

**A FRAMEWORK IN SUPPORT OF STRUCTURAL  
MONITORING BY REAL TIME KINEMATIC GPS  
AND MULTISENSOR DATA**

By

**Clement Ogaja**

B.Sc., University of Nairobi, Nairobi, Kenya, 1997

A thesis submitted to The University of New South Wales  
in partial fulfilment of the requirements for the Degree of  
Doctor of Philosophy

School of Surveying and Spatial Information Systems  
(Formerly the School of Geomatic Engineering)  
The University of New South Wales  
Sydney NSW 2052, Australia

May, 2002

## ABSTRACT

---

---

Due to structural damages from earthquakes and strong winds, engineers and scientists have focused on performance based design methods and sensors directly measuring relative displacements. Among the monitoring methods being considered include those using Global Positioning System (GPS) technology. However, as the technical feasibility of using GPS for recording relative displacements has been (and is still being) proven, the challenge for users is to determine how to make use of the relative displacements being recorded. This thesis proposes a mathematical framework that supports the use of RTK-GPS and multisensor data for structural monitoring. Its main contributions are as follows:

- (a) Most of the emerging GPS-based structural monitoring systems consist of GPS receiver arrays (dozens or hundreds deployed on a structure), and the issue of integrity of the GPS data generated must be addressed for such systems. Based on this recognition, a methodology for integrity monitoring using a data redundancy approach has been proposed and tested for a multi-antenna measurement environment. The benefit of this approach is that it verifies the reliability of both the measuring instruments and the processed data contrary to the existing methods that only verifies the reliability of the processed data.
- (b) For real-time structural monitoring applications, high frequency data ought to be generated. A methodology that can extract, in real-time, deformation parameters from high frequency RTK measurements is proposed. The methodology is tested and shown to be effective for determining the amplitude and frequency of structural dynamics. Thus, it is suitable for the dynamic monitoring of towers, tall buildings and long span suspension bridges.
- (c) In the overall effort of deformation analysis, large quantities of observations are required, both of causative phenomena (e.g., wind velocity, temperature, pressure), and of response effects (e.g., accelerations, coordinate displacements, tilt, strain, etc.). One of the problems to be circumvented is that of dealing with excess data generated both due to process automation and the large number of instruments employed. This research proposes a methodology based on multivariate statistical process control whose benefit is that excess data generated on-line is reduced, while

maintaining a timely response analysis of the GPS data (since they can give direct coordinate results).

Based on the above contributions, a demonstrator software system was designed and implemented for the Windows operating system. Tests of the system with datasets from UNSW experiments, the Calgary Tower monitoring experiment in Canada, the Xiamen Bank Building monitoring experiment in China, and the Republic Plaza Building monitoring experiment in Singapore, have shown good results.

## ACKNOWLEDGMENTS

---

---

I wish to acknowledge and thank the Almighty God, and the individuals and groups who contributed to my study. Without their support, this thesis would not have been possible.

Firstly, I would like to express special thanks to my supervisor Professor Chris Rizos for accepting me as his student so that I had an opportunity to study in the School of Surveying and Spatial Information Systems (formerly School of Geomatic Engineering) at the University of New South Wales (UNSW). Many encouragements, numerous supports, valuable suggestions and patient guidance by Prof. Rizos led to my successful study at UNSW. Much appreciation also goes to my Co-supervisor Dr. Jinling Wang for his encouragement and valuable suggestions.

I wish to thank all members of the Satellite Navigation And Positioning (SNAP) group, Dr. Toshiaki Tsujii, Dr. Horng-yue Chen, Dr. Joel Barnes, Dr. Linlin Ge, Dr. Chalermchon Satirapod, Dr. Craig Roberts, Mr. Liwen Dai, Mr. Volker Janssen, Mr. Michael Moore, Mr. Jun Zhang, Mr. HungKyu Lee, Mr. Binghao Li, Ms. Yonghong Li, Ms Diana Polonska and Mr. Yufei Wang for their support in a variety of ways. Special thanks also goes to the staff members of the School for the numerous ways in which they supported my study, in particular, Prof. Bill Kearsley, Prof. J. M. Rueger, Helve Frangoulis, Leon Daras, Maria Ponce, Philip Lam, Chris Ryan and Brian Donnelly.

I would like to gratefully acknowledge the University of New South Wales as a whole, the Faculty of Engineering, and the SNAP group for respectively awarding me the International Postgraduate Research Scholarship (IPRS), the Supplementary Engineering Postgraduate Award (SEPA) scholarship and the SNAP scholarship to pursue my Ph.D. studies at the UNSW. Much gratitude to the U.S. Institute of Navigation (ION) for awarding me a student competition winner scholarship to support my attendance at the 14th International Technical Meeting of the ION Satellite Division, held in Utah, USA, 11-14 September 2001, and for awarding me a best presentation prize at that meeting. Thanks to the IAG Special Commission 4 for awarding me a student prize to partially support my attendance at the 2<sup>nd</sup> Symposium on

Geodesy for Geotechnical and Structural Engineering, held in Berlin, Germany, 21-24 May 2002.

Most importantly, I would like to extend my deepest appreciation to my family and my beloved wife Julie (and unborn baby), for their love, encouragement, moral support and understanding during the period of this study.

## TABLE OF CONTENTS

---

---

ABSTRACT .....	i
ACKNOWLEDGMENTS .....	iii
TABLE OF CONTENTS .....	v
LIST OF FIGURES .....	x
LIST OF TABLES .....	xiii
PROGRAM LISTINGS .....	xiv
LIST OF ABBREVIATIONS .....	xv

### 1. INTRODUCTION

1.1 Background .....	1
1.2 Research Objectives .....	3
1.3 Structure of the Thesis .....	5
1.4 Contributions to Research .....	7

### 2. STRUCTURAL MONITORING

2.1 Introduction .....	9
2.2 Observables and Instrumentation .....	10
2.3 Non-GPS Methods .....	13
2.3.1 Surveying Methods .....	14
2.3.1.1 Electronic Distance and Angle Measurements .....	14
2.3.1.2 Levelling and Trigonometric Heighting .....	16
2.3.1.3 Photogrammetric Methods .....	17
2.3.2 Geotechnical Measurement Techniques .....	18
2.3.2.1 Extension and Strain Measurements .....	18
2.3.2.2 Tilt and Inclination Measurements .....	19
2.3.3 Other Non-GPS Techniques .....	19
2.3.4 Advantages and Limitations .....	20
2.4 Recent Activities .....	23

---

3. INTRODUCING GPS POSITIONING	
3.1 Introduction	26
3.2 GPS Positioning Modes	27
3.2.1 Point Positioning	30
3.2.2 Relative Positioning	30
3.3 RTK-GPS Positioning	32
4. GPS APPLICATIONS TO STRUCTURAL MONITORING	
4.1 Introduction	36
4.2 Slow Structural Deformation	39
4.3 Fast Structural Deformation	40
4.4 Commercial Off-the-Shelf RTK-Based Software Systems	42
4.4.1 Operational RTK-Based Structural Monitoring Systems	43
4.4.1.1 Tsing Ma Suspension Bridge Monitoring	43
4.4.1.2 Republic Plaza Building Monitoring	45
5. GPS BIASES AND INTEGRITY MONITORING	
5.1 Error Sources in GPS Observations	48
5.1.1 Satellite Related Biases	48
5.1.2 Receiver Related Biases	49
5.1.3 Signal Propagation Biases	51
5.2 Multipath	53
5.2.1 Modes of Multipath	53
5.2.2 Example of Low Frequency Multipath	54
5.2.3 Multipath in GPS-Based Structural Monitoring	59
5.2.3.1 Introduction	59
5.2.3.2 Multipath Minimisation Techniques	59
5.3 Integrity Monitoring	61
5.3.1 Definition and Concepts	61

---

5.3.2 Ground-Based Integrity Monitoring .....	62
5.3.3 Receiver Autonomous Integrity Monitoring.....	63
4.4 Concluding Remarks .....	64
6. INTEGRITY MONITORING IN THE POSITION DOMAIN	
6.1 Introduction.....	65
6.2 On-line Change Detection Algorithms .....	66
6.2.1 Shewhart Control Charts.....	66
6.2.2 CUSUM Test Algorithms .....	70
6.2.2.1 One-Sided CUSUM Test.....	70
6.2.2.2 Two-Sided CUSUM Test .....	72
6.2.3 Summary and Discussion.....	73
6.2.3.1 Estimating the Mean and Standard Deviation .....	73
6.2.3.2 Choosing the Anticipated Shift and Threshold.....	74
6.2.4 Choice of Criteria.....	74
6.3 CUSUM Application to Integrity Monitoring .....	75
6.3.1 The Proposed Approach.....	75
6.3.2 Experiment at UNSW .....	78
6.3.3 Data Normality and Statistical Independence .....	79
6.3.4 Integrity Tests .....	81
7. ANALYSIS OF RTK-GPS AND MULTISENSOR MEASUREMENTS	
7.1 Introduction.....	87
7.2 Estimating Fast Deformation Parameters .....	90
7.2.1 Fast Fourier Spectra .....	90
7.2.2 Experiment at UNSW .....	91
7.2.3 On-line Estimation .....	95
7.2.3.1 Time-Frequency Approach .....	95
7.2.3.2 On-line Analysis .....	97
7.2.4 Test Example .....	98
7.3 Multivariate Analysis .....	100



---

7.3.1 Introduction.....	100
7.3.2 Multivariate Statistical Process Control.....	101
7.3.3 Test Example .....	103
7.3.4 Analysis by Wavelet Transformation .....	108
7.3.4.1 Methodology.....	108
7.3.4.2 Test Results.....	111
8. TEST RESULTS OF A SOFTWARE IMPLEMENTATION	
8.1 Introduction.....	113
8.2 Integrity Monitoring of GPS Data in the Position Domain .....	113
8.3 Time and Frequency Domain Analysis.....	116
8.3.1 Case I – UNSW Dataset.....	116
8.3.2 Case II – Calgary Tower Dataset .....	120
8.3.3 Case III – Xiamen Building Dataset .....	124
8.4 GPS and Multisensor Data Analysis.....	128
8.4.1 Data Description .....	128
8.4.2 Test Results .....	129
9. CONCLUSIONS AND RECOMMENDATIONS	
9.1 Concluding Remarks.....	136
9.1.1 Integrity Monitoring of GPS Data in the Position Domain.....	136
9.1.2 Time and Frequency Domain Analysis.....	137
9.1.3 GPS and Multisensor Data Analysis .....	138
9.2 Recommendations and Future Work .....	138
REFERENCES .....	141
APPENDIX I. AUTHOR-DEVELOPED SOFTWARE	
I-1 Introduction .....	157
I-2 Programming Language and Coding Style .....	157

I-3 Framework Core Classes .....	160
I-4 Software Modules and Sample Window Interfaces .....	168
I-5 Concluding Remarks .....	174
APPENDIX II. GLOSSARY OF TERMS .....	176
VITA .....	187

## LIST OF FIGURES

### Figures

3.1	Geometric range from a receiver to a satellite.....	29
3.2	The RTK-GPS concept.....	33
3.3	Satellite-receiver double-difference ( $\Delta\nabla$ ).....	34
4.1	A schematic of GPS deployment on a structure (Celebi & Sanli, 2002).....	38
4.2	Tsing Ma Suspension Bridge.....	44
4.3	Republic Plaza Building (RPB).....	45
4.4	Layout of the GPS monitoring system at the RPB .....	46
5.1	The multipath environment surrounding a GPS receiver .....	53
5.2	Plan view of the UNSW stations used for the multipath experiment.....	55
5.3	Photo of UNSW multipath experiment setup (a) and the surrounding environment (b) .....	55
5.4	Comparison of the measurements and regression curves for the base-alpha baseline (Day 1 vs. Day 2).....	56
5.5	Comparison of the measurements and regression curves for the base-beta baseline (Day 1 vs. Day 2).....	57
5.6	Comparison of the measurements and regression curves for the alpha-beta baseline (Day 1 vs. Day 2).....	57
5.7	Frequency-domain representations of multipath on baseline results.....	58
6.1	A Shewhart example of random data simulated using Matlab random number generator .....	69
6.2	Typical behaviour of the log-likelihood ratio corresponding to an increase in the mean (top) and a decrease in the mean (bottom) .....	71
6.3	Typical behaviour of the CUSUM decision function.....	72
6.4	FDE in the measurement domain (Ober, 2000).....	75
6.5	FDE in the position domain (Ober, 2000) .....	76
6.6	Experimental setup at UNSW (26 November 2001).....	78
6.7	Time series of baseline residuals (UNSW – 26 November 2001) .....	79
6.8	Normal Distribution histogram plots for Easting residuals .....	80
6.9	Normal Probability plots for Easting residuals.....	80
6.10	Correlation analysis for Easting residuals .....	81
6.11	Time series of baseline residuals with 1-sigma biases (PMDEs) introduced into ROV2 components .....	82
6.12	Time series of baseline residuals with 2-sigma biases (PMDEs) introduced into ROV2 components .....	83
6.13	Hypothetical abrupt "failure" in ROV2 components.....	84
6.14	Bias/Failure detection and exclusion: 1-sigma case (top), 2-sigma case (middle), simulated failure (bottom).....	85
7.1	The experiment at UNSW (24th January 2001) -- The 'rover' antenna atop the mechanical shaker .....	92
7.2	RTK-GPS time series of the height component (UNSW, 24 Jan. 2001).....	93
7.3	High frequency RTK-GPS time series (a) and corresponding amplitude spectra (b) .....	94

7.4	Short-Time Fourier Transform .....	96
7.5a	Power spectrum (Left) and IF tracking (Right) for 2 – 3Hz .....	99
7.5b	Power spectrum (Left) and IF tracking (Right) for 0.2 – 0.3Hz .....	99
7.5c	Power spectrum (Left) and IF tracking (Right) for 0.5 – 0.7Hz .....	99
7.5d	Power spectrum (Left) and IF tracking (Right) for 0.7 – 1.2Hz .....	99
7.6	Simultaneous GPS positioning, wind, accelerometer and temperature sensor data. Units: GPSN [cm], GPSE [cm], UE [m/s], UW [m/s], $\delta E$ [mm/s <sup>2</sup> ], $\delta N$ [mm/s <sup>2</sup> ], T [°C].....	104
7.7	Normal Distribution histogram plots for the Multivariate Data .....	105
7.8	Multivariate SPC chart .....	106
7.9	Multivariate SPC chart for GPS data (top), wind data (middle), and accelerometer data (bottom) .....	107
7.10	MH/Median hybrid filter example. <b>Top left panel:</b> original data signal; <b>top right panel:</b> signal with Gaussian random noise, <b>bottom left panel:</b> filtered signal after 50 consecutive passes and a window half-width of 9; <b>bottom right panel:</b> a superposition of the filtered and the uncorrupted signal .....	109
7.11	Wavelet Transform of FMH filtered GPS data signals. <b>Top panel:</b> DHWT of FMH filtered GPSE data signals; <b>bottom panel:</b> DHWT of FMH filtered GPSN data signals.....	111
7.12	MSPC charts of (a) original GPSE and GPSN signals (top), and (b) wavelet transformed FMH filtered GPSE and GPSN signals (bottom) .....	112
8.1	Screen image of Integrity Test – Case I .....	114
8.2	Screen image of Integrity Test – Case II .....	115
8.3	Screen image of Integrity Test – Case III.....	116
8.4	Screen image of frequencies and amplitudes (UNSW) – (1) .....	118
8.5	Screen image of frequencies and amplitudes (UNSW) – (2) .....	119
8.6	Screen image of frequencies and amplitudes (UNSW) – (3) .....	119
8.7	Screen image of frequencies and amplitudes (UNSW) – (4) .....	120
8.8	Movement of Calgary Tower .....	121
8.9	Frequency Domain of Movement of Calgary Tower .....	121
8.10	Dominant Frequency of Movement of Calgary Tower .....	122
8.11	Screen Image of frequencies and amplitudes (Calgary Tower) – Set A .....	123
8.12	Screen Image of frequencies and amplitudes (Calgary Tower) – Set B.....	123
8.13	Screen Image of frequencies and amplitudes (Calgary Tower) – Set C.....	124
8.14	Time series of X-component of Xiamen Bank Building data .....	125
8.15	Time series of Y-component of Xiamen Bank Building data .....	125
8.16	Time series of H-component of Xiamen Bank Building data .....	126
8.17	Screen image of frequencies and amplitudes (Xiamen Building) – Set A .....	127
8.18	Screen image of frequencies and amplitudes (Xiamen Building) – Set B .....	127
8.19	Screen image of frequencies and amplitudes (Xiamen Building) – Set C .....	128
8.20	Multisensor instrumentation at Republic Plaza (RP) Building during the trial experiment of 17 to 25 February 2000. (a) Sonic anemometer at east corner, (b) Sonic anemometer at west corner, and (c) close up on the brackets .....	129
8.21	Screen image of multisensor signal .....	130
8.22	Time series of 1-second GPS solutions – NTU, 18 February 2000 .....	131
8.23	Screen image of frequencies and amplitudes (RP Building) – Set 1A.....	131
8.24	Screen image of frequencies and amplitudes (RP Building) – Set 1B .....	132

---

8.25	Screen image of frequencies and amplitudes (RP Building) – Set 1C .....	132
8.26	Time series of 1-second GPS solutions – NTU, 19 February 2000 .....	133
8.27	Screen image of frequencies and amplitudes (RP Building) – Set 2A .....	134
8.28	Screen image of frequencies and amplitudes (RP Building) – Set 2B .....	134
8.29	Screen image of frequencies and amplitudes (RP Building) – Set 2C .....	135
9.1	An integrated analysis model .....	140
I-1	Microsoft Visual C++ 6.0 project workspace.....	159
I-2	An opened Microsoft Visual C++ 6.0 project workspace .....	161
I-3	Overall structure of the author-developed system .....	168
I-4	A flowchart of some of the key functions of the author-developed system .....	169
I-5	Flow diagram of the module for RTK data integrity monitoring .....	170
I-6	Flow diagram of the Module for multisensor data analysis .....	171
I-7	"Dialogue One" of RTSM version 1.0 interface.....	172
I-8	Alarm message box of RTSM .....	173
I-9	"Dialogue Two" of RTSM version 1.0 interface .....	173
I-10	"Dialogue Three" of RTSM version 1.0 interface .....	174

## LIST OF TABLES

---

---

### Tables

2.1	Non-GPS instruments for measuring deformation. ....	15
2.2	Non-GPS surveying methods .....	22
2.3	Geotechnical and other instrument methods .....	23
5.1	Estimated quality of the IGS orbit products (GPS broadcast values included for comparison).....	49
6.1	Sigmas for baseline residuals .....	79
6.2	1-sigma PMDEs.....	82
6.3	2-sigma PMDEs.....	83
7.1	The test frequencies for the experiment at UNSW .....	93
8.1	The test frequencies for the experiment at UNSW (2) .....	117

## PROGRAM LISTINGS

---

---

### Listings

I-1	Class <b>CMyAlgorithms</b> (contained in CMYALGORITHMS.H) .....	163
I-2	Class <b>CTabOne</b> (contained in CTABONE.H).....	164
I-3	Class <b>CTabTwo</b> (contained in CTABTWO.H) .....	165
I-4	Class <b>CTabThree</b> (contained in CTABTHREE.H).....	166
I-5	Class <b>CTabFour</b> (contained in CTABFOUR.H).....	167
I-6	Class <b>COMPLEX</b> (contained in RTDSPC.H).....	167

## LIST OF ABBREVIATIONS

---

---

ANCOLD	Australian National Committee on Large Dams
C/A	Coarse Acquisition or Civilian Access code
CCD	Charge Couple Device
cm	Centimetre
CORS	Continuously Operating Reference Stations
CUSUM	Cumulative Sum
DHWT	Discrete Haar Wavelet Transformation
EDM	Electronic Distance Measurement
FDE	Fault Detection and Exclusion
FFT	Fast Fourier Transform
FIG	International Federation of Surveyors
FIG SG6C	International Federation of Surveyors Study Group 6C
FIR	Finite Impulse Response
FMH	FIR Median Hybrid
GEONET	GPS Earth Observation Network
GIC	Ground Integrity Channel
GOCA	GPS-based Online Control and Alarm system
GPS	Global Positioning System
GPSE	GPS Easting Component
GPSN	GPS Northing Component
GPS-OSIS	GPS On-Structure Instrumentation System
HWT	Haar Wavelet Transform
Hz	Hertz
IF	Instantaneous Frequency
IABSE	International Association for Bridge and Structural Engineering
IABSE WC1	IABSE Working Commission 1
IAG	International Association of Geodesy
IAG SC4	International Association of Geodesy Special Commission IV
ICOLD	International Commission on Large Dams
IGS	International GPS Service
ION	Institute of Navigation



IPRS	International Postgraduate Research Scholarship
Km	Kilometre
KSMB	Kap Shui Mun Bridge
LADGS	Local Area Differential GPS
LCL	Lower Control Limit
LMS	Least Mean Square
L1	First frequency sent out by GPS satellites (1.5GHz)
L2	Second frequency sent out by GPS satellites (1.2 GHz)
mm	Millimetre
m/s	Metres per second
MCS	Master Control Station
MDE	Marginally Detectable Error
NTU	Nanyang Technological University
PANDA	PC software for optimisation, Adjustment and Deformation Analysis
PC	Personal Computer
PCMCIA	Personal Computer Memory Card International Association
PMDEs	Persistent Marginally Detectable Errors
RAIM	Receiver Autonomous Integrity Monitoring
RLS	Recursive Least Squares
ROV1	Rover Station 1
ROV2	Rover Station 2
ROV3	Rover Station 3
RP	Republic Plaza
RPB	Republic Plaza Building
RTK	Real-Time Kinematic
RTK-GPS	Real-Time Kinematic GPS
RTSM	Real-Time System Monitor
RTCM	Radio Technical Committee for Maritime Applications
SCIGN	Southern California Integrated Geodetic Network
SEPA	Supplementary Engineering Postgraduate Award
SNAP	Satellite Navigation and Positioning Group
SPC	Statistical Process Control
SPP	Single Point Positioning

sps	Samples per second
STFT	Short Time Fourier Transform
TEC	Total Electron Content
TFD	Time Frequency distribution
TKB	Ting Kau Bridge
TMB	Tsing Ma Bridge
UCL	Upper Control Limit
UE	Wind Velocity in the Orthogonal Direction E
UNSW	University of New South Wales
USACE	United States Army Corps of Engineers
USSD	United States Society on Dams
UW	Wind Velocity in the Orthogonal Direction W
UVW	Three Orthogonal Directions of Wind Velocity
WAAS	Wide Area Augmentation System
WADGPS	Wide Area Differential GPS
WASHMS	Wind and Structural Health Monitoring System
WGS84	World Geodetic System 1984
WVD	Wigner-Ville Distribution
1D, 2D, 3D	One-Dimensional, Two-Dimensional, Three-Dimensional

## **1.1 Background**

Higher, bigger and wider structures (buildings, bridges, towers) form an integral part of the modern national infrastructure. Structural monitoring can help to gather data whose many uses include improvement of building codes and design, assessment of earthquake and wind hazards, and correlation of structural response with damage. The benefits from such programs include safety to users (e.g. building occupants) and the public, and to protect the public property from damage. For example, in the United States several programs have been instituted through the National Earthquake Hazard Reduction Act 1977 to support instrumentation of federal buildings especially those located in the seismic zones (Celebi et al. 1984, 1985, 1986, 1987, 1988, 1989, 1998b; Celebi, 2000b).

Until recently, only accelerometers (single, biaxial or triaxial) were used to instrument structures. However, due to structural damages observed from the 1994 Northridge and 1995 Kobe earthquakes, engineers and scientists have now focused on performance based design methods and sensors directly measuring relative displacements (Celebi et al. 1998a; 2000b). Among the monitoring methods being considered include those using Global Positioning System (GPS) technology. Early work by researchers have already shown the technical feasibility of using GPS methods for recording relative displacements of structures (e.g., Celebi, 2000a; Celebi & Sanli, 2002).

However, as the technical feasibility of recording relative displacements with GPS has been (and is still being) proven, the challenge for users of such data is to determine how to make use of the relative displacements being recorded. Real-time kinematic (RTK) GPS technology, is now advanced to record at 10 sps (or better [e.g. 20 sps]) with an accuracy of  $\pm 1$  cm horizontally and  $\pm 2$  cm vertically. This provides an opportunity to

measure directly and with sufficient accuracy, the relative displacements in real-time. The possible potential uses of such data include:

- (1) Real-time monitoring by configuring the GPS units to provide streams of data to indicate excessive displacements, average drift ratios or changes in the dynamic characteristics of tall buildings and long-span bridges. This information can be made available to site managers (or interested parties) in real-time or near real-time or whenever a predetermined displacement threshold is reached. The managers can then assess the response of the structure according to the different threshold displacements or temporally changing dynamic characteristics. If the situation is serious, the management can make decisions to evacuate the building (or close the bridge) for additional inspection and to secure the safety of the users and the structure.
- (2) The collected information on the response of the structure during strong motion events can be used to make decisions for further evaluation of the serviceability of the structure.
- (3) The recorded data can be used to analyse the performance of the structure, and the results can be used to improve future analyses/design procedures.

Each deformable structure may obviously require different parameters to be observed, different instrumentation, different accuracies, and different observation frequencies. For example, measuring the rooftop displacement of a building has the potential use in advancing and verifying performance-based design procedures for tall buildings (Celebi & Sanli, 2002). A minimum of three GPS units should be deployed – two on the roof to detect translational and torsional motions, and the third to serve as a reference station for calculation of relative displacements. Similarly, several dozens of GPS units deployed on bridge decks and towers can be configured to compute direct displacements of the bridge towers with respect to the deck. Thus, one should expect that large datasets are generated as well as several GPS units are used. However, GPS data alone have some shortcomings (e.g., multipath effects, low sampling rates) when used for precise engineering applications. Therefore, an important consideration is to allow comparison of relative displacements measured by GPS and those obtained by conventional methods such as the double integration of accelerations (Roberts et al. 2000). Thus, GPS

units should be deployed on a structure that is also instrumented with other sensors (e.g. accelerometers).

For checking the reliability of a monitoring system, redundant monitoring (in terms of instrumentation and stations) is necessary. In addition, it should be emphasised that the monitoring instrumentation, even if permanently installed, can be vulnerable to defects and failures. Thus, employing parallel but separate instrument sets, and the means for evaluating data by, for instance, double-checking using alternative methods, is advisable. A proper monitoring scheme should incorporate redundant measurements and a system for "self-checking".

In general, the quality of data analysis depends on the frequency, type and reliability of the measurements. Data frequency and reliability can be enhanced through an automatic system of data acquisition and processing. In such a case, a data system encompassing everything that happens to the data from the instant at which it is generated by a sensor to the time of analysis can be designed. The time interval between sensing and analysis may extend over minutes, hours or days under normal conditions or may have to be instantaneous under critical conditions in order to provide a warning of imminent failure. The many advantages of such a system include increased sensitivity to abrupt changes resulting in the possibility to measure structural deflections and movements, the possibility of data retrieval from remote inaccessible locations, near real-time or real-time results of trends and analysis, elimination of data reading and recording errors, and so forth. On the other hand, problems that are likely to be encountered while dealing with such systems include the fact that data may be blindly accepted leading to wrong conclusions (hence the need for data integrity), generation of excess data leading to lack of timely response, and the need for compatibility between different observables.

## **1.2 Research Objectives**

The main objective of this research is to define a mathematical framework that supports the use of RTK-GPS and multisensor data for structural monitoring. New methods are proposed for real-time integrity checking of a GPS array monitoring system using time

domain data, real-time analysis of fast structural deformations and the use of long-term multisensor observations to aid the monitoring of fast deformations from high frequency RTK measurements. The developed mathematical framework is evaluated through a simple software demonstration with test datasets.

Structural monitoring with GPS requires high precision and reliability for the raw GPS measurements and subsequent position results. High precision can be achieved by using a carrier phase-based differential positioning mode (see Chapter 3). However, precise positioning is not necessarily the most important issue. High integrity of the GPS antenna coordinates is also required in order to guard against false information. This can be achieved through data-based quality control methods (e.g., GPS fault detection and integrity tests). Some researchers (e.g., Chang and Paige, 2000; Ober, 2000; Ochieng et al., 2001, 2002; Cross et al., 1994) have developed methods based on *equation removal* and *satellite removal* approaches that are implemented at the GPS data processing step. Such methods removes a biased measurement or all measurements corresponding to a given satellite at one time step. Thus, they can be implemented for quality control and integrity monitoring at one or two GPS reference stations (e.g., De Jong et al., 2001).

Most of the emerging GPS-based structural monitoring systems consist of GPS receiver arrays (dozens or hundreds deployed on a structure), and the issue of integrity of the GPS data generated must be addressed for such systems. One way to address this issue is through the GPS reference station(s) as explained above. The other possible way is to utilise the redundancy of the measuring system to perform an integrity check based on the GPS data generated from multiple GPS units. Such an approach is now feasible due to the availability of 3D monitoring systems (e.g., <http://www.3d-gps.com/>) supporting multiple GPS receivers, located on the target structure, transferring data in real-time via modem, wireless radio or network connection to a personal computer which processes the data in real-time. The benefit of the approach is that it verifies the reliability of both the measuring instruments and the processed data. This is one of the objectives of this research.

The process of deformation analysis involves estimating the deformation parameters. In the case of a long series of observations taken and/or averaged over a prolonged

period of time, plotting of individual observables versus time helps to establish the deformation trend and is a means of visualising the deformation model in the time domain. During analysis, one has to separate the known trend(s) from the superimposed investigated deformation. For example, one has to distinguish between the cyclic (seasonal) thermal expansion of a structure with known period of oscillation, and deformation caused by other effects which are, for instance, linear in time. For near-real-time or real-time applications, the observation data ought to be generated more frequently (e.g. sampling rate  $> 1$  Hz). In this thesis, the term "high frequency" is used to refer to such data, for which one of the challenges is to convert into information as soon as possible. A methodology that can extract, in real-time, deformation parameters from high frequency RTK measurements, is one of the research emphases of this thesis.

In the overall effort of deformation analysis, large quantities of observations are required, both of causative phenomena (e.g., wind velocity, temperature, pressure), and of response effects (e.g., accelerations, coordinate displacements, tilt, strain, etc.). It is generally expected that if long sets of observation data are available, portions of the response data would be strongly correlated with changes in wind, temperature or pressure. As already pointed out in the previous section, one of the problems to be circumvented is that of dealing with excess data generated both due to process automation and the large number of instruments employed. This research proposes a methodology based on multivariate statistical process control (e.g., Kourti & MacGregor, 1996). The term "multivariate process" is used to refer to GPS data along with the data from other sensors such as accelerometers, anemometers, and temperature sensors. The benefit of the proposed methodology is that excess data generated on-line is reduced, while maintaining a timely response analysis of the GPS data (since they can give direct coordinate results).

### **1.3 Structure of the Thesis**

This thesis consists of nine chapters and two appendices.

The first chapter is a brief introduction of the research objectives and the overview of this thesis.

Chapter 2 briefly introduces structural monitoring and the traditional (non-GPS) structural monitoring methods and instrumentation. It reviews the terrestrial methods, including the conventional geodetic survey methods and the geotechnical techniques.

Chapter 3 is devoted to an overview of GPS positioning methods that are of interest in this thesis. Different modes of GPS positioning are briefly discussed followed by the concept of real-time kinematic GPS (RTK-GPS).

Chapter 4 gives the background to structural monitoring with GPS. It reviews some of the current developments and research activities relating to GPS-based structural monitoring.

GPS biases that are common to GPS positioning as a whole, and to the RTK-GPS technique in particular, are summarised in Chapter 5. Issues concerning multipath in GPS-based structural monitoring and minimisation techniques are discussed. A section is also devoted to introducing the concept of integrity monitoring.

The first part of the mathematical algorithms that have been developed for the proposed framework is presented in Chapter 6. The basic mathematical assumptions and concepts upon which the proposed methodology for integrity monitoring (fault/defect detection) of RTK data is based are outlined. The theories are described in detail, and illustrated with examples.

Chapter 7 is a continuation of the proposed framework. It introduces deformation analysis and outlines an approach to the estimation of fast deformation parameters from RTK observations. The first part of the approach is based on a direct estimation of the parameters where only fast RTK data are available, while the second part is an estimation based on indicative information from auxiliary multisensor data.



Chapter 8 presents the results of this research and includes some tests of an author-developed software system. The test results are based on actual data obtained from trial experiments with towers and tall buildings. The analysed datasets include those from UNSW experiments, the Calgary Tower monitoring experiment in Canada, the Xiamen Bank Building monitoring experiment in China, and the Republic Plaza Building monitoring experiment in Singapore.

Chapter 9 draws some conclusions and makes recommendations for future work.

Appendix I is a description of the author-developed software system.

Finally in Appendix II is a glossary of terms which may be unfamiliar to the reader.

#### **1.4 Contributions to Research**

The contributions of this research can be summarised as follows:

1. Most of the emerging GPS-based structural monitoring systems consist of GPS receiver arrays (dozens or hundreds deployed on a structure), and the issue of integrity of the GPS data generated must be addressed for such systems. Based on this recognition, a methodology for integrity monitoring using a data redundancy approach has been proposed and tested for a multi-antenna measurement environment. The benefit of this approach is that it verifies the reliability of both the measuring instruments and the processed data contrary to the existing methods that only verifies the reliability of the processed data.
2. For real-time structural monitoring applications, high frequency data ought to be generated. A methodology that can extract, in real-time, deformation parameters from high frequency RTK measurements is proposed. The methodology is tested and shown to be effective for determining the amplitude and frequency of structural dynamics. Thus, it is suitable for the dynamic monitoring of towers, tall buildings and long span suspension bridges.

3. In the overall effort of deformation analysis, large quantities of observations are required, both of causative phenomena (e.g., wind velocity, temperature, pressure), and of response effects (e.g., accelerations, coordinate displacements, tilt, strain, etc.). One of the problems to be circumvented is that of dealing with excess data generated both due to process automation and the large number of instruments employed. This research proposes a methodology based on multivariate statistical process control whose benefit is that excess data generated on-line is reduced, while maintaining a timely response analysis of the GPS data (since they can give direct coordinate results).

## **2.1 Introduction**

Buildings, towers, bridges, dams, and other large engineering structures are subject to external loading that causes deformation. Any abnormal behaviour may indicate a threat to the safety of the structure as well as that of its users and the general public. Careful monitoring of the loads acting on a structure, and its response to those loads, can aid in identifying the deformational behaviour of that structure.

Deformations and their observations will vary according to the structure. Differences in construction materials is one of the larger influences on how a structure deforms. For example, deformation is mainly elastic, dependent on reservoir water pressure and temperature variations for concrete dams (cf. earthen dams). Such deformations can be measured by configuring to observe movement trends over long periods of time. Similarly, deformation in flexible steel-framed structures (tall buildings and suspension bridges) are elastic and relative movements between short time intervals may occur due to abrupt seismic loading, wind loading or traffic loading. In that case, fast deformation of such structures can be determined from high frequency measurements.

Depending on the type and condition of a structure, monitoring systems may need to be capable of measuring both long-term trends and short-term loading deformations. Long-term permanent deformations are those that occur over long time intervals (months or years) and can be assessed from absolute data (i.e. displacement obtained from episodic observations). Short-term deformations are those that occur over short time intervals (at 1 second or less) and can be assessed from high frequency data.

Episodic observations can be either made to monitoring points on the structure from external reference points, or made relative to absolute (external) reference points. The reference points are established on stable ground located outside the actual structure,

and beyond the area that may be affected by the structure. The external reference points are termed "Reference Network". The reference network should also be monitored at less frequent intervals to ensure that the reference points have not themselves moved. Traditional geodetic survey instruments and techniques may be used to establish and monitor the reference network.

A more routine and more frequent monitoring process can be employed to track the short-term behaviour of a structure by simply confining observation to trends at selected points along the span, and sometimes lateral lines. Such monitoring is cost-effective when the measuring instruments can lend themselves to automation, and continuous and direct measurements.

Some traditional monitoring techniques (e.g., accelerometers, tiltmeters, strain gauges) require that the reference points are located on the structure itself. When such techniques are employed, relative as well as localised deformations can be established.

## **2.2 Observables and Instrumentation**

In general, structural monitoring schemes include i) monitoring of deformations through the determination of the geometrical change in shape and size, and rigid body translations and rotations (absolute and/or relative) of the monitored object, and ii) monitoring of the acting forces (loading) which can either be measured directly or derived from measurements. The measurement objectives would, however, depend on whether the scheme is designed to monitor slow (long-term) or fast (short-term) deformations, or both.

Slow deformations due to dead loading, temperature loading, pressure loading, tectonic activities (e.g. seismic swarms) and so forth, can be assessed by distance or point displacements (distortions, translations), angular displacements (rotations), and strain/stress conditions. Fast deformations due to abrupt wind loading, seismic loading, or traffic loading can be assessed by relative distance, point or angular displacements, station acceleration response data and strain/stress conditions.

Distance and angular measurements are traditionally used to derive absolute displacements of selected points on the surface of objects with respect to some reference network. The "absolute values" can be obtained only if the reference network itself is stable. Horizontal absolute displacements can be surveyed with alignment techniques while vertical absolute displacements can be determined by levelling techniques.

Station acceleration response measurements, extension and strain measurements, tilt and inclination measurements, and pressure measurements should provide information on the relative movements (deflections or inclinations) within the body of the deformable structure and its surroundings.

Temperature measurements would provide information on the thermal state of the construction material and atmospheric temperature at various levels (and/or water temperature at various levels in the case of dam monitoring).

Wind velocity and wind direction are an important consideration in schemes where fast deformations or structural response are a candidate for validating the design assumptions and parameters due to wind conditions. They generally require recording of measurements made in three orthogonal directions.

Three-dimensional coordinates or baseline components of points located on the surface of a structure, if obtained in real-time, relative to a reference network, can be used to deduce absolute displacements, as well as the deflections or fast movements due to abrupt loading conditions.

There is a vast array of measurement techniques and instrumentation that can observe or provide angular measurements, distance measurements, temperature measurements, strain/stress measurements, acceleration measurements, pressure measurements, wind velocity, wind direction, and position coordinates (see, e.g., Dunnycliff, 1988, 1993; Rueger, 1996; USACE, 1994, 1996). This thesis will categorise these techniques and instrumentation according to two main groups, namely:

- 1) The traditional terrestrial structural monitoring techniques (Non-GPS methods), which include the conventional geodetic surveys (e.g. Electronic Distance Measurement (EDM), precise levelling, terrestrial close range photogrammetric techniques, laser interferometry, etc), and geotechnical measurements of local deformations using titlometers, strianometers, extensimeters, joint meters, etc.
- 2) The satellite positioning-based monitoring techniques (i.e., GPS methods) which can provide, in real-time, the three-dimensional coordinates of a point located on the Earth surface by measurements to satellites (Chapter 3).

Each type of measurement has its own pros and cons. Geodetic surveys through a network of points interconnected by angle and/or distance measurements, usually supply sufficient redundancy of observations for the statistical evaluation of their quality and error detection. They give global information on the behaviour of the deforming structure. On the other hand, the geotechnical measurements give very localised information without any checking unless compared with some other independent measurements. However, geotechnical instruments are easier to adapt for automatic and continuous monitoring than is the case with geodetic instruments. Geodetic surveys are labour intensive and require skilful observations, while geotechnical instruments, once installed, only require infrequent checks on their performance. GPS positioning methods offers sub-centimetre accuracy in differential mode over medium-range distances (e.g., < 100Km), and are currently replacing the conventional terrestrial surveys for deformation applications, and especially in establishing the reference networks. They have several advantages over the conventional terrestrial methods (see Chapter 4).

Geodetic surveys with optical and electromagnetic instruments (including GPS) are always contaminated by atmospheric (tropospheric and ionospheric) refraction which limits their positioning accuracy to about  $\pm 1$  ppm to  $\pm 2$  ppm (at the standard deviation level) of the distance. For instance, with the average distance between the object and reference points of 500 m, the absolute displacements of the object points cannot be determined with an accuracy better than about  $\pm 2$  mm at the 95% probability (USACE, 1994). However, the high precision electro-optical geodetic instruments for EDM, with

accuracies of about  $\pm 0.3$  mm over short distances, may be more suitable for relative deformation surveys. Similarly, geodetic levelling with achievable accuracies of better than  $\pm 0.1$  mm over 20m distances will provide better accuracy for tilt determination ( $\pm 1$  second of arc). New developments in three-dimensional coordinate systems with electronic theodolites can provide relative positioning to an accuracy of  $\pm 0.05$ mm over distances of several metres. The same applies to photogrammetric techniques with CCD (charge couple device) sensors.

The advent of the GPS technology has facilitated automated structural monitoring with real-time direct precise position information (3D coordinates or baseline components). With the advantages of the GPS technology and other new sensor technologies, in addition to the current advances in desktop computational flexibility, the possibilities of automated intelligent signal processing and health monitoring systems are today within reach. Numerous feasibility studies have confirmed that GPS-based hardware and software monitoring systems can play a role in monitoring manmade structures. However, for such purposes, the GPS technology also has some limitations if used in isolation from other sensors. Consequently, some studies have recently identified the complementary benefits of integrating GPS positioning with additional sensors. For example, Roberts et al. (2000) have carried out a series of tests of an integrated GPS/accelerometer system. Their work showed that the integration of the two sensor sub-systems is possible, and that it results in a system that addresses the shortcomings of each sub-system, in addition to providing higher levels of quality control.

### **2.3 Non-GPS Methods**

A full review of all the traditional non-GPS methods (and instruments) available for structural deformation monitoring would far exceed the scope of this thesis. The material in this section is limited only to some comments on the basic types of terrestrial surveying techniques with electronic instrumentation for distance, height difference and angle measurements, photogrammetric techniques, geotechnical techniques for the measurements of tilt, inclination, changes in distance/strain, and other non-GPS displacement determination techniques (e.g., interferometers and optical fibre sensors).

In general, the instruments for measuring deformations can be grouped in the categories listed in Table 2.1 (see, e.g. Dunicliff, 1988, 1993).

### **2.3.1 Surveying Methods**

Surveying methods are applicable for monitoring the magnitude and rate of horizontal and vertical deformation of accessible parts of structures, normally over a period of time. In most circumstances, they are adequate for monitoring over long periods of time. It only becomes necessary to use geotechnical instruments if greater accuracy is required, or if the measuring points are inaccessible to the surveying methods (Ibid, 1988). The following section will introduce the categories of surveying methods, as applicable to structural monitoring. The textbooks that can be consulted for more details include Bannister et al. (1998), Brinker & Minnick (1995), Kavanagh (2001), Moffitt & Bossler (1998), Murchison (1977), Perrott (1970), Rueger (1996), and Uren & Price (1994).

#### **2.3.1.1 Electronic Distance and Angle Measurements**

Theodolites are mostly used to carry out traversing and triangulation surveys, in which distances and angles are measured to determine change in lateral position. Electronic theodolites with automatic digital and electronic data collectors have superseded the labour intensive methods of making and recording distance and angle measurements.

However, as far as accuracy is concerned, electronic theodolites have not brought about any drastic improvements in effectiveness in comparison to precision theodolite systems (USACE, 1994). Most precision electronic theodolites are equipped with sensors for the automatic sensing of mislevelment, and can automatically correct both vertical and horizontal readouts, while mislevelment in optical theodolites is controlled by a spirit level.



Table 2.1. *Non-GPS instruments for measuring deformation (Dunnicliff, 1988)*

Instrument category	Type of measured deformation					
	↔	↕	↗↘	↻	—•	—•
<b>SURVEYING INSTRUMENTS</b>						
Optical and electronic theodolites	✓	✓	✓			✓
EDM	✓	✓	✓			✓
Total stations and survey robots	✓	✓	✓			✓
Optical, digital and laser beam levels		✓				✓
Photogrammetric and CCD cameras	✓	✓	✓			✓
<b>GEOTECHNICAL INSTRUMENTS</b>						
Extensometers	✓	✓	✓			✓
Tiltmeters				✓	✓	✓
Inclinometers	✓	✓	✓	✓		✓
Transverse deformation gauges	✓	✓	✓			✓
Liquid level gauges		✓				✓
Miscellaneous deformation gauges	✓	✓	✓		✓	✓
<b>OTHER NON-GPS INSTRUMENTS</b>						
Laser interferometers, optical fibre sensors, etc.	✓	✓	✓			
Key: ↔ horizontal deformation ↗↘ axial deformation —• surface deformation ↕ vertical deformation ↻ rotational deformation —• subsurface deformation						

Three-dimensional coordinating systems consisting of two or more electronic theodolites that are linked to a microcomputer can be used for on-line calculation of point coordinates (Ibid, 1994). Such systems can be used for high precision monitoring over small areas (over ranges of tens of metres in industrial-type environments).

EDMs are used for accurate measurement of distances, either for direct determination of distance change or for the determination of lateral position change by trilateration. EDM equipment uses the velocity of electromagnetic radiation to measure the distance between the instrument and a reflector prism at the measuring point. The Mekometer, an

older model developed in England in the 1960s, with an accuracy of  $\pm 0.3$  mm over a 3km range, has been used for monitoring movements of dams (Dunicliff, 1988). The USACE manual EM 1110-1-1004 (1994) describes the operating principle of precision EDM and discusses its usefulness in structural deformation monitoring.

A total surveying station (i.e, electronic theodolite integrated with EDM, and linked to a computer) permits the simultaneous measurement of distance, horizontal direction and vertical angle, from which relative horizontal and vertical positions of the observed points can be determined directly in the field. For continuous (or frequent) deformation monitoring, computerised and motorised total stations can be programmed for sequential self-pointing to a set of prism targets, at predetermined time intervals, measuring distances, horizontal and vertical angles, and transmitting the data to an office location via a telemetry link (e.g., Booth, 2002a, 2002b; Kahmen, 1994; Katowski, 1995, 1996). Information on such systems are available at the homepages of manufacturers, for example, [www.leica-geosystems.com](http://www.leica-geosystems.com), [www.surveysupplies.co.uk](http://www.surveysupplies.co.uk), [www.pentax.co.uk](http://www.pentax.co.uk), [www.sokkia.com](http://www.sokkia.com), [www.topcon.co.uk](http://www.topcon.co.uk), and [www.trimble.com](http://www.trimble.com).

### 2.3.1.2 Levelling and Trigonometric Heighting

Levelling techniques are used to determine the height difference between an instrument station and the target point. Geometric (or optical) levelling with horizontal lines of sight (using spirit or compensated levels) is slow, but reliable and accurate. On the other hand, digital levels with automatic height and distance readouts from encoded levelling rods increases the levelling speed. High precision "total stations" (integrated electronic theodolites and EDMs) can be used for trigonometric height difference measurement. Trigonometric levelling uses EDM to determine the slope distance from the instrument to a prism placed at the measuring point. The height difference is calculated from the measured slope distance and the vertical angle (between the sloping line and a horizontal plane). Trigonometric levelling is more economical than optical techniques, and is particularly useful when measuring to points which are physically inaccessible. Laser beam levels can be used for alignment measurements and levelling, for example, in dam deformation monitoring. When the atmospheric refraction is low, high

accuracies can be achieved over short distances. For instance, accuracies of 0.2-0.3mm over 200m have been reported by Jian et al. (1996).

### **2.3.1.3 Photogrammetric Methods**

Terrestrial photogrammetric methods can be used to monitor engineering structures (aerial photogrammetric techniques are extensively used for determining ground subsidence in mining areas). The main advantages being reduced time of fieldwork, simultaneous provision of three-dimensional coordinates, and an unlimited number of points can be monitored (e.g., Mikhail et al., 2001).

The principle is based on taking overlapping photographs of an object from one or two fixed stations with known coordinates and with a known relative orientation of the camera(s). Relative position coordinates of points identifiable on the photograph of the object surface can then be determined from the geometrical relationship between the intersecting optical rays which connect the image and object points, a procedure similar to triangulation. Phototheodolites (cameras integrated with theodolites) and stereocameras (two cameras mounted on a bar of known length) use this principle. They can be employed to determine the relative movements of points over time (Lichti & Chapman, 1996; Obidowski & Teskey, 1996).

According to the USACE manual EM 1110-1-1004, using a camera with, for instance, a focal length of 100 mm at a distance of 100 m, with assumed accuracy of the image coordinates of 10  $\mu\text{m}$ , coordinates of the object points can be determined with an accuracy of 10 mm.

Solid-state cameras based on CCD sensors have also become available for close-range terrestrial photogrammetry, for static as well as dynamic applications (Fraser, 1996). Continuous monitoring with real-time photogrammetry is possible with the latest developments in the CCD cameras and digital image processing techniques.

## 2.3.2 Geotechnical Measurement Techniques

### 2.3.2.1 Extension and Strain Measurements

Extensometers, also referred to as strain-meters, convergence-meters or fissure-meters depending on the application, are mechanical or electro-mechanical devices used for monitoring changes in the distance between two points on the surface of a structure (or ground) (Dunicliff, 1988; 1993). The various instruments differ from each other by the method of "linking" the points between which the change in the distance is to be determined, and the kind of sensor employed to measure the change. The sensors are usually mechanical, but can be adapted to automatic and continuous data recording by using electronic transducers. They, for example, include dial gauges, wire and tape extensometers, and sometimes precision EDMs when used over short distances may also be employed as extensometers.

Strainmeters or jointmeters are used for monitoring tension in the body of the structure, or between joints in the structure. If an extensometer is installed inside the body of a structure with a homogeneous strain field, then the measured change  $\Delta l$  of the distance  $l$  gives directly the strain component  $\Delta l/l$  in the direction of the measurements. In order to determine the total strain tensor in a plane (two normal strains and one shearing), a minimum of three extensometers must be installed in three different directions. Precise wire extensometers, if properly calibrated, can give accuracies of 0.05 mm or better in measuring changes over 1–20 m length distances (USACE, 1994). The accuracies of other types include: special high precision strainmeters for shorter distances (up to a few decimetres) with relative precision of one microstrain ( $10^{-6}$ ). This corresponds to 0.15 $\mu$ m relative displacements over 150 mm; and torpedo extensometers with typical accuracies of 0.1 mm to 0.5 mm over a total length of up to 200 m (usually in segments of 3 m to 6 m). In general, however, the actual accuracy depends on the quality of the temperature corrections that are applied and the care with which the installation has been carried out.

### 2.3.2.2 Tilt and Inclination Measurements

Tiltmeters (or inclinometers) are used to monitor the change in the tilt or inclination (rotation) of points on a structure. They consist of a gravity-sensing transducer within an appropriate housing, for installation either on or below the surface of the structure. Applications include monitoring of the tilt of retaining walls, dams, and very precise tiltmeters can sometimes be used over short time periods to provide indication of deformation trends due to earthtides and other geodetic or seismic events. This makes them very suitable for monitoring the safety of buildings alongside excavations, to provide forewarning of distress where, for instance, a rotational deformation is expected. Deformation profiles of tall structures may be determined by placing a series of tiltmeters at different levels of the structure.

The tiltmeter instruments that are available today include pendulum-type tiltmeters, accelerometer transducer tiltmeters, vibrating wire tiltmeters, and electrolyte level transducer tiltmeters. For the servo-accelerometer tiltmeters (small horizontal pendulum-type), the output signal (volts) is proportional to the sine of the angle of tilt. The angular resolution depends on the tilt range of the tiltmeter, with the typical output voltage range being  $\pm 5$  V, corresponding to the maximum range of the tilt. Tiltmeters may be either fixed-in-place or portable.

Factors that affect the accuracy of tilt sensing include temperature changes affecting the mechanical parts, changes to the properties of the damping oil in the pendulum tiltmeters, and drifts of tilt indications and fluctuations of the readout.

### 2.3.3 Other Non-GPS Techniques

There are a range of other displacement measurement sensors and techniques that can be applied to structural monitoring. A complete list cannot be provided in this thesis. Some of the more common include:

- 1) Accelerometers. These are devices for measuring the rate of change of velocity (acceleration) of a point. Hence measurements require double integration to arrive at displacement values. Several reports of studies on structural monitoring with such devices can be found in the literature (e.g., Brownjohn & Ang, 1998; Brownjohn & Pan, 2001; Brownjohn et al., 1998; Kahmen et al., 1994; Tao & Brownjohn, 1998, etc.).
- 2) Laser interferometers. These can determine precise interferometric distances by using monochromatic radiation, and optical fibre sensors (a comparatively new technology) where changes in length of the optical fibre are sensed electro-optically.
- 3) Dynamic pressure transducers. They compare the measured pressure with the atmospheric pressure. Dynamic pressure transducer falls in the class of displacement transducers.

Temperature measurements may be necessary when temperature itself is the parameter of interest (e.g., for correlation), or where temperature causes deformation or stress, or where a transducer is sensitive to temperature (or its changes). Temperature transducers (thermometers, thermistors, thermocouples, etc.) should be placed at locations on the structure, or at least as close as possible to the structure.

In the case of monitoring the dynamics of tall or long structures, wind transducers such as anemometers may be used to measure the wind velocities and direction(s) in several directions. Many integrated real-time structural health monitoring systems incorporate wind transducers (e.g., Aktan, 2000).

#### **2.3.4 Advantages and Limitations**

From the point of view of achievable instrument accuracy, there is no clear distinction between the majority of surveying and geotechnical methods. Tables 2.2 and 2.3 give a summary of some of the major advantages and limitations of the traditional surveying methods, and the geotechnical and other non-GPS methods. In general, as far as the

non-GPS methods are concerned, other limiting factors, mainly a result of environmental and human influences, can be enumerated:

- They are limited in range and do not provide absolute position.
- Temperature influences may affect the mechanical, electronic or optical components of the instruments.
- Majority of the methods, whether requiring manual handling or automated, are influenced by the prevailing weather conditions.
- Most surveying methods are labour intensive, and are prone to human error.
- Station intervisibility is required, reducing the flexibility in selecting the monitoring points.
- Most survey measurements must be made during the day, and sometimes require near-perfect visibility conditions.
- Even though some of the methods (both surveying and geotechnical) can capture dynamic events, direct measurements may not be available in real-time during the actual event, for instance, during wind/earthquake loading. Moreover, in such circumstances, both the reference point(s) and the monitoring point(s) may be simultaneously affected.
- Though highly accurate, geotechnical sensors can typically only measure one-dimensional deformation. This makes it difficult to extract three-dimensional motions in the horizontal and vertical planes, and hence they may be unable to detect certain modes of deformation.
- Sensors must be installed, maintained and frequently recalibrated.

Table 2.2. *Non-GPS surveying methods*

Method	Advantages	Limitations	Approx. Accuracy
<i>Distance and angle measurement methods</i>			
Distance measurements by taping (now largely superseded by EDM)	Direct measurement of distances where theodolites, EDMs, and total stations are not available.	Requires clear accessibility between the reference and measured points. Requires calibration.	3 <sup>rd</sup> order: $\pm \frac{1}{6,000}$ of distance 2 <sup>nd</sup> order: $\pm \frac{1}{50,000}$ of dist. 1 <sup>st</sup> order: $\pm \frac{1}{300,000}$ of dist.
Traversing	Applied when direct measurements are not possible.	Accuracy decreases as the no. of legs in the traverse increases.	$\pm \frac{1}{30,000} - \frac{1}{150,000}$ of distance
Triangulation	Applied when direct measurements are not possible.	Requires accurate angles and baselines. Very slow compared to trilateration by EDM.	$\pm \frac{1}{30,000} - \frac{1}{1,000,000}$ of distance
Electronic distance and angle measurements	Long range, fast and convenient, highly accurate.	Accuracy influenced by atmospheric conditions.	For distance: ( $\pm 0.3-10$ mm) $\pm 2-5$ ppm. Lateral position change by trilateration: ( $\pm 2-10$ mm) $\pm 2-5$ ppm.
<i>Levelling methods</i>			
Optical levelling	Fast with self-levelling instruments.	Requires high-grade equipment and careful adherence to observational procedures.	3 <sup>rd</sup> order: $\pm 12 \text{ mm} \times \sqrt{\text{km}}$ 2 <sup>nd</sup> order: $\pm 6-8 \text{ mm} \times \sqrt{\text{km}}$ 1 <sup>st</sup> order: $\pm 3-5 \text{ mm} \times \sqrt{\text{km}}$
Laser beam levelling	Faster than optical methods, readings can be made by one person.	Affected by air turbulence, humidity and temperature differential. Requires curvature and refraction correction beyond 200m.	$\pm 3-10$ mm
Trigonometric levelling	Long range, fast and convenient, can be done simultaneously with traversing.	Accuracy influenced by atmospheric conditions. Requires very accurate measurement of vertical angle.	3 <sup>rd</sup> order: $\pm 12 \text{ mm} \times \sqrt{\text{km}}$ 2 <sup>nd</sup> order: $\pm 6-8 \text{ mm} \times \sqrt{\text{km}}$
<i>Photogrammetric methods</i>			
Photogrammetric techniques	Can record movements of many points at one time for determination of overall deformation.	Requires skilled interpretation. For good accuracy the baseline should not be less than 1/5 of the sighting distance.	$\pm \frac{1}{5,000} - \frac{1}{100,000}$ of distance



Table 2.3. *Geotechnical and other instrument methods*

Method	Advantages	Limitations	Approx. Accuracy
<i>Extension and strain measurement techniques</i>			
Extensometers	Mostly inexpensive. Highly accurate.	Span limited. Errors due to temperature and electrical connections are possible.	$\pm 0.003$ – $0.5$ mm
<i>Tilt and inclination measurement techniques</i>			
Tiltmeters	Highly accurate.	Temperature changes may affect mechanical parts. Drifts may occur.	$\pm 0.03$ – $5$ mm
Inclinometers	Highly accurate.	Temperature changes may affect mechanical parts. Drifts may occur.	$\pm 0.03$ – $5$ mm
<i>Other Techniques: accelerometers, laser Interferometry, etc.</i>			
Accelerometers	Very accurate. Large frequency bandwidth. Can operate at very low temperatures. Orthogonal measurements (bi- or tri-axial).	Requires double integration to arrive at the displacement values, hence cannot offer direct measurements. Drifts may occur.	$\pm 0.03$ – $0.5$ ms <sup>-2</sup>
Laser interferometers	Very accurate.	Requires stable temperature and pressure corrections.	Up to $1$ $\mu$ m per m

## 2.4 Recent Activities

The development of techniques and instrumentation for structural monitoring, including new methods for deformation analysis and modelling, has been the focus for many individual researchers, organisations and professional groups. For example, among the many active international organizations concerned with deformation studies are:

- International Federation of Surveyors (FIG), whose Study Group 6C (FIG SG6C) has made significant contributions to the development of new methods and concepts for the design, modelling and analysis of integrated deformation

surveys. For instance, several topics on the latest developments in relation to deformation measurements were recently addressed by the 19-22 March 2001, "10<sup>th</sup> FIG International Symposium on Deformation Measurements", held in Orange, California. In particular, contributions to non-GPS methods of structural deformation measurement included those by Breumso (2001), Garcia & Orteu (2001), Gordon et al. (2001), Kayser & Schwarb (2001), Paxton (2001), Pretorius et al. (2001), Proszynski & Stanczyk (2001), Radovanovic & Teskey (2001), Szostak-Chrzanowski et al. (2001), Tsan-wing & Kin-wah (2001), and many others.

- International Association of Geodesy (IAG) Special Commission IV (IAG SC4) which organises international symposia on studies related to geodynamic processes and structural deformation. In 2001, the first IAG SC4 workshop was held in Wuhan (China) on "Monitoring of Constructions and Local Geodynamic Processes". Topics presented at this workshop included those related to non-GPS techniques for structural monitoring (see, e.g., Lam & Tang, 2001; Mentis & Fabian, 2001a; 2001b). A follow-up IAG SC4 symposium on "Geodesy for Geotechnical and Structural Engineering" was held in Berlin, Germany, during 21-24 May 2002.
- International Association for Bridge and Structural Engineering (IABSE) has an active Working Commission 1 (IABSE WC1), which provides a forum for discussion of problems related to structural performance and safety. The IABSE WC1 deals with structural performance under various conditions (both manmade and natural), the methodologies of structural analysis, assessment of design loads, material properties, structural resistance, and problems related to structural safety and serviceability, for buildings, bridges and other civil engineering structures (<http://www.iabse.ethz.ch/>). The IABSE WC1 is responsible for many symposia, journal publications and technical reports on structural monitoring (see, e.g., Gentile, et al., 2001; Hearn, 1998; Kashima et al., 2001; and others).

Since 1975 the FIG SG6C has been the most active group dealing with practically all aspects of deformation monitoring and analysis (USACE, 1994), and has organised ten international symposia, with the eleventh one planned for Greece, in May 2003. Although originally biased toward the development of geodetic surveying monitoring techniques, new concepts for integrated monitoring systems (e.g. integration of geodetic and geotechnical measurements) and other sensory systems have also been developed (see, e.g., Kahmen et al., 1994; Kahmen, 1994; 1996; Katowski, 1995, 1996; Dale, 1996; Setan & Nyet, 2001).

Various other national and international professional groups such as the Australian National Committee on Large Dams (ANCOLD, 1994), the International Commission on Large Dams (ICOLD) and the U.S. Society on Dams (USSD), are involved in dam deformation studies and the development of structural monitoring guidelines. The USSD has, for example, organised the 3<sup>rd</sup> U.S.-Japan Workshop on "Advanced Research on Earthquake Engineering for Dams", to be held in San Diego, in June 2002. This workshop will address instrumentation, monitoring and condition assessment as one of its main themes.

### **3.1 Introduction**

GPS is a satellite-based radio-positioning and time-transfer system developed by the U.S. Department of Defense to support real-time navigation anywhere on the Earth (Parkinson & Spilker, 1996). The system has the advantage of being globally accessible, functioning independent of the local weather conditions, and being able to provide three-dimensional position, velocity and time in a common reference system, anywhere on or near the surface of the Earth, on a continuous basis.

The GPS system consists of three segments, namely the Space Segment, the Control Segment and the User Segment.

The Space Segment nominally comprises 24 satellites, deployed in six circular orbital planes of about 20,200 km altitude above the Earth's surface, with an orbital inclination of 55 degrees. There are four satellites in each orbital plane. The constellation design is such that at least four satellites are simultaneously visible above the horizon anywhere on the Earth, 24 hours a day.

The Control Segment consists of the ground facilities carrying out the task of satellite tracking, orbit computations, telemetry and supervision necessary for the continuous operation of the Space Segment. There are five ground facility stations located around the world, owned and operated by the U.S. Department of Defense, which primarily functions as tracking stations. The Master Control Station is located in Colorado Springs, and the processing of the tracking data in order to generate the satellite orbits and satellite clock corrections is performed at this station. Three of the ground facility stations, located at Ascension Island, Diego Garcia and Kwajalein, are also upload stations that uplink data to the GPS satellites.

The User Segment is the entire spectrum of applications equipment and computational techniques that are available to both the military and civilian users. The military research and development programs have concentrated on accomplishing a high degree of miniaturisation, modularisation and reliability, while the civilian user equipment manufacturers have, in addition, sought to bring down costs and to develop features that enhance the capabilities of the positioning system.

Each GPS satellite continuously transmits a unique navigational signal centred on two L-band frequencies, L1 at 1575.42 MHz and L2 at 1227.60 MHz (Spilker, 1978). The signals basically consist of three main components, the two L-band carrier waves, the navigation message and the ranging codes. Each satellite's navigation message contains information about its orbit (or ephemeris), the satellite clock model, satellite status, and other pieces of information. The ranging codes and the navigation message are modulated on the carrier waves. The Coarse/Acquisition code (C/A-code) is modulated only on the L1 carrier, while the Precise code (P-code) is modulated on both the L1 and L2 carriers. The P-code has higher measurement resolution and therefore allows more precise code measurements than the C/A-code.

More details on the GPS system can be found in any of a number of GPS textbooks, see, e.g., Hofmann-Wellenhof et al. (2001); Leick (1995); Parkinson (1994); Parkinson & Spilker (1996); Rizos (1997); Seeber (1993).

### 3.2 GPS Positioning Modes

The two fundamental GPS measurements for position determination are the *pseudorange* and *carrier phase* observations. The basic observation equations for these measurements are (e.g., Lachapelle et al., 1992; Langley, 1993):

$$P_r^s = \rho_r^s + d\rho^s + c(dt^s - dT_r) + d_{\text{ion}}^s + d_{\text{trop}}^s + \varepsilon(p_{\text{rx}}) + \varepsilon(p_{\text{mult}})_r^s \quad (3.1)$$

$$\Phi_r^s = \rho_r^s + d\rho^s + c(dt^s - dT_r) + \lambda N_r^s - d_{\text{ion}}^s + d_{\text{trop}}^s + \varepsilon(\Phi_{\text{rx}}) + \varepsilon(\Phi_{\text{mult}})_r^s \quad (3.2)$$

where

$P_r^s$	is the pseudorange measurement by the GPS receiver to the satellite (m)
$\rho_r^s$	is true range or "geometric" range (m)
$d\rho^s$	is the orbit error term (m)
$dt^s$	is the satellite clock error (m)
$dT_r$	is the receiver clock error (m)
$d_{\text{ion}}^s$	is the ionospheric delay term (m)
$d_{\text{trop}}^s$	is the tropospheric delay term (m)
$\varepsilon(p_{rx})$	is the error in pseudorange measurement due to receiver noise (m)
$\varepsilon(p_{\text{mult}})_r^s$	is the error in pseudorange measurement due to multipath (m)
$c$	is the speed of light ( $\text{ms}^{-1}$ )
$\Phi_r^s$	is the carrier phase measurement by the GPS receiver to the satellite (m)
$N_r^s$	is the carrier phase ambiguity between the GPS receiver and the satellite (cycles)
$\lambda$	is the wavelength of the carrier phase (m)
$\varepsilon(\Phi_{rx})$	is the error in carrier phase measurement due to receiver noise (m)
$\varepsilon(\Phi_{\text{mult}})_r^s$	is the error in carrier phase measurement due to multipath (m)

The true range, or geometric range, from the receiver to the satellite (Figure 3.1), can be represented in terms of the World Geodetic System 1984 (WGS-84) coordinates:

$$\rho_r^s = |\mathbf{r}^s - \mathbf{r}_r| = \sqrt{(x^s - x_r)^2 + (y^s - y_r)^2 + (z^s - z_r)^2} \quad (3.3)$$

where

$\rho_r^s$	is the geometric range from the receiver to the satellite (m)
$\mathbf{r}^s$	is the satellite position vector referenced to the WGS-84 (m)

- $\mathbf{r}_r$  is the receiver position vector referenced to the WGS-84 (m)  
 $x^s, y^s, z^s$  are the satellite WGS-84 coordinates  
 $x_r, y_r, z_r$  are the receiver WGS-84 coordinates

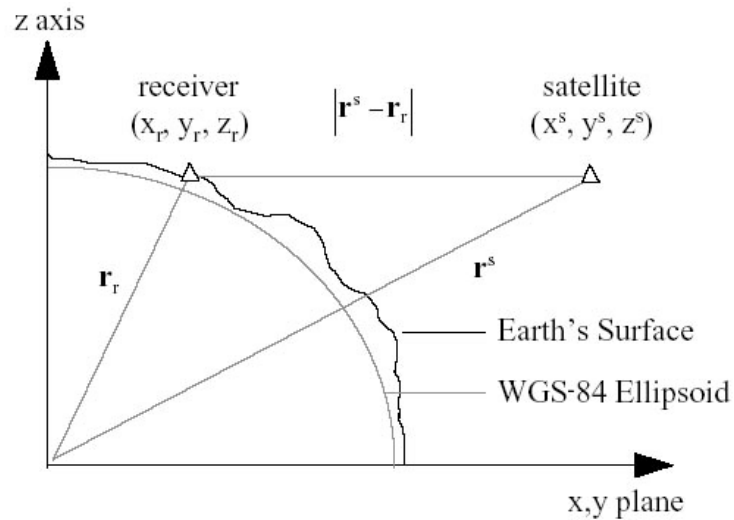


Figure 3.1. *Geometric range from a receiver to a satellite*

Notice the similarity between Equation (3.1) and Equation (3.2), the major differences being the presence of the integer carrier phase ambiguity term ( $\lambda N_r^s$ ) in the carrier phase measurements, and the reversal of sign for the ionospheric bias term ( $d_{\text{ion}}^s$ ).

The level of carrier phase measurement noise (at the mm level) is much lower than the level of the pseudorange measurement noise (typically at the metre level). The inability of civilian users to access the P-code pseudorange measurements (under the policy of Anti-Spoofing) reduces the accuracy of GPS pseudorange positions. Therefore, pseudorange measurements are generally used in applications where the accuracy requirement is not high (few metre level), as is typical for single-epoch navigation applications. On the other hand, carrier phase measurements are extensively used in precise (cm level) GPS surveying applications.

### 3.2.1 Point Positioning

If one receiver is used to determine the absolute coordinates of any point on Earth, with respect to the reference frame WGS-84, the positioning technique is known as *single point positioning (SPP)*. This technique can be further divided into two classes depending on the measurements used, namely *pseudorange-based point positioning* and *carrier phase-based point positioning*.

In the pseudorange-based point positioning mode, the basic principle is to use resection by distances to determine the receiver's coordinates. If the satellite coordinates are assumed to be known (as they are provided to the user within the navigation message), the receiver's coordinates can be computed from the resection using the measured pseudoranges. The accuracy of this the pseudorange-based SPP is currently about 7 metres in the horizontal component and 12 metres in the vertical component (at the 95% confidence level) for civilian users.

Due to the availability of precise GPS orbits and satellite clock corrections, precise carrier-phase based SPP has recently been proposed by the Jet Propulsion Laboratory (Zumberge et al., 1997; Zumberge, 1999). This technique mainly uses the carrier phase measurements from both frequencies (L1 and L2), with the post-mission information in the estimation procedure, producing high-precision positioning results. Nevertheless, it requires a reasonably large amount of data, implying that *instantaneous* solutions are not yet possible, and currently can only be used when the receiver is stationary.

### 3.2.2 Relative Positioning

In the relative positioning method, sometimes also referred to as *differential positioning*, two GPS receivers are used to observe the same satellites simultaneously. One receiver, designated as "the base", is set up at a reference station whose coordinates are known. The other receiver, designated as "the rover", is used to determine its coordinates with respect to the reference station. In this case, by subtracting the observations at the reference station from those at the rover, the *single-difference* equations are derived



from Equations (3.1) and (3.2). This technique reduces many of the systematic biases (e.g. satellite orbit bias, satellite clock error, ionospheric and tropospheric delays), and is extensively used in data processing schemes for applications requiring centimetre-level accuracy. However, the effectiveness of the relative positioning technique is largely dependent on the distance between the two receivers. The residual error increases as the distance between the receivers increases.

Relative positioning can further be divided into two classes depending on the measurements used, namely *pseudorange-based differential positioning* and *carrier phase-based differential positioning*.

The pseudorange-based differential positioning method is commonly referred to as Differential GPS (DGPS). The estimation of the range error for each satellite is carried out at the reference station. The estimated range errors (or corrections to the measurements) are broadcast to the users by an appropriate communication link (Parkinson & Enge, 1996). For operations over a small area one reference station is typically used, and the technique is generally referred to as *Local Area Differential GPS* (LADGPS). However, if a network of reference stations is employed to generate the range corrections for each satellite, the correction data model is valid over a much larger area, and the technique is referred to as *Wide Area Differential GPS* (WADGPS). Finally, in a case where the geostationary satellites transmit to users the DGPS corrections for each satellite, together with additional GPS-like ranging signals and an integrity message, the concept is known as *Wide Area Augmentation System* (WAAS). Detailed explanations of these DGPS techniques can be found in Enge & Van Dierendonck (1996).

Carrier phase-based differential positioning is realised by either differencing the carrier-phase measurements made to the same satellite by two receivers, at the same time, or differencing the carrier-phase measurements to two satellites made by the same receiver, at the same time. The former method is referred to as *single-differencing between receivers* while the latter is referred to as *single-differencing between satellites*. If the difference between the single-differenced observations is formed, a process

referred to as *double-differencing*, the resultant double-differenced observable is the standard input for carrier phase-based data processing.

Carrier phase-based differential positioning can be carried out in static or kinematic mode. If carried out in kinematic mode, the technique is referred to as *kinematic positioning*, implying that either (or both) the reference and user receivers are in motion (Remondi, 1985). Today, with advanced receiver technology and improved data processing algorithms, it is possible to obtain high precision results (sub-cm) in "real-time" using the "real-time kinematic" (RTK) GPS positioning method.

### 3.3 RTK-GPS Positioning

The RTK-GPS positioning concept is represented in Figure 3.2. RTK-GPS consists of a reference station and one or more rover station installations. The hardware requirements are identical at each station. The reference station is placed at a location with good sky visibility in order to minimise station-dependent errors that may be introduced due to signal obstructions or reflections. Raw pseudorange and carrier phase data, or their corrections to the GPS satellite ranges, are collected at the reference station, and transmitted to the rover station(s) via a communication link using either proprietary message formats or an industry standard format (RTCM, 1994). In the standard RTK configuration, the rover receiver combines this transmitted data with its own measurements in order to calculate its position in real-time (Langley, 1998; Talbot, 1993). When measurements from the two receivers are combined, correlated errors (such as satellite orbital errors, satellite clock errors, ionospheric and tropospheric errors -- Chapter 5) are significantly reduced. However, the spatial correlation of the errors is largely dependent on the inter-receiver distance. Beyond 10 or so kilometres the degree of decorrelation may be so high as to significantly impact on the baseline solution.

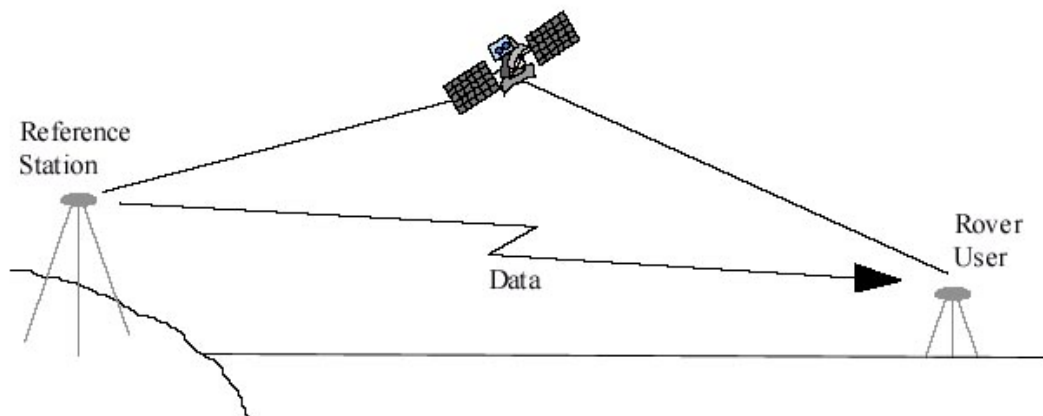


Figure 3.2. *The RTK-GPS concept*

In order to achieve high positioning accuracies (centimetre level or better) in real-time, the processing of double-differenced carrier phase measurements is carried out. In that case, the number of L1/L2 carrier cycles between the satellite and the reference and rover stations (the integer ambiguities) must be determined (Han, 1997; Han & Rizos, 1995, 1996, 1997a; Hatch & Euler, 1994). If the changing number of cycles is measured by the receiver, the problem is essentially one of determining the initial ambiguities at signal lock on. The basic approach to determining the integer ambiguities is to use the relatively noisy pseudorange measurements to define a volume which is assumed to contain the correct set of integer ambiguities. All possible integer ambiguity combinations are then tested to determine the best set, the test criterion often being the set that minimises the sum of squared carrier phase residuals. A ratio test is performed between the sum of squared carrier phase residuals of the "best" and "second best" sets, and if the ratio exceeds a certain threshold, then the "best" set is accepted for fixing the carrier phase ambiguities.

The double-differencing data processing strategy for a single epoch is illustrated in Figure 3.3. At each of the stations (reference and rover), the observations from the "base satellite" are subtracted from the observations to all other satellites at that epoch. The differences for the reference station are then subtracted from the differences at the rover station to create a "double-difference" observable.

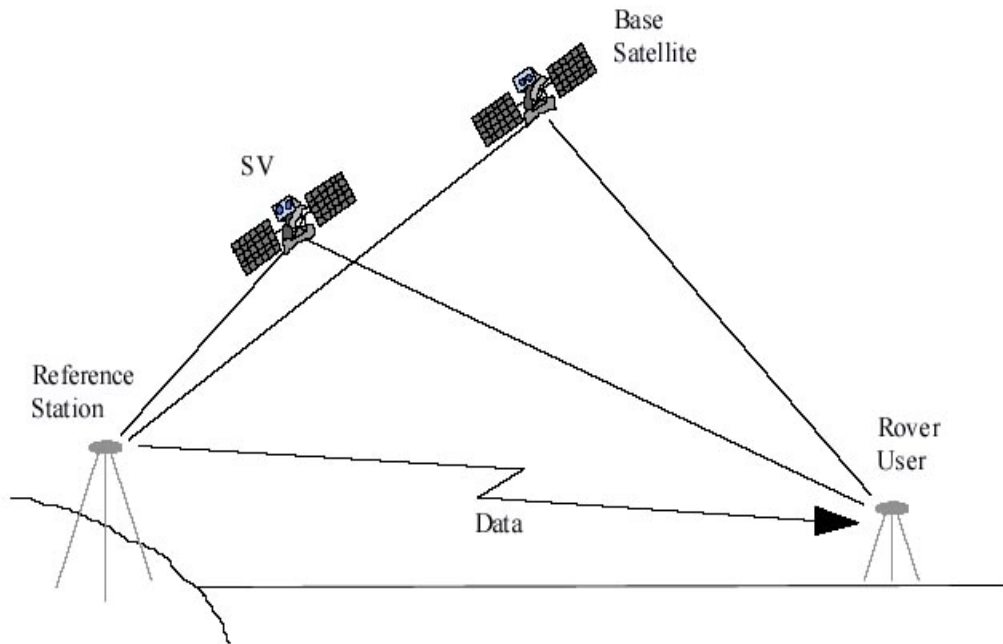


Figure 3.3. *Satellite-receiver double-difference ( $\Delta\nabla$ )*

The satellite-receiver double-difference is generally given as (Morley, 1997):

$$\Delta\nabla = \left\{ (\text{data})^{\text{sat}} \right\}_{\text{rem}} - \left\{ (\text{data})^{\text{base}} \right\}_{\text{rem}} - \left\{ (\text{data})^{\text{sat}} \right\}_{\text{ref}} + \left\{ (\text{data})^{\text{base}} \right\}_{\text{ref}} \quad (3.4)$$

where  $\Delta\nabla$  is the satellite-receiver double difference, the operator  $\Delta$  implies a between-receiver difference and  $\nabla$  implies a between-satellite difference

$(\text{data})^{\text{sat}}$  is the data from the satellite (other than the base satellite)

$(\text{data})^{\text{base}}$  is the data from the base satellite, and

$\left\{ \right\}_{\text{rem}}$  and  $\left\{ \right\}_{\text{ref}}$  are respectively the differenced data calculated by the rover station and the reference station.

The resulting satellite-receiver double-differenced phase observable is:

$$\Delta\nabla\Phi = \Delta\nabla\rho + \Delta\nabla d\rho + \lambda\Delta\nabla N - \Delta\nabla d_{\text{ion}} + \Delta\nabla d_{\text{trop}} + \varepsilon\Delta\nabla(\Phi_{\text{rx}}) + \varepsilon\Delta\nabla(\Phi_{\text{mult}}) \quad (3.5)$$

where the satellite and receiver clock error terms are eliminated, and the orbital and atmospheric effects are greatly reduced (and can be ignored), while the receiver noise

and multipath are slightly increased. In single epoch solution, using carrier phase data, accuracies in the range sub-cm to sub-dm can be obtained, depending on the baseline length and other factors (Hatch, 1986; Goad, 1987). Typical single epoch accuracy is  $\pm 1\text{--}2$  cm for the horizontal components and about  $\pm 2$  cm for the vertical component, for short baselines (typically  $< 10$  km). However, higher accuracies have been claimed with recent receiver technology and refined Kalman filter data processing procedures (Remondi & Brown, 2000; Rutledge et al. 2001).

**CHAPTER 4**

**GPS APPLICATIONS TO STRUCTURAL MONITORING**

---

---

#### **4.1 Introduction**

GPS surveying methods have several advantages over the conventional terrestrial methods described in Chapter 2. The advantages that the GPS technology can offer include the following:

- The need for intervisibility between the measuring stations is not necessary, and hence there is greater flexibility in the selection of station locations than is the case with the terrestrial methods.
- Measurements can be made at any time of the day or night, and in varying weather conditions.
- GPS can provide direct instantaneous 3-D displacement, and absolute position on a well-defined global reference frame (WGS-84), permitting near-real-time trend analysis. The connection to the WGS-84 frame makes it easier to assess how the structure might have moved with respect to the surrounding bedrock, for example, after a shock such as an earthquake.
- GPS has global coverage, and can be used at any location on the earth, making it suitable for remote automated monitoring.
- Although relative movements in the lateral and vertical directions are available from the integration of accelerometer data, only part of the movement vector (non-continuous) is available. GPS can function as an independent checking system.
- Obtainable accuracies of 1 cm (instantaneous) to 1 mm (with averaging), making GPS suitable for a variety of monitoring scenarios.
- GPS does not encounter sensor drifts that are common with accelerometers.

Though already widely used in many monitoring applications, GPS methods also have some limitations. For example, one has to be aware that although GPS does not require intervisibility between the observing stations, the receivers do require an unobstructed view to the satellites. This limits the use of GPS to reasonably open areas (unobstructed grounds, building rooftops, top surface of dam wall, bridge decks and towers, etc.). Secondly, the accuracy of GPS relative positioning depends on the distribution (spatial geometry) of the observed satellites in space with respect to the receiver, the data processing strategies and algorithms, and the modelling of the various error sources that contaminate the measurements (see, e.g., Parkinson & Spilker, 1996; Rizos, 1997). The common biases that affect GPS relative positioning are later discussed in Chapter 5.

Although accuracies provided by most GPS methods are less than those of the most precise terrestrial techniques, the RTK-GPS technique does provide sufficient accuracy for most long-term continuous monitoring applications.

As discussed in Chapter 2, there are different modes of structural deformation. These can be classified into two kinds. The first is the long-term slow movements due to water pressure, temperature differentials, or slow tectonic activities. The second kind is the short-term fast movements due to irregular wind, earthquake, or traffic loading. Fast deformations are generally much more important in terms of disaster mitigation and damage analyses, and are difficult to monitor with episodic static GPS observations. Slow displacements, thermal expansion/contraction or settlements occur over relatively long periods of time, and averaging times of GPS data of a few hours or more can be used to produce baseline solutions at, or near, the millimetre-level accuracy, to derive the deformation trend from repeated surveys. To measure fast deformations that occur over a time span of a few seconds, RTK-GPS with high sampling rates (up to 20 Hz), and little or no averaging is used. This restricts the utility of RTK-GPS in structural monitoring to the more flexible structures (suspension bridges, towers, tall buildings) where vehicular or wind effects cause movements of detectable magnitude ( $> 1$  cm) and frequency ( $< 10$  Hz) (Roberts et al., 2000).

When RTK-GPS is used to monitor a structure, one or more GPS rover antennas are usually attached to the structure of interest, while the reference station(s) is located at a

nearby site (perhaps a few kilometres away) with clear sky visibility (Figure 4.1). It should also be noted that if measurements are taken over short baselines, then the influence of the errors due to atmospheric effects is considered to be negligible. However, those errors due to signal obstructions by dense cables, crane towers or due to signal reflections by the bridge decks, building walls, or dam walls (i.e., multipath) are largely unavoidable, and must be carefully studied for the particular monitoring environment.

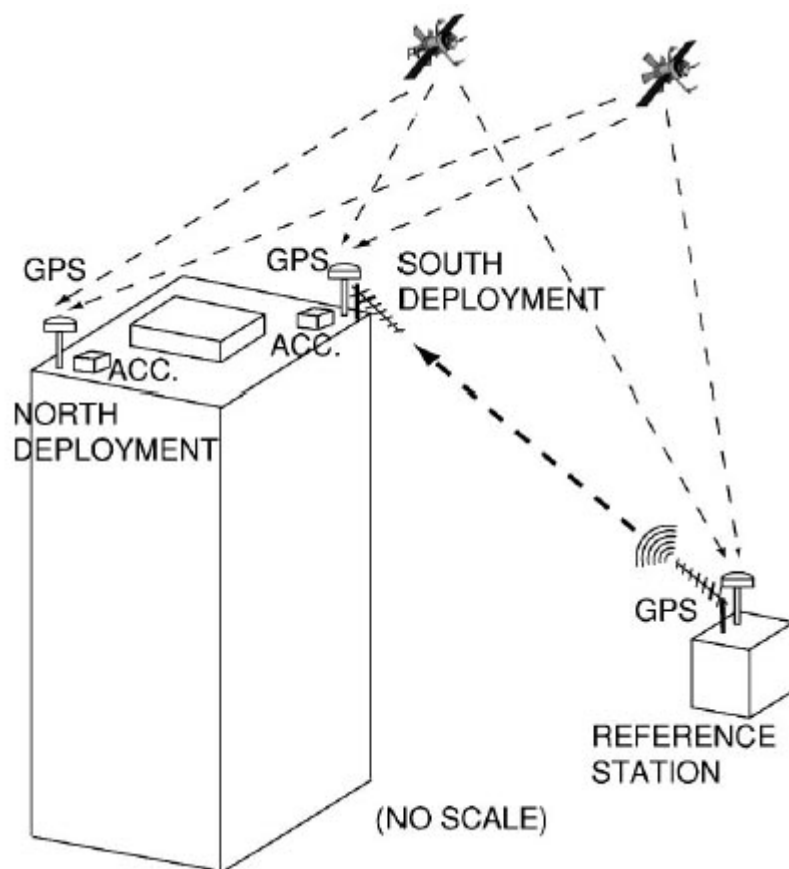


Figure 4.1. A schematic of GPS deployment on a structure (Celebi & Sanli, 2002)

The use of RTK-GPS at strategic points on a structure permits close monitoring of its behaviour through the analysis of absolute and relative measurements. Time-dependent displacements of critical points on the structure can be obtained. For example, in the case of a bridge, GPS receivers placed at suitable locations can indicate, in real-time, the amplitude of the displacements of the deck and towers, as well as movements of key



bridge elements relative to local reference points. Movements of the piers relative to the abutments, the top of a tower with respect to its base, or the span with respect to the ground, can be obtained with centimetre-level accuracy.

With its real-time capabilities, information provided by a RTK-GPS system deployed on a structure can be obtained without delay. The structural response can then be assessed according to different threshold displacements or changing dynamic characteristics, and such real-time monitoring can be used to warn of anomalous structural behaviour.

## 4.2 Slow Structural Deformation

The RTK-GPS surveying technique was introduced in the mid-1990s (see, e.g., Lowry & MacLeod, 1997; Kondo & Cannon, 1995), for a variety of monitoring applications. Prior to this, some limited studies on structural monitoring with GPS were carried out using static (receiver) observations, post-processed using commercial software available at the time. Such studies were therefore limited to detection of slow deformations, as expected on large structures such as dams. Hollmann & Welsch (1992), for example, describes one of such project in which a high precision dam monitoring network relied on static GPS observations. In their dam monitoring network example they proved that, for accuracy requirements of the order of a few millimetres, periodic static GPS observations could be used. A similar study is reported in DeLoach (1989).

Though RTK-GPS systems are not necessarily the appropriate technique for slow deformation structural monitoring, a number of dam deformation studies using RTK-based small scale, continuously-operating reference stations (CORS) are currently in progress (e.g., Duffy & Whitaker, 1999). For example, due to the high risk of earthquakes in the state of California, a number of dams are being monitored by both conventional means and continuously-operating GPS receiver arrays. Hudnut & Behr (1998) and Behr et al (1998) describe a continuous monitoring program for the Pacoima Dam located in Southern California. They have shown periodic (quarterly-daily) GPS baseline solutions from the 1996-1997 campaign, in which they used two GPS antennas installed on the dam, a reference antenna installed about 2.5 km from the dam site, and

three continuous monitoring stations (about 30 km away from the dam site) that form part of the Southern California Integrated GPS Network (SCIGN) (Hudnut et al., 2001).

In the Perth region of Western Australia, episodic GPS trials have been carried out alongside other techniques, including geotechnical instrumentation and conventional surveying (total stations and electronic levels), in order to monitor the North Dandalup Dam (Duckrell & Stewart, 1998; Stewart & Tsakiri, 2001). With the dam monitoring network consisting of some 40 points, geodetic quality receivers were used during each site survey, with two of the receivers situated on bedrock control points and the "roving" receiver visiting each monitoring point. The study proved that GPS technology had the potential for dam surface monitoring, when a large number of points are to be visited. However, the investigators have not offered an optimal solution in terms of attainable accuracies and mitigation of adverse factors for dam monitoring requirements. Stewart & Tsakiri (2001) have further discussed a related project on Harvey Dam, also located in Western Australia, for which a multi-antenna GPS array has been proposed. According to the authors, this project is meant to combine the best features of continuous and episodic GPS monitoring techniques, in order to produce an economical monitoring system.

Other reports of feasibility studies, and system developments, by various individuals and research institutions can be found, for example, in the proceedings of symposia organised by organizations such as FIG SG6C, IAG SC4 and IABSE WC1. Examples include Bock et al. (2001), Dale (1996), Duffy et al. (2001), and Qin et al. (2001).

### **4.3 Fast Structural Deformation**

More recently, due to the enhanced capability of GPS technology to provide high data sampling rates (up to 20Hz), there has been an increased interest in using RTK-GPS to measure fast structural deformations. Most of the reports available in the literature describe system trials on towers, tall buildings, and long suspension bridges.

The work by Lovse et al. (1995) is one of the earliest to use GPS technology for the dynamic monitoring of tall structures. They carried out a field trial to measure the vibrations of the Calgary Tower in Canada, a structure that is approximately 160m high. The researchers measured a single dominant frequency of 0.36Hz, with an amplitude of  $\pm 16$ mm, from their *post-mission* analysis of the movements caused by a 60–100km/h wind.

In China, Guo & Ge (1997) carried out a GPS experiment to measure the displacement and frequency signature of the 68-storey Diwang Tower (325m high) in the Shenzhen City, caused by a strong typhoon which measured 25 m/s. Using high quality GPS receivers they recorded data at a sample rate of 10Hz from 2:00 to 5:00 am on 9 September, 1996, over the period of the typhoon. A *post-mission* analysis of their data showed that it was possible to monitor the amplitude and frequency of deflections of a high-rise building using GPS measurements. Other reports of studies of GPS measurements of tall structures can be found in the literature (e.g, Aziz et al., 2001; Celebi et al., 1998; and others).

Ashkenazi et al. (1997) reports on real-time GPS tests that were carried out at strategic points on three different bridges in the United Kingdom, the Humber Bridge, the Nottingham Clifton Bridge and the Dee Bridge. Their trials demonstrated that RTK-GPS may be used to monitor the movements of large bridges. Since then other related studies have been carried out (e.g., Roberts et al., 1999), and the latest concern the integration of GPS with accelerometers (Roberts et al., 2000). More studies on suspension bridges have been carried out elsewhere. For example, in Australia, Watson & Coleman (1998) have monitored the dynamic movement of the Batman Bridge in Northern Tasmania using GPS. Nakamura (2000) reports on the RTK-GPS monitoring of a Japanese suspension bridge with a main span of 720m, and compares GPS results to the measurements of wind velocities and acceleration data.

Other reports can be found in the proceedings of symposia of FIG WG6C, IAG SC4 and IABSE WC1, and related journal articles (e.g., Ogaja et al., 2001a; Radovanovic & Teskey, 2001; Roberts et al., 2001; Schaal & Larocca, 2002; Shengxiang & Xianglin, 2001; and others).

#### 4.4 Commercial Off-the-Shelf RTK-Based Software Systems

The last few years have seen the development of commercial off-the-shelf RTK-GPS-based systems capable of continuous automated 3-D monitoring. Two examples include the 3-D Tracker software system developed by Condor Earth Technologies Inc. (<http://www.3d-gps.com/>), and the GPS-based On-line Control and Alarm (GOCA) software system developed by the University of Applied Sciences in Karlsruhe (Kälber et al., 2000).

The 3-D Tracker software, according to the developers, can simultaneously compute 3-D millimetre-level accuracy positions of dozens of GPS receivers deployed on dams, bridges, oil platforms, buildings and other large structures, and has been specifically designed for continuous operation. It can process data from single- or dual-frequency receivers, or a combination of both. It uses an approach slightly different from the standard RTK in which instead of raw data from reference station(s) and rover station(s) being processed at the rover(s), all data are processed at a centralised station. Both triple-differenced and double-differenced data are processed to provide epoch-by-epoch Kalman-filtered solutions.

The GOCA software has been designed to receive GPS baseline solutions from either single-frequency or dual-frequency GPS systems. In this system the raw data observed at the GPS base station(s) are transmitted to GPS rover station(s), where the baseline solutions are computed. The baseline solutions are then transmitted via radio modems back to the GOCA centre, where through subsequent network adjustment analysis, any motions of the receivers between the observation epochs are detected.

Most of the current operational RTK-based structural monitoring systems are based on commercial off-the-shelf software. Such GPS receiver array systems have been commissioned in many parts of the world. Among them is the *Wind and Structural Health Monitoring System* (WASHMS) for the Tsing Ma Bridge in Hong Kong, the world's longest span suspension bridge, which initially consisted of 774 sensors (of

seven major types: anemometers, temperature sensors, dynamic weigh-in-motion sensors, accelerometers, displacement transducers, level sensing stations, and strain gauges) and has now been upgraded to include an additional 29 GPS receivers for real-time displacement monitoring (Wong et al., 2001). Similarly, in Singapore a building monitoring system initially consisting of accelerometers and anemometers has been upgraded with a RTK-GPS system since November 2001 (Ogaja et al., 2001a; 2001b; 2001c). These two projects are briefly described in the following section.

#### **4.4.1 Operational RTK-Based Structural Monitoring Systems**

##### **4.4.1.1 Tsing Ma Suspension Bridge Monitoring**

The Tsing Ma Bridge has become internationally known engineering and a major Hong Kong landmark (Figure 4.2). Its construction commenced in May 1992, and it was completed in May 1997 (<http://crucial.ied.edu.hk/airport/tsingma.html>, [http://www.hyd.gov.hk/airport/mw\\_f.htm](http://www.hyd.gov.hk/airport/mw_f.htm)). It is part of the Lantau Link, which comprises the Tsing Ma suspension bridge, viaducts crossing Ma Wan and the Kap Shui Mun cable-stayed bridge.

The clear span of the 2.2km long Tsing Ma Bridge is 1377m, three times the length of the Sydney Harbour Bridge, and 97m longer than San Francisco's Golden Gate Bridge. "Officially opened in 27th April 1997, the Tsing Ma will rate an entry in the Guinness Book of Records as the world's longest suspension bridge for both rail and road traffic" (Leica Geosystems, 2002).



Figure 4.2. *Tsing Ma Suspension Bridge*

The WASHMS was designed at the early stages of the construction of the bridge to monitor its responses (Wong et al., 2001). At the initial design stage, measurement technologies such as infrared and laser were considered for displacement monitoring, but later on were dropped due to constraints such as limited visibility distances and inoperability in severe weather conditions. Level sensing stations were installed to monitor bridge deck displacements with measurement accuracy of approximately 2 millimetres. However, these instruments were only capable of measuring at vertical planes but could not measure the lateral and longitudinal displacements in the horizontal plane. High precision servo-type accelerometers were also installed to monitor local vertical, lateral and rotational accelerations, whose double integration could provide estimates of displacement.

"After trial tests in 1999 and 2000 demonstrated GPS applicability and the required accuracy level, the Hong Kong Highways Department decided to employ GPS with Real Time Kinematic (RTK) function to monitor displacements of the three cable-supported bridges (Kap Shui Mun Bridge (KSMB), Ting kau Bridge (TKB), Tsing Ma Bridge (TMB))" – *Ibid* (2001). Today, the GPS receiver array system at the Tsing Ma Bridge consists of two reference stations and 27 dual-frequency, carrier phase tracking rover receivers, collecting data at a 10Hz sampling rate. Referred to as "the real-time GPS On-Structure Instrumentation System (GPS-OSIS)", it monitors real-time motions of the main suspension cables, decks and bridge towers of KSMB, TKB and TMB, and operates along with the other WASHMS instrumentation systems to monitor overall bridge health. The "GPS-OSIS plays an important role in plotting wind speeds against

bridge motion since the GPS data can display the global motion over the full length of the bridge, which in the past could not be accurately obtained by accelerometers" – *Ibid* (2001).

#### 4.4.1.2 Republic Plaza Building Monitoring

In Singapore, traditional monitoring devices for measuring wind-induced excitation, including accelerometers and anemometers, were installed on the Republic Plaza (Figure 4.3) since 1996. To further the objective of monitoring the dynamic response characteristics of a tall building, a GPS system with RTK capability was incorporated to allow for a complete monitoring of displacements at up to 10 Hz ([http://www.gmat.unsw.edu.au/snap/work/singapore\\_rpb.htm](http://www.gmat.unsw.edu.au/snap/work/singapore_rpb.htm), <http://www.ntu.edu.sg/home/cjames/gps2.htm>).



Figure 4.3. *Republic Plaza Building (RPB)*

The existing instrumentation was upgraded to incorporate the new GPS component, as shown in Figure 4.4. The GPS component is composed of three main sub-systems:

- i) One reference station comprising a dual-frequency, geodetic GPS receiver installed at a nearby location, complete with mounting brackets, accessories and battery backup for operation for up to one day without power.
- ii) Two 'rover' stations, comprising a pair of dual-frequency GPS receivers installed on existing masts attached to the 66th level parapet of the Republic Plaza Building.
- iii) Control centre PC running the real-time monitoring software.

The system is designed to allow the analysis of data downloaded automatically from the RPB, and to occasionally adjust, by remote control, the system parameters. The logging computer is located at the RPB for storing raw GPS data on event trigger, and the communication link is provided via a leased line link to the reference station and RS-232 connections to the 'rover' receivers. The leased line transmits the reference receiver data to the rover receiver, allowing for continuous RTK solutions to be generated.

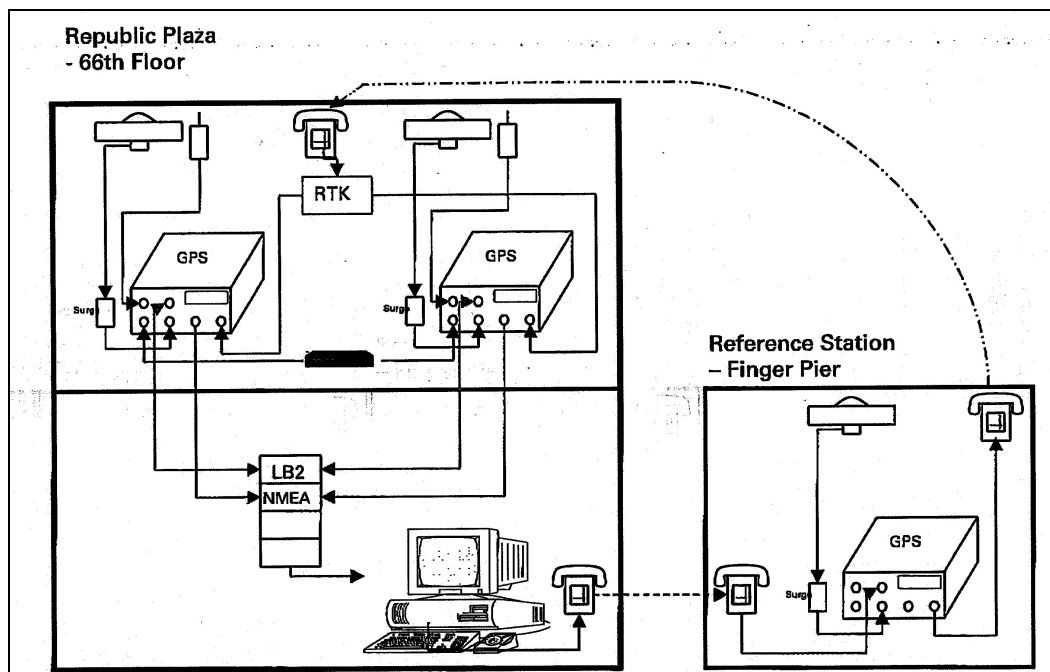


Figure 4.4. *Layout of the GPS monitoring system at the RPB*



Other components of the integrated RPB monitoring system include analog-to-digital converter for the continuous output of a pair of accelerometers on the rooftop and in the basement, and a pair of sonic UVW anemometers.

**CHAPTER 5**

**GPS BIASES AND INTEGRITY MONITORING**

---

---

**5.1 Error Sources in GPS Observations**

GPS observations are subject to a number of errors, both random and systematic. The major error sources include satellite orbital and clock errors, receiver noise and clock errors, and signal propagation errors (ionospheric effects, tropospheric effects, and multipath). They are briefly discussed in this chapter.

**5.1.1 Satellite Related Biases**

The satellite related biases (or systematic errors) include satellite orbit bias and satellite clock bias. The satellite orbit information is generated from the tracking data collected by the monitor stations within the Control Segment (Section 3.1). The Master Control Station (MCS) processes the tracking data, and predicted satellite ephemerides and clock error behaviour is formatted into the navigation message transmitted by each satellite. In reality, it is impossible to perfectly model the satellite orbit. Hence, the predicted satellite ephemeris would differ from the true satellite orbit. This discrepancy is the *satellite orbit bias*.

Since 1 January 1994 the International GPS Service (IGS) has carried out routine operations necessary to generate precise post-processed GPS orbits. An international network of nearly 200 continuously operating GPS stations is used to track the satellites. The satellite orbit bias can therefore be mitigated by using the precise orbits obtained from the IGS in place of the broadcast orbits. Table 5.1 is the estimated quality of the IGS orbit products (IGS, 2001).

Table 5.1. *Estimated quality of the IGS orbit products (GPS broadcast values included for comparison)*

Orbit Type	Accuracy	Latency
Broadcast Orbits	~260 cm	Real time
Predicted Orbits	~25 cm	Real time
Rapid Orbits	~5 cm	After 17 hours
Final Orbits	<5 cm	After 13 days

The *satellite clock bias* is the difference between the satellite clock time and true GPS time. Despite the fact that high quality cesium, or rubidium, atomic clocks are used in the GPS satellites, the satellite clock bias is still unavoidable. In the case of SPP, a typical way to account for the satellite clock bias is to use the broadcast clock error model generated by the MCS, and defined by polynomial coefficients. Even with the best efforts in monitoring the behaviour of each satellite clock, their behaviour cannot be precisely predicted (JPS, 1998). As a result there is a *residual* error after applying the broadcast clock error model. In the case of relative positioning, the satellite clock bias can be eliminated by differencing the measurements obtained from two receivers (Section 3.3), since the satellite clock bias is the same for two receivers observing the same satellite, at the same time.

### 5.1.2 Receiver Related Biases

The receiver related biases include the receiver clock bias, internal inter-channel biases, antenna phase centre variation and receiver noise. Similar to the satellite clock bias, the receiver clock bias is an offset between the receiver clock time and true GPS time. Due to the fact that GPS receivers are usually equipped with relatively inexpensive clocks, the receiver clock bias is very large compared to the satellite clock bias. In the case of SPP, a typical way to account for the receiver clock bias is to treat it as an additional unknown parameter in the estimation procedure. In the case of relative positioning, the receiver clock bias can be eliminated by differencing the measurements made at the same receiver (Section 3.3), since the receiver clock bias would be the same for all measurements made at the same receiver, observing all satellites, at the same time.

The inter-channel bias arises because a multi-channel receiver takes the measurements to different satellites, using different hardware tracking channels. However, multiplexing and sequential single-channel receivers were generally free of the inter-channel bias (Seeber, 1993). With modern GPS receiver technology, the inter-channel bias can be calibrated at the sub-millimetre level or better (Hofmann-Wellenhof et al., 2001).

In GPS positioning, the measurements made by the receiver are usually referred to the distance between the electrical centre of the satellite's transmitter and the electrical centre of the receiving antenna. The discrepancy between the electrical centre and the physical centre is the *phase centre offset*. The electrical centre tends to vary with the direction and strength of the incoming signal. In addition, the phase centre variations for the L1 and L2 carriers may have different properties (Leick, 1995; Rothacher et al., 1990). For most antenna types, the antenna phase variation is usually calibrated by the manufacturers. In addition, the antenna phase centre models for various antennas can be obtained from the National Geodetic Survey (NGS, 2001). These models can subsequently be applied to mitigate the effect of antenna phase variations. It is, however, recommended that for high-precision applications, that care be taken not to mix antenna types, or to swap antennas between sites and receivers during a survey (Rizos, 1997).

The magnitude of the receiver noise is dependent on parameters such as the signal-to-noise ratio and tracking bandwidth. According to a rule of thumb for classical receivers the measurement noise is approximately 1% of the signal wavelength. Therefore, the level of noise in pseudorange measurements is about 3 metres (~300 m wavelength) for C/A-code and of the order of 0.3 metres (~30 m wavelength) for P-code, while the level of noise in carrier phase is a few millimetres for L1 (~ 19 cm wavelength) and L2 (~ 24 cm wavelength). Modern receiver technology tends to bring the internal phase noise below 1 millimetre, and to reduce the C/A-code noise to the decimetre level (JPS, 1998; Qiu, 1993; Seeber, 1993).

### 5.1.3 Signal Propagation Biases

When the satellite signals travel from the satellite to the receiver, the signals will be affected by the atmospheric delay, and possibly, multipath effects. The atmosphere consists of two main layers, the *ionosphere* and *troposphere*, that affect the propagation of GPS signals. Thus, the atmospheric signal propagation biases include the ionospheric and tropospheric delays.

The ionosphere is that band of the atmosphere from around 50km to 1000km above the earth's surface (Hofmann-Wellenhof et al., 2001; Seeber, 1993). Because of free electrons in this layer, the GPS signals do not travel at the speed of light as they transit this region (Parkinson, 1996). As a result, the measured pseudoranges become too long (Equation (3.1)), while on the other hand, the measured phase ranges become too short (Equation (3.2)). The ionospheric delay is a function of the Total Electron Content (TEC) along the signal path, and the frequency of the propagated signal (Lin, 1997). The TEC depends on time, season and geographic location, with major influencing factors being the solar activity and the geomagnetic field (Klobuchar, 1991; Leick, 1995; Seeber 1993). In extreme cases, the ionospheric delay can range from about 50m for signals at the zenith to as much as 150m for measurements made at the receiver's horizon.

Due to the fact that the ionospheric delays are highly correlated over distances of up to a few tens of kilometres, the impact of the ionospheric delay can be significantly reduced by forming a difference between the measurements made by two receivers on short baselines to the same satellite (Section 3.3).

The troposphere is that band of the atmosphere from the earth's surface to about 50km (Spilker, 1996). The tropospheric delay is a function of elevation and altitude of the receiver, and is dependent on many factors such as the atmospheric pressure, temperature and water vapour content. The tropospheric delay ranges from approximately 2m for signals at the zenith to about 20m for signals at an elevation angle of 10 degrees (Brunner & Welsch, 1993). Unlike the ionospheric delay, the tropospheric

delay is not frequency-dependent. It cannot therefore be eliminated through linear combinations of L1 and L2 observations.

Several "standard" troposphere models can be used to estimate the magnitude of the tropospheric delay (e.g. Saastamoinen model, Hopfield model, Black model, and others). The signal refraction due to the troposphere is separated into two components, the dry component and the wet component. Due to the high variation in the wet component, it is difficult to predict or model this component. As a result, the standard models can account for about 90% of the total delay (the dry component). Similar to the ionospheric delay, the tropospheric delay can be largely eliminated by forming a difference between the measurements made by two receivers on short baselines to the same satellite (Section 3.3). For high-precision static applications, the residual tropospheric delays in the double-differenced observables may be treated as additional unknown parameters in the baseline estimation procedure (e.g. Rothacher et al., 1990).

The environment surrounding the antenna of a GPS receiver significantly affects the signal propagation, thereby introducing noise into the measured pseudorange and carrier phase observables. Multipath is the error caused by nearby reflecting surfaces. GPS signals can arrive at the receiver via multiple paths due to reflections from nearby objects such as trees, buildings, the ground, water surfaces, vehicles, etc (Fig. 5.1). Theoretically, the maximum pseudorange multipath error is approximately one chip length of the code (that is, about 300m for the C/A-code, and approximately 30m for the P-code), while the maximum carrier phase multipath error is about a quarter of the wavelength (that is, about 5cm for the L1 carrier, and 6 cm for the L2 carrier) (Georgiadou & Kleusberg, 1989; Lachapelle, 1990; Wells et al., 1987). Since the multipath error depends on the receiver's environment, it cannot be eliminated or reduced by using the data differencing technique (Section 3.3). However, the following options for reducing the effect of multipath have been suggested by Rizos (1997):

- Make a careful selection of the antenna site (reference and observation site) in order to avoid reflective environments.
- Use a good quality antenna that is multipath-resistant.
- Use a receiver that can internally digitally filter out the multipath disturbance.

- Do not observe low elevation satellites (signals are more susceptible to multipath).

## 5.2 Multipath

### 5.2.1 Modes of Multipath

Figure 5.1 depicts the multipath effects of the environment surrounding a GPS observation station. These effects cannot be easily characterised by mathematical means because multipath changes its phase and amplitude with changes in the GPS satellite constellation geometry.

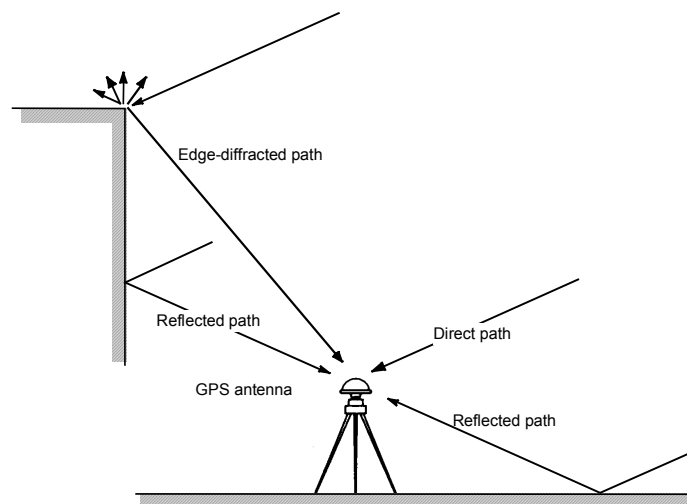


Figure 5.1. *The multipath environment around a GPS receiver*

Multipath generates distortions in phase measurements due to interference of the direct and reflected signals. In general, its effects can be classified into two major categories, *common mode multipath* and *differential multipath* (El-Mowafy, 1994). Common mode multipath occurs when the GPS antennas are very close (e.g., in the range of centimetres to a few metres). In this mode, the reflected signals producing multipath virtually take the same path to the antennas, and thus the correlation between multipath effects at the two antennas is strong enough such that the differencing technique (Equation 3.4) eliminates most of the multipath effects. On the other hand, differential multipath occurs when the antennas are further apart and the multipath effects at the different antennas

are less correlated, since the geometry between satellite, reflector surface and antenna becomes less similar. In this case, the multipath effects cannot be eliminated by data differencing techniques.

Multipath effects can also be classified according to whether the receiver platform is stationary or mobile. For example, in vehicle mode applications, multipath may occur from signal reflections from the surrounding buildings, vehicles, the ground and the body of the vehicle itself. During motion of the receiver, signal diffractions due to the rapidly changing satellite-reflector-antenna geometry will result in randomisation of the multipath effects. This scenario will cause what may be generally termed as the "high-frequency multipath effects" with a period of sub-minute to 2-3 minutes. On the other hand, if the receiver platform is stationary, the multipath error will be characterised as a very slow frequency fluctuation, with the period being dependent on the reflective surfaces in the vicinity of the antenna (e.g., 5-10 minutes due to specular reflections in the vicinity of the antenna, or 50-60 minutes for water surfaces) (*Ibid*, 1994).

### 5.2.2 Example of Low Frequency Multipath

An experiment was carried out at The University of New South Wales (UNSW) to investigate the low frequency multipath effects on short, static baselines. Figure 5.2 shows the plan view of the experiment setup on the rooftop of the Electrical Engineering (EE) Building. The design of the experiment included one base station (**1**) and two rover stations (**2** & **3**). In Figure 5.3, station **1** is designated as **base**, while stations **2** & **3** are designated as **alpha** & **beta** respectively. Dual-frequency Leica System500 GPS receivers were used. Station **base** was equipped with a choking antenna, while stations **alpha** & **beta** were equipped with standard antennas. Note that stations **alpha** & **beta** were located in the close vicinity of a large solar panel structure, thus placing them in a high multipath environment. Station **1** was located on top of the elevator tower A, in a relatively clear space with minimal multipath disturbance.



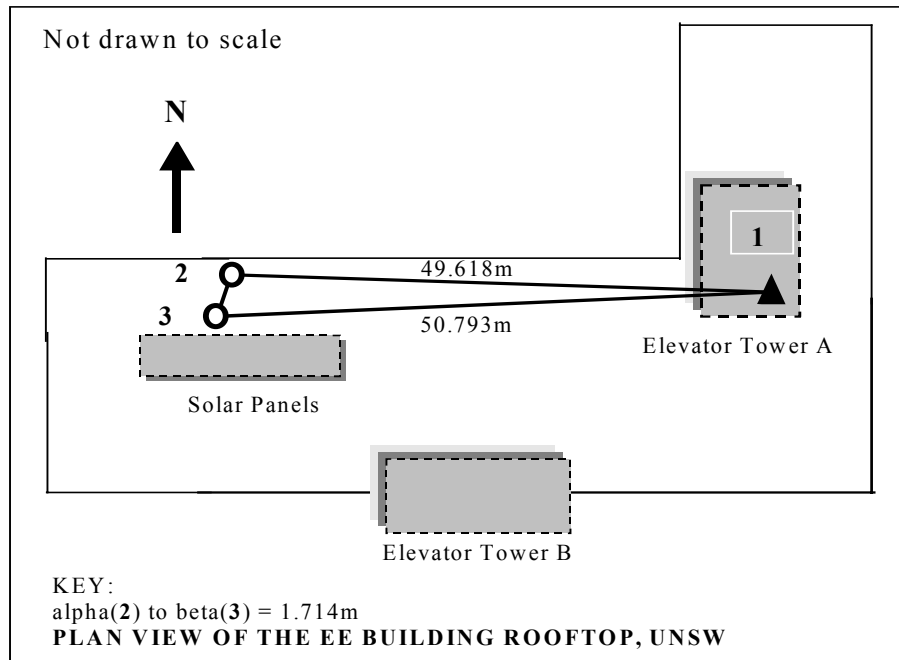


Figure 5.2. Plan view of the UNSW stations used for the multipath experiment

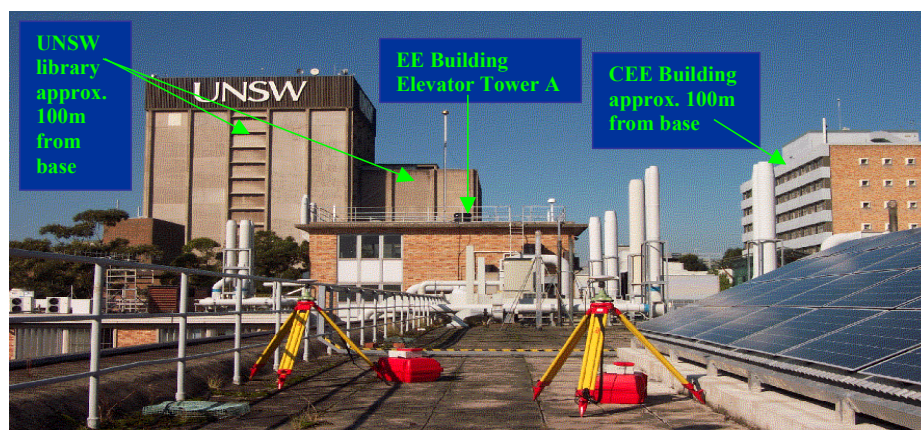
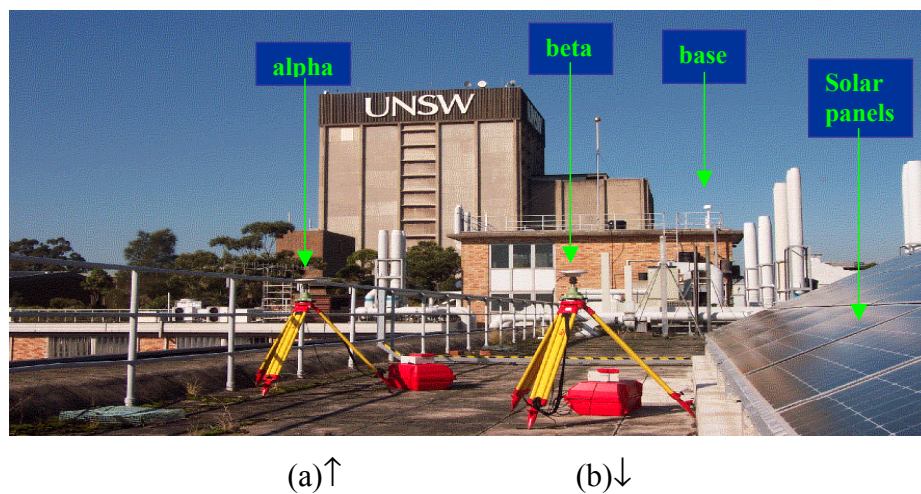


Figure 5.3. Photo of UNSW multipath experiment setup (a) and the surrounding environment (b)

The data were collected at all stations at a 1 second data rate over the same period of nearly 1 hour on two successive days, 23<sup>rd</sup> and 24<sup>th</sup> April 2002, and logged in Leica binary format. All processing was carried out using the Leica SKIPro software. The coordinates of **base** were available from a previous GPS survey. To obtain the mean baseline lengths (shown in Fig 5.2), in the case of the first processing the elevation mask angle was set at 15° for all stations and the data processed in static mode. In the second processing strategy the elevation mask angle was set at 15° and 0°, for the base station and the two rover stations (to permit the maximum influence of multipath on the results), and the data processed to give epoch-by-epoch solutions.

Figures 5.4, 5.5 and 5.6 show the residuals for the base-alpha, base-beta and alpha-beta baselines respectively. The following assumptions can be made with regard to these residuals:

- Because the baseline lengths are very short (~50m, ~50m, ~2m respectively), the systematic biases such as orbit bias, tropospheric delay, and ionospheric delay are assumed to be absent. These residuals therefore show only the multipath effects and observational noise.

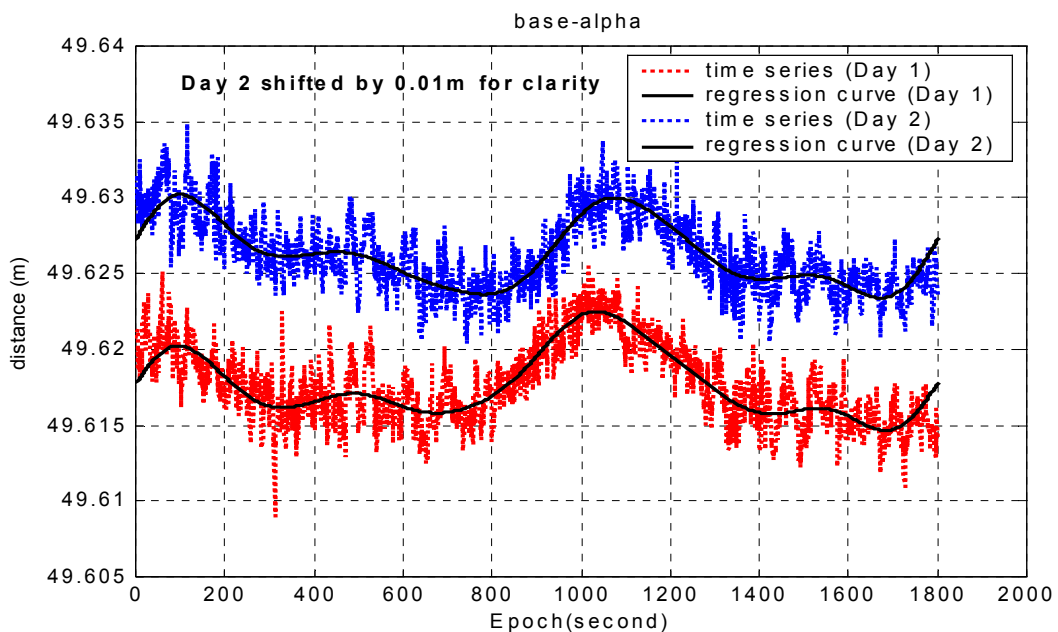


Figure 5.4. Comparison of the measurements and the regression curves for the base-alpha baseline (Day 1 vs. Day 2)

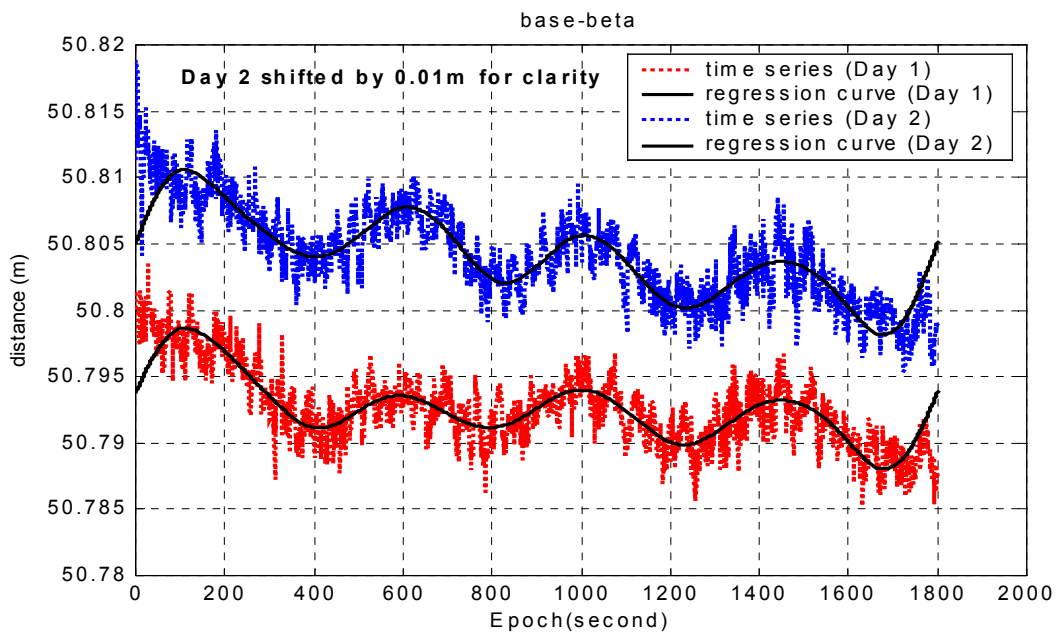


Figure 5.5. Comparison of the measurements and the regression curves for the base-beta baseline (Day 1 vs. Day 2)

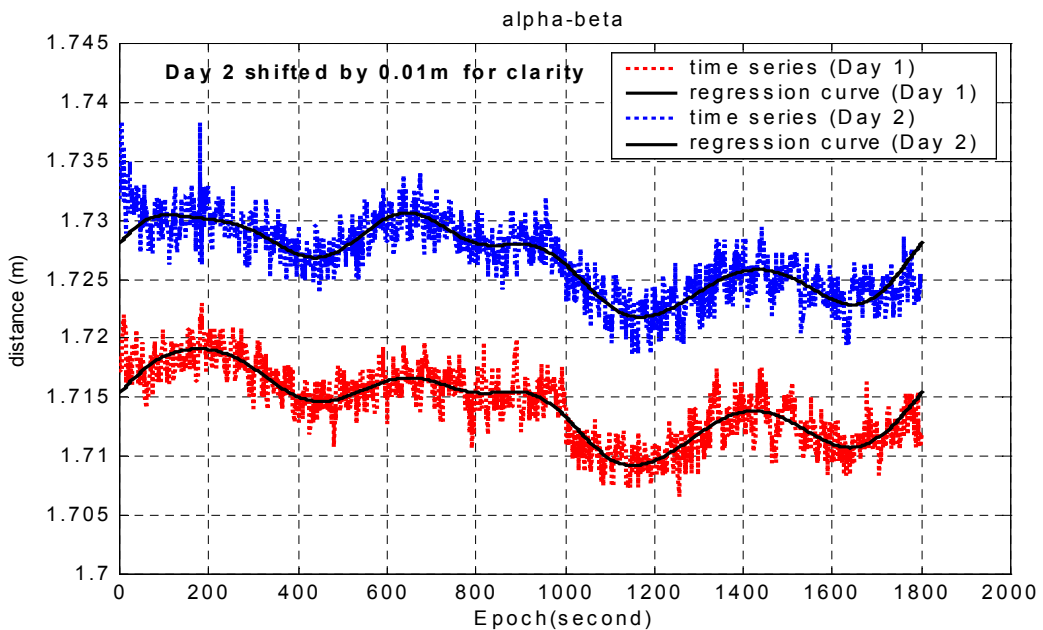


Figure 5.6. Comparison of the measurements and the regression curves for the alpha-beta baseline (Day 1 vs. Day 2)

- The base station is located in a comparatively multipath-free environment. An attempt to further minimise the multipath effects at the base station was made by using a  $15^\circ$  elevation mask angle during data processing. Hence it is assumed that the multipath effects in the residuals are due to the rover stations.

All the plots display the repeated trend between Day 1 and Day 2 of the experiment, which demonstrates clearly that multipath is present. The frequency-domain representations of the time series indicates that the frequency band between 0.0005Hz to 0.01Hz is repeated for all the baseline residuals on the two successive days (Figure 5.7). The frequency higher than 0.01Hz cannot be distinguished from the observation noise. This implies that "low frequency multipath" in the band 0.0005Hz to 0.01Hz is present. Bandpass filtering can be used to extract or delete such multipath trends (e.g., Han & Rizos, 1997; Schwarz et al., 1993) from the baseline residuals. The reader is referred to these articles for a detailed explanation.

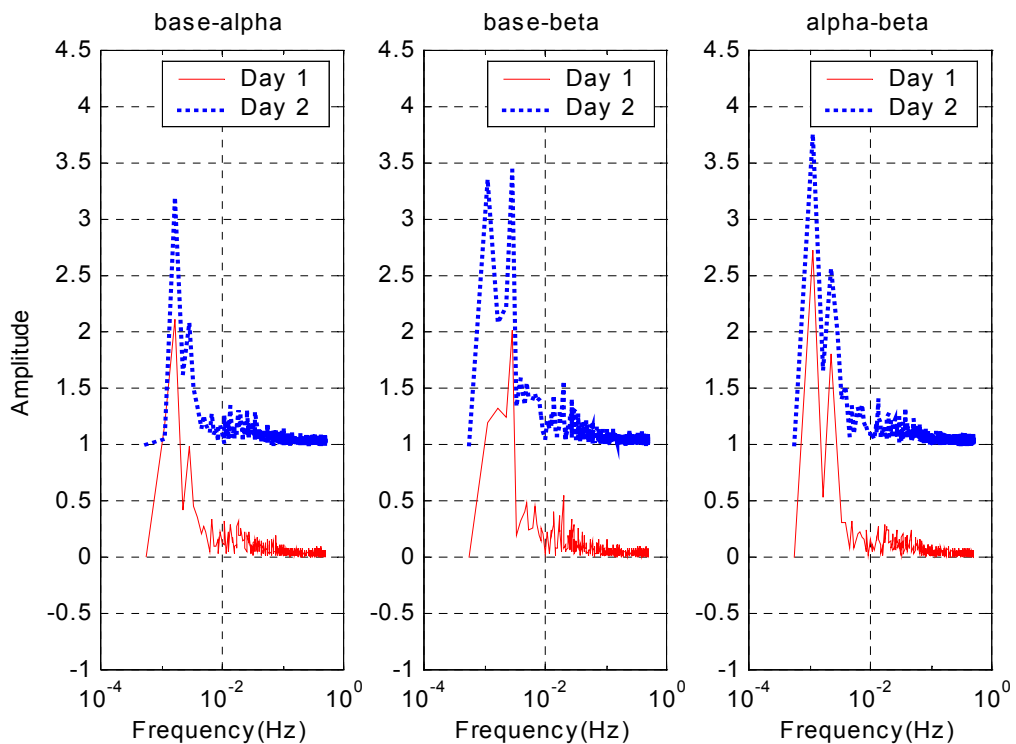


Figure 5.7. Frequency-domain representations of multipath on baseline results

### 5.2.3 Multipath in GPS-Based Structural Monitoring

#### 5.2.3.1 Introduction

In structural monitoring applications the antennas are permanently installed. Therefore, only the low frequency multipath phenomena are expected. Research shows that typical low frequency multipath errors have sinusoidal oscillations of periods of 6–10 minutes (0.001–0.003 Hz) (Qiu, 1993). This implies that multipath can become a dominant error source for deformation scenarios where monitoring points move very slowly (say, < cm a day). On the other hand, when detecting deformations (or motions) with shorter periods (say, > 0.05 Hz), then multipath effect may be treated as negligible. Moreover, GPS-based structural monitoring is a special application of GPS relative positioning, where short baseline lengths are used (< 10 km). Thus, the long-term systematic errors, such as orbital and atmospheric errors can also be assumed to cancel out in the double-differenced carrier phase observable (Equation 3.5).

#### 5.2.3.2 Multipath Minimisation Techniques

Many hardware and software multipath *mitigation* techniques have been developed by researchers, but none of the techniques can be considered ideal for all environments and scenarios. The University of Calgary have proposed a multiple antenna for mitigating multipath (see Ray et al., 1998; Ray, 1999), by using the spatial correlation of multipath over short distances. Since this method is based on the use of multiple antennas located at one point, it is more suited for multiple reference station multipath mitigation, but is unfortunately less cost-effective for deformation monitoring networks where a great number of points are monitored. Ge et al. (2000b; 2000c) have proposed adaptive filtering of multipath for continuous GPS applications, while Dodson et al. (2001) have recently studied the feasibility of the approach to mitigate multipath for structural deflection monitoring applications. Other related studies can be found in the literature (e.g., Schaal & Netto, 2000).

A characteristic of multipath is that its effect repeats when the satellite geometries relative to the static GPS antenna repeats, e.g. after one sidereal day. In other words, the effects of multipath on the GPS (carrier phase) measurements are similar from day-to-day when the satellite-reflector-receiver geometry is repeated. Day-to-day correlation is about 85% depending on how static the reflective environment is (Radovanovic, 2000). This characteristic of multipath can be exploited to improve the positioning accuracies. For instance, if there is a series of baseline solutions over several days, then the multipath error can be calculated at every epoch, and subsequently subtracted, from data collected on the subsequent day(s).

And as previously mentioned, multipath errors may have periods ranging from less than a minute to several hours. The errors may have low frequency sinusoidal patterns (Figures 5.4 - 5.7) arising from the motion of the satellite and the receiver with respect to the reflector(s). Noise-like high frequency patterns may arise from changes in the signal reflections and diffractions (e.g., in vehicle mode applications). Low frequency multipath errors can be removed through long-term averaging, while the noise-like multipath errors can be minimised through filtering (El-Mowafy, 1994). For example, according to Radovanovic (2000), tests performed on static and slowly deforming baselines indicate that by averaging the corrected 1Hz position estimates over 30 seconds, improvements in positioning accuracies of up to 50% (to less than the 5 mm level) can be realised. For example, in static mode applications, the low frequency multipath is dominant. For the noise-like multipath errors, spectral techniques such as direct and inverse Fast Fourier Transforms (FFTs) have been suggested for multipath detection and removal (e.g., Schwarz et al., 1993). Similarly, Han & Rizos (1997b) proposed an approach to mitigate the multipath effect by transforming the measured data into the spectral domain, and removing the multipath using a FIR (Finite Impulse Response) filter.

Improved antenna design with lower gain at low elevations reduces the influence of ground-reflected signals (Ding et al., 1999). Based on this principle, new types of antennas that can reject multipath signals have been designed. These include the chokerings and groundplanes (e.g., Leica chokerings and NovAtel GPSAntenna Model 600). Much effort has also been invested to refine the GPS receiver processing

algorithms in order to help reduce multipath at the internal receiver signal processing stage. The processing algorithms aim at both reducing the threshold for multipath detection and rejection, and improvement in the measurement accuracy (e.g., Townsend & Fenton, 1994).

Multipath mitigation can also be achieved by setting a cut-off angle for signal reception at the data processing stage, so that the signal(s) reflected from surfaces and the low elevation satellites are rejected. This approach may, however, only be desirable for some applications (e.g., deformation monitoring) but not for others. For example, for airborne applications, using a cut-off angle may mask off useful satellites. However, this technique can be applied for monitoring applications, especially for base stations.

### 5.3 Integrity Monitoring

#### 5.3.1 Definition and Concepts

The *integrity* of a navigation system is defined as the trust that can be placed in the correctness of the information supplied by the system (Brown 1996; Cohen et al., 1996). It relates to the ability of the system to issue timely warnings to the user when the system fails to meet its stated accuracy. Thus, the system is required to deliver a warning (*alarm*) whenever an error or bias in the delivered user position solution exceeds an allowable level (*alarm limit*). *Integrity* is one of the four parameters by which the required navigation performance of a system can be specified. The other three parameters include *accuracy*, *continuity*, and *availability*. These parameters can be defined as follows (e.g., Ochieng et al., 2001, 2002):

- *Accuracy* is the degree of conformance of the estimated position results to the *true* value(s), at a given time.
- *Continuity* is the ability of the navigational system to perform its function without interruption during the intended period of operation. *Continuity risk* is a

measure of the system unreliability (i.e., the probability that the system will be interrupted for the intended period of operation).

- *Availability* is the percentage of time during which the system is available for use, having taken into account all outages. Thus a system is available if all the *accuracy*, *integrity* and *continuity* requirements are satisfied.

Of the four parameters *integrity* is the one that is crucial for safety-critical applications such as aircraft precision approach and landing. Similarly, GPS-based real-time structural health monitoring systems require high integrity of the antenna position coordinates in order to guard against the *risk of false alarms*.

At a more general level, two subclasses of integrity monitoring of GPS systems are of interest: *ground-based integrity monitoring* (based on an independent network of monitoring stations), and *Receiver Autonomous Integrity Monitoring (RAIM)*.

### 5.3.2 Ground-Based Integrity Monitoring

One of the strategies for providing an independent assurance of integrity is to have a network of ground monitoring stations whose purpose is to monitor the health of the GPS satellite data (Brown 1996; Ochieng et al., 1996, 2001, 2002). The ground-based integrity monitoring approach uses a number of strategically located integrity monitoring stations, whose locations are established using precise geodetic techniques, to the highest level of accuracy. The stations track signals in space from the GPS satellites, the data then being used to determine the satellite integrity (health). In the event that an alarm is detected, the information is transmitted to the system users via a Ground Integrity Channel (GIC) within a specified time period (*time-to-alarm*).

Ground-based integrity monitoring is also carried out through augmentation of the GPS satellite system with additional ranging signals. For example, in aircraft approach and landing applications, it might be possible to use an additional augmentation by "pseudolites" (ground transmitters sending pseudo-GPS signals) for ground-based integrity monitoring (Pervan, 1994; Cohen et al., 1993, 1996). This concept can be



extended to the structural monitoring application when the obstruction of GPS satellite signals becomes a problem, or when additional ranging signals are necessary to improve solutions (especially in the height component) (e.g. Dai et al., 2001a, 2001b, 2002; Wang et al., 2001).

### 5.3.3 Receiver Autonomous Integrity Monitoring

Receiver Autonomous Integrity Monitoring (RAIM) is a method based on some kind of self-consistency check among the available raw GPS measurements (Brown, 1996). It is a technique applied by the user (i.e. the receiver) to estimate the quality of the position results obtained by raw measurements from different satellites. For the RAIM methods to be effective, they require redundant measurements and good satellite geometry. A minimum of five satellites are required in order to permit an anomaly to be detected in range measurements, while a minimum of six satellites are required to remove the faulty satellite observations from the solution (Ochieng et al., 2002).

Examples of RAIM methods can be found in articles and textbooks. For example, *Ibid* (1996) has made a detailed analysis of three common methods: the range comparison method, the least-squares-residuals method, and the parity method.

Most of the RAIM schemes are based on statistical detection theory in which the hypothesis-testing questions for detecting a failure and identifying the failed satellite (if any) are posed (it is usually assumed that there is only one failure at a time). More specifically, such schemes consist of two distinct parts: satellite fault detection/exclusion and bad geometry detection/exclusion (e.g., Chang & Paige, 2000; De Jong et al., 2001; Ober, 2000; Pervan et al., 1994). In essence, the models are based on a set of linearised observations equations at one time step. Since, in general, there is one equation per satellite in the observation model, removing an equation is equivalent to removing a satellite.

## 5.4 Concluding Remarks

For differential operations (e.g. RTK systems), most biases will be removed by the double-difference data processing technique (Equation 3.4). Short baseline lengths will minimise the atmospheric biases, and careful site selection helps to mitigate multipath effects. Gross errors or outliers that are often large and occur due to a sudden change in the prevailing physical circumstances, for example, the acquisition of a new, very low elevation satellite or sudden signal loss/obstructions (cycle slips), can be handled well by statistical modelling at the data processing step (Chang & Paige, 2000; Cross et al., 1994; De Jong, 2000; Ober, 2000; Wieser, 2001).

For differential operations, the concept of integrity monitoring concerns the reference station and the rover station (Morley, 1997). The concept of integrity monitoring at the reference station has received special attention in recent years (e.g. De Jong et al., 2001; Jonkman & De Jonge, 2000a, 2000b, 2000c). The current research assumes that the reference receiver data have passed all integrity checks, and are "blunder-free". It is considered important that the rover station should have the ability to assess the quality of the position solutions, and to detect and (if necessary) exclude one or more erroneous observations from the processing step. If an error in the position solution cannot be guaranteed to be below the threshold limit, then an alert message must be sent to the user. However, in case the error cannot be detected by the existing methods of integrity monitoring, then the term "loss-of-integrity" is implied. Based on this new definition, an approach for detecting a "loss-of-integrity" event in the position domain is proposed in the following Chapter.

CHAPTER 6

INTEGRITY MONITORING IN THE POSITION DOMAIN

---

---

## 6.1 Introduction

The purpose of this chapter is to introduce a new approach to integrity monitoring of GPS receiver arrays based on position domain data. The proposed method is intended for the detection of unscheduled "failures" under the following assumptions:

- a) Valid data have been generated by the reference station(s), and the rover station(s) have carried out data processing as well as performed *Failure Detection and Exclusion (FDE)* (see, e.g., Chang & Paige, 2000).
- b) The position solutions reported by the rover station(s) in a GPS receiver array system are consistent except for unscheduled failures. It will be assumed that such failures are abrupt (but not necessarily of large magnitudes) and are due to unknown sensor defects, faults or any other unknown biases that will be persistent from the time of their occurrence.

It is common to test the hypothesis that only one observation is corrupted by a *Marginally Detectable Error (or bias) (MDE)* at any one time, and that the rest of the observations are assumed to be unbiased (Cross et al., 1994). Hence, one may calculate a *MDE* for each observation. In this research, it must be emphasised that the proposed method is concerned with the detection of *persistent biases (= Persistent MDEs (PMDEs))* that may otherwise be mistaken for deformation signals by a GPS-based monitoring scheme. Before presenting details of the proposed method, it is necessary to understand the basis of on-line statistical change detection.

## 6.2 On-line Change Detection Algorithms

In designing change detection procedures two tasks are involved (e.g., Baseville & Nikiforov, 1993; Mertikas, 2001). First, the "residuals" that will reflect direct changes in the data have to be generated. The residuals are ideally close to a constant value (e.g., zero, mean value, standard deviation) when no change occurs and significantly different from this value when a change has occurred. Secondly, algorithms have to be developed, using the statistical methods for declaring an abrupt change in the data and estimating the exact time of change. Numerous algorithms concerned with on-line detection of "shifts" in systems and data, and "quality control" of data, have been proposed (e.g., Baseville, 1988; Baseville & Nikiforov, 1993; Cox, 1988-89; Keats et al., 1995; Kourti & MacGregor, 1996; Lu, 1999; McReynolds, 1994; Mertikas, 2001; Mertikas & Rizos, 1996, 1997, 1998; Samuel et al., 1998; Sullivan & Woodall, 1996).

Because of the mathematical complexities and the wide range of possible applications, it is generally sufficient to select the appropriate algorithms on the basis of the application. For instance, *Shewhart control charts* can be implemented to directly monitor excessive displacements (or trends) in GPS data. They can be used to indicate whenever a predetermined threshold is reached or exceeded. However, this algorithm can only detect large shifts in the mean long after the change has occurred, but cannot detect moderate or slight shifts (e.g., due to the onset of a bias or fault) even if they persist (Mertikas, 2001). On the contrary, *cumulative sum (CUSUM) test* algorithms are sensitive to small persistent changes in the mean or standard deviation of measurements, and they permit a prompt detection delay. The two algorithms are described next as used in the development of the proposed mathematical framework.

### 6.2.1 Shewhart Control Charts

Limit checking detectors were initially introduced in the field of quality control under the title *continuous inspection schemes*. The concept underpinning these schemes can be mathematically explained as follows (Baseville & Nikiforov, 1993). Assume that  $K$

samples of data with fixed size  $N$  are taken. At the end of each sample a decision rule is computed to test between the following two hypotheses:

$$\begin{aligned} \mathbf{H}_0 &: \theta = \theta_0 \\ \mathbf{H}_1 &: \theta = \theta_1 \end{aligned} \quad (6.1)$$

where  $\theta$  is the mean of the samples. If the decision is taken in favour of  $\mathbf{H}_0$ , the sampling and test continues. However, the sampling is stopped after the first sample of observations for which the decision is taken in favour of  $\mathbf{H}_1$ . For a fixed sample, the decision rule  $d_K$  is given by:

$$d_K = \begin{cases} 0 & \text{if } S_1^N < \lambda; \mathbf{H}_0 \text{ is chosen} \\ 1 & \text{if } S_1^N \geq \lambda; \mathbf{H}_1 \text{ is chosen} \end{cases}, \quad K = 1, 2, 3, \dots, N \quad (6.2)$$

where  $S_1^N$  is a decision function and  $\lambda$  is a conveniently chosen threshold. The decision is taken with the aid of a *stopping rule*, in this case defined by:

$$t_a = N \cdot \min\{K : d_K = 1\} \quad (6.3)$$

where  $d_K$  is the decision rule for the sample number  $K$  (of fixed size  $N$ ) and  $t_a$  is the number of steps of the process when an alarm is issued. In other words, the sampling stops after the first sample of fixed size  $N$  for which the decision is in favour of  $\mathbf{H}_1$ .

Consider a case where the distribution of  $y$  is Gaussian with mean value  $\theta = \mu$  and constant variance  $\sigma^2$ . The probability density for  $y$  is given by:

$$p_\theta(y) = \frac{1}{\sigma\sqrt{2\pi}} e^{-\frac{(y-\mu)^2}{2\sigma^2}} \quad (6.4)$$

A Shewhart control chart is constructed for which when  $\mu_1 > \mu_0$ , the alarm is set the first time at which (Ibid, 1993):

$$\bar{y}(K) \geq \mu_0 + c \frac{\sigma}{\sqrt{N}}, \quad K = 1, 2, 3, \dots, N \quad (6.5)$$

where the mean of  $y$  at the  $k^{\text{th}}$  sequential sample is:

$$\bar{y}(K) = \frac{1}{N} \sum_{i=N(K-1)+1}^{NK} y_i \quad (6.6)$$

$c$  and  $N$  are the tuning parameters of the Shewhart control chart. They can be defined *a priori*. The right side of the inequality (6.5) is referred to as the *upper control limit (UCL)*, and hence it can only detect an increase (or positive change). However, it is often more useful to detect deviations from  $\mu_0$  in both directions. This requires the assumption that the mean value after the change is either  $\mu_1^+ = \mu_0 + v$  or  $\mu_1^- = \mu_0 - v$ . In that case, the *lower control limit (LCL)* is also defined:

$$LCL = \mu_0 - c \frac{\sigma}{\sqrt{N}} \quad (6.7)$$

with which the alarm can be set the first time  $K$  at which:

$$|\bar{y}(K) - \mu_0| \geq c \frac{\sigma}{\sqrt{N}}, \quad K = 1, 2, 3, \dots, N \quad (6.8)$$

Figure 6.1 is a Shewhart example of random data simulated using a Matlab random number generator. The Shewhart control charts are suitable for application in GPS deformation monitoring schemes to detect sudden jumps or slow linear drifts in the mean value (and/or standard deviation) of station coordinates (or baseline solutions) as long as those data follow a normal distribution, are statistically independent and their true mean(s) and standard deviation(s) are known. Mertikas (2001) has presented an

example of a practical evaluation of the Shewhart control charts using station coordinates from the GPS crustal deformation monitoring network, the GEONET in Japan.

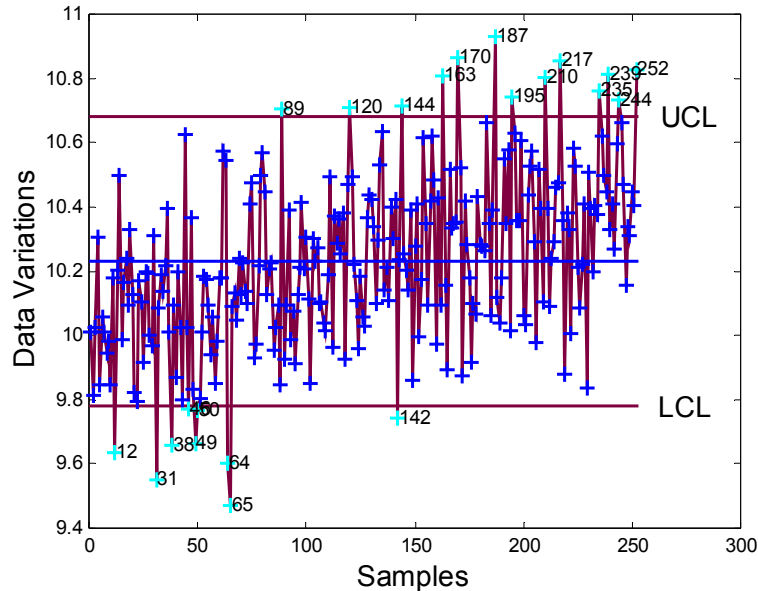


Figure 6.1. *A Shewhart example of random data simulated using Matlab random number generator*

The ability of a Shewhart control chart to detect either a short-period or a long-period deformation will depend on the GPS data rate. For the detection of abrupt short-period deformations more frequent sampling is required. For the detection of slow long-period deformations less frequent sampling would suffice. For example, for long-period (slow) deformations, every value of the coordinates can correspond to the mean from daily or quarter-daily observations, while for short-period (fast) deformation(s), every value of the coordinates can correspond to 0.1 of a second (10Hz). Even so, to construct the control charts, samples of fixed size  $N$  (e.g.  $N = 5$ ) are sequentially taken from the observations, and at the end of each sample the sample mean of the  $N$  observations and the standard deviation are computed. The derived sample means are then plotted as a function of the sample number.

## 6.2.2 CUSUM Test Algorithms

CUSUM algorithms can be classified into two types. The first type is the one-sided CUSUM, which can be used when both the means before and after change are known. The second type is the two-sided CUSUM, to be used when the change magnitude is unknown.

### 6.2.2.1 One-Sided CUSUM Test

Define the function (Baseville & Nikiforov, 1993):

$$S_n = \sum_{i=1}^n z_i \quad (6.9)$$

where:

$$\begin{aligned} z_i &= \ln \frac{p_{\theta_1}(y_i)}{p_{\theta_0}(y_i)} = \frac{\mu_1 - \mu_0}{\sigma^2} \left( y_i - \frac{\mu_0 + \mu_1}{2} \right) \\ &= \frac{b}{\sigma} \left( y_i - \frac{\mu_0 + \mu_1}{2} \right) = \frac{b}{\sigma} \left( y_i - \mu_0 - \frac{\nu}{2} \right) \end{aligned} \quad (6.10)$$

is the log-likelihood ratio for the observations from observation  $y_1$  to  $y_n$ ,  $\nu = \mu_1 - \mu_0$

is the change magnitude and  $b = \frac{\mu_1 - \mu_0}{\sigma}$ . In other words, at the  $n^{\text{th}}$  sampling point, the

decision function is cumulative and is expressed as:

$$S_n = \frac{b}{\sigma} \sum_{i=1}^n \left( y_i - \mu_0 - \frac{\nu}{2} \right) \quad (6.11)$$

The typical behaviour of the above function shows a negative drift before change, and a positive drift after change in the case of a positive shift in the mean, and vice versa in the case of a negative shift (see Figure 6.2).



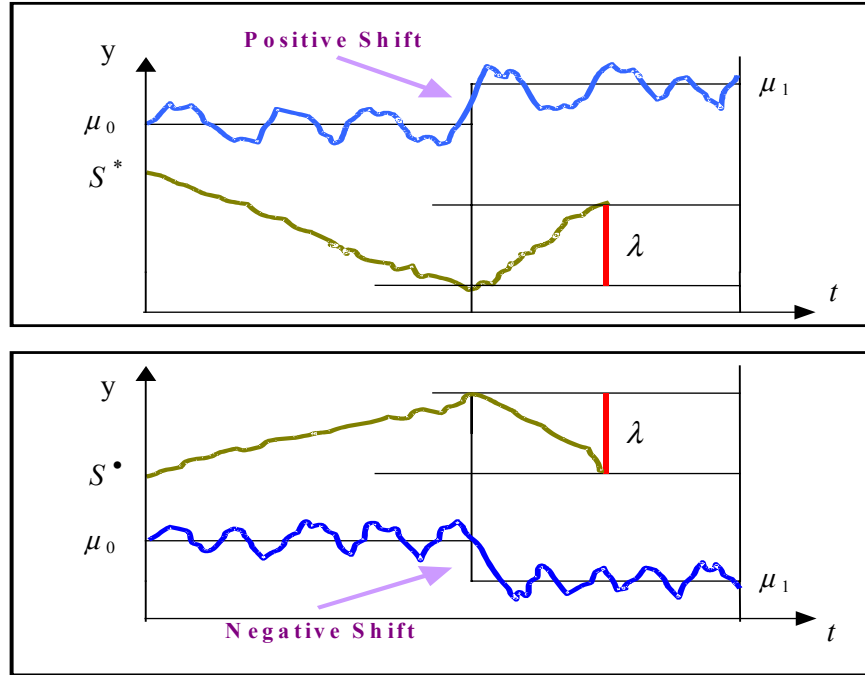


Figure 6.2. Typical behaviour of the log-likelihood ratio corresponding to an increase in the mean (top) and a decrease in the mean (bottom) of a process

The basic assumption in the one-sided case is that either a positive or a negative shift of known magnitude has occurred. For the positive shift case, for instance, the relevant change information lies in the difference between the value of the log-likelihood ratio and its current minimum value; and the corresponding decision rule is, at each time instant, to compare this difference to a threshold. Thus, an alarm will be issued if:

$$g_n^* = S_n^* - \min_{0 \leq t \leq n} S_t^* \geq \lambda \quad (6.12)$$

where

$$S_t^* = \left( S_{t-1}^* + y_t - \mu_0 - \frac{v}{2} \right)^+, \quad S_0^* = 0$$

and  $g_n^*$  is the CUSUM decision function depicted in Figure 6.3.

### 6.2.2.2 Two-Sided CUSUM Test

A more realistic case of change detection using the CUSUM algorithm is where the change magnitude is unknown. However, an *a priori* minimum jump magnitude  $\nu$  must still be applied, so that the implied mean value after change is either  $\mu_1^+ = \mu_0 + \nu$  or  $\mu_1^- = \mu_0 - \nu$ . In such a case, it is relevant (Basseville, 1988; Basseville & Nikiforov, 1993; Hinkley, 1970; Page, 1954, 1957) to use two CUSUM algorithms in parallel; the first one for detecting an increase in the mean, and the second for detecting a decrease in the mean of the sequence. Thus, an alarm will be issued if:

$$\begin{cases} g_n^* = S_n^* - \min_{0 \leq t \leq n} S_t^* \geq \lambda \\ g_n^\bullet = \max_{0 \leq t \leq n} S_t^\bullet - S_n^\bullet \geq \lambda \end{cases} \quad (6.13)$$

where

$$S_t^* = \left( S_{t-1}^* - y_t + \mu_0 - \frac{\nu}{2} \right)^+, \quad S_0^* = S_0^\bullet = 0 \quad (6.14)$$

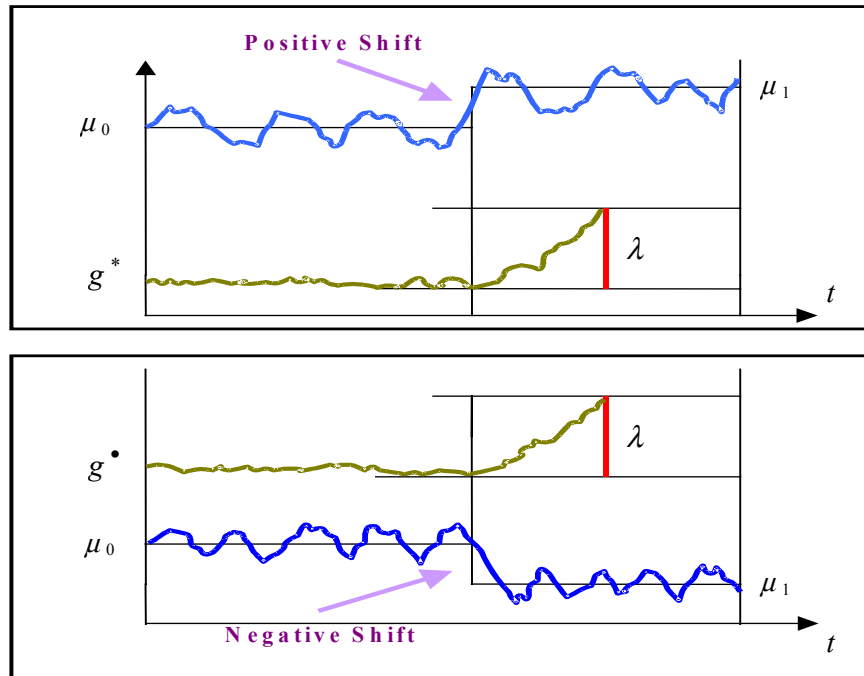


Figure 6.3. Typical behaviour of the CUSUM decision function

The resulting alarm time is given by:

$$t_a = \min\{t \geq 1 : (g_t^* \geq \lambda) \cup (g_t^\bullet \geq \lambda)\} \quad (6.15)$$

In most practical cases, very little is known about the change magnitude  $\nu$ . Three possible *a priori* choices can be made with respect to this parameter. The first is to choose  $\nu$  as a minimum possible jump magnitude (limit case being  $\nu = 0$ ). The second is to choose *a priori* the most likely jump magnitude. Third choice is a worst-case value from the point of view of the cost of missed detection(s).

Along with the Shewhart control charts, the practical evaluation of the CUSUM algorithm for the online detection of abrupt shifts in GPS baseline vector solutions (or station coordinates) from the GEONET of Japan is also found in Mertikas (2001).

### 6.2.3 Summary and Discussion

The basic principles of the *limit checking algorithms* and the *CUSUM algorithms* have been presented. It has also been pointed out that practical examples of the implementation of these algorithms using GPS station coordinates can be found in Mertikas (2001). Related work and discussions on quality control and monitoring with GPS can also be found in the literature (e.g., Mertikas, 1998; Mertikas & Rizos, 1996, 1997, 1998). Section 6.3 will describe the proposed application of the two-sided CUSUM algorithm to the problem of integrity monitoring. In that respect it is necessary to emphasise two important issues, namely, the estimation of the *a priori* mean and standard deviation, and the choice of anticipated shift and detection threshold. A few comments will be made below, however Mertikas (2001) has addressed these two issues in detail.

#### 6.2.3.1 Estimating the Mean and Standard Deviation

The mis-specification of the mean and/or standard deviation of the data being monitored will lead to undesired *false alarms*. In most cases, historical in-control data (if available)

can be used to estimate the mean value and the standard deviation of the process. Once the initial estimates of these parameters are available, they would be used to calibrate the CUSUM. However, in the case of a lack of sufficient in-control data for such an estimation, a self-starting CUSUM can be used instead. In such a case the mean and the standard deviation are computed in real-time (and as soon as the CUSUM starts) using all the data accumulated to date. In such a scheme these values will be updated sequentially and in real-time.

### **6.2.3.2 Choosing the Anticipated Shift and Threshold**

For an optimal CUSUM, the anticipated shift value  $\nu$  must be chosen carefully in order to avoid missed detection(s) and false alarms. The optimality criterion is to choose the shift value that will offer fast detection with few false alarms. For example, the anticipated shift of the order of one or two standard deviations of the in-control data can be used. Along with the anticipated shift, the choice of the threshold value  $\lambda$  also affects the detection delay. A common approach is to first specify the anticipated shift value, and then determine the threshold value.

### **6.2.4 Choice of Criteria**

For deformation studies, the detection method should be capable of discerning between biases (or errors) and deformation. The standard performance index for on-line change detection is the delay for detection, which has to be minimised for a fixed false alarm rate (Page 1954). Baseville & Nikiforov (1993) give a clear definition of the criteria that can be used for deriving optimal stopping times for change detection. The criteria should favour fast detection with only a few false alarms. Fast detection is necessary because, between the failure onset time and its detection, incorrect interpretation of the measurements continue to be made, which is clearly undesirable.

Apart from the trade off between the mean time between false alarms and the delay for detection (both increasing when the sensitivity of the detector to high frequencies

decreases), there exists another trade off which is closely related to the first one, efficiency versus complexity. When the designed monitoring system involves, at each alarm, a complex time consuming processing and/or a reconfiguration of the control, false alarms are more dramatic. It should also be noted that the complexity of a change detection system is not only of a computational nature but also of a technological one. For example, some failure detection procedures can make use of the redundancy in the data obtained from several identical sensors. For such systems, reducing the complexity without degrading the performance of the detector may be of interest.

### 6.3 CUSUM Application to Integrity Monitoring

#### 6.3.1 The Proposed Approach

In order to provide integrity, the user should be warned in case of system failures. There are different ways to deal with failures. A more widely used approach is the failure detection and exclusion (FDE) algorithms.

Traditionally, FDE is performed in the measurement domain (e.g., Figure 6.4). The conformance of the raw measurements with the theoretical models is examined using results from statistical outlier detection (Ober, 2000).

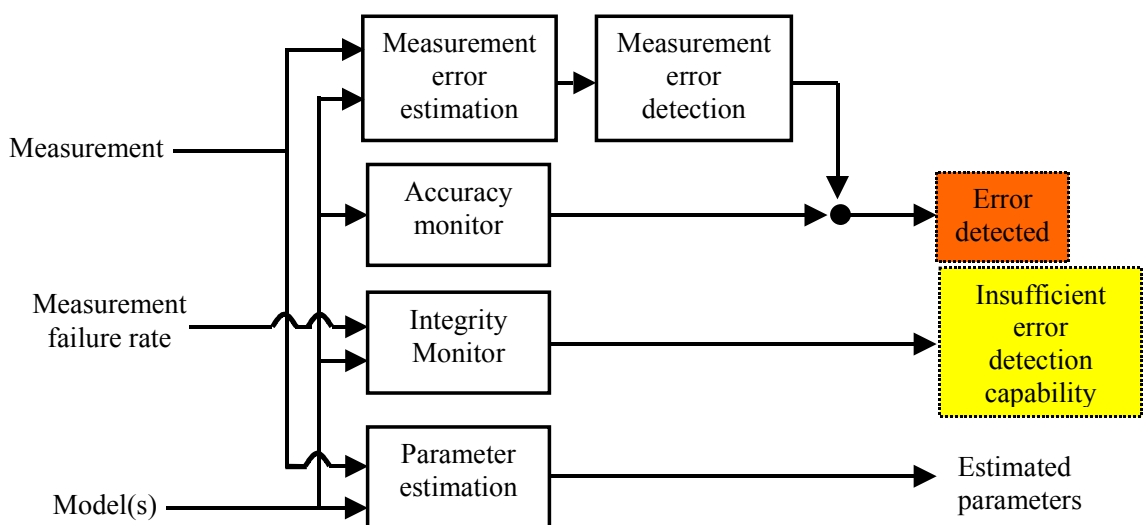


Figure 6.4. FDE in the measurement domain (Ober, 2000)

When failure detection is done explicitly in the position domain (Fig. 6.5), performance (or on-line) monitoring becomes the basis of failure detection: a failure is detected as soon as the integrity requirements are not met.

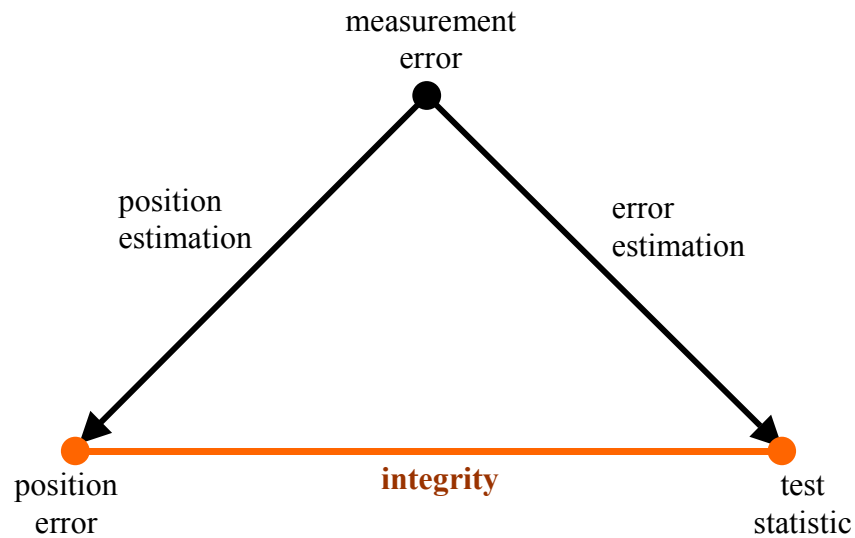


Figure 6.5. *FDE in the position domain (Ober, 2000)*

In this research, a CUSUM approach to perform the integrity monitoring (or FDE) in the position domain is proposed. As for any other detection algorithm, the procedure comprises two main steps. Firstly, the minimum size of errors (or bias) in the data should be specified. Any errors larger than the specified size will be detected, smaller errors will not. Secondly, the impact that the smallest detectable error would have on the data is quantified through a predetermined threshold. Hence, the algorithm proceeds as follows:

- a) Determine the *PMDEs*
- b) Compute the residuals (or innovations) of the data
- c) Test for shifts in the residuals (or innovations) against preset threshold(s)
- d) If the shifts are within the threshold(s) then there is no error (or bias).

The proposed approach uses redundancy in the data obtained by several identical sensors (such as GPS arrays). However, it is possible to use only three GPS rovers, as

discussed later, to generate data redundancy between stations (i.e., baselines) for an on-line implementation. For example, three GPS rover station antennas can be installed on a structure (e.g. building rooftop), simultaneously generating baseline solutions. In that case, the FDE proceeds as discussed below.

Having determined the PMDEs, assume that an error (or bias) is present in the baseline solutions of one of the GPS sensors, which makes itself apparent at an unknown time. The problem is to detect and isolate the responsible station, as soon as possible.

For the  $r^{\text{th}}$  GPS station ( $r = 1, 2, 3$ ), consider that a sequence of independent random variables:

$$\{\mathbf{X}_n^r\} \text{ with } n = 1, 2, 3, \dots \quad (6.16)$$

is a normal Gaussian process. Let the sequence  $\{\mathbf{X}_n^r\}$  represent the residuals of the vector components  $\{dX_n^r - d\bar{X}^r, dY_n^r - d\bar{Y}^r, dZ_n^r - d\bar{Z}^r\}$  of a baseline,  $\{d\bar{X}^r, d\bar{Y}^r, d\bar{Z}^r\}$  are the known (or true) values of those vector components. If an error occurs in the solutions of the  $i^{\text{th}}$  GPS station at time  $t_0$ , then it follows that:

$$E\{\mathbf{X}_n^r\} = \begin{cases} \mathbf{0} & \text{if } n < t_0, \\ \mathbf{b} & \text{if } n \geq t_0 \text{ and } r = i \end{cases} \quad (6.17)$$

where  $\mathbf{b}^T = [0, 0, 0, \delta_x^i, \delta_y^i, \delta_z^i, 0, 0, 0]$  = PMDEs represents the errors (or biases) in the three baseline components of the  $i^{\text{th}}$  GPS station.

In order to detect and isolate the faulty  $i^{\text{th}}$  GPS station, all combinations of receiver pairs are used to compute between-receiver differences of the baseline residuals in (6.16). This should give rise to three sequences of between-receiver differenced residuals. If an error(s) occurred in the solutions from one of the stations, then it would also exist in two of the between-receiver differenced residuals. Each component of these residuals is tested for a change-point. If two change-points are detected simultaneously, then the

isolation of the faulty receiver is realised by voting. The receiver that is common to the two between-receiver residuals with the change-points is the faulty receiver. This method is satisfactory for receiver fault detection applications when no more than one receiver fails at any one time.

### 6.3.2 Experiment at UNSW

Figure 6.6 shows the setup of an experiment that was carried out on the rooftop of the Electrical Engineering Building of The University of New South Wales (UNSW) on 26 November 2001. In the setup a total of four dual-frequency NovAtel GPS receivers were used to collect data at a 1 second data rate, over a period of more than twenty minutes. One receiver was designated as the base station, while the remaining three were the rover stations (designated as ROV1, ROV2, ROV3). The data were collected using specially developed UNSW software (RTFour). All four receivers were connected to a single PC via 4 RS232 serial cables joined together by a PCMCIA card. The data from the three rovers and the base station were logged simultaneously in binary format and post-processed using baseline software, also developed at UNSW. Baseline residuals for all the rovers were saved to the PC harddisk (Figure 6.7).

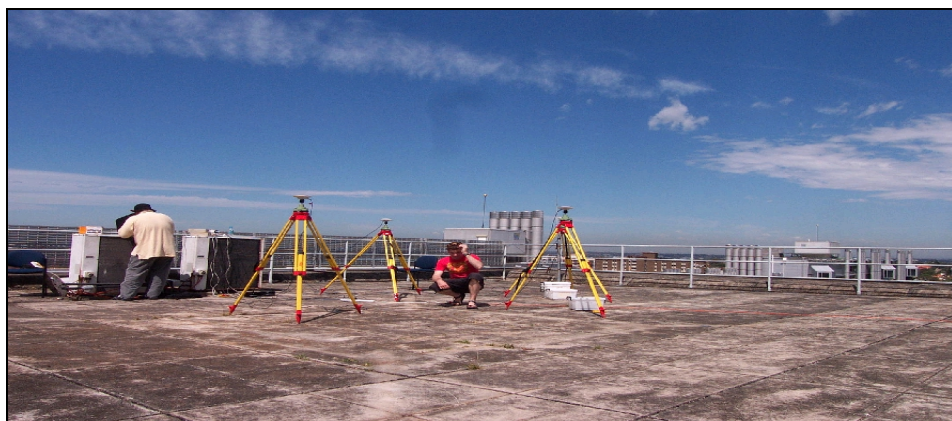


Figure 6.6. *Experimental setup at UNSW (26 November 2001)*



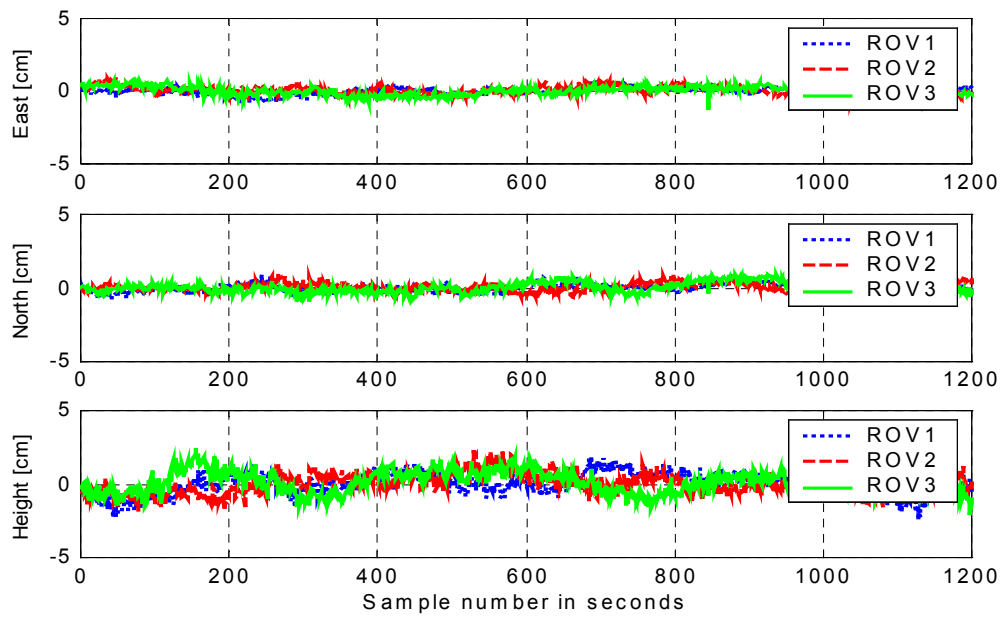


Figure 6.7. Time series of baseline residuals (UNSW – 26 November 2001)

Table 6.1. Sigmas for baseline residuals

Station	$\sigma_{\text{East}}$	$\sigma_{\text{North}}$	$\sigma_{\text{Height}}$
ROV1	$\pm 0.25$ cm	$\pm 0.26$ cm	$\pm 0.72$ cm
ROV2	$\pm 0.33$ cm	$\pm 0.32$ cm	$\pm 0.68$ cm
ROV3	$\pm 0.30$ cm	$\pm 0.35$ cm	$\pm 0.75$ cm

### 6.3.3 Data Normality and Statistical Independence

The basic detection approach upon which the CUSUM algorithms are based assumes that the data are normally distributed and are statistically independent of one another. The normality of the baseline residuals (Figure 6.7) can be studied through histogram or normal probability plots. For the sake of the present discussion the easting components of the baseline residuals (i.e. one-dimensional case) will be studied (only a matter of choice). Their normality is assessed using Figure 6.8, which indicates that these data are normally distributed. This can be further verified by inspection of the normal probability plots (Figure 6.9). The purpose of the probability plots is to assess whether these data follow a normal distribution. If the data are normally distributed the plots will be linear (as is the case), while other distribution types will introduce curvature into the

plots. Note that there is no restriction on which of the baseline components (East, North, Height) are processed for change detection, as long as they meet the normality requirement. However, caution should be exercised when using the height components as they are invariably the noisiest.

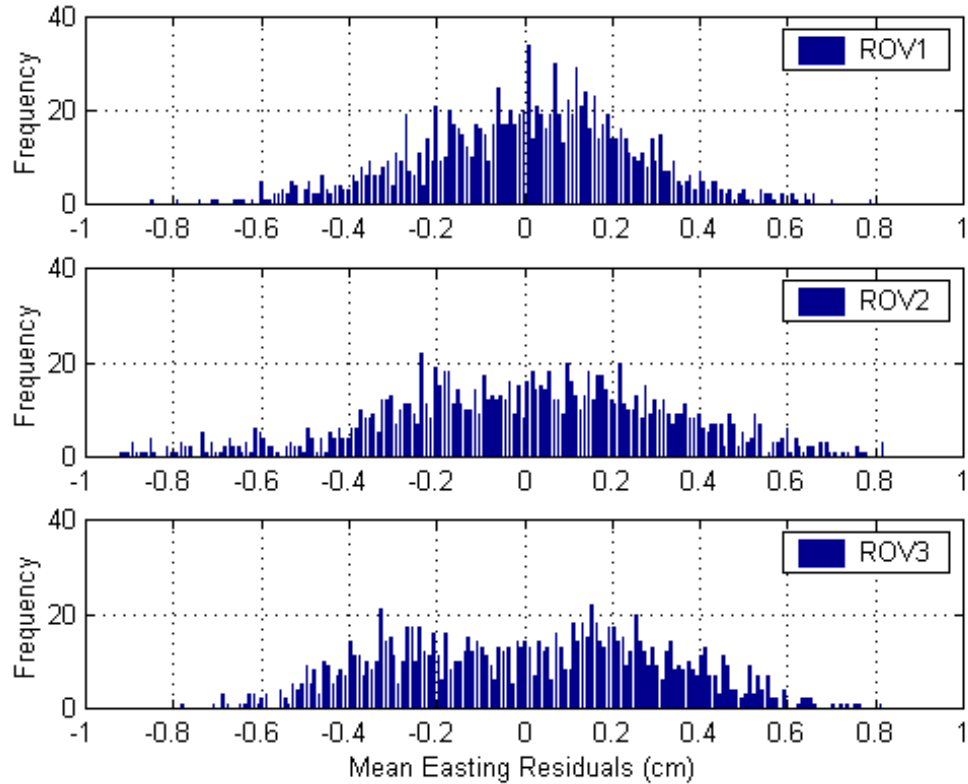


Figure 6.8. Normal Distribution histogram plots for Easting residuals

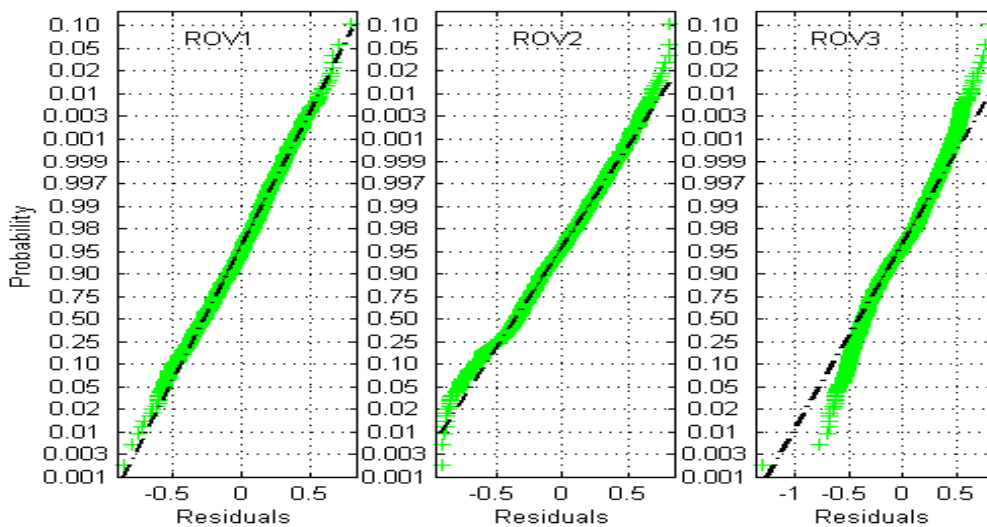


Figure 6.9. Normal Probability plots for Easting residuals

The requirement for statistical independence should also be taken seriously since correlation has a significant effect on the rate of false alarms. Observations that are taken close in time may have some degree of serial correlation, a problem that can be tackled by, for instance, using standardised variates (Mertikas, 2001). As far as the GPS measurements are concerned, Ge et al. (2000a) have recently demonstrated, through correlation analysis, that L1 and L2 phase measurements are truly and partially independent respectively for up to a 10Hz sampling rate. In Figure 6.10, correlation analysis indicates that the residuals are reasonably independent.

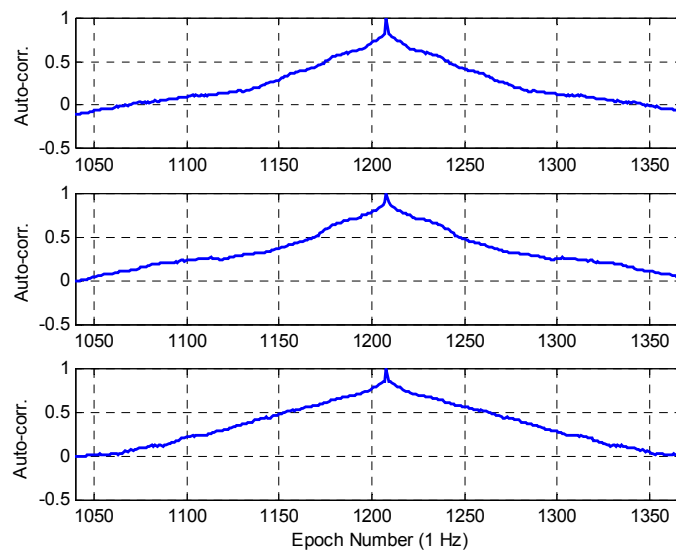


Figure 6.10. *Correlation analysis for Easting residuals*

### 6.3.4 Integrity Tests

Under normal operating conditions, the measurements from a GPS receiver array will contain valid information and experience normal random errors. If a failure occurs at one of the stations, then the measurements contain additional error term(s). The additional error terms can be masked by the signals if they are marginally small. For this reason the useful signals can be removed by using redundant measurements (Section 6.3.1). For example, for an individual baseline component (East, North or Height), the between-station difference of baseline residuals of two closely spaced stations can be used in order to remove useful signals. The data from the experiment (Figure 6.7) have

been shown to be normally distributed and statistically independent. Thus, they can be tested for errors (or biases) by using the multi-antenna approach described in Section 6.3.1. Three particular cases will be considered for the two-sided CUSUM algorithm.

**Case I: 1-sigma biases**

The first case considers that hypothetical biases are introduced into the ROV2 baseline residuals at the 430<sup>th</sup> sampling epoch, of the order of one standard deviation of those baseline residuals, as small persistent marginally detectable biases (1-sigma *PMDEs*). The magnitudes of the introduced hypothetical biases are shown in Table 6.2, while the corresponding time series of the baseline residuals after the biases are introduced is shown in Figure 6.11.

Table 6.2. 1-sigma *PMDEs*

Station	$\delta_{\text{East}}$	$\delta_{\text{North}}$	$\delta_{\text{Height}}$
ROV1	0.00 cm	0.00 cm	0.00 cm
ROV2	+0.33 cm	+0.32 cm	+0.68 cm
ROV3	0.00 cm	0.00 cm	0.00 cm

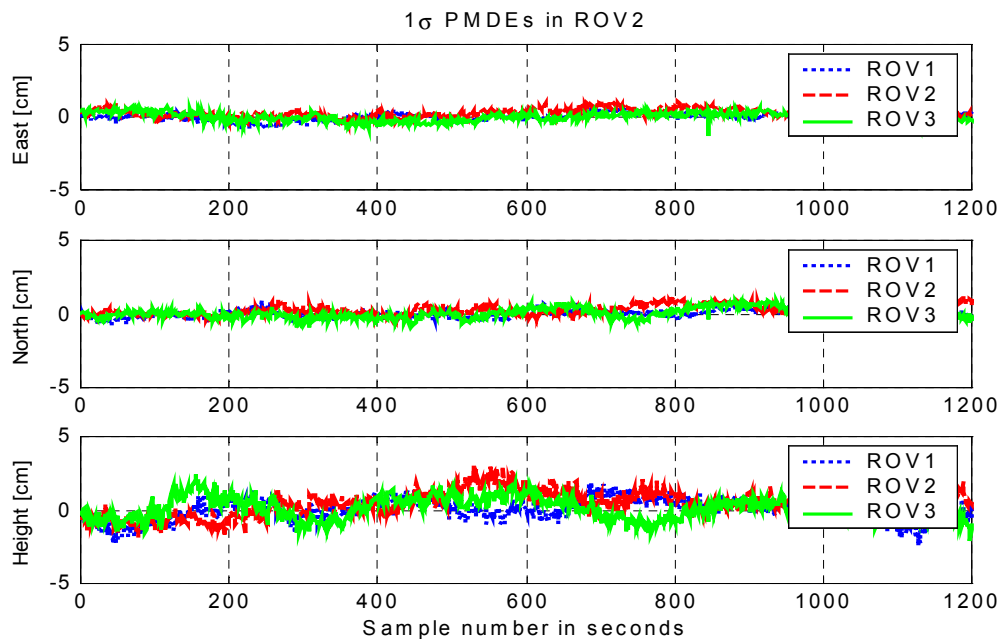


Figure 6.11. Time series of baseline residuals with 1-sigma biases (*PMDEs*) introduced into ROV2 components

**Case II: 2-sigma biases**

Similarly, in the second case, biases of the order of two standard deviations of the baseline residuals from ROV2 are introduced into those residuals at the 430<sup>th</sup> sampling epoch as hypothetical persistent biases. The magnitudes of the hypothetical biases are shown in Table 6.3, while the corresponding time series of the baseline residuals after the biases are introduced is shown in Figure 6.12.

Table 6.3. 2-sigma *PMDEs*

Station	$\delta_{\text{East}}$	$\delta_{\text{North}}$	$\delta_{\text{Height}}$
ROV1	0.00 cm	0.00 cm	0.00 cm
ROV2	+0.65 cm	+0.64 cm	+1.36 cm
ROV3	0.00 cm	0.00 cm	0.00 cm

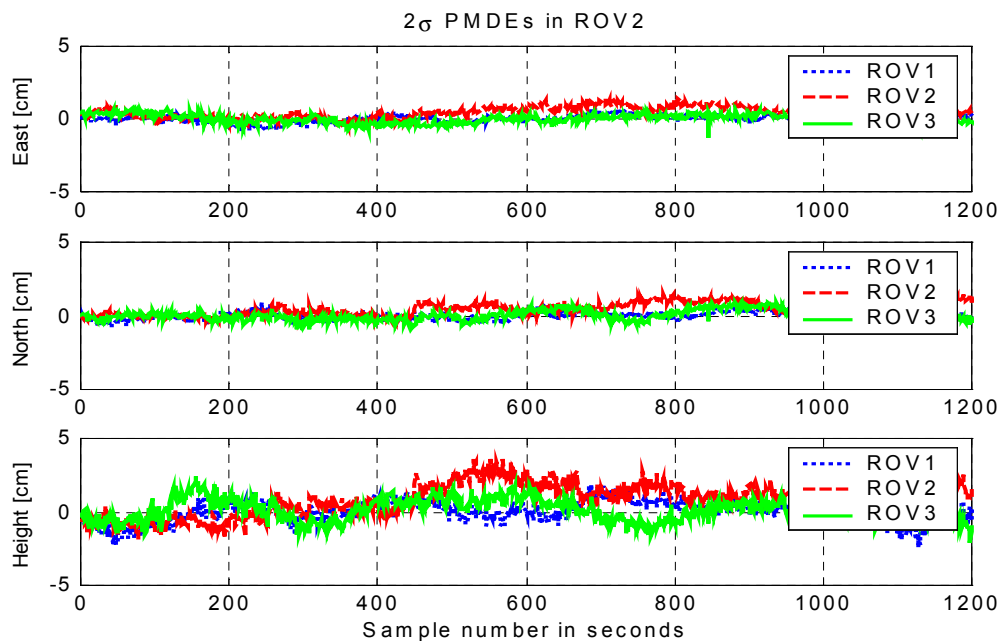


Figure 6.12. Time series of baseline residuals with 2-sigma biases (*PMDEs*) introduced into ROV2 components

**Case III: Abrupt "failure"**

The third case considers a hypothetical "failure" at the 430<sup>th</sup> sampling epoch for the ROV2 measurements (Figure 6.13).

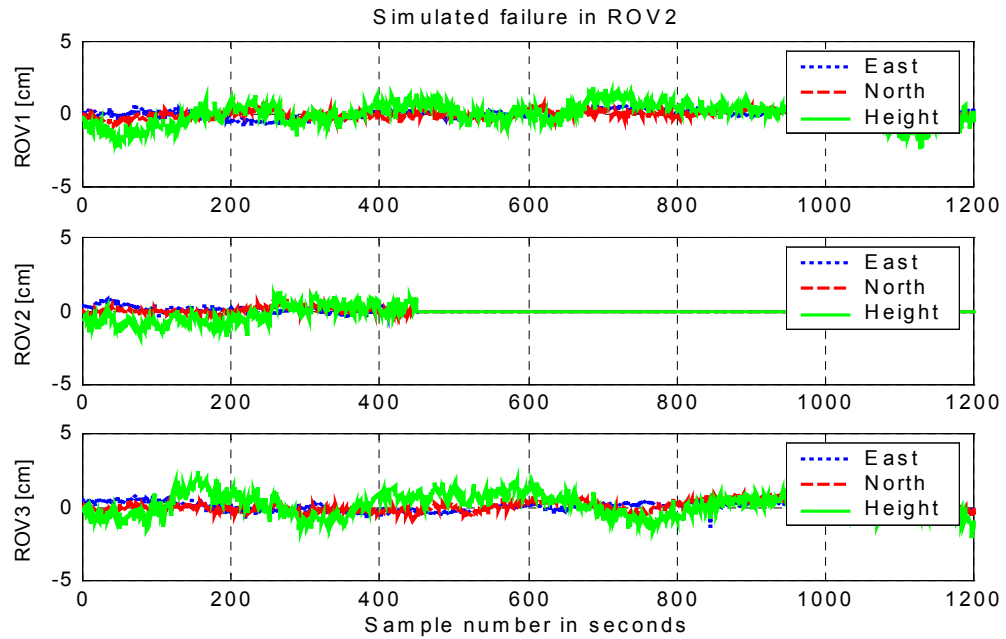


Figure 6.13. Hypothetical abrupt “failure” in the ROV2 components

For each of the three abovementioned cases, the minimal absolute value of anticipated bias  $|\nu|$  in the baseline residuals which leads to an inadmissible error (i.e., fault), but not necessarily obvious to the naked eye, is determined. For each rover, assume  $y_t$  to be the easting residuals. Thus, using the multi-antenna method, three innovation sequences  $y^{12}$ ,  $y^{13}$ ,  $y^{23}$  are obtained and processed by the two-sided CUSUM algorithm. Assume that a fault or bias is detected if an alarm is given by at least one of the two-sided tests in Equation (6.13). If alarms are given by the two two-sided tests processing the same baseline component (in this case the easting component), the isolation of the “failed” GPS station is realised by voting. For example, if alarms are detected in  $y^{12}$  and  $y^{23}$ , the following hypothesis:

$$\mathcal{H}_2 = \{\text{ROV2 is the biased GPS station}\}$$

is accepted.

The tuning parameters of the two-sided CUSUM test are the assumed change magnitude  $\nu$  and the detection threshold  $\lambda$ . The parameter  $\nu$  is selected for a typical random

noise sequence for a marginal bias (e.g.,  $1\text{-}\sigma$  or  $2\text{-}\sigma$  *PMDEs*). A bias which is lower than its minimal level does not lead to a sustained increase of the cumulative sum, hence an alarm does not occur. Consequently, the two-sided CUSUM algorithm is tuned for low values, and all biases (or failures) which have change magnitudes greater than this level will be detected.

The threshold  $\lambda$  of the two-sided CUSUM algorithm is selected in accordance with the desired (or specified) mean time between false alarms  $\bar{T}$  and the measurement sampling rate. Generally, the tuning parameters  $\nu$  and  $\lambda$  can be checked by using simulations, which takes into account the normal operating conditions of the monitoring system, failures of different kinds, etc.

The proposed scheme (a set of two-sided CUSUM + voting) has been tested on experimental data to generate the results shown in Figure 6.14.

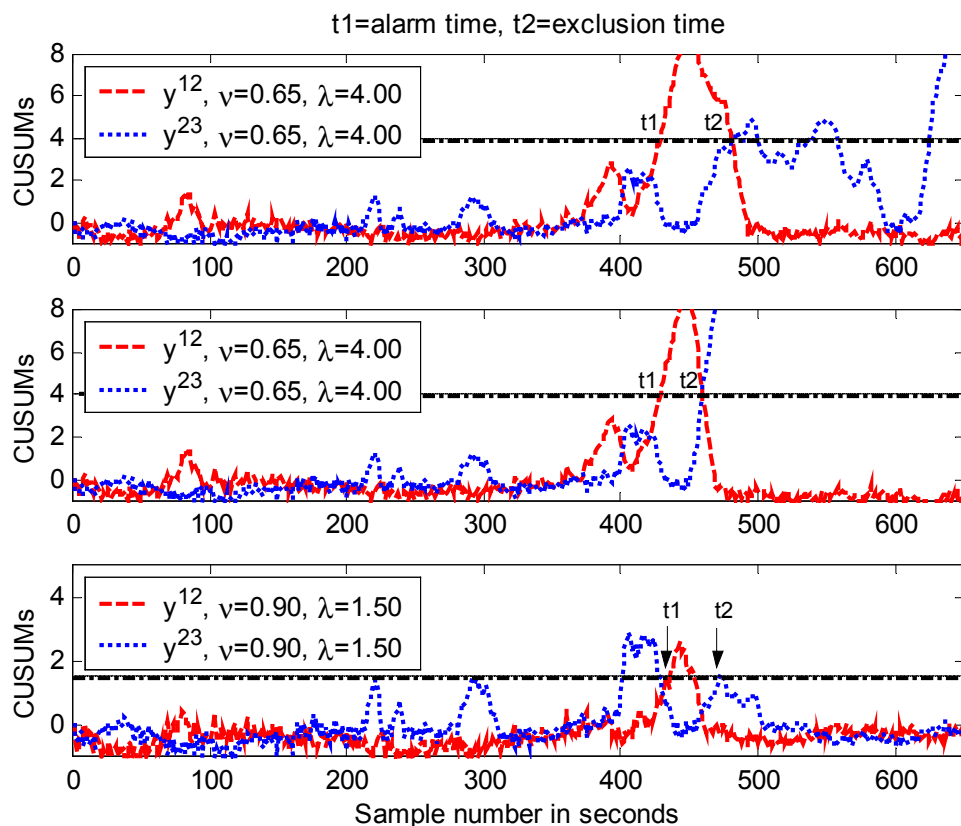


Figure 6.14. Bias/Failure detection and exclusion: 1-sigma case (top), 2-sigma case (middle), simulated failure (bottom)

With the GPS sampling rate of 1 second, the detection delay of alarm and exclusion of the failed station for the three cases considered are as follows (Figure 6.14):

- For the 1-sigma *PMDEs* case, the delay is about 1–80 seconds for detecting a 0.65 cm bias with the threshold  $\lambda=4.00$
- For the 2-sigma *PMDEs* case, the delay is about 1–30 seconds for detecting a 0.65 cm bias with the threshold  $\lambda=4.00$

For the failure case, the delay is about 1–40 seconds for detecting a 0.90 cm bias with the threshold  $\lambda=1.50$ . There is one false alarm.

The main conclusions of these tests are:

- The 1- $\sigma$  and 2- $\sigma$  biases, and "failure", were detected, and the responsible station isolated. The behaviour of the decision functions is shown in Figure 6.14.
- The behaviour of the tested residuals were in sufficiently good agreement with a normally distributed sequence of statistically independent samples.

Two of the benefits of using the two-sided CUSUM algorithm for this type of detection are: a) it is powerful at detecting small sustained changes in a zero-mean random noise environment, and b) it characterises the origin of such changes. The proposed scheme is therefore suitable for screening GPS position residuals for small persistent biases, especially in a monitoring application where deformation signals must be carefully interpreted.



## **7.1 Introduction**

The forms of analysis of deformational signal derived from different types of surveying data (conventional and GPS surveys) and geotechnical/structural measurements includes (USACE, 1994):

- **Geometrical analysis**, which describes the geometrical stability of the deformable structure, its change in shape and dimensions, as well as rigid body movements (translations and rotations) of the whole structure with respect to a stable reference frame. The results of the geometrical analysis of the actual deformations can be compared with the expected (or predicted) deformation to improve the understanding of the deformation mechanisms. Such prediction models can provide information on the expected deformation, hence facilitating the design of the monitoring scheme and the deformation analysis strategy.
  
- **Physical interpretation**, consisting of: (a) a stochastic component, which analyses the correlations between the observed deformation and observed loads (external and internal causes producing the deformation), and (b) a deterministic component, which utilises information on the loads, properties of the materials, and physical laws governing the stress-strain relationship, to describe the state of internal stresses and the relationship between the causative effects (loads) and the deformations. Deterministic and statistical modelling of deformations have been used in the analysis of dam deformations, at least in some countries, for many years.

Several software packages have been developed for the geometrical analysis of deformations. Some of them are limited to the analysis of geodetic survey (conventional and GPS) networks only, for example, the PANDA software (Niemeier & Tengen, 1988), and the GeoGenius<sup>®</sup> software (<http://www.terrasat.de/>), while others are applicable to the integrated analysis of any type of deformations (as discussed below).

In general deformation analysis consists of the identification of deformation models (displacement functions) and the estimation of deformation parameters. A vector of changes in any type of observations, for instance, changes in observed strain, in tilts, or in distances, can always be expressed in terms of the displacement function:

$$\Delta(x, y, z, t - t_0) = (u, v, w)^T \quad (7.1)$$

where  $\Delta$  is the displacement function of a point  $(x, y, z)$  at time  $t$  with respect to a reference time  $t_0$ ; and  $u$ ,  $v$ , and  $w$  are components of the displacement function in the  $x$ -,  $y$ -, and  $z$ -directions respectively. Examples of typical deformation models (displacement functions) in 2-D analysis include (USACE, 1994):

- The model for homogeneous strain in the whole body and differential rotation, which may be expressed in terms of the strain components  $(\varepsilon_x, \varepsilon_y, \varepsilon_{xy})$  and differential rotation  $(\varpi)$ :

$$\begin{bmatrix} u \\ v \end{bmatrix} = \begin{bmatrix} \varepsilon_x & \varepsilon_{xy} \\ \varepsilon_{xy} & \varepsilon_y \end{bmatrix} \begin{bmatrix} x \\ y \end{bmatrix} + \begin{bmatrix} -\varpi y \\ \varpi x \end{bmatrix} \quad (7.2)$$

- For a horizontal tiltmeter, the change  $d\tau$  of tilt between two survey campaigns may be expressed in terms of the vertical component ( $w$ ) of the displacement function:

$$d\tau = (\partial w / \partial x) \sin \alpha + (\partial w / \partial y) \cos \alpha \quad (7.3)$$

where  $\alpha$  is the orientation angle of the tiltmeter.

- The relationship between a displacement function and a change  $ds$ , in the distance observed between two points  $i$  and  $j$ , in two monitoring campaigns (epochs) may be written as:

$$ds_{ij} = [(x_j - x_i / s)]u_j + [(y_j - y_i / s)]v_j - [(x_j - x_i / s)]u_j + [(y_j - y_i / s)]v_j \quad (7.4)$$

where  $u_j$ ,  $v_j$ ,  $u_i$ , and  $v_i$  are components of the displacement function at points  $(x_j, y_j)$  and  $(x_i, y_i)$  respectively.

The "best" deformation model (or displacement function) is based on either *a priori* knowledge of the expected deformations (for instance, from finite element analysis), or a qualitative analysis of the deformation trend from all the observations taken together. In the case where observables are relative displacements (e.g., from conventional and/or GPS surveys), if a series of observations are taken over a long period of time, plotting of the individual (averaged) observables versus time helps to establish the deformation trend and the deformation model in the time domain. However, any data, or derived data, whether geotechnical or geodetic (so long as it has been repeated in a suitable time series), can be brought together in an integrated deformation analysis. In the process a time series is analysed for trend, with the separation of systematic and long-term behaviour. Thus, the data ("y", the change in the value of an observed or derived quantity) against time ( $t$ ) is described by the function:

$$y = \alpha_0 + \alpha_1 \cos(\omega t) + \alpha_2 \sin(\omega t) + \alpha_3 t + \alpha_4 \delta(t_i) + \dots \quad (7.5)$$

in which

$\alpha_0$  = the y-intercept,

$\alpha_1, \alpha_2$  = constants for deriving the cyclic deformation parameters,

$\alpha_3$  = the "rate" or long-term trend, and

$\alpha_4$  = possible values of slips accounting for discontinuities in the data.

For the near-real-time or real-time analysis of data from a monitoring system, the observation data ought to be generated more frequently. One of the challenges is then to convert the high frequency observations into information as soon as possible. In that case, Equation (7.5) may be adopted only to the order of the first three terms, to estimate the period (or phase) and amplitude as the short-term deformation parameters. Such an approach will assume that the long-term trend,  $\alpha_3$ , is not of interest and that there are no slips,  $\alpha_4$ , in the data. Based on such assumptions, the following section will discuss the estimation of fast deformation parameters from high frequency RTK-GPS measurements.

## 7.2 Estimating Fast Deformation Parameters

### 7.2.1 Fast Fourier Spectra

State-of-the-art GPS receivers with high sampling rates of up to 10Hz have recently become available and can be used to track high-frequency deformation signals. For real-time deformation measurements, it has been shown (e.g., Ge et al., 2000) that at such high sampling rates that RTK-GPS measurements are, respectively, truly and partially independent in the carrier phase and pseudo-range modes. In order to obtain real-time deformation information one needs to deal with the errors and biases associated with such measurements. If the interest is to track high-frequency deformation (say,  $> 0.05\text{Hz}$ ), then the multipath effect (typical multipath errors have sinusoidal oscillations of periods of 6–10 minutes (0.001–0.003Hz) (Qiu, 1993)) can be ignored. However, high rate RTK normally produces noisy results, which may obscure cyclic deformations of smaller magnitudes. Thus, from Equation (7.5), consider that a one-dimensional sequence of GPS measurements (i.e., a single baseline component) may be written as:

$$y(t) = \alpha_0 + \alpha_1 \cos(\omega t) + \alpha_2 \sin(\omega t) + \varepsilon(t) \quad (7.6)$$

where  $\varepsilon(t)$  is the random noise term at time  $t$ .

Spectrum analysis through Fourier transformation is a common method of mapping time series (e.g. fast RTK-GPS data) into its frequency domain. The discrete time series  $y(t)$  can be expressed in terms of the Fourier progression (e.g. Blais, 1988):

$$y(t) = A_0 + \sum_{n=1}^{\infty} (a_n \cos 2\pi nft + b_n \sin 2\pi nft) \quad (7.7a)$$

$$= A_0 + \sum_{n=1}^{\infty} A_n \sin(2\pi nft + \phi_n) \quad (7.7b)$$

where  $f = 1/T$  is the dominant frequency of  $y(t)$ ;  $T$  is the period;  $A_n = \sqrt{a_n^2 + b_n^2}$  is the amplitude of the Fourier progression; and  $\phi_n = \tan^{-1}(a_n/b_n)$  is the phase spectrum of the Fourier progression.

If  $N$  is of the form  $N = 2^L$ , where  $L$  is a positive integer, and  $y(t_k)$  is the discrete observation at time  $t_k$  ( $k = 0, 1, 2, \dots, N-1$ ):

$$a_n = \frac{2}{N} \sum_{k=0}^{N-1} y(t_k) \cos 2\pi nk / N, \text{ and } b_n = \frac{2}{N} \sum_{k=0}^{N-1} y(t_k) \sin 2\pi nk / N \quad (7.8)$$

where  $n = 1, 2, \dots, M$ , and  $M$  satisfies the condition  $N \geq 2M + 1$ . Generally, the spectrum analysis involves computing the coefficients in Equation (7.8) and knowing  $f$  over  $N$ .

### 7.2.2 Experiment at UNSW

Based on the above considerations, a trial experiment with RTK-GPS was carried out on 24 January 2001, on the rooftop of the Geography and Surveying Building, at The University of New South Wales (UNSW), to measure vibrations. A baseline of approximately 10m was established and the observations were made over a period of 1 hour 50 minutes (see Table 7.1).

The setup included two Leica CRS1000 GPS receivers, a signal generator and a mechanical shaker. The base station antenna was set up on one of the astronomical pillars while the 'rover' antenna sat on top of the mechanical shaker (Figure 7.1). Corrections generated at the base station were communicated to the 'rover' receiver through a RS232 cable connection, and RTK position results were recorded at a 10Hz sample rate. The signal generator supplied the mechanical shaker with random sine waves of both 'low' and 'high' frequencies within the range of 0.2Hz to 5Hz, simulating the response of a dynamic structure under varying loading conditions. The 'low' frequencies were selected so that they were representative of values determined from past structural monitoring experiments (e.g., Celebi et al., 1998; Guo & Ge, 1997; Lovse et al., 1995). The 'high' frequency values simulate the scenario of fast changing vibrations during the onset of some extreme loading event, such as an earthquake or typhoon. Table 7.1 gives information concerning the design of the experiment over a period of 1 hr 50 mins, with the corresponding RTK-GPS time series over the period also plotted in Figure 7.2. Note that only the height component results were selected for analysis since the mechanical shaker was excited only in the vertical direction.



Figure 7.1. *The experiment at UNSW (24th January 2001) -- The 'rover' antenna atop the mechanical shaker*

Table 7.1. *The test frequencies for the experiment at UNSW*

Time	Frequency	Antenna Orientation
'high' frequency		
11:30 - 11:40	DC	Vertical
11:40 - 11:50	2.0Hz	Vertical
11:50 - 12:00	3.0Hz	Vertical
'low' frequency		
12:00 - 12:10	DC	Vertical
12:10 - 12:20	0.2Hz	Vertical
12:20 - 12:30	0.3Hz	Vertical
'low' frequency		
12:30 - 12:40	0.5Hz	Vertical
12:40 - 12:50	0.7Hz	Vertical
'high' frequency		
12:50 - 13:00	1.2Hz	Vertical
13:00 - 13:10	1.4Hz	Vertical
13:10 - 13:20	1.7Hz	Vertical

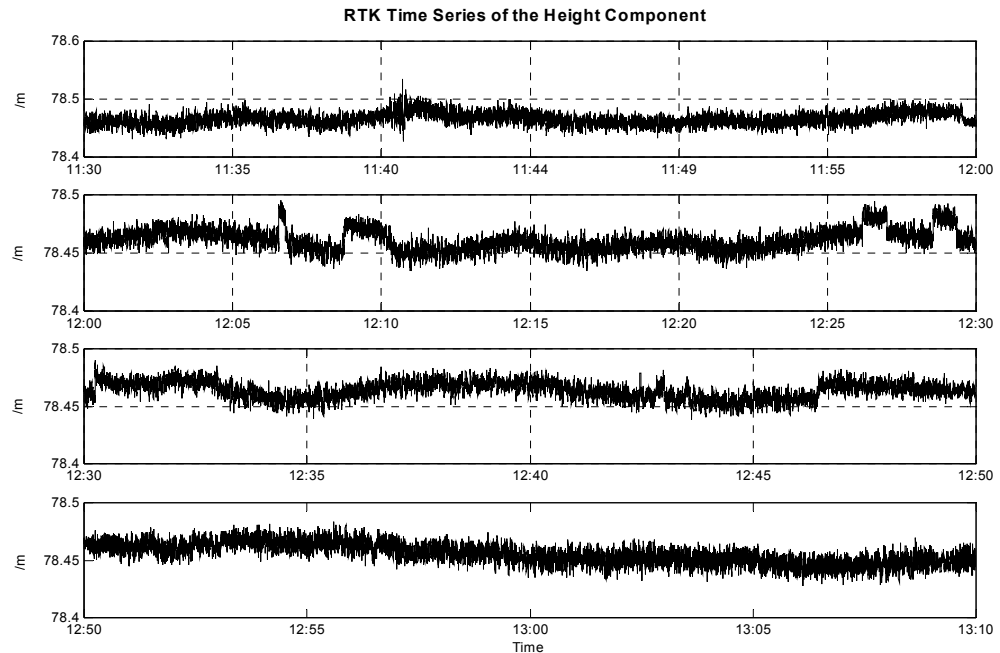
Figure 7.2. *RTK-GPS time series of the height component (UNSW, 24 Jan. 2001)*

Figure 7.3 gives the RTK-GPS time series and the corresponding Fourier amplitude spectra. Note that for the distinctive shaker motions (or vibrations), their amplitudes varied from 4mm to 6mm. For the low frequency bands (0 – 2Hz), there is a concentration of amplitudes of 2mm and higher in the very low frequency part of the spectrum (0 – 0.05Hz). This approximately represents the random noises (and other noises of unknown source) as well as multipath errors (0.001 – 0.003Hz).

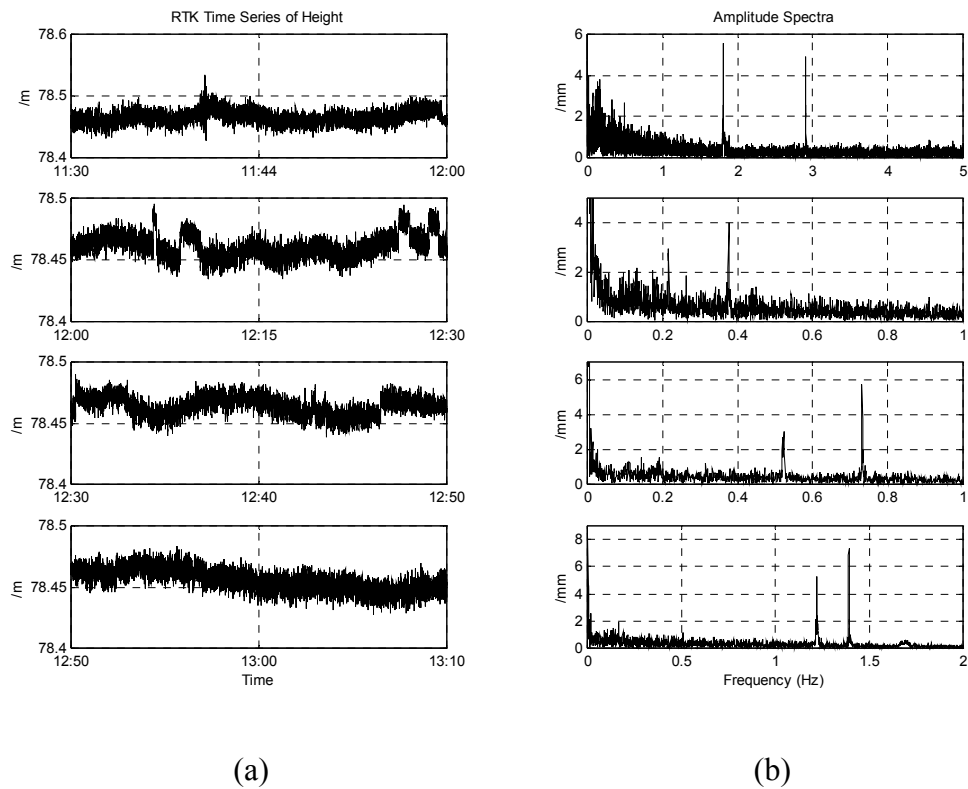


Figure 7.3. High frequency RTK-GPS time series (a) and corresponding amplitude spectra (b)

The spectrum analysis has shown that high frequency RTK-GPS measurements reveal signatures (frequency and amplitudes) due to short period motions. However, the spectrum analysis result shown in Figure 7.3 can only give such information over the whole of the time span of such measurements, and hence information about the "exact" times when the motions occurred is lost. A procedure that can approximate the spectrum (frequency and amplitude) on a time basis would be useful for monitoring purposes. This is the basis of the following discussion.



### 7.2.3 On-line Estimation

#### 7.2.3.1 Time-Frequency Approach

To monitor the periodic behaviour of fast deformation signals, an online estimation of frequencies (with amplitudes) can be implemented. For such a requirement, two basic assumptions should be made about the GPS measurements. The first assumption is that the spectral content of the RTK-GPS results are time-varying. Secondly, the GPS sampling rate must obey the *Nyquist sampling theorem* (see, e.g., Blais, 1988; Embree, 1995; Embree & Danieli, 1999; Haykin, 1995): that is, for a band limited signal, the signal can be recovered from discrete sampled values if the sampling rate is  $f_s \geq 2f_{\max}$  where  $f_{\max}$  is the highest frequency in the signal. This condition was met in the experiment for which  $f_s$  was 10Hz and the highest frequency recovered in the spectrum analysis was 3Hz.

The issue of estimating the instantaneous frequency (IF) of a signal has been intensively researched and many estimators have been proposed, across several applied fields (e.g. Boashash, 1992; Petranovic et al., 1997; Rao & Taylor, 1990; Stankovic & Katkovnik, 1998). In particular, Boashash (1992) has presented a very good review of the various estimation techniques:

- a) *The general phase difference IF estimators*
- b) *Zero-crossing IF estimators*
- c) *Adaptive IF estimators (Least-Mean-Square (LMS) & Recursive-Least-Squares (RLS) estimators)*
- d) *IF Estimators Based on the moments of Time-Frequency Distributions (TFD)*
- e) *Time-Varying Autoregressive (AR) Model Based IF Estimators*
- f) *IF Estimators Based on the Peak of TFDs (peak of the Short-Time-Fourier-Transform (STFT) and Wigner-Ville Distributions (WVDs))*

In this research, for the sake of simplicity, the STFT will be applied to estimate the time-frequency of RTK-GPS data, which will be denoted as  $f_{\kappa}$ .

The STFT is a two-dimensional time-frequency representation algorithm  $STFT(t, f)$  of the signal  $y(t)$ , composed of spectral characteristics depending on time, with the local frequency  $f_\kappa$  being defined through an appropriate definition of  $STFT(t, f)$ . In a discrete sense, the STFT is defined by assuming that the signal  $y(t)$  is stationary when seen through a window  $\gamma(t)$  of short time duration, centred at time location  $\kappa$ . Thus (Qian & Chen, 1996):

$$STFT[\kappa, n] = \sum_{i=0}^{L-1} y[i] \gamma[i - \kappa] W_L^{-ni} \quad (7.9a)$$

where

$$STFT[\kappa, n] \equiv STFT(t, f) \Big|_{t=\kappa\Delta t, f=2\pi n/(L\Delta t)}, \text{ and } W_L = \exp\left\{j \frac{2\pi}{L}\right\} \quad (7.9b)$$

and where  $\Delta t$  denotes the time sampling interval.  $\gamma[\kappa] \equiv \gamma(\kappa\Delta t)$  is the  $L$ -point window function. Figure 7.4 depicts the procedure for computing the STFT, that is, first multiply the function  $\gamma(t)$  with the signal  $y(t)$  and then compute the Fourier transform of the product. Moving  $\gamma(t)$  and repeating the process gives the signal's local frequencies over time.

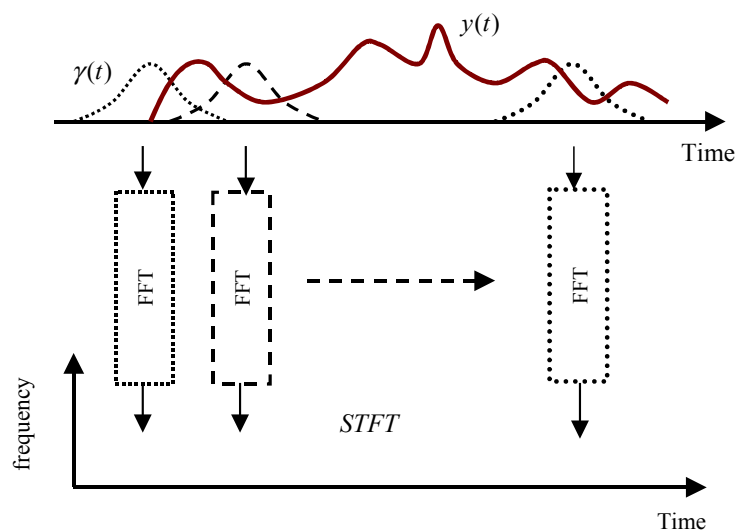


Figure 7.4. Short-Time Fourier Transform

At the time location  $\kappa$ , the frequency  $f_{\kappa}$  that maximises the STFT over the selected window is identified. Thus the time location of each frequency is known, as opposed to the global Fast Fourier Transform (FFT) analysis, which only gives the frequency composition of a signal under the assumption that all of the component frequencies are present from the origin to the end of the 'infinite' signal. If the RTK-GPS sample rate is high enough (e.g. in the range 1–10Hz), the STFT will give rise to a sequence  $f_{\kappa} (\kappa = 1, 2, \dots)$  whose mean and variance can be defined. The sequence can then be tested for changes in its mean value.

### 7.2.3.2 On-line Analysis

For on-line frequency tracking, the CUSUM algorithm (Section 6.2.2) is implemented as follows.

The time-dependent frequency estimates  $f_{\kappa} (\kappa = 1, 2, \dots)$  are assumed to have the initial mean value of  $\mu_0$ , and a new mean  $\mu_1$  after some change has occurred. For practical cases, the two-sided CUSUM algorithm is used to test for the unknown change time. Hence, two tests are run in parallel, corresponding to an *a priori* minimum detectable change  $\nu$ , and in two possible directions (increase or decrease in the mean). For a decrease:

$$\begin{cases} S_0 = 0 \\ S_{\kappa} = \sum_{j=1}^{\kappa} \left( f_j - \mu_0 + \frac{\nu}{2} \right) \\ Mx_{\kappa} = \max_{0 \leq j \leq \kappa} S_j \\ \text{alarm when } Mx_{\kappa} - S_{\kappa} > \lambda \end{cases} \quad (7.10)$$

and for an increase:

$$\begin{cases} S_0 = 0 \\ S_{\kappa} = \sum_{j=1}^{\kappa} \left( f_j - \mu_0 - \frac{\nu}{2} \right) \\ Mn_{\kappa} = \min_{0 \leq j \leq \kappa} S_j \\ \text{alarm when } S_{\kappa} - Mn_{\kappa} > \lambda \end{cases} \quad (7.11)$$

The decision which is taken corresponds to the rule which stops first, and the estimate of the change time is the last maximum (respectively minimum) time before detection.

An alternative approach in the case of the unknown jump magnitude  $\nu$  may consist of replacing it by its Maximum Likelihood Estimate (MLE) (see, e.g., Ogaja, 2001).

#### 7.2.4 Test Example

The proposed frequency tracking methodology was tested using the data from the RTK-shaker experiment. Figures 7.5a, 7.5b, 7.5c, and 7.5d show a selection of the test results. In each of the figures a section of the noisy RTK-GPS time series containing the change-point is plotted in the top panel on the left. The results are very noisy due to the random observational errors. Thus any information concerning frequency will not be obvious to the unaided eye. The plots in the bottom panels on the left are the Fourier transforms, which reveal the occurrence of different frequencies in the original time series data, but cannot indicate when the particular components occurred within the data. The plots in the top panels on the right show the instantaneous frequencies obtained using the STFT algorithm. They indicate that a change has occurred in the frequency at some point. This change could be detected using the two-sided CUSUM algorithm. The plots in the bottom panels on the right show the change detector given by testing the log-likelihood ratio of the CUSUM algorithm against a threshold under the hypothesis that 'the mean of frequency has changed'.

The CUSUM algorithm operates under the assumption that the data are statistically independent. With respect to the frequency estimation, the important factor in reducing serial correlation is the number of samples between successive estimation – the time resolution. The upper limit on the time resolution is one sample. However, a resolution

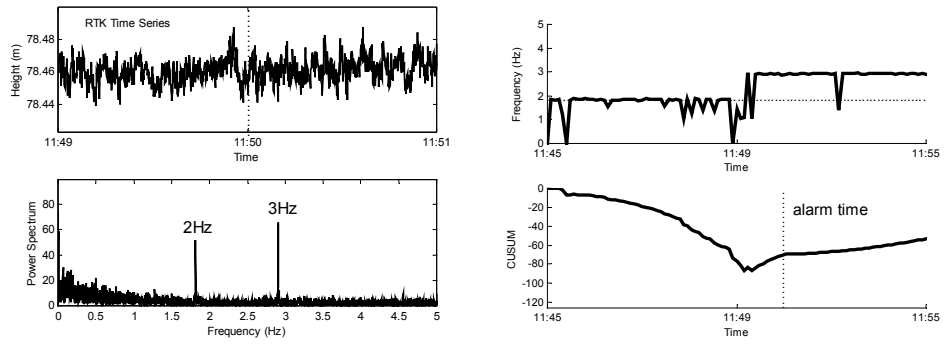


Figure 7.5a. Power spectrum (Left) and IF tracking (Right) for 2–3Hz

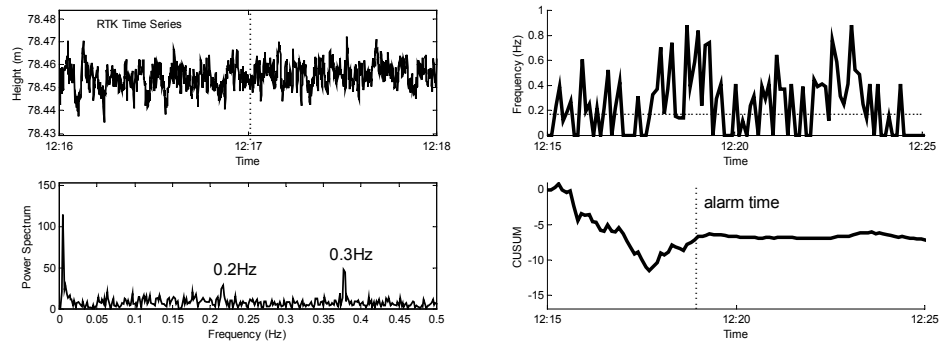


Figure 7.5b. Power spectrum (Left) and IF tracking (Right) for 0.2–0.3Hz

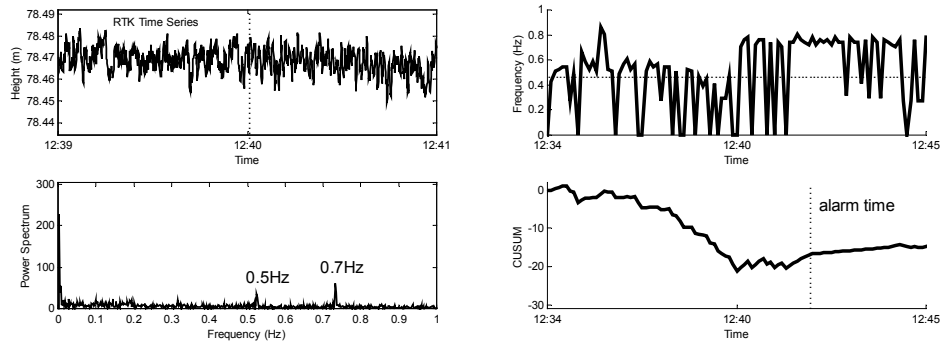


Figure 7.5c. Power spectrum (Left) and IF tracking (Right) for 0.5–0.7Hz

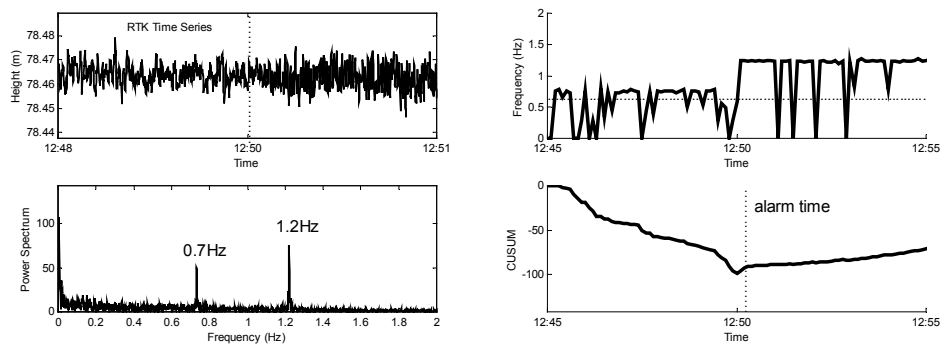


Figure 7.5d. Power spectrum (Left) and IF tracking (Right) for 0.7–1.2Hz

of 16-64 samples is taken to be adequate for most applications. Thus, the time resolution was defined to be 60 samples, which is a multiple of the GPS sample rate, in order to produce the estimates at time instants without overlapping between the FFT bins. A typical FFT length of 512 points for the STFT, which implies a frequency resolution of 256 points, was applied. A higher frequency resolution is desired as well as a low time resolution.

For the online monitoring process, the initial mean of the IF estimates was defined to be computed in real-time, through the self-starting CUSUM. Hence, the running mean and standard deviation values were updated sequentially. For each case of detection, the anticipated jump and threshold values were tuned for the minimum number of false alarms and minimum delay.

### **7.3 Multivariate Analysis**

#### **7.3.1 Introduction**

In the overall effort of deformation analysis, a large volume of observations are required, both of causative quantities (wind velocity, temperature, pressure) and of response effects (e.g., accelerations, displacements, tilt, strain, etc.). It is generally expected that if long sets of observation data are available, portions of the response data would be strongly correlated with the changes in wind, temperature or pressure effects.

This section discusses a methodology in which long observations are analysed to obtain an indicator of the status of monitoring (for trigger conditions), which can then aid the analysis of RTK-GPS data for fast deformations (Section 7.2). The benefit of the approach is that excess data generated online is reduced, while maintaining a timely response analysis with the RTK-GPS data (since they can give direct coordinate results for the near-real-time knowledge of the system). The term "multivariate process" is referred to the GPS measurements along with those of other sensors, such as accelerometers, anemometers, temperature sensors, and so forth.

The proposed methodology is based on a multivariate statistical process control (SPC) in which the mean of the multivariate process is monitored by using a multivariate statistic. The term "in-control" is used to indicate that the process is on-target (i.e, close to a constant value such as zero, mean, standard deviation) with respect to its mean. Conversely, the term "out-of-control" is used to indicate that the mean of the multivariate process has changed. In the first instance it is assumed that the process dispersion is stable and is not prone to changes.

### 7.3.2 Multivariate Statistical Process Control

It is common to use the SPC approach to chart a small number of variables, and examine them one at a time (Shewhart, cumulative sum (CUSUM) or exponentially weighted moving average (EWMA) charts). For example, the CUSUM algorithm, which was described earlier in Chapter 6, is for a single variable (a baseline component) of one measurement type (i.e., GPS positioning). However, when a process is defined by more than one measurement type (GPS positioning, accelerations, wind velocities, temperature, etc.), all the measurement properties may be studied collectively. In such a case, Multivariate SPC (MSPC) charts that have been developed for the purpose of studying variables of different properties may be used. The MSPC charts have been based on the chi-squared statistic or on Hotelling's  $T^2$  statistic (Gnanadesikan, 1997; Jackson, 1985; Pignatiello & George, 1990; Sullivan & Woodall, 1996). The traditional MSPC approach is discussed by Kourti & MacGregor (1996), and can be summarised as follows.

Given a vector of measurements  $\mathbf{z}$  of  $n$  normally distributed variables, with an in-control covariance matrix  $\Sigma$ , one can test whether the current mean of the multivariate process is at its population mean  $\boldsymbol{\mu}$ , by computing the statistic:

$$\chi^2 = (\mathbf{z} - \boldsymbol{\mu})^T \Sigma^{-1} (\mathbf{z} - \boldsymbol{\mu}) \quad (7.12)$$

The statistic in Equation (7.12) will be distributed as a central chi-squared distribution with  $n$  degrees of freedom if the mean is equal to  $\boldsymbol{\mu}$ . A multivariate chi-squared chart

can be constructed by plotting  $\chi^2$  versus time with an upper control limit (UCL) given by  $\chi_{\alpha,n}^2$ , where  $\alpha$  is an appropriate significance level for performing the test (e.g.,  $\alpha = 0.01$  or  $\alpha = 0.05$ ). The  $\chi^2$  statistic in Equation (7.12) represents the directed or weighted distance (Mahalanobis distance) of any point from  $\boldsymbol{\mu}$ .

For two variables  $z_1, z_2$ , if Equation (7.12) is set equal to  $\chi_{\alpha,n}^2$ , the solution in the  $z_1, z_2$ -space is an ellipse centered at  $\boldsymbol{\mu}$ . All points on the ellipse have the same Mahalanobis distance,  $\chi_{\alpha,n}^2$ . One can plot the variables against each other and check if the points fall within the elliptical control region, with the same degree of confidence (the perimeter of the ellipse corresponds to the UCL of the chart).

When the in-control covariance matrix  $\boldsymbol{\Sigma}$  is not known and must be estimated from a limited amount of data, it is more appropriate to plot Hotelling's  $T^2$  statistic:

$$T^2 = (\mathbf{z} - \boldsymbol{\mu})^T \mathbf{S}^{-1} (\mathbf{z} - \boldsymbol{\mu}) \quad (7.13)$$

where  $\mathbf{S}$  is an estimate of  $\boldsymbol{\Sigma}$ . An upper control limit  $T_{\text{UCL}}^2$  is then obtained based on the  $F$  distribution, and depends upon the degrees of freedom available for the estimate  $\mathbf{S}$  (Jackson, 1985; Seber, 1984; Gnanadesikan & Kettenring, 1972). For a new  $n \times 1$  multivariate observation vector and an estimate  $\mathbf{S}$  based on  $m$  past multivariate observations (Kourti & MacGregor, 1996):

$$T_{\text{UCL}}^2 = \frac{(m^2 - 1)n}{m(m - n)} F_{\alpha}(n, m - n) \quad (7.14)$$

where  $F_{\alpha}(n, m - n)$  is the upper  $100\alpha\%$  critical point of the  $F$  distribution with  $(n, m - n)$  degrees of freedom.

The  $T^2$  in Equation (7.13) can also be expressed in terms of the principal components of the multinormal variables (Ibid, 1996):



$$T^2 = \sum_{a=1}^n \frac{s_a^2}{e_a} = \sum_{a=1}^n \frac{s_a^2}{\sigma_a^2} \quad (7.15)$$

where  $e_a$ ,  $a = 1, 2, \dots, n$ , are the eigenvalues of  $\mathbf{S}$  (variances of principal components),  $s_a$  are the scores from the principal component transformation, and  $\sigma_a^2$  is the variance of  $s_a$ . Each score  $s_a$  can be expressed as:

$$s_a = \mathbf{p}_a^T (\mathbf{z} - \boldsymbol{\mu}) = \sum_{j=1}^n p_{a,j} (z_j - \mu_j) \quad (7.16)$$

where  $\mathbf{p}_a$  is the eigenvector of  $\mathbf{S}$  corresponding to  $e_a$ , and  $p_{a,j}$ ,  $z_j$ ,  $\mu_j$  are elements of the corresponding vectors associated with the  $j^{\text{th}}$  variate.

Alternatively other types of multivariate charts, such as Multivariate CUSUM and Multivariate EWMA charts, may be used.

### 7.3.3 Test Example

Consider the data plotted in Figure 7.6. These represent components in the differential easting (GPSE) and northing (GPSN) of GPS observations, the corresponding wind velocity (UE & UW), the accelerometer response ( $\delta E$  &  $\delta N$ ) and temperature (T). These measurements were made on the rooftop of Singapore's tallest building, the Republic Plaza Building, during a pilot experiment executed between 17 and 25 February 2000. The original GPS data were measured using two Trimble 4700 receivers ( $\pm 1$  cm horizontal accuracy and  $\pm 2$  cm stated vertical accuracy) sampling at 1Hz. The wind velocity data and accelerometer response were recorded using two UVW Gill windmaster anemometers (recording U, V, and W components of the wind) and QA-700 accelerometers (located on Basement 1) respectively. The resolutions of the QA-700 accelerometers and the Gill windmaster anemometers are 1 micro-g ( $\approx 0.01$  mm/s<sup>2</sup>) and 0.01 m/s for wind speed and 1° for wind direction respectively. The temperature sensors

were accurate to about  $0.5^{\circ}\text{C}$ . The reference station for the GPS sub-system was located on the rooftop of a nearby low-rise building approximately 1km away. This experiment covered two periods of maximum wind conditions reaching more than 10 m/s, during 19 and 22 February 2000.

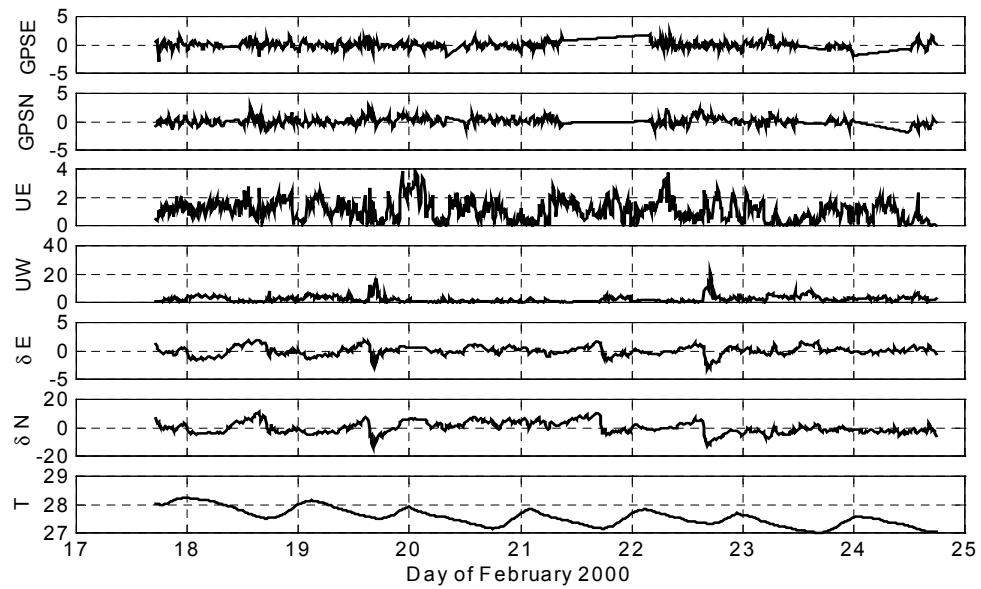


Figure 7.6. *Simultaneous GPS positioning, wind, accelerometer and temperature sensor data. Units: GPSN [cm], GPSE [cm], UE [m/s], UW [m/s],  $\delta E$  [mm/s<sup>2</sup>],  $\delta N$  [mm/s<sup>2</sup>],  $T$  [ $^{\circ}\text{C}$ ]*

The experiment involved simultaneous measurement of multivariate data consisting of seven variables: two horizontal GPS positioning components (GPSN & GPSE), two wind velocity vector components (UE & UW), two accelerometer response vector components ( $\delta E$  &  $\delta N$ ), and one temperature vector component ( $T$ ). The normality of the individual variables is studied through the normal distribution plots in Figure 7.7. The components (GPSN, GPSE,  $\delta E$ ,  $T$ ) are individually normally distributed. However, the components (UE, UW,  $\delta N$ ) appear to be skewed (indicating that outlying data may be present).

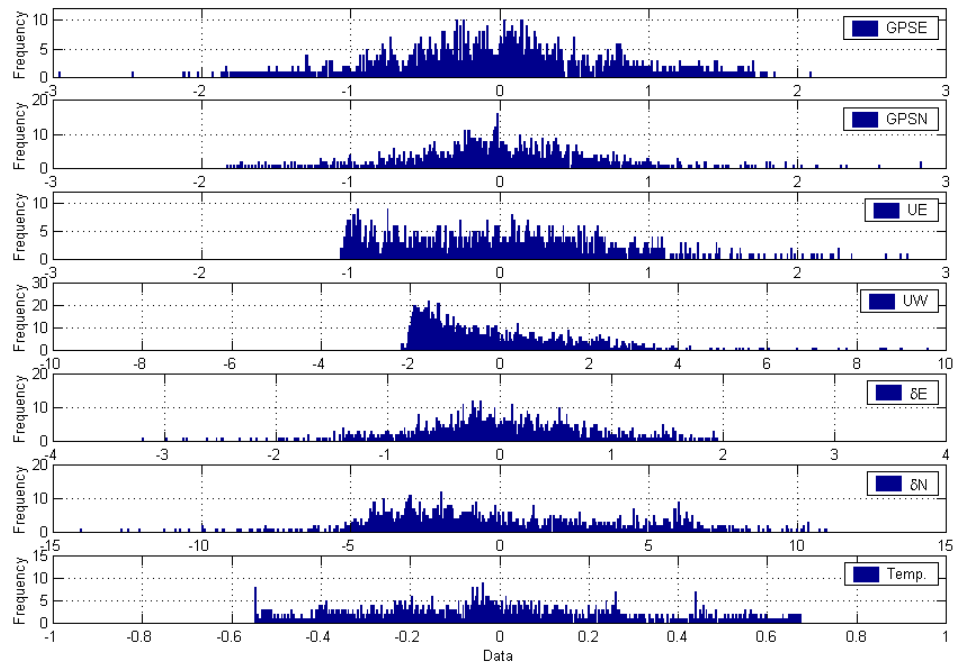


Figure 7.7. Normal Distribution histogram plots for the Multivariate Data

There were 1112 observations of the seven variables, hence  $m = 1112$  and  $p = 7$ . The vector of sample means was calculated as:

$$\bar{\mathbf{Y}}_{1112} = \begin{bmatrix} 0.00 \text{ cm} \\ 0.00 \text{ cm} \\ 1.08 \text{ m/s} \\ 2.34 \text{ m/s} \\ 0.00 \text{ mm/s}^2 \\ 0.00 \text{ mm/s}^2 \\ 27.56 \text{ }^\circ\text{C} \end{bmatrix} \quad (7.17)$$

The sample correlation matrix  $\mathbf{R}_m$  is made up of elements  $r_{kl}$  representing the pair-wise correlation coefficient between the element in the  $k^{\text{th}}$  row and the  $l^{\text{th}}$  column in the covariance matrix. For this example, the correlation matrix  $\mathbf{R}_{1112}$  is:

$$\mathbf{R}_{1112} = \begin{bmatrix} 1 & 0.126 & 0.066 & -0.038 & -0.019 & 0.111 & -0.005 \\ 0.126 & 1 & 0.114 & -0.062 & 0.083 & 0.189 & 0.094 \\ 0.066 & 0.114 & 1 & -0.106 & -0.101 & 0.075 & 0.245 \\ -0.038 & -0.062 & -0.106 & 1 & -0.489 & -0.658 & -0.014 \\ -0.019 & 0.083 & -0.101 & -0.489 & 1 & 0.779 & -0.282 \\ 0.111 & 0.189 & 0.075 & -0.658 & 0.779 & 1 & -0.058 \\ -0.005 & 0.094 & 0.245 & -0.014 & -0.282 & -0.058 & 1 \end{bmatrix} \quad (7.18)$$

Using Equation (7.13), the values of the statistic  $T^2$  are computed. The corresponding control limit is  $T_{UCL}^2 = 20.6$ , from Equation (7.14), with significance level  $\alpha = 0.01$ . Figure 7.8 shows the resulting MSPC chart. The MSPC chart shows a number of peaks lying outside the control limits during the 18, 19, 22, 23 and 24 February. The two periods, during the 19 and 22 February, with the strongest peaks (2 & 4) indicate that significant events occurred during these periods.

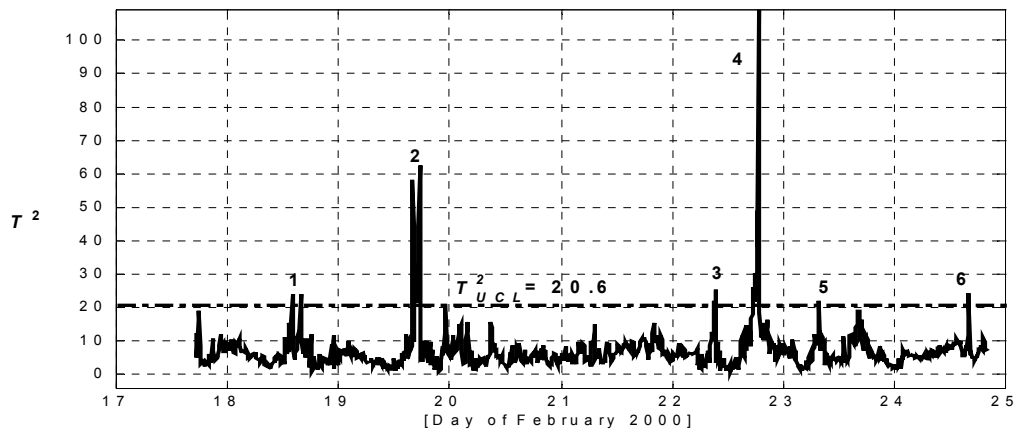


Figure 7.8. Multivariate SPC chart

Figure 7.9 shows the bivariate counterparts in which the statistic  $T^2$  are computed separately for the GPS components (GPSN & GPSE), the wind velocity components (UE & UW) and the acceleration components ( $\delta E$  &  $\delta N$ ), and for which the corresponding control limit is  $T_{UCL}^2 = 10.7$ .

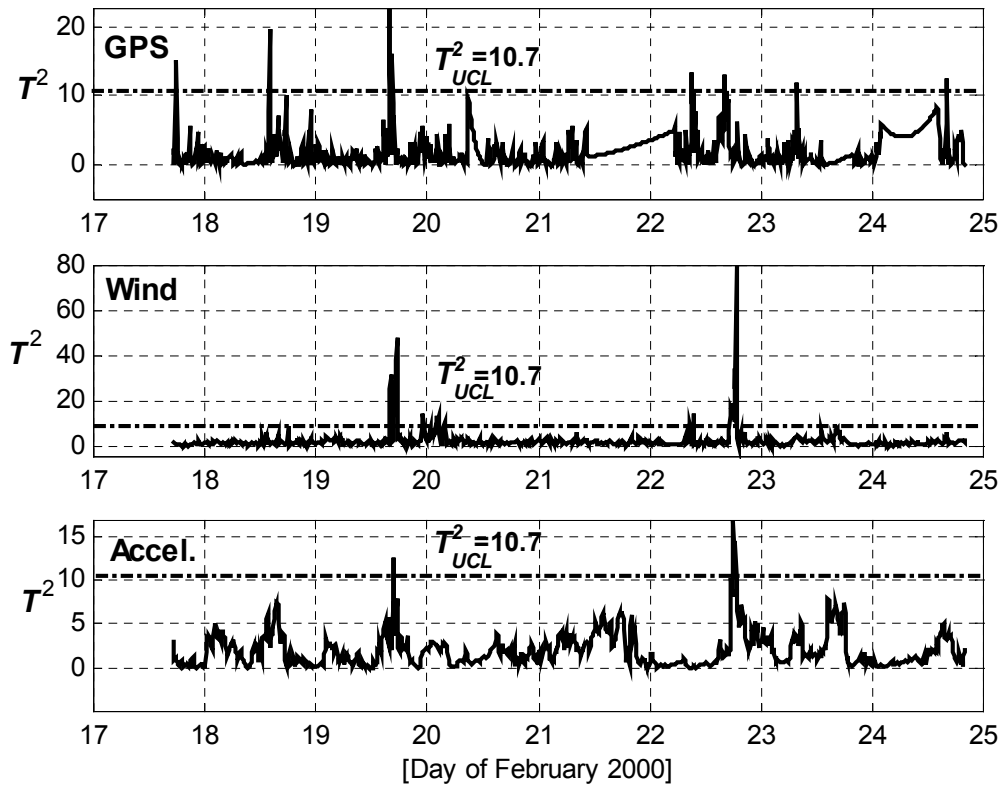


Figure 7.9. Multivariate SPC chart for GPS data (top), wind data (middle), and accelerometer data (bottom)

Since, in general, the wind data are observations of the causative quantities (for use in correlation analysis), while the GPS and accelerometer data are observations of the response effects, one is more interested in the further analysis of the latter for the recovery of deformational signals. The acceleration response data have a clear trend but they do not give the direct displacement information. On the other hand, the GPS data has direct displacement information but their MSPC trend is "unclear". For this reason, the following section will discuss a monitoring model in which the analysis of the GPS components can be enhanced.

### 7.3.4 Analysis by Wavelet Transformation

#### 7.3.4.1 Methodology

A monitoring model is further defined based on two pre-processing techniques, namely:

- a Finite Impulse Response (FIR) Median Hybrid Filter (FMH), and
- the Haar Wavelet Transformation (HWT)

The proposed methodology is a three-step procedure:

- I. Apply a FIR Median Hybrid (or FMH) filter iteratively to the GPS data to reduce the level of noise (if any).
- II. Compute the wavelet coefficients of the results from step I using the wavelet transform, in this case the Haar wavelet transform (HWT).
- III. Compute the multivariate statistic  $T^2$  from the wavelet coefficients obtained from step II.

#### *FIR Median Hybrid Filter*

In contrast to the usual linear filters, the Finite impulse response Median Hybrid (or FMH) filter (Heinonen & Neuvo, 1987) is able to reduce the noise, and preserve sudden "jumps" in data. These jumps are the sudden events which have to be detected during the pre-processing. For a time series  $\{y_1, \dots, y_N\}$ , the  $(K + 1)^{\text{st}}$  FMH filter output is given by:

$$y_{k+1}^{FMH} = \text{median}\{\hat{y}_{k+1}, \bar{y}_{k+1}, y_{k+1}\} \quad (7.19)$$

where

$\hat{y}_{k+1}$  is the average of  $K$  past samples, and

$\bar{y}_{k+1}$  is the average of  $K$  future samples.

The filter at Equation (7.19) is applied iteratively to enhance noise reduction. It involves the determination of the median of three elements, where  $K$  is the window half-width.  $K > 0$  but smaller than half the length of the shortest expected region of constant value in the data. This is referred to as a steady-state region. Large values of  $K$  will result in the distortion of a signal whose constant region is of a duration shorter than  $K$ , however, a large  $K$  does contribute to improving the noise suppression capabilities. Ideally,  $K$  should be chosen as large as possible without losing steady-state information.

Figure 7.10 illustrates the performance of the FMH filter on a signal that is corrupted with Gaussian noise. Using a window half-width of 9 and 50 consecutive passes of the filter, the noise is essentially filtered from the signal while preserving the steady-state regions.

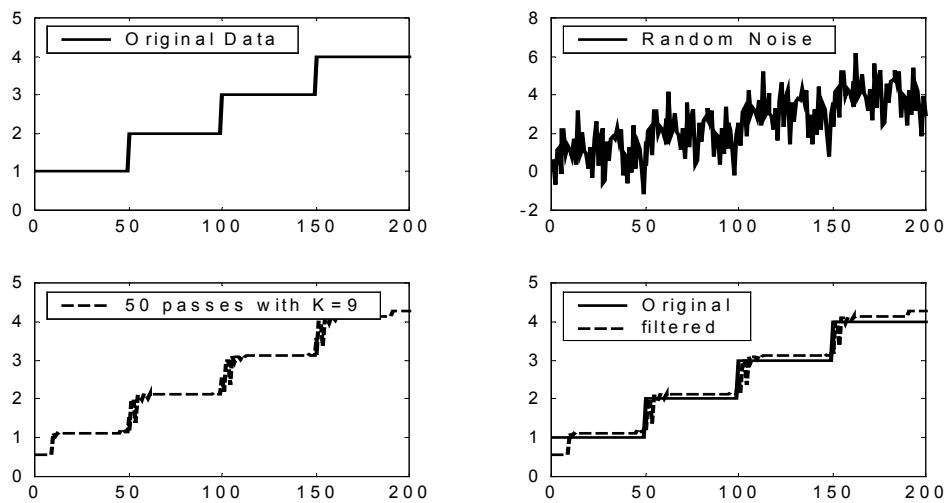


Figure 7.10. *FMH/Median hybrid filter example. Top left panel: original data signal; top right panel: signal with Gaussian random noise, bottom left panel: filtered signal after 50 consecutive passes and a window half-width of 9; bottom right panel: a superposition of the filtered and the uncorrupted signal*

### Wavelet Transform

Wavelet transformation involves representing general functions in terms of simple, fixed blocks at different scales and positions. These blocks are a family of wavelet functions generated from a prototype function, called a "mother" wavelet, by translation

and scaling operations. The prototype function must satisfy certain admissibility conditions (Chui, 1992).

One way to distinguish between the various types of wavelet transforms is whether the time and scale parameters are continuous or discrete. Continuous signals lead to Continuous Wavelet Transforms (CWT) if the parameters are continuous, and to a Wavelet Series Expansion if the parameters are discrete. Discrete signals lead to Discrete Wavelet Transforms (DWT) if the parameters are chosen to be discrete. The type of "mother" wavelet applied can also be used to describe the transformation process.

In this investigation, the use is made of the Haar Wavelet Transform (HWT), whose continuous form is given by (Olivier & Vetterli, 1991; Wang, 1995):

$$Tf(s,t) = \int \psi_s(t-u)f(u)du \quad (7.20)$$

The notation  $\psi$  in Equation (7.20) is the prototype function, and the transform  $Tf(s,t)$  is a function of both the scale, or frequency,  $s$  and the spatial position, or time,  $t$ . The plane defined by the pair of variables  $(s,t)$  is called the scale-space, or time-frequency plane, and the value of  $Tf(s,t)$  depends upon the value of function  $f()$  in the neighbourhood of  $t$  of size proportional to the scale  $s$ . At small scales  $Tf(s,t)$  provides localised information.

In practice, the measured data are normally observed only at discrete values. The discrete Haar Wavelet Transform (DHWT), a discretised version of the continuous transform in Equation (7.20), is therefore applied. In such a case, the simple prototype Haar function, developed around 1910, is used (Chui, 1992):

$$\psi_H(t) = \begin{cases} 1 & 0 \leq t \leq 1/2 \\ -1 & 1/2 \leq t \leq 1 \\ 0 & \text{otherwise} \end{cases} \quad (7.21)$$



and the time-scale parameters are discretised. Thus, if  $s = 2^j$  and  $u = k2^j$ , the corresponding wavelets become a function of two integer parameters,  $j$  and  $k$ . For this case, the wavelets form a dyadic series whose coefficients are easily calculated for combinations of the parameters  $j$  and  $k$ .

### 7.3.4.2 Test Results

With respect to the GPS components (Figure 7.9), the significant events that occurred during 19 and 22 February 2000 are not clearly revealed by the time series of the GPS data. The DHWT is applied to the mean-centred data after the data are pre-filtered by the FMH filter to remove the high frequency (noise) and gross outliers. Figure 7.11 shows the results of applying the DHWT to FMH-filtered GPS components. In each of the panels, the top plot indicates the original GPS vectors, the middle plot are the results after applying the FMH filter using 20 passes and with a half-window size of 9, and the bottom plot indicates the empirical wavelet coefficients from a DHWT of the FMH filtered data. The steady-state conditions of the data are preserved after the FMH filtering, hence the important information are not filtered out.

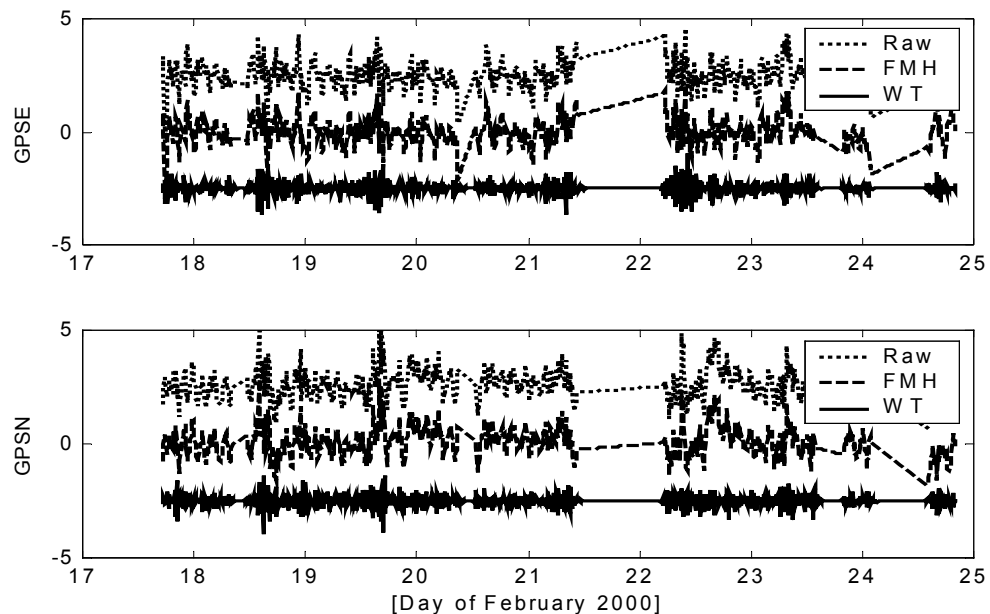


Figure 7.11. *Wavelet Transform of FMH filtered GPS data signals. Top panel: DHWT of FMH filtered GPSE data signals; bottom panel: DHWT of FMH filtered GPSN data signals.*

The multivariate statistic  $T^2$  computed from the wavelet-transformed data reveals three significant out-of-control peaks, including the two wind conditions of 19 and 22 February 2000. The comparative plots of the statistic for both the original unfiltered GPS signals and the wavelet transform of the FMH-filtered GPS signals are shown in Figure 7.12, the horizontal lines representing the 99% confidence limits.

The test results demonstrate that pre-filtering of the data with a Finite impulse response Median Hybrid filter (FMH), and developing the monitoring model from a set of coefficients obtained from a discrete Haar wavelet transform (DHWT) of the FMH-filtered data, produces a model with better (sharper) classification features.

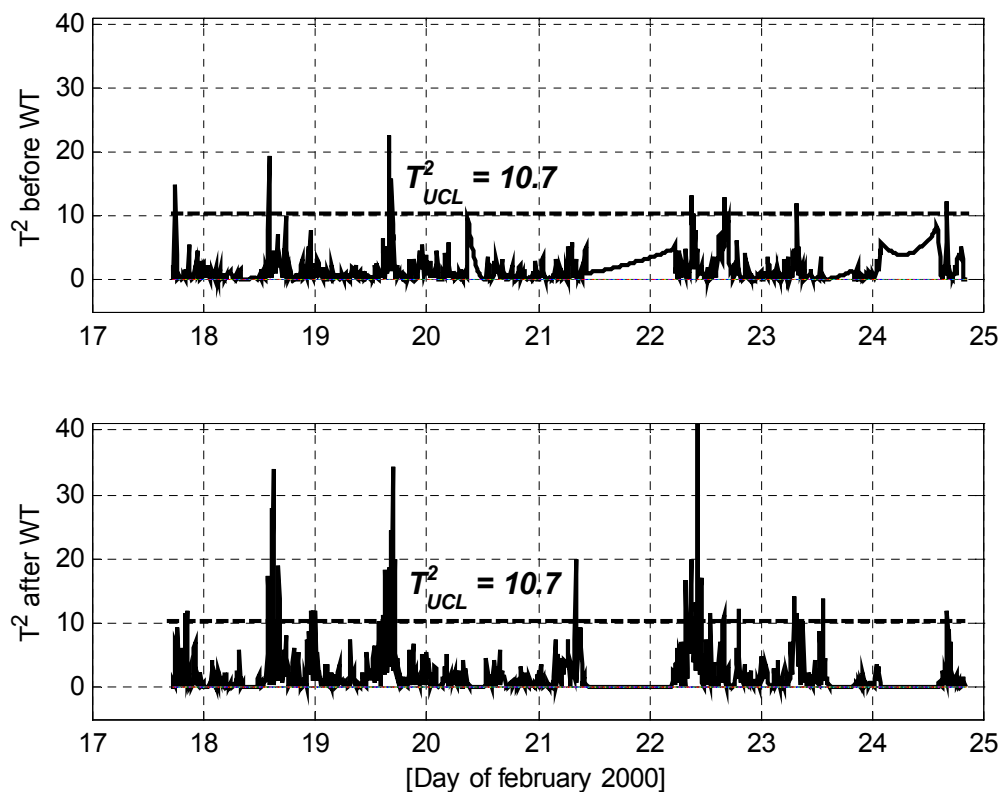


Figure 7.12. MSPC charts of (a) original GPSE and GPSN signals (top), and (b) wavelet transformed FMH filtered GPSE and GPSN signals (bottom)

## **8.1 Introduction**

In Chapters 6 & 7, the algorithms and methodologies that have been proposed in support of structural monitoring with GPS and multisensor data were described and illustrated with examples. This chapter presents some test results of a simple Windows software implementation of the proposed algorithms. The author-developed software is called "Real-Time System Monitor" (RTSM). A detailed description of its design and implementation is given in the Appendix.

The test results presented here highlight three important goals. First, Section 8.2 is to verify, through a real-time emulation, the methodology proposed in Chapter 6 of this study. Secondly, Section 8.3 is to verify the methodologies discussed in Chapter 7 by testing whether the system can accurately extract, 'on-the-fly', the frequencies and amplitudes of fast periodic deformations buried in RTK-GPS time series, as well as monitor the time series themselves. Thirdly, Section 8.4 is to verify the multisensor analysis option of the proposed methodologies.

## **8.2 Integrity Monitoring of GPS Data in the Position Domain**

The data from the UNSW experiment described in Section 6.3.2 have been used to test the integrity monitoring option of the software. Three cases are considered.

### ***Case I – No Bias Introduced***

Figure 8.1 shows the screen image of the RTSM interface that emulates real-time plotting of the position residuals from the three rovers. The data rate is set to 1,

representing 1 sample per second, and the sensitivity to bias is set to 1.5, in this case representing 1.5 cm bias. No bias is detected in the datasets as evidenced by the CUSUMs and the sensor flags.

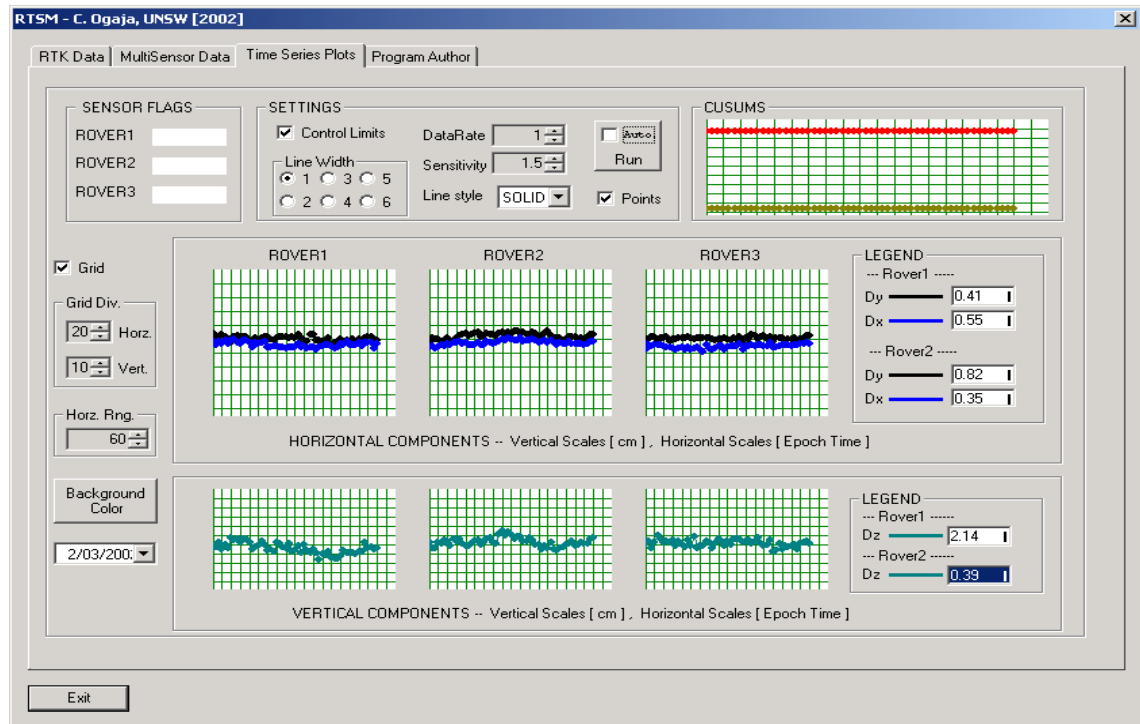


Figure 8.1. Screen image of Integrity Test – Case I

### Case II – $2\sigma$ Biases Introduced into ROVER1

In a second test, a bias of constant magnitude was introduced into the residuals of each of the vector components obtained from one of the rovers, identified as ROVER1. The bias introduced into each component was of the order of two standard deviations, with a known onset time (i.e., the 430<sup>th</sup> sampling point). Thus, from the standard deviation values of  $\pm 0.25\text{cm}$ ,  $\pm 0.26$  and  $\pm 0.72\text{cm}$ , the quantities  $-0.50\text{cm}$ ,  $+0.52\text{cm}$  and  $-1.44\text{cm}$  were introduced as biases to the easting, northing and height components of ROVER1 (the positive and negative signs are arbitrary). Figure 8.2 emulates the online process in which the bias is detected and ROVER1 is isolated as the faulty sensor (as indicated by the red flag). The message box issues an alert message to this effect.

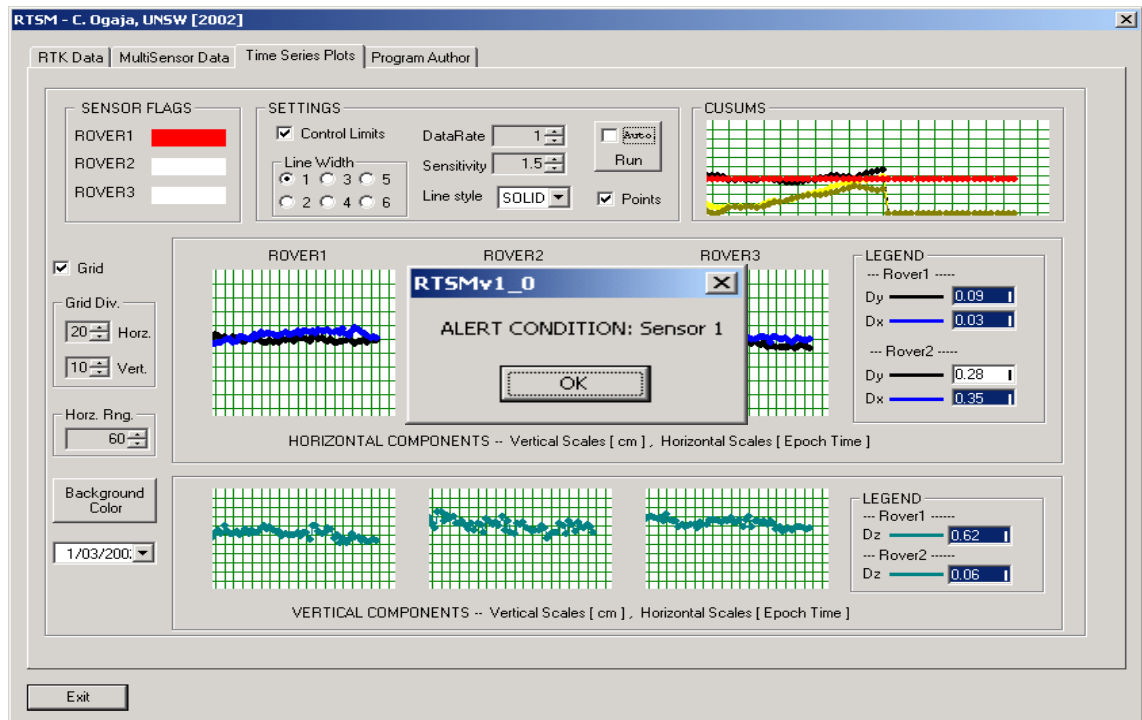


Figure 8.2. Screen image of Integrity Test – Case II

### ***Case II – $2\sigma$ Biases Introduced into ROVER2***

In a third test, a bias of constant magnitude was introduced into the residuals of each of the vector components obtained from a second rover, identified as ROVER2. Similar to Case II, the standard deviations of each of its components were computed, and a bias introduced into each component of the order of two standard deviations, with the onset time at the 430<sup>th</sup> sampling point. From the standard deviation values of  $\pm 0.33\text{cm}$ ,  $\pm 0.32$  and  $\pm 0.68\text{cm}$ , the quantities  $+0.66\text{cm}$ ,  $-0.64\text{cm}$  and  $-1.36\text{cm}$  were introduced as biases to the easting, northing and height components of ROVER2 (the positive and negative signs of the biases are arbitrary). Figure 8.3 emulates the online process in which the bias is detected and ROVER2 is isolated as the faulty sensor (as indicated by the red flag). The message box issues an alert message to this effect.

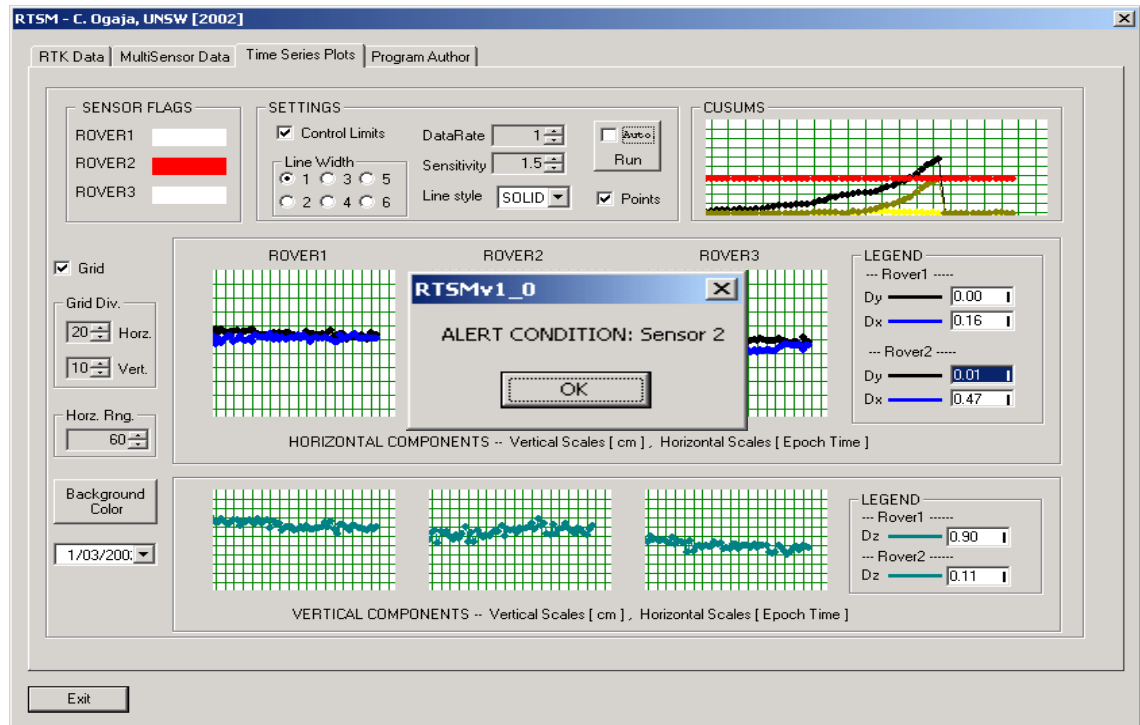


Figure 8.3. Screen image of Integrity Test – Case III

### 8.3 Time Domain and Frequency Domain Analysis

#### 8.3.1 Case I – UNSW Dataset

**Data Description:** The data from the experiment described in Section 7.2.2 have been used in an evaluation of the second option of the implemented software. These datasets were obtained at 1 sample per 0.1 second (10 Hz), and thus provide the opportunity for monitoring at a high sample rate.

Because the software is currently designed to monitor three rovers simultaneously, the data shown in Table 7.1 (p. 93) have been reformatted into four sets to appear as though they were simultaneously obtained from three rovers, for each of the sets. Table 8.1 summarises the characteristics of this scenario.

Table 8.1. *The test frequencies for the experiment at UNSW (2)*

Time	Frequency	Antenna Orientation
Session 1		
Rover1	0.2Hz	Vertical
Rover2	0.3Hz	Vertical
Rover3	0.5Hz	Vertical
Session 2		
Rover1	DC	Vertical
Rover2	0.5Hz	Vertical
Rover3	0.7Hz	Vertical
Session 3		
Rover1	1.2Hz	Vertical
Rover2	1.4Hz	Vertical
Rover3	1.7Hz	Vertical
Session 4		
Rover1	DC	Vertical
Rover2	2.0Hz	Vertical
Rover3	3.0Hz	Vertical

Again only the height component data were used since the mechanical shaker only operated in the vertical direction. Each of the sets was used in turn to evaluate the RTSM software via the "RTK Data" dialogue.

**Test Results:** Figures 8.4, 8.5, 8.6 and 8.7 are the screen images of the test results for the four sets described in Table 8.1. Only height component values (i.e.,  $Dz[Hz]$  and  $Dz[mm]$ ) are useful as the horizontal components are all set to zero.

In Figure 8.4, for instance, notice from the upper panel "MOVING WINDOW SUMMARIES", the frequencies 0.21Hz, 0.37Hz, 0.52Hz, with their respective amplitudes of  $\pm 4mm$ ,  $\pm 4mm$ ,  $\pm 2mm$ , obtained for Rover1, Rover2, and Rover3 respectively during session 1 of monitoring. These values are in agreement with those obtained in the earlier analysis in Section 7.2.2 (see Figure 7.3). The results during session 2 of monitoring are also in agreement, except for Rover1 (0.13Hz extracted instead of 0.2Hz). This misdetection could be attributed to signal aliasing and the presence of random noise in the dataset.

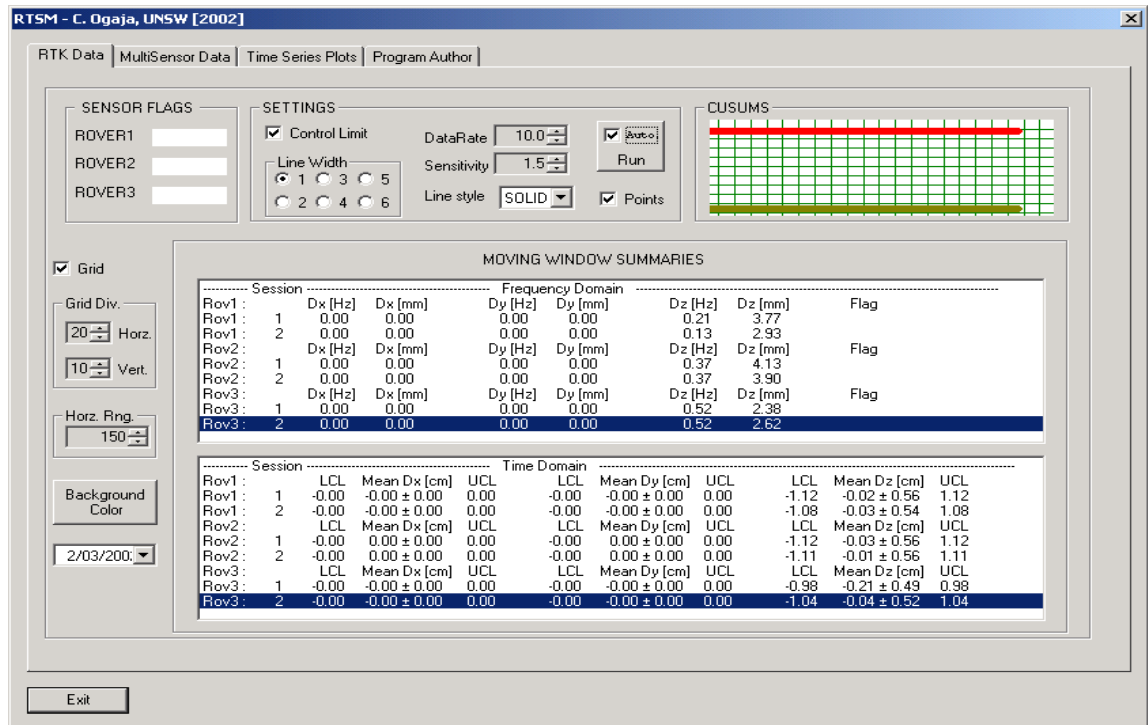


Figure 8.4. Screen Image of frequencies and amplitudes (UNSW) – (1)

The lower panel of Figure 8.4 monitors the data in the time domain according to the methodology discussed in Section 6.2.1. The data are shown to be in-control.

Similarly, the upper panel "MOVING WINDOW SUMMARIES" of Figures 8.5, 8.6 and 8.7 shows the frequencies with their respective amplitudes obtained from Session 2, Session 3 and Session 4 respectively, for Rover1, Rover2, and Rover3. The frequencies extracted are in agreement with their simulated values (Table 8.1). However, note that in Figures 8.5 and 8.7, the frequencies extracted for Rover1 do not correspond well to the simulated values (aliasing). The corresponding time domain monitoring results shown in the lower panels of the figures indicate that the data are in-control.



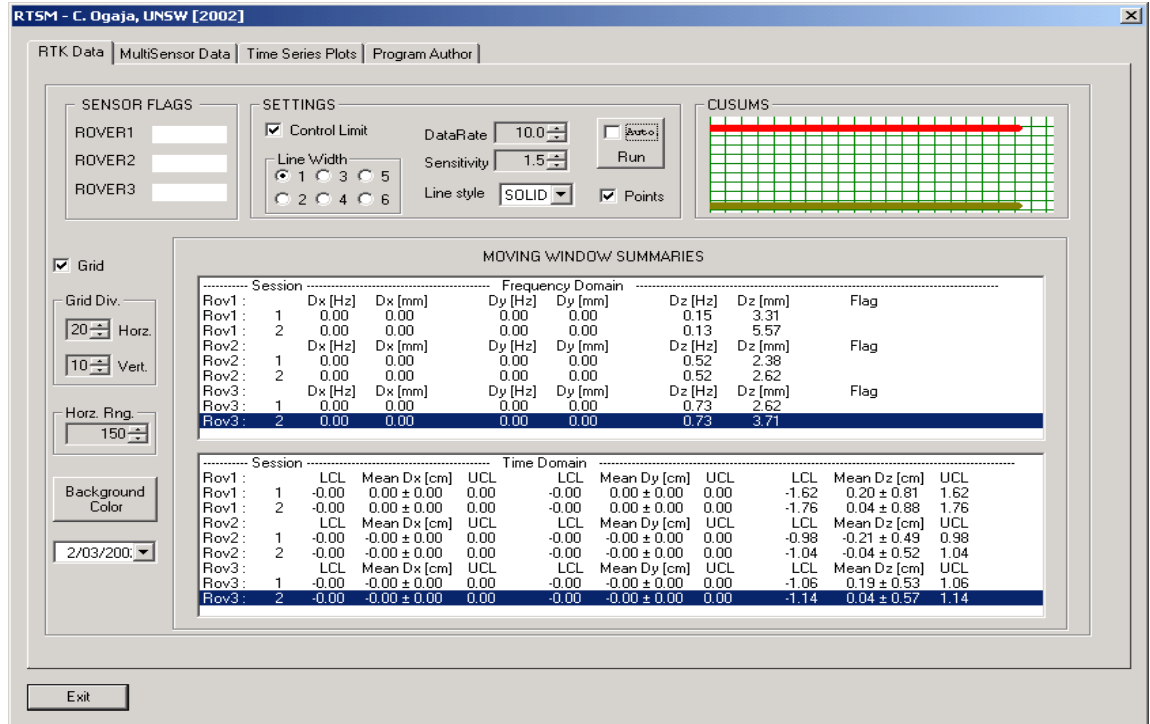


Figure 8.5. Screen Image of frequencies and amplitudes (UNSW) – (2)

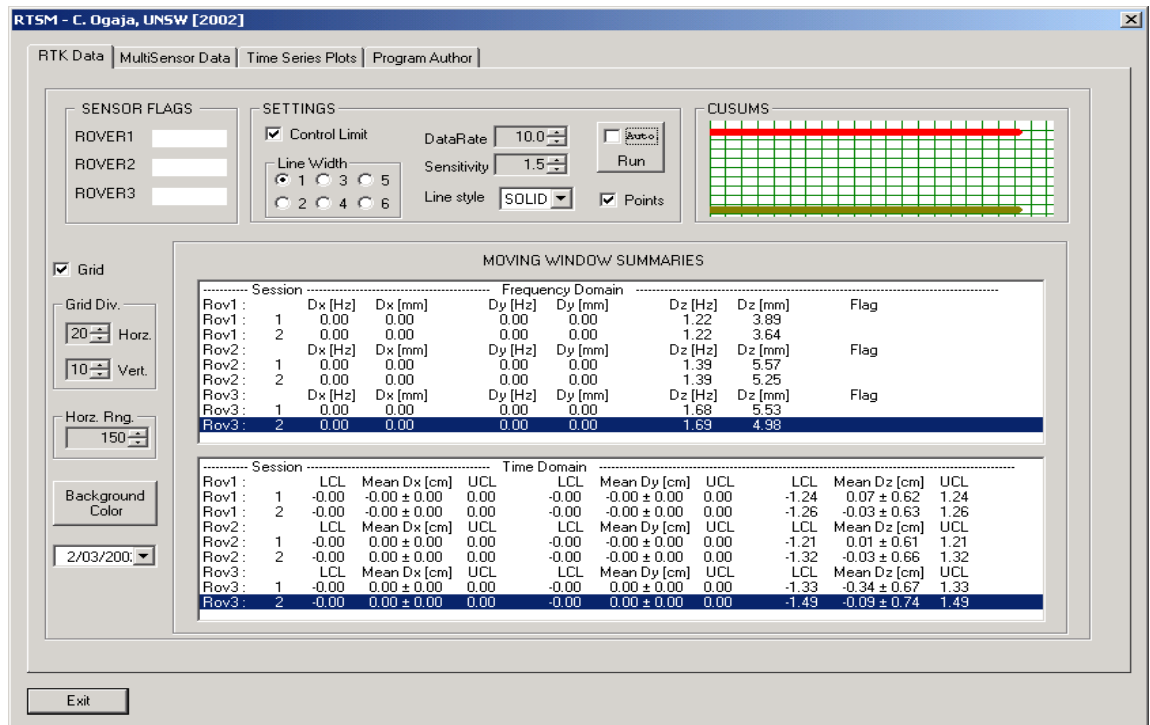


Figure 8.6. Screen Image of frequencies and amplitudes (UNSW) – (3)

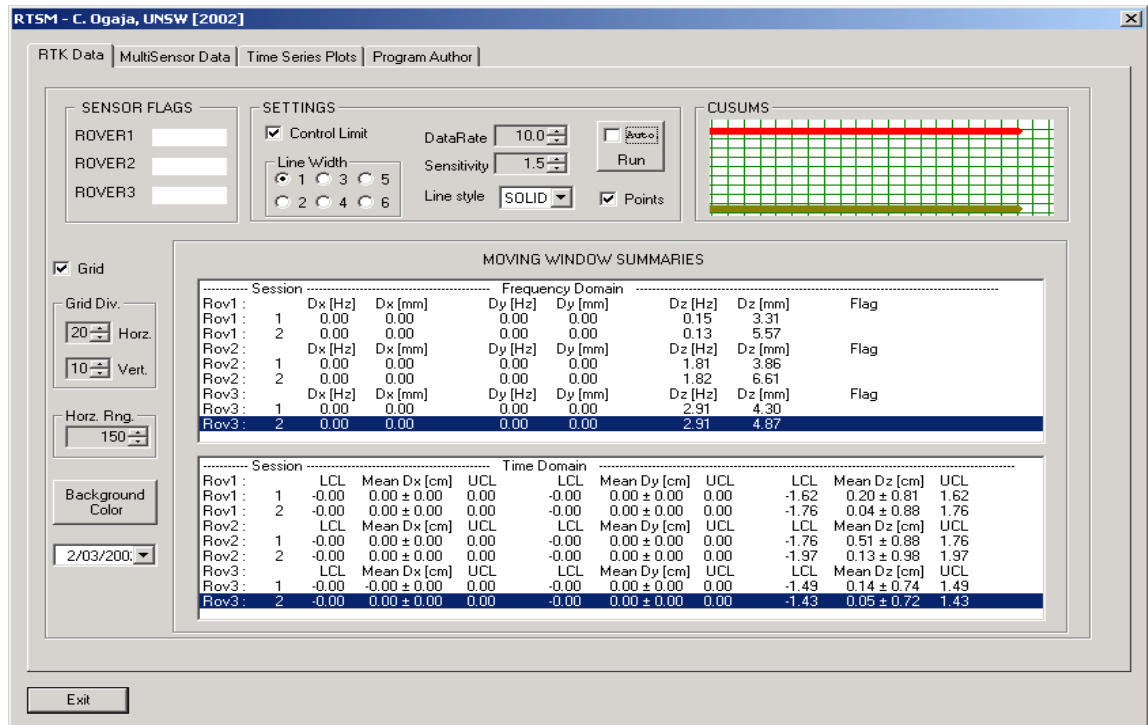


Figure 8.7. Screen Image of frequencies and amplitudes (UNSW) – (4)

### 8.3.2 Case II – Calgary Tower Dataset

**Data Description:** A dynamic deformation monitoring experiment was carried out by Lovse et al. (1995), involving the measurement of the structural vibrations of the Calgary Tower in Alberta, Canada. The data from this experiment have been obtained from the authors, and used with their permission to demonstrate the second option of the implemented software. The experiment consisted of logging data from one GPS receiver at a reference station (located on a low-rise three-storey apartment building situated approximately 1 km north of the tower), and from two GPS receivers on the tower. The receivers were the NovAtel GPSCard Model 951. The data were collected at 10Hz for about 15 minutes at a time during which the wind speed was 60km/h-100km/h. Figure 8.8 shows the north-south (longitude) and east-west (latitude) movements of the tower obtained from the analysis of the raw data at 1Hz. Figures 8.9 and 8.10 show the corresponding fast Fourier transforms (FFTs) of the data.

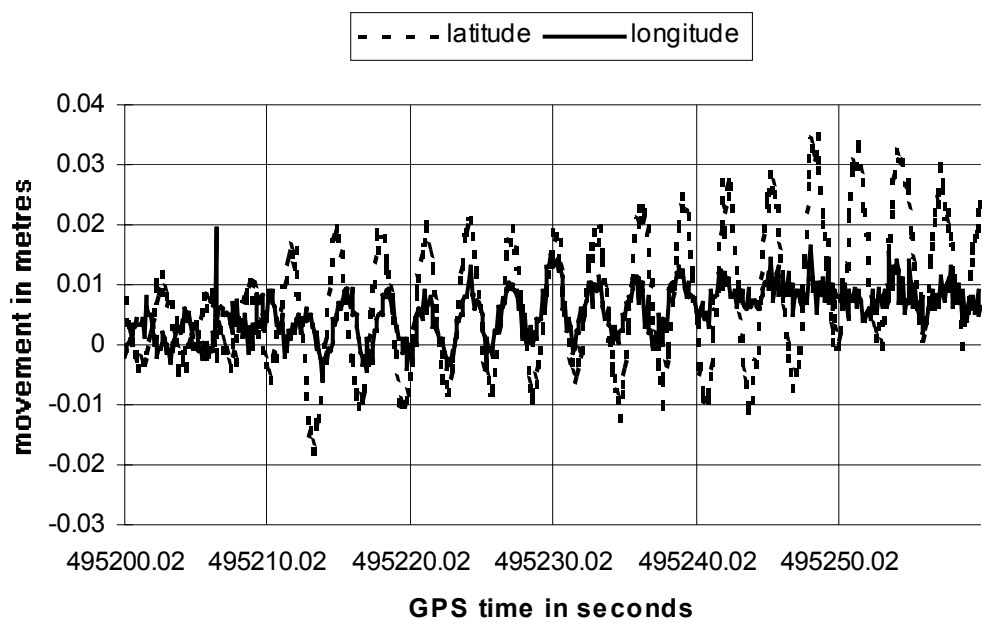


Figure 8.8. *Movement of the Calgary Tower*

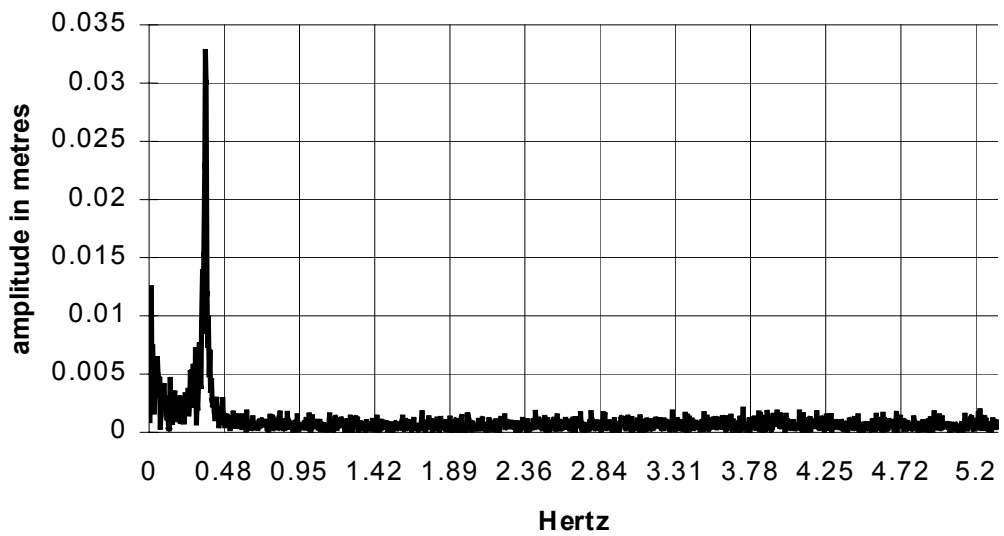


Figure 8.9. *Frequency Domain of Movement of the Calgary Tower*

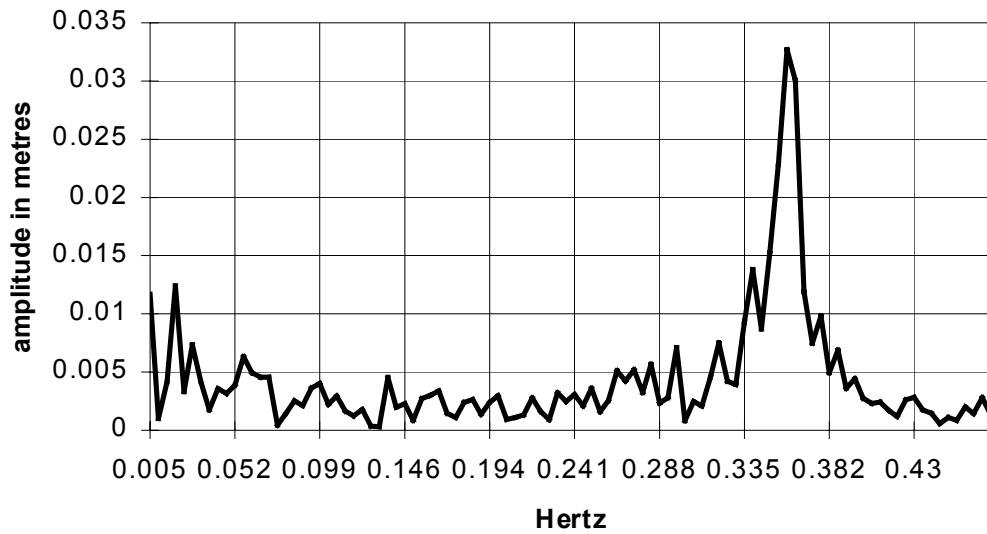


Figure 8.10. *Dominant Frequency of Movement of the Calgary Tower*

**Tests Results:** The north-south and east-west movements (Figure 8.8), together with the height components (not plotted) have been input to the RTSM software at 1Hz sample rate for evaluation. Again, for convenience, the data are analysed in three different sets in time order. The three sets of data, designated as Set A, Set B and Set C, are assigned to Rover 1, Rover2 and Rover3 respectively. Figure 8.11 is the screen image of the Set A data analysis. Note that for the north-south component, frequencies in the range 0.01–0.34Hz have been extracted, in real-time, with amplitudes in the range  $\pm 5$  to  $\pm 7$ mm. Similarly, frequencies in the range 0.01–0.02Hz have been extracted with amplitudes of  $\pm 4$  to  $\pm 8$ mm, in the east-west components. However, the frequency of 0.01Hz common to the height components, represents the noise level. The time domain data, as indicated by the results in the lower panel "MOVING WINDOW SUMMARIES", are all in-control.

Figures 8.12 and 8.13 show that as time progresses, the dominant frequency varies between 0.33Hz to 0.34Hz with an amplitude in the range of  $\pm 7$ mm to  $\pm 17$ mm. This is in agreement with the results reported by Lovse et al. (1995), that is, a single dominant frequency of 0.36Hz, with an amplitude of  $\pm 16$ mm for the north-south movement.

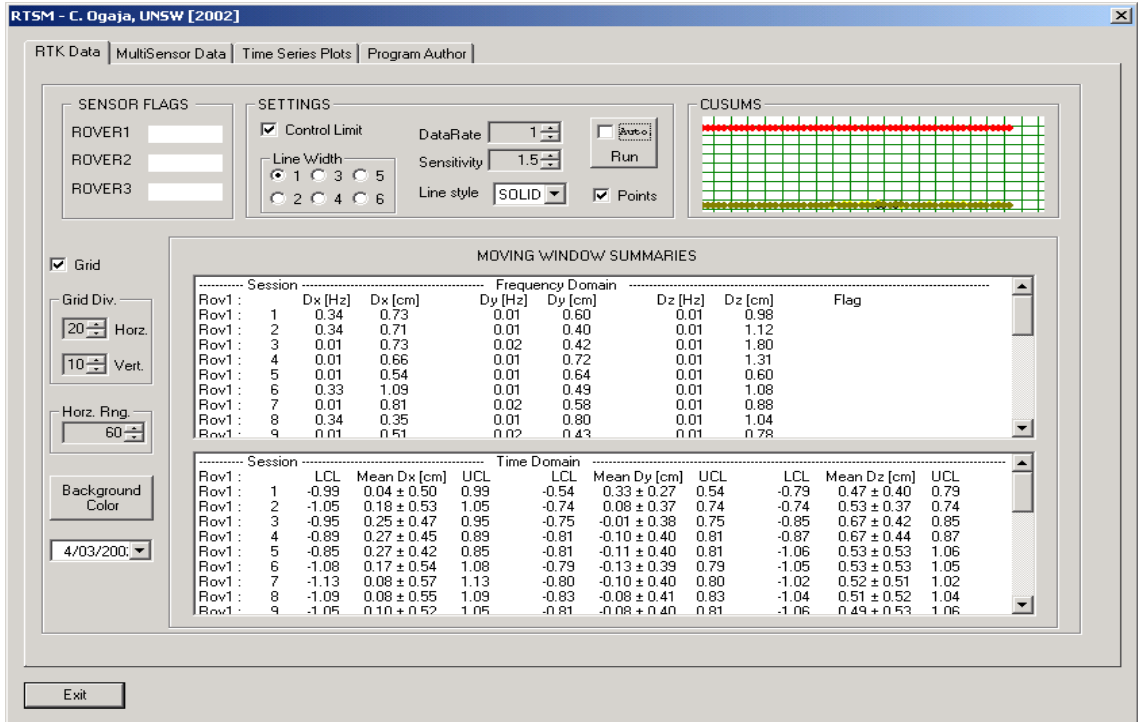


Figure 8.11. Screen Image of frequencies and amplitudes (Calgary Tower) – Set A

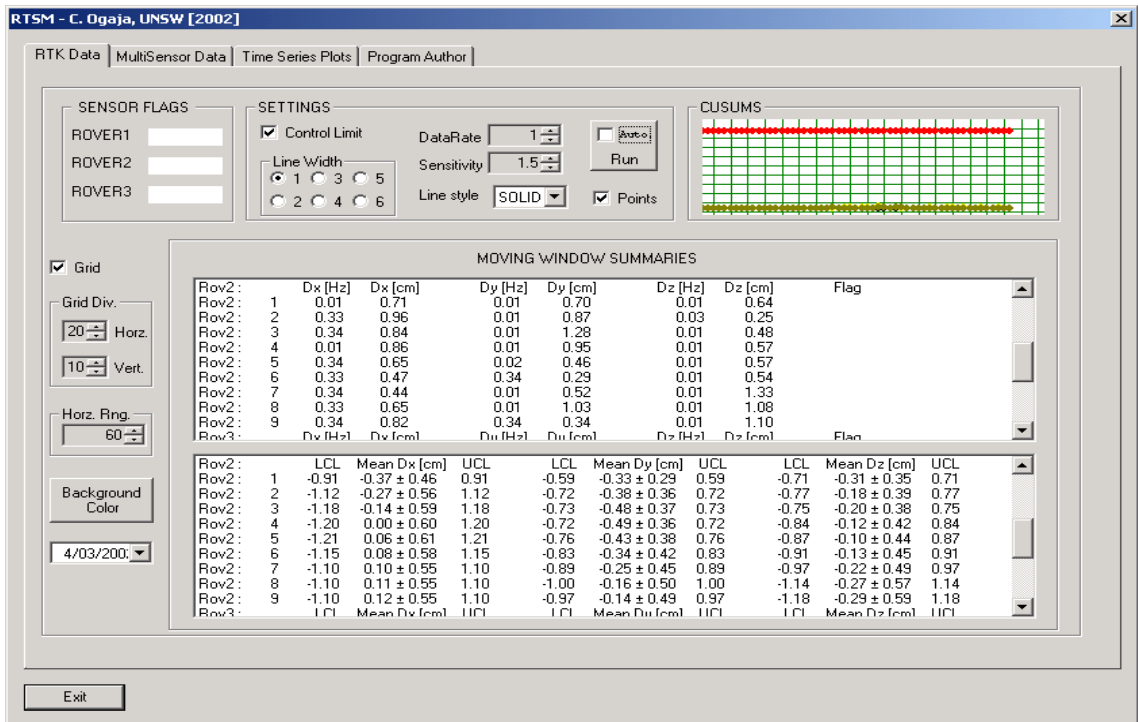


Figure 8.12. Screen Image of frequencies and amplitudes (Calgary Tower) – Set B

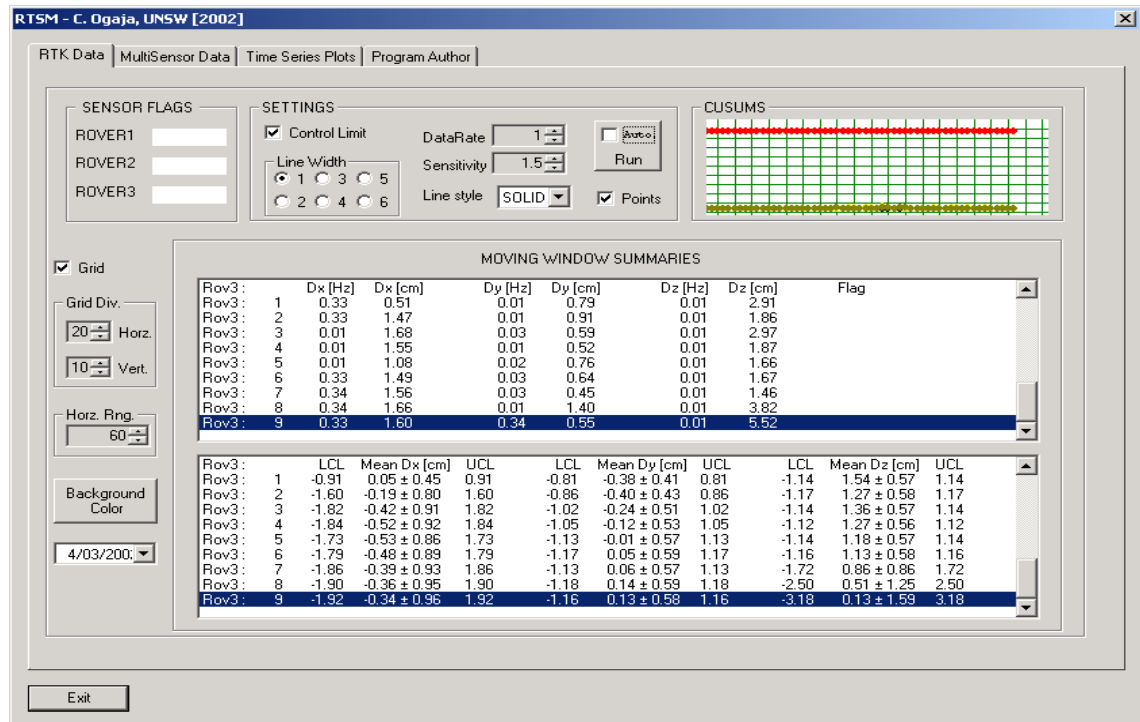


Figure 8.13. Screen Image of frequencies and amplitudes (Calgary Tower) – Set C

### 8.3.3 Case III – Xiamen Building Dataset

**Data Description:** The third test of the RTSM "RTK Data" option involves data obtained from another tall structure monitoring experiment, this time carried out in China. The data, analysis of which was reported in Shengxiang & Xianglin (2001), was provided by the authors for this evaluation and used with their permission. The experiment was carried out on 5 October 2000 during which the self-vibration and movements of the Xiamen Bank Building in China, during its construction, were observed by Trimble 4000ssi dual-frequency receivers. Two receivers were installed at two reference sites 219m apart, and 170m and 208m away from the monitoring receiver installed on the building (approximately 148.5m above ground level at that time). The raw data were collected at 2Hz for about 30min, the coordinate results subsequently generated off-line. The data simultaneously collected at the two reference sites were used in an attempt to remove systematic errors and multipath during baseline processing. Further details of this work can be found in *Ibid* (2001). The data plotted in Figures 8.14, 8.15 and 8.16 are the time series of the residuals of the X-, Y- (horizontal)

and H- (height) components for one of the reference stations (bottom) and the monitoring station (top) respectively.

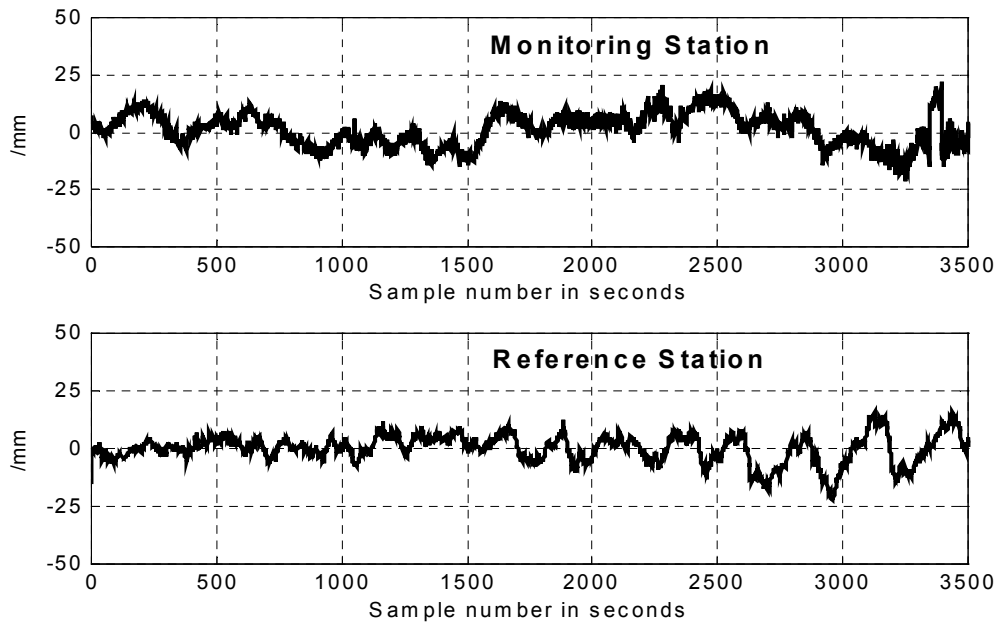


Figure 8.14. *Time series of X-component of the Xiamen Bank Building data*

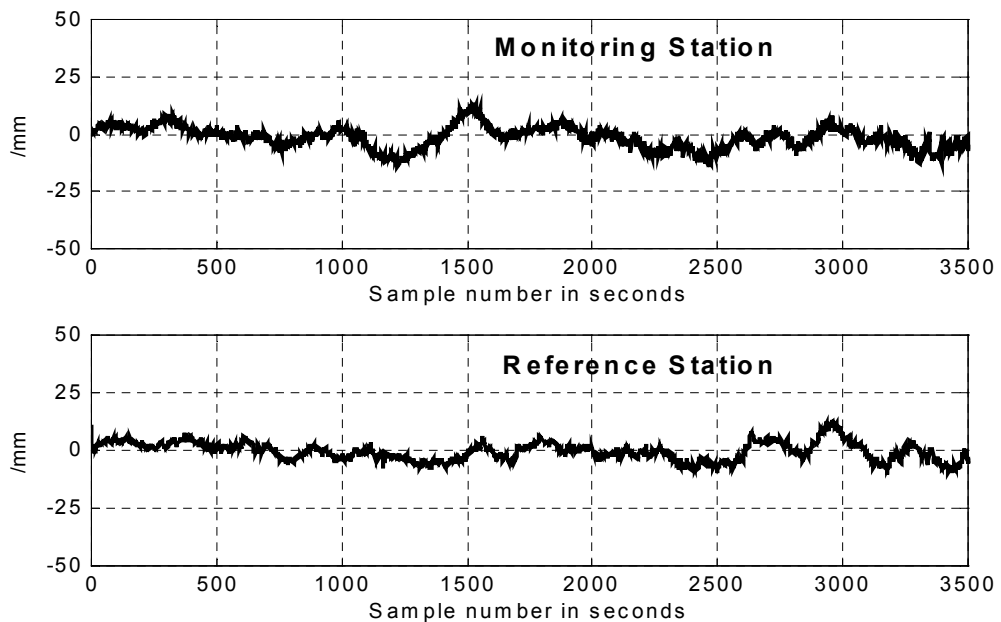


Figure 8.15. *Time series of Y-component of the Xiamen Bank Building data*

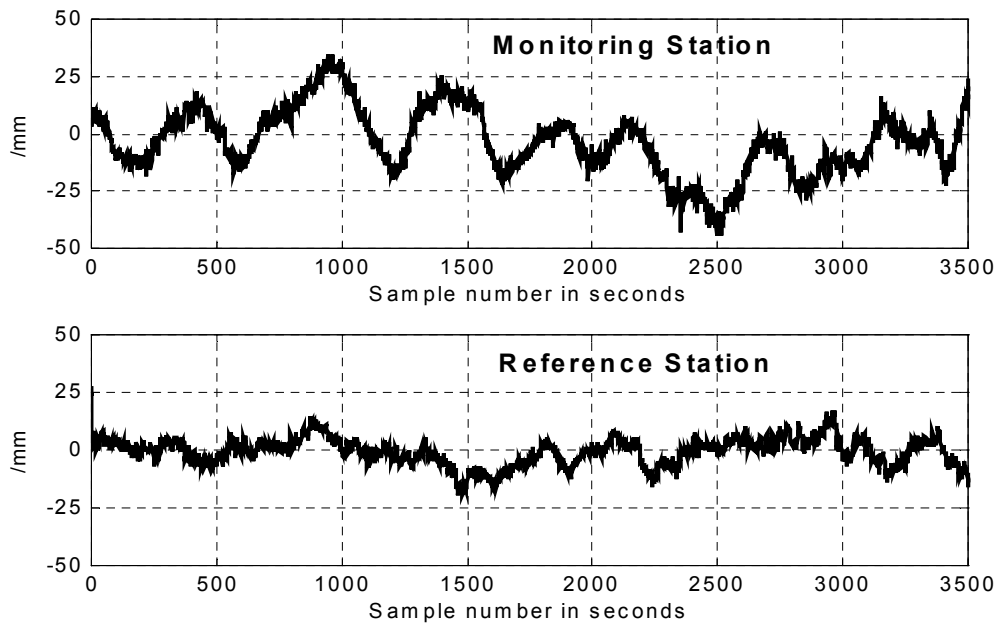


Figure 8.16. *Time series of H-component of the Xiamen Bank Building data*

**Tests Results:** In this study, only the data obtained from the monitoring station as shown in the upper plots of Figures 8.14 to 8.16, were input to the RTSM software. The data are analysed in three different sets in time order, designated as Set A, Set B and Set C, each set assigned to each of the rovers.

Figure 8.17 shows the analysis results of the Set A data. The dominant frequencies from both the X-component ( $D_x$ ) and H-component ( $D_z$ ) are 0.01Hz, with corresponding amplitude ranges of  $\pm 1$  to  $\pm 3$ mm and  $\pm 1$  to  $\pm 6$ mm respectively. However, the dominant frequency from the Y-component ( $D_y$ ) is in the range of 0.01–0.07Hz with amplitudes of  $\pm 0.2$  to  $\pm 2$ mm. In comparison, the analysis results of Set B (Fig. 8.18) and Set C (Fig. 8.19) show a single dominant frequency concentrated around 0.01Hz with three-dimensional amplitudes in the range of  $\pm 1$  to  $\pm 4$ mm (north-south direction),  $\pm 0.5$  to  $\pm 3$ mm (east-west direction), and  $\pm 1$  to  $\pm 8$ mm (vertical direction). These results are partially in agreement with those presented in Shengxiang & Xianglin (2001). The low frequencies, with their corresponding large amplitudes, may be attributed to the multipath influence from the construction equipment such as tower cranes and the safety meshwork. In this analysis, no dominant frequency of the building movement was detected. Such a frequency would be expected to be in the range 0.30–0.35Hz.



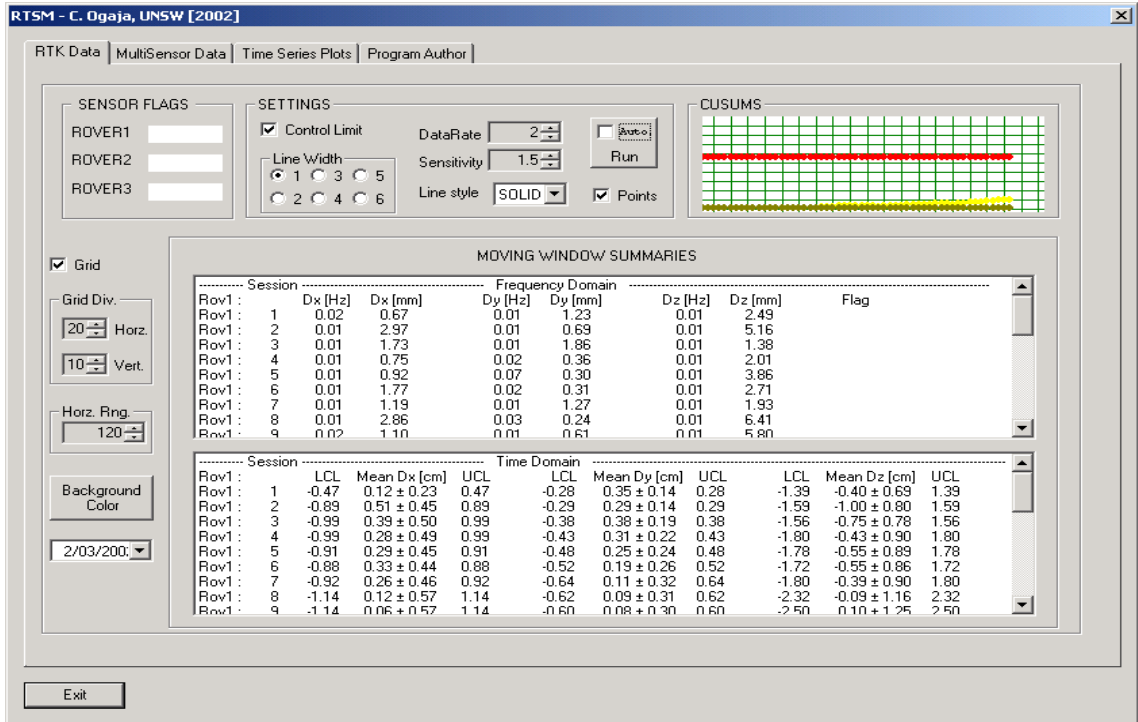


Figure 8.17. Screen Image of frequencies and amplitudes (Xiamen Building) – Set A

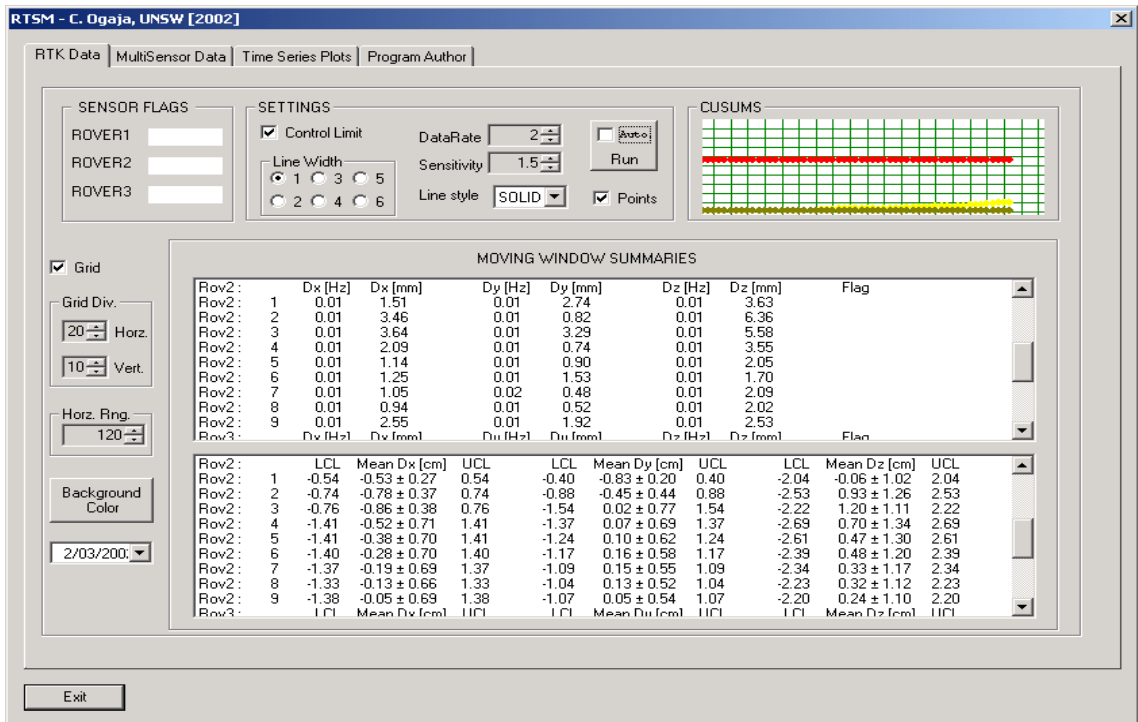


Figure 8.18. Screen Image of frequencies and amplitudes (Xiamen Building) – Set B

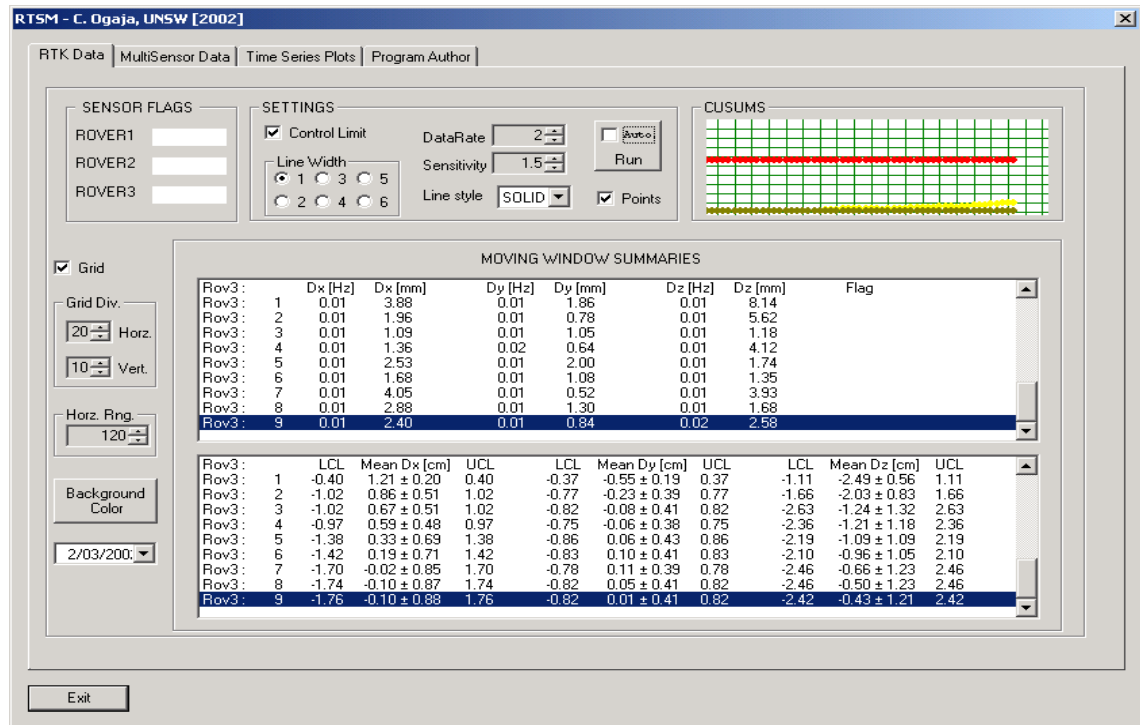


Figure 8.19. Screen Image of frequencies and amplitudes (Xiamen Building) – Set C

## 8.4 GPS and Multisensor Data Analysis

### 8.4.1 Data Description

In this test, the data previously described in Section 7.3.3 have been considered, together with two additional datasets of GPS-only coordinate solutions. The GPS measurements were taken simultaneously with the auxiliary sensor measurements during the period 17 to 25 February 2000, in a trial experiment to test the monitoring equipment being installed on the Republic Plaza Building in Singapore (see Figure 8.20). The means of GPS and the corresponding multisensor signals were extracted at regular intervals and recorded for the analysis of the long-period behaviour (Figure 7.6). At the same time, the raw GPS data were recorded at a rate of 1Hz, and later processed by off-line commercial baseline processing software to give the corresponding 1-second coordinate solutions.

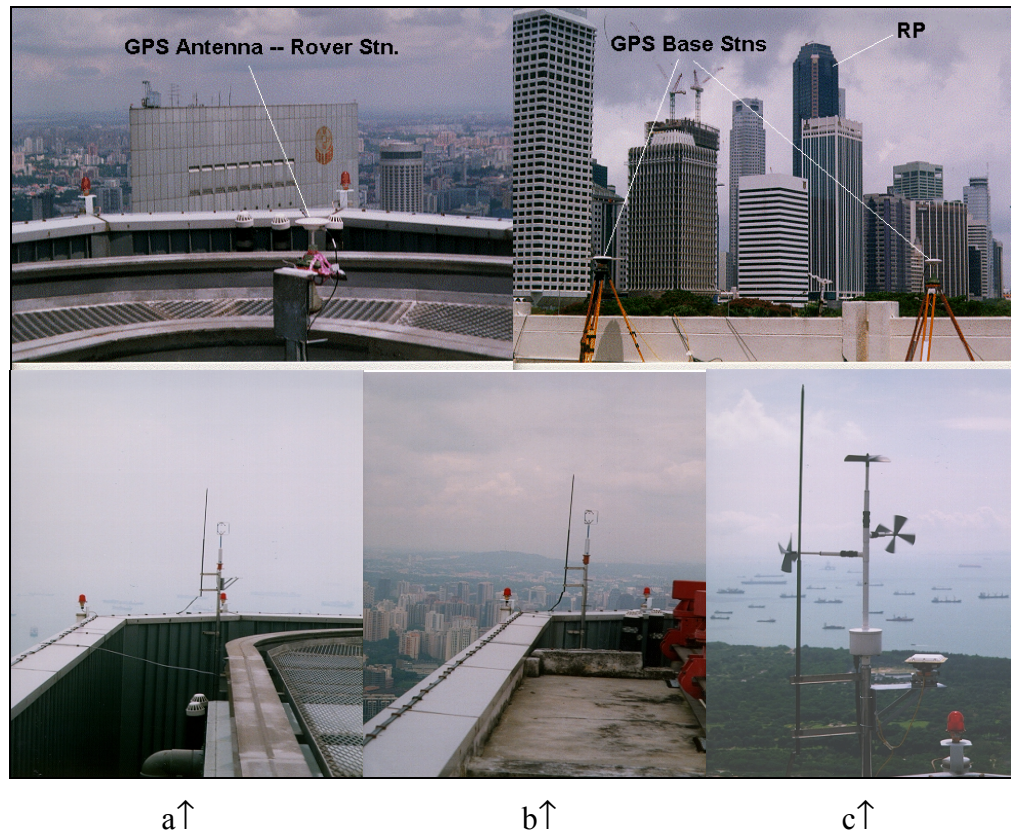


Figure 8.20. *Multisensor instrumentation at Republic Plaza (RP) Building during the trial experiment of 17 to 25 February 2000. (a) Sonic anemometer at east corner, (b) Sonic anemometer at west corner, and (c) close up on the brackets*

## 8.4.2 Tests Results

### *Case I – Multivariate Analysis of GPS and Multisensor data*

The methodology described in Section 7.3.2 was implemented within the RTSM software. The recorded means of GPS and the corresponding multisensor signals from the experiment described above were input to the RTSM through its "MultiSensor Data" dialogue. Figure 8.21 emulates the online process in which the multivariate statistic displays two distinct out-of-control signals. These two signals correspond to the windy sessions during 19 and 22 February 2000, as earlier revealed in the analysis in Section 6.3.3. Note that in this case, even though the data rate setting is 1, it doesn't imply a 1-second data rate, but rather the sampling interval for the means. Thus no building vibration is present at this stage of the analysis.

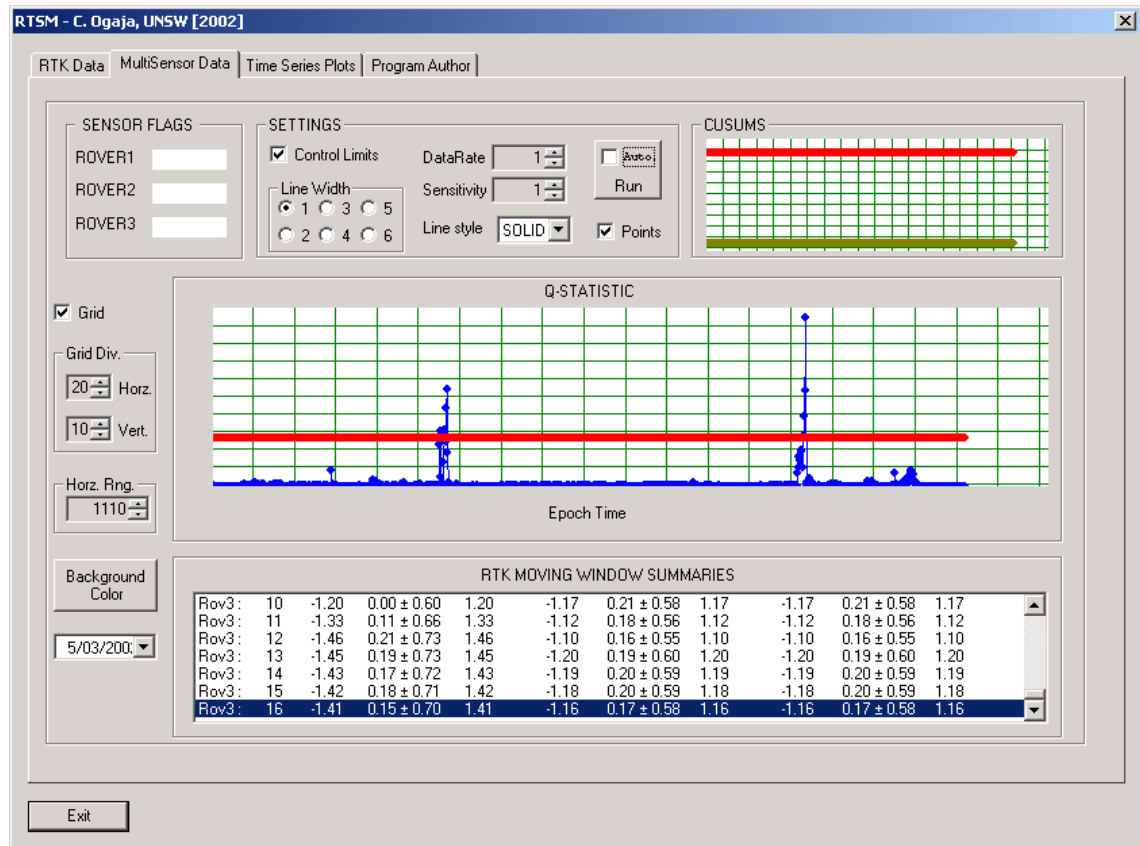


Figure 8.21. Screen Image of multisensor signal

### Case II – Analysis of 4-hr GPS data observed on 18 February 2000 (no wind)

Figure 8.22 shows a 4-hr period of the 1-second GPS coordinate solutions obtained from the raw GPS data recorded during 18 February 2000, corresponding to a period of no wind. This section of the data was selected for more detailed scrutiny at a higher temporal resolution. The data were analysed in three sets, Set 1A, Set 1B and Set 1C, in time order (as already explained in earlier sections). From the RTSM results presented in Figures 8.23, 8.24 and 8.25, the dominant frequency is at its lowest, 0.01Hz, with amplitudes ranging from  $\pm 0.1$  to  $\pm 2$ mm. This represents noise, and thus no building vibration is extracted from this part of the GPS results. All the time-domain data are in-control.

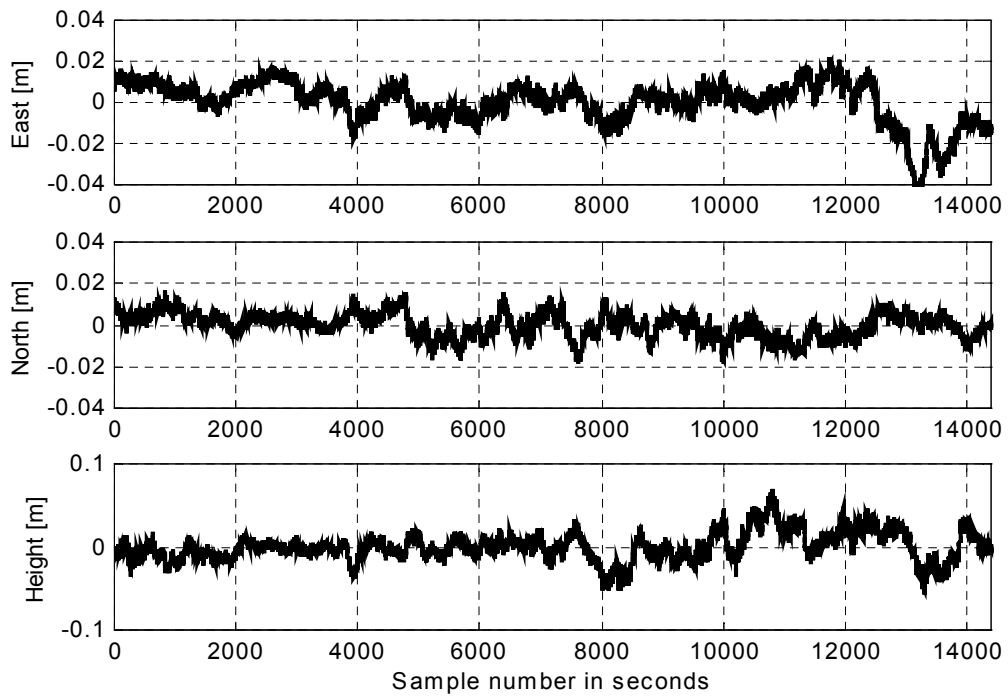


Figure 8.22. Time series of 1-second GPS solutions – NTU, 18 February 2000

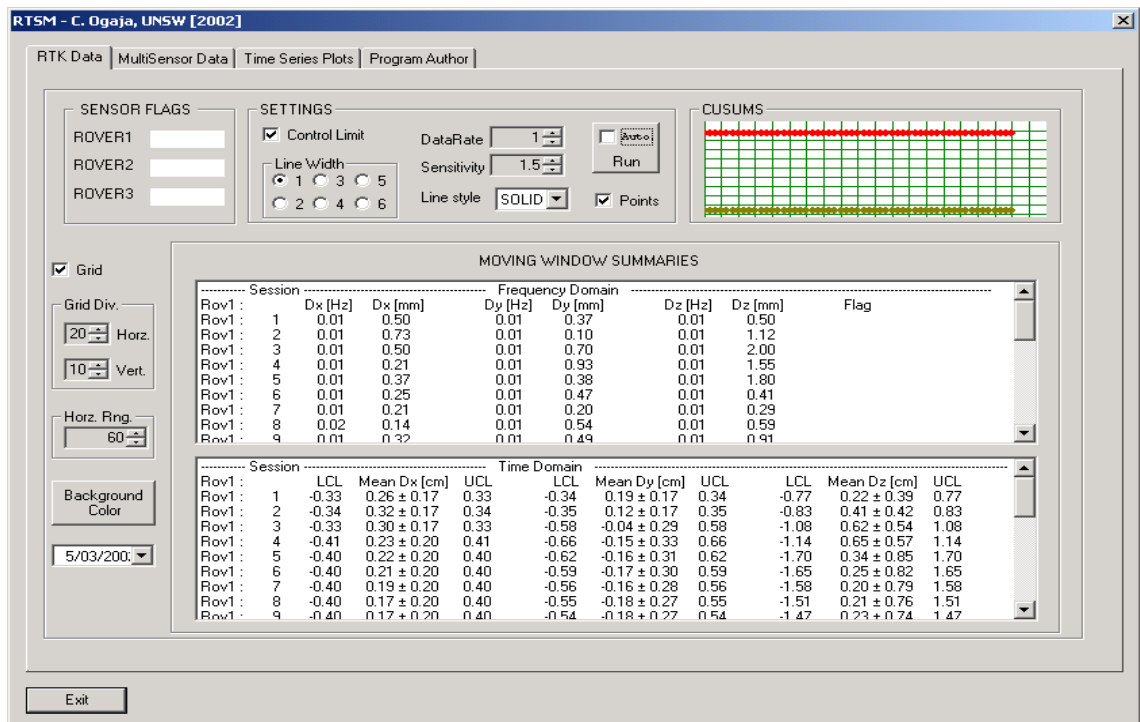


Figure 8.23. Screen Image of frequencies and amplitudes (RP Building) – Set 1A

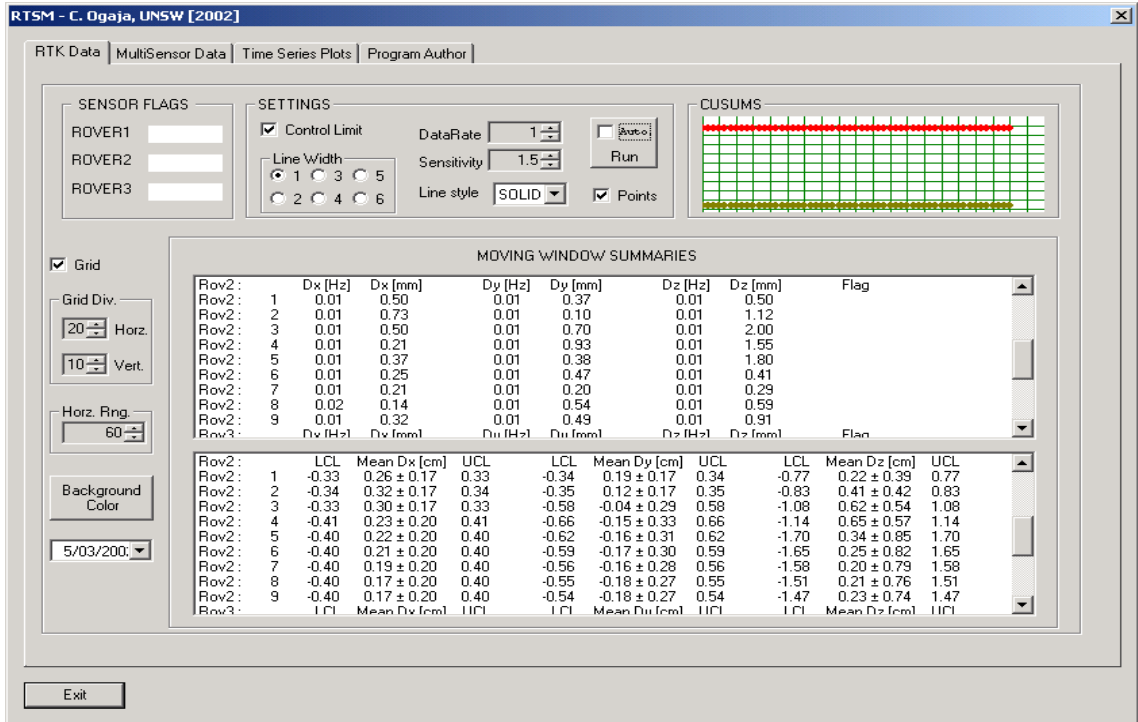


Figure 8.24. Screen Image of frequencies and amplitudes (RP Building) – Set 1B

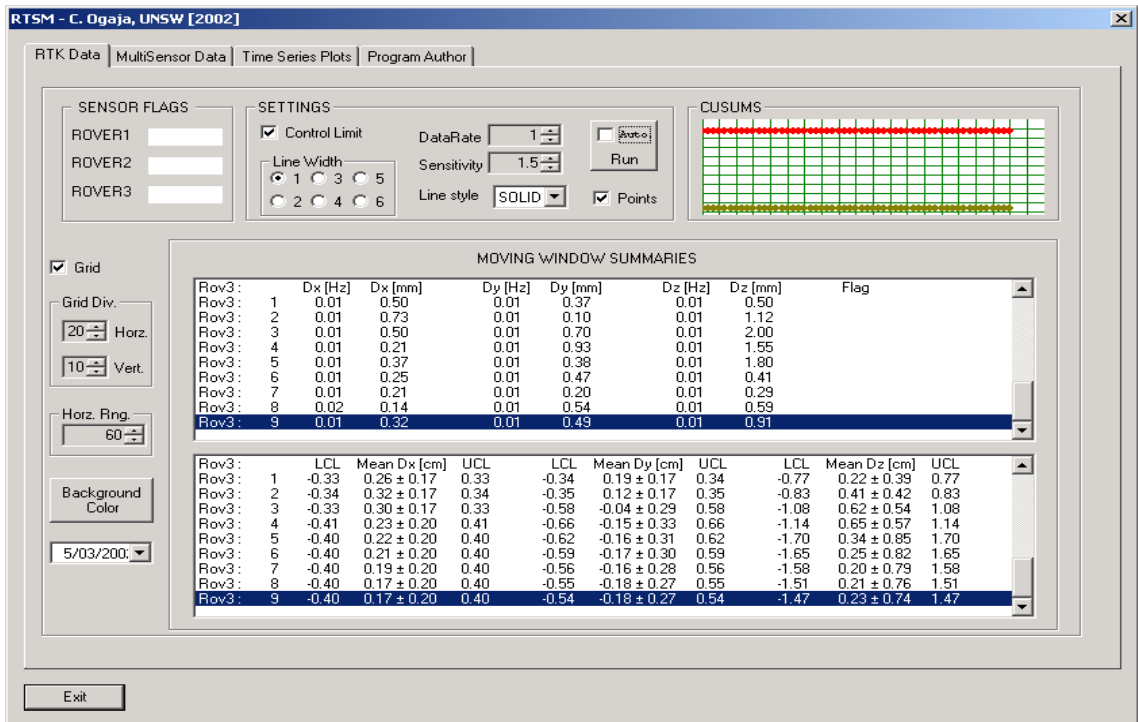


Figure 8.25. Screen Image of frequencies and amplitudes (RP Building) – Set 1C

**Case III – Analysis of GPS data observed on 19 February 2000 (windy)**

In another case, a 4-hr period of the 1-second GPS coordinate solutions, obtained from the raw GPS data recorded during a windy period on 19 February 2000, was selected for comparative analysis. Figure 8.26 is the plot of the data from this period. The data were analysed in three sets, Set 2A, Set 2B and Set 2C, in time order, in an attempt to extract the signature of the building dynamics.

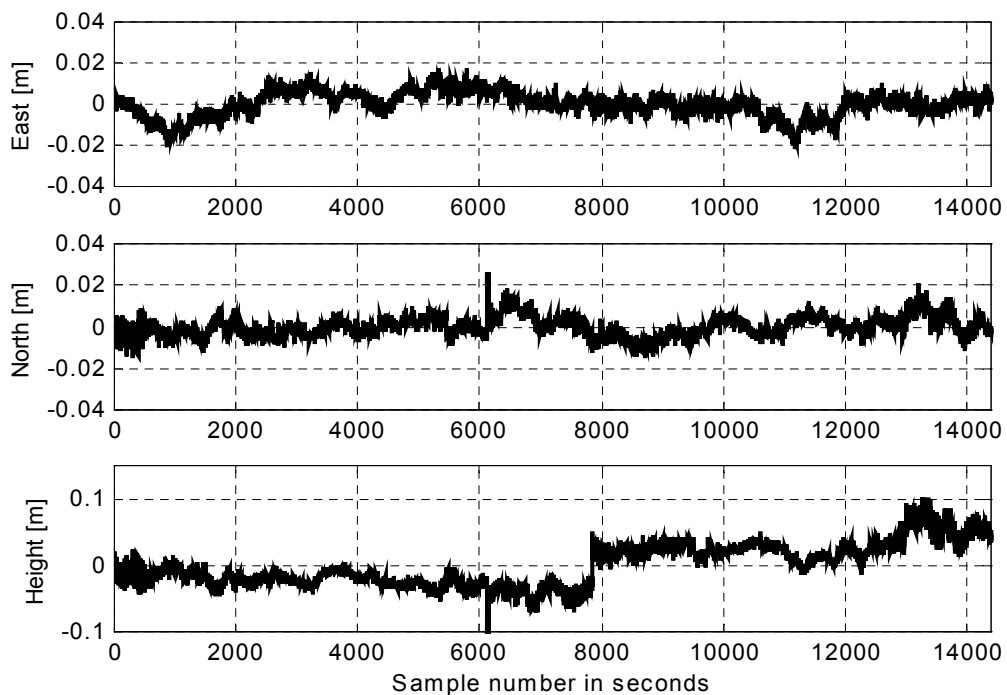


Figure 8.26. Time series of 1-second GPS solutions – NTU, 19 February 2000

Figure 8.27 shows the dominant frequencies of 0.01–0.05Hz, 0.01–0.16Hz, and 0.01–0.16Hz for the East ( $D_y$ ), North ( $D_x$ ), and Height ( $D_z$ ) components respectively. The corresponding amplitudes are  $\pm 0.2$  to  $\pm 2$ mm (East),  $\pm 0.2$  to  $\pm 1$ mm (North) and  $\pm 1$ mm (Height). The results in Figures 8.28 and 8.29 show a similar analysis. The conclusion from these results is that the RP Building responded to the short period of wind loading on the 19 February 2000. This is in agreement with an earlier analysis by Ogaja et al. (2000).



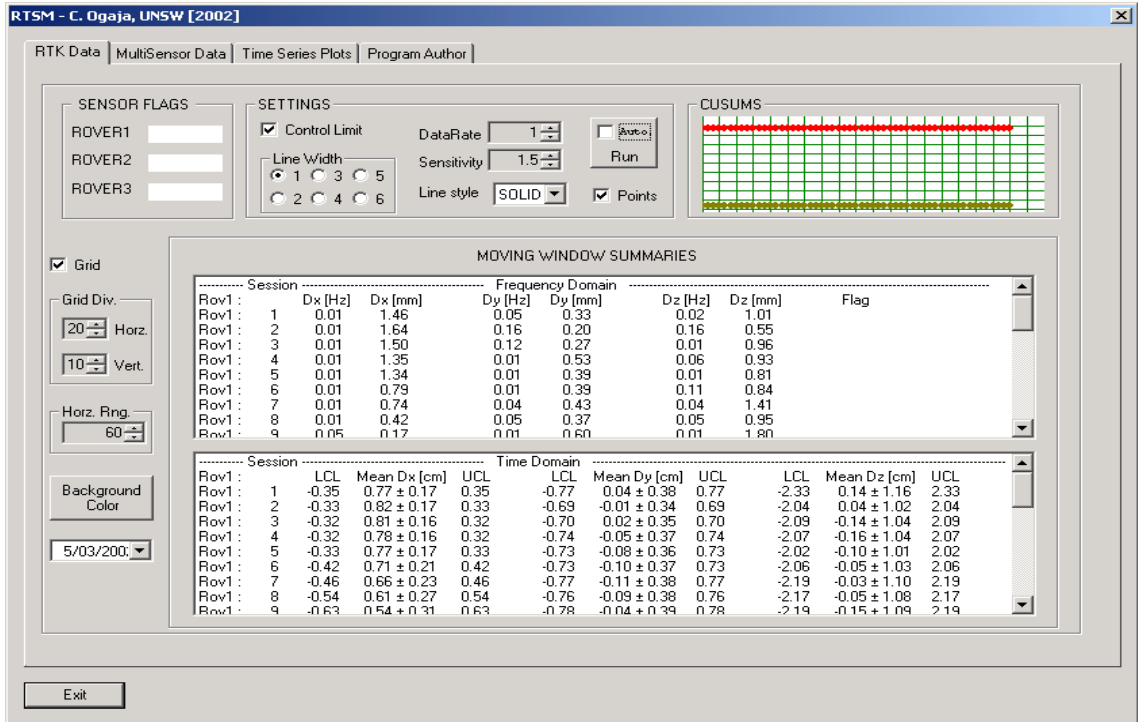


Figure 8.27. Screen Image of frequencies and amplitudes (RP Building) – Set 2A

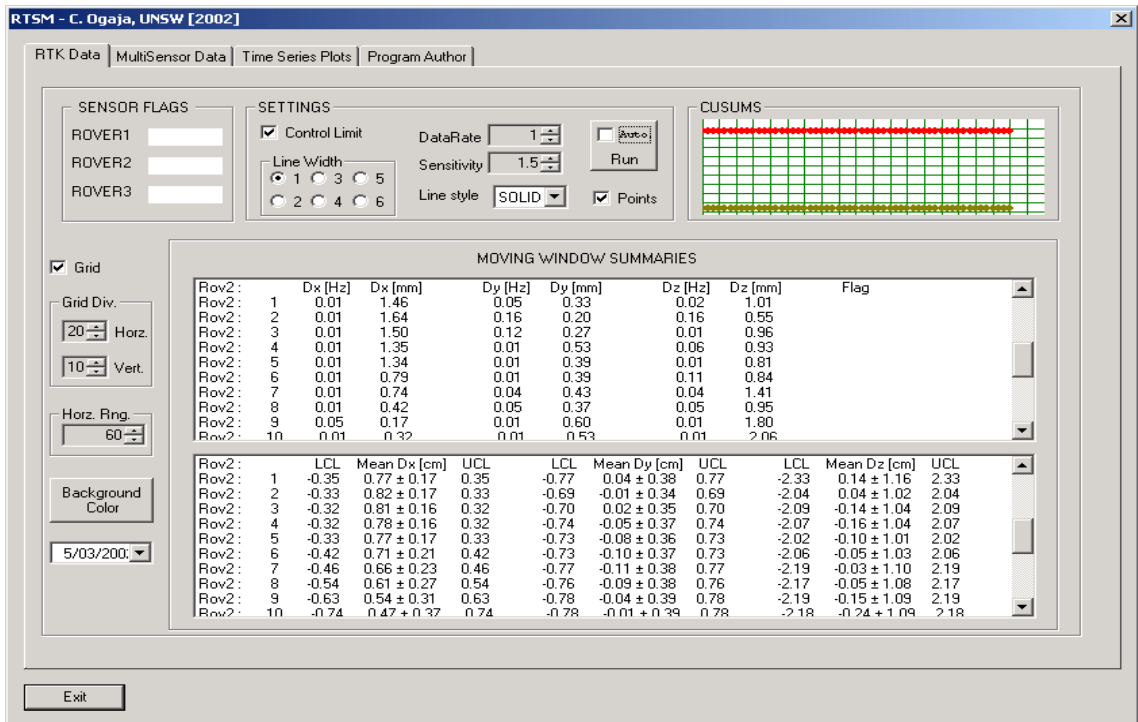


Figure 8.28. Screen Image of frequencies and amplitudes (RP Building) – Set 2B



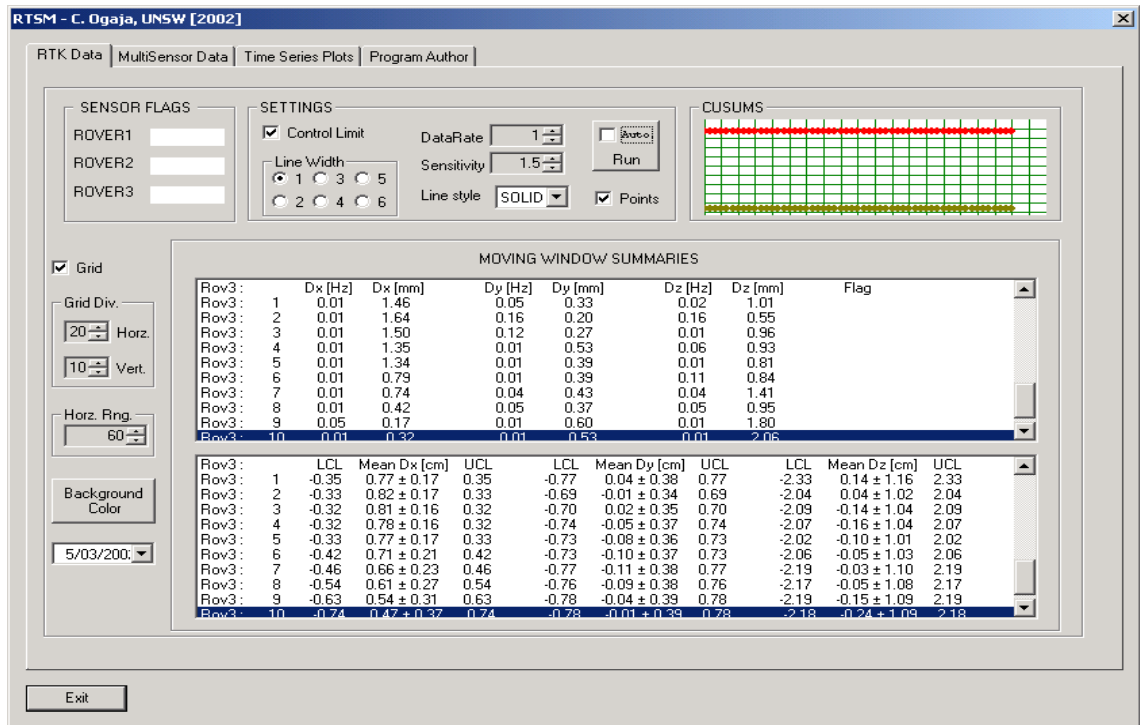


Figure 8.29. Screen Image of frequencies and amplitudes (RP Building) – Set 2C

## **9.1 Concluding Remarks**

One of the major challenges encountered in designing monitoring systems consisting of multiple GPS units, and a variety of additional sensors, is the volume of data that will be generated in real-time. Such systems require reliable but sensitive procedures for the screening, analysis and interpretation of the sensor data. The work described in this thesis introduces a general theoretical framework, and an associated software system, to support real-time structural monitoring using RTK-GPS and multisensor data as input. The implemented software system uses RTK position results and auxiliary measurements to provide information for system integrity purposes, as well as for short-period and long-period monitoring. Initial tests with numerical simulations and real datasets have demonstrated the capability of the system to extract dynamic information about structures.

The implemented software system was developed to run in the Microsoft Windows environment, providing several advantages, including a graphical-user-interface which is familiar to users of other Windows applications. The principal aim of developing the software was to provide a simple demonstrator system for GPS data integrity assessment, time domain and frequency domain monitoring, and GPS and multisensor unit monitoring.

### **9.1.1 Integrity Monitoring of GPS Data in the Position Domain**

For high precision and reliability, a GPS system should provide the user with some form of assurance as to the integrity of the system. In most cases this is accomplished by

designing the system so that the processing software handles all possible scenarios relating to degraded solution accuracy. The monitoring system should provide the user with timely warnings when either the total system, or any of its sub-systems, should not be used for monitoring.

Integrity of the GPS antenna position solutions is desired in order to guard against false alarms. Most of the current GPS fault detection and integrity monitoring methodologies are based on satellite fault detection/exclusion or bad geometry detection/exclusion approaches. In such methodologies either the *equation removal approach* or the *satellite removal approach* is used to ensure that reliable results are obtained at the GPS data processing step.

This study has considered a new approach to integrity assessment, which monitors for soft sensor faults (defects or biases) by using a multi-antenna method. The methodology has been designed as a basic approach that can be extended to application in multi-antenna GPS-based monitoring projects. However, it is currently intended for the minimum requirement of three receivers located on the structure being monitored.

### **9.1.2 Time Domain and Frequency Domain Analysis**

One aspect of real-time monitoring using GPS is the ability to measure slight but persistent variations in the horizontal or vertical components. In the context of the present study, structural monitoring can be accomplished by considering both the short-term dynamic information and the long-term information extracted from the measured data. The CUSUM algorithm is one of the methods appropriate for on-line time domain monitoring of variations in the GPS station coordinates. It has been successfully implemented in this study. The short-term dynamic information that relates to the periodic movements or structural vibrations due to wind loading, for example, is one of the main subjects of this study. It has been shown that sometimes, due to the high GPS sampling rate and receiver-induced noise, the dynamic information can best be extracted by spectrum analysis, as opposed to a mere time domain interpretation. Based on this principle, a methodology has been developed for extracting the dynamic information 'on

the fly', in the form of the dominant frequencies and their corresponding amplitudes. Several tests of the proposed methodology with numerical simulations and experimental datasets have shown the approach to be feasible.

### **9.1.3 GPS and Multisensor Data Analysis**

Many experiments have shown that the GPS technology can be integrated with other sensors to improve the reliability (and accuracy) of deformation monitoring. In this study, a multivariate monitoring procedure based on a single statistic has been proposed to deal with correlated measurements that are simultaneously generated by GPS and complementary sensors. It is shown that the proposed procedure can be used as an option for handling the large amounts of data that are typically generated by such sensors, and still be capable of extracting the important information contained within the individual measurements. Thus an immediate advantage is the reduction in data dimensionality. Through test examples, it has been demonstrated that the multivariate statistical process control can be applied to identify the trigger conditions during the measurement process, and thus to give an indication as to which sections of the data to analyse for an event capture. A wavelet transformation process is proposed for an improved interpretation of the multisensor data. Results from the combination of the wavelet transformation and multivariate Statistical Process Control (SPC) are encouraging. However, in the current demonstrator software system only the multivariate SPC component has been implemented.

## **9.2 Recommendations and Future Work**

Based on both the theoretical studies and experimental results described in this study, the following recommendations are made for further research work.

- 1) As demonstrated in Chapter 6, initial experiments with the proposed GPS data integrity monitoring technique have shown promising results. However, the current technique is based on the minimum number of monitoring stations, that is, three rovers, and on the assumption that a fault in only one of the rovers is detectable at

any one time. In practice, the number of rovers installed for monitoring a large bridge or a tall building may be many more. Consequently, it is considered a challenge that this issue must be addressed in the immediate future. The following are recommended:

- An optimal model should be designed to extend the concept of the multi-antenna method to handle more than the minimum three rover stations simultaneously. In such future work, the assumptions and challenges with regard to the inter-receiver distances and the influences of the immediate monitoring environments (e.g. in the case of long bridges) should be appropriately addressed.
  - The integrity monitoring model should be further optimised to take into account the fact that multiple rovers can be biased at the same time. In the present work it has been assumed that only one of the rovers can be at odds with the rest, at any instant in time.
- 2) As demonstrated in Chapter 7, a methodology based on the combination of the multivariate SPC and a wavelet transformation technique has been shown to improve the interpretation of multisensor data. An integrated analysis model has therefore been designed, as shown in Figure 9.1. It is proposed that this system be developed and implemented in an operational software system. In order to optimise the model, issues such as sensitivity to directional variations and efficient wavelet transformation should be addressed.
- 3) The demonstrator software system has been shown to be adequate for the tasks for which it was initially designed. However, a few other features and improvements that should be implemented include:
- Support for RTK-GPS data input from a larger number of rover stations.
  - Support for a more elaborate multisensor option (Figure 9.1).
  - Incorporation of a more sophisticated graphics display, with more capabilities.

- Inclusion of full online help facilities and a reference manual.

For the present study, the developed software system has been used in an offline mode, in which the data files are located on the harddisk of a PC. In the near future it is intended that this system will be further enhanced for implementation in an operational (i.e. real-time) monitoring system.

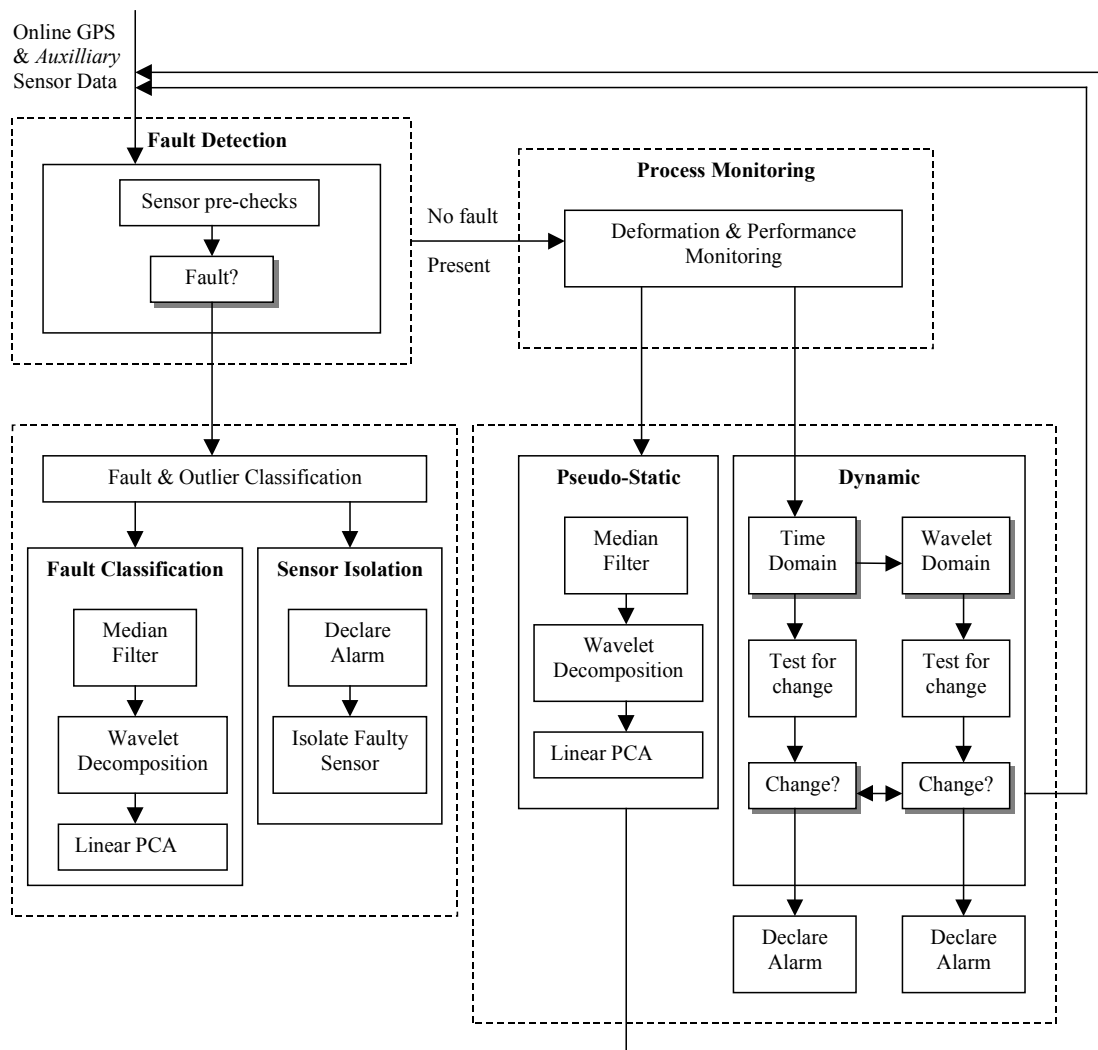


Figure 9.1. An integrated analysis model

## REFERENCES

---

---

- ANCOLD, (1994). Guidelines for Dam Instrumentation and Monitoring Systems. Australian National Committee on Large Dams. <http://www.damsafety.nsw.gov.au/ANCOLD/ANCOLD.htm>
- Aktan, A. E., F. N. Catbas & M. Pervizpour (2000). Real-time bridge health monitoring for management, *2<sup>nd</sup> Workshop on Advanced Technologies in Urban Earthquake Disaster Mitigation*, Kyoto, Japan, 9-14 July, 14pp. <http://www.parameterid.com/~mesut/>
- Ashkenazi, V., A.H. Dodson, T. Moore & G.W. Roberts (1997). Monitoring the movements of bridges by GPS, *10th Int. Tech. Meeting of the Satellite Division of the U.S. Inst. of Navigation*, Kansas City, Missouri, 16-19 September, 1165-1172.
- Aziz, W., W. A. Othman & H. Najib (2001). Monitoring high-rise building deformation using Global Positioning System, *The Asian GPS Conference*, New Delhi, 29-30 October, 13-18.
- Ballard, C. M. & S. S. Chen (1997). An internet structural monitoring system: In "Intelligent Civil Engineering Materials and Structures", a collection of state-of-the-art papers in the applications of emerging technologies to civil structures and materials published by the ASCE (American Society of Civil Engineers), New York, 229-242.
- Bannister, A., S. Raymond and R. Baker (1998). *Surveying*, 7<sup>th</sup> ed., Addison Wesley Longman Ltd., England, ISBN 0582302498, 502pp.
- Basseville, M. (1988). Detecting changes in signals and systems – a survey, *Automatica*, 24 (3), 309-326.
- Basseville, M. & V. Nikiforov (1993). *Detection of Abrupt Changes – Theory and Applications*, Prentice Hall, New Jersey, ISBN 0-13-126780-9, 441pp.
- Behr, J. A., K. Hudnut, & N. King (1998). Monitoring structural deformation at Pacoima Dam, California, using continuous GPS, *11<sup>th</sup> Int. Technical Meeting of the Satellite Division of the Institute of Navigation*, Nashville, Tennessee, 15-18 September, 59-68.
- Blais, J. A. R. (1988). *Estimation and Spectral Analysis*, The University of Calgary Press, Calgary, Alberta, Canada, ISBN 0-919813-41-0, 132pp.
- Boashash B. (1992). Estimating and interpreting the instantaneous frequency of a signal – part 2: Algorithms and applications, *IEEE*, 80(4), 540-568.
- Bock, Y., P. J. de Jong, D. Honcik, M. Bevis, L. Bock & S. Wilson (2001). Epoch-by-epoch positioning applied to dam deformation monitoring at Diamond valley lake,

- Southern California, *10th FIG Int. Symp. on Deformation Measurements*, Orange, California, 19-22 March, 78-87.
- Booth S. (2002a). Total stations today, *Engineering Surveying Showcase*, A GITC Brochure, GITC, Netherlands, 15-28.
- Booth S. (2002b). Monitoring station deformation, *Engineering Surveying Showcase*, A GITC Brochure, GITC, Netherlands, 42-43.
- Breumso S. (2001). Deformation measurement on bridge and tunnel of the fixed link between Sweden and Denmark, *10th FIG Int. Symp. on Deformation Measurements*, Orange, California, 19-22 March, 259-267.
- Brinker, R. C. & R. Minnick (1995). *The Surveying Handbook*, 2<sup>nd</sup> ed., Chapman & Hall, New York, ISBN 041298511X, 967pp.
- Brown, R. G. (1996). Receiver Autonomous Integrity Monitoring, In: Parkinson, B.W. et al. (eds.), *Global Positioning System: Theory and Applications*, Progress in Astronautics & Aeronautics, ISBN 1-56347-107-8, 164, 143-165.
- Brownjohn, J. M. W. & C. K. Ang (1998). Full-scale dynamic response of a high rise building subject to lateral loading, *ASCE Journal of Performance of Constructed Facilities*, 12(1), 33-40.
- Brownjohn, J. M. W. & T. C. Pan (2001). Response of a tall building to long distance earthquakes, *Earthquake Engineering and Structural Dynamics*, 30, 709-729.
- Brownjohn, J. M. W., M. Boccione, A. Curami, M. Falco & A. Zasso (1994). Humber Bridge full scale measure campaigns 1990-1991, *Wind Engineering & Industrial Aerodynamics*, 52, 185-218.
- Brownjohn, J. M. W., T. C. Pan & H. K. Cheong (1998). Dynamic response of Republic Plaza, Singapore, *The Structural Engineer*, 76(11), 221-226.
- Brunner, F.K. & Welsch, W.M. (1993) Effect of the troposphere on GPS measurements, *GPS World*, 4(1), 42-51.
- Çelebi, M., C. Arnold C., V. Bertero, Borchardt, D. Roger, G. Brady, J. Fedock, J. Gates, R. Maley, C. Mortgat, C. Rojahn, E. Safak, H. Shah & E. Zacker (1984). Report on recommended list of structures for seismic instrumentation in the San Francisco Bay region, USGS OF 84-0488, [http://nsmp.wr.usgs.gov/publications/online\\_reports.html](http://nsmp.wr.usgs.gov/publications/online_reports.html), 36pp.
- Çelebi, M., G. Brady, C. Rojahn, W. Iwan, G. Hart, G. Pardo, L. Schoelkopf, R. Haskell, K. Topping, E. Safak & R. Maley (1985). Report on recommended list of structures for seismic instrumentation in San Bernardino county, California, USGS OF 85-583, [http://nsmp.wr.usgs.gov/publications/online\\_reports.html](http://nsmp.wr.usgs.gov/publications/online_reports.html), 18pp.



- Çelebi, M., J. Bagwell, R. Elling, C. Lindberg, R. Maley, R. Pool, J. Radzimirski, C. Simmons, D. Smits, P. Sparks & P. Talwani (1986). Report on recommended list of structures for seismic instrumentation in Southeastern United States, USGS OF 86-398, [http://nsmp.wr.usgs.gov/publications/online\\_reports.html](http://nsmp.wr.usgs.gov/publications/online_reports.html), 22 pp.
- Çelebi, M., M. Cassaro, W. Durbin, P. Gould, W. Graham, A. Johnston, H. Karabinis, A. Lin, R. Maley, O. Nuttli, G. Schwalbe, J. Theiss, M. Walsh & T. Winstead (1987). Report on recommended list of structures for seismic instrumentation in the New Madrid region, USGS OF 87-59, [http://nsmp.wr.usgs.gov/publications/online\\_reports.html](http://nsmp.wr.usgs.gov/publications/online_reports.html), 37pp.
- Çelebi, M., G. Brady, K. Deppe, W. Gates, G. Hart, R. Haskell, W. Iwan, J. Lord, R. Maley, D. Ostrom, C. Rojahn, E. Safak, B. Schmid, L. Schoelkopf, B. Zaropapel & E. Zeller (1988). Report on recommended list of structures for seismic instrumentation in the Los Angeles region, USGS OF 88-277, [http://nsmp.wr.usgs.gov/publications/online\\_reports.html](http://nsmp.wr.usgs.gov/publications/online_reports.html), 23pp.
- Çelebi, M., B. Olsen, L. Bush, J. Clark, R. Crosson, P. Grant, H. Halverson, N. Hawkins, W. Hancock, T. Kinsman, R. Maley, L. Noson, C. Pearson & U. Vasishth (1989). Report on list of structures recommended for seismic instrumentation in the Puget Sound area, Washington, USGS OF 89-374, [http://nsmp.wr.usgs.gov/publications/online\\_reports.html](http://nsmp.wr.usgs.gov/publications/online_reports.html), 61pp.
- Celebi, M., W. Prescott, R. Stein, K. Hudnut, J. Behr & S. Wilson (1998a). Structural monitoring using GPS, *11th Int. Tech. Meeting of the Satellite Division of the U.S. Inst. of Navigation*, Nashville, Tennessee, 15-18 September, 929-935.
- Çelebi, M., S. Nishenko, C. Astill & R. Chung (1998b). Seismic instrumentation of federal buildings; A proposal document for consideration by federal agencies: USGS OF 98-117, [http://nsmp.wr.usgs.gov/publications/online\\_reports.html](http://nsmp.wr.usgs.gov/publications/online_reports.html), 38pp.
- Celebi, M. (2000a). GPS in dynamic monitoring of long-period structures, *Soil Dynamics and Earthquake Engineering*, 20, p. 477-483.
- Celebi, M. (2000b). Seismic instrumentation of buildings, USGS OF 00-157, [http://nsmp.wr.usgs.gov/publications/online\\_reports.html](http://nsmp.wr.usgs.gov/publications/online_reports.html), 37pp.
- Celebi, M. & Sanli, A. (2002). GPS in pioneering dynamic monitoring of long-period structures, *Earthquake Spectra*, 18(1), 47-61.
- Chang, X.W. & C.C. Paige (2000). Two carrier phase based approaches for autonomous fault detection and exclusion, *13th Int. Tech. Meeting of the Satellite Division of the U.S. Inst. of Navigation*, Salt Lake City, Utah, 19-22 September, 1895-1905.
- Chui, C. K. (1992). *An Introduction to Wavelets*. Academic Press, New York, ISBN 0121745848, 264pp.
- Cohen, C. E., B. S. Pervan, D. G. Lawrence, H. S. Cobb, J. D. Powell & B. W. Parkinson (1993). Real-time flight test evaluation of the GPS marker beacon concept

- for category III kinematic GPS precision landing, *6th Int. Tech. Meeting of the Satellite Division of the U.S. Inst. of Navigation*, Salt Lake City, Utah, 22-24 September, 841-849.
- Cohen, C. E., B. S. Pervan, H. S. Cobb, D. G. Lawrence, J. D. Powell & B. W. Parkinson (1996). Precision Landing of Aircraft Using Integrity Beacons, In: Parkinson, B.W. et al. (eds.), *Global Positioning System: Theory and Applications*, Progress in Astronautics & Aeronautics, ISBN 1-56347-107-8, 164, 427-459.
- Cox, M. A. A. (1988-89). Control charts on spreadsheets: A tutorial guide or poor man's persuader, *Quality Engineering*, 1(2), 135-155.
- Cross, P., D. J. Hawksbee & R. Nicolai. (1994). Quality measures for differential GPS positioning, *The Hydrographic Journal*, 72, 17-22.
- Dai, L., J. Wang, C. Rizos & S. Han (2001a) Applications of pseudolites for deformation monitoring systems, *10th FIG Int. Symp. on Deformation Measurements*, Orange, California, 19-22 March, 11-22.
- Dai, L., C. Rizos, & J. Wang (2001b). The role of pseudo-satellite signals in precise GPS-based positioning, *Journal of Geospatial Eng., HK Inst. of Engineering Surveyors*, 3(1), 33-44.
- Dai, L., J. Wang, C. Rizos, & S. Han (2002). Pseudo-satellite applications in deformation monitoring, *GPS Solutions*, 5(3), 80-87.
- Dale, R. (1996). Deformation surveys at Mangahao power station, North Island, New Zealand, *8th FIG Int. Symp. on Deformation Measurements*, Hong Kong, 25-28 June, 325-334.
- De Jong, K. (2000). Minimal detectable biases of cross-correlated GPS observations, *GPS Solutions*, 3(3), 12-18.
- De Jong, C. D., H. van der Marel & N. F. Jonkman (2001). Real-time GPS and GLONASS integrity monitoring and reference station software, *Phys. Chem. Earth*, 26(6-8), 545-549.
- DeLoach, S.R. (1989). Continuous deformation monitoring with GPS, *Journal of Surveying Engineering*, 115(1), 93-110
- Ding, X., Y. Chen, J. Zhu & D. Huang (1999). Surface deformation detection using multipath signals, *12th Int. Tech. Meeting of the Satellite Division of the U.S. Inst. of Navigation*, Nashville, Tennessee, 14-17 September, 53-62.
- Dodson, A H, X. Meng & G. W. Roberts (2001). Adaptive method for multipath mitigation and its applications for structural deflection monitoring, *Proc. of International Symposium on Kinematic Systems in Geodesy, Geomatics and Navigation (KIS 2001)*, Banff, Canada, 5-8 June, 101-108.

- Duckrell, R. & M.P. Stewart (1998). GPS monitoring of North Dandalup Dam, Western Australia, '*Advances in GPS Deformation Monitoring*', Perth, Australia, 24-25 September, Paper No. 10.
- Duffy, M. A. & C. Whitaker (1999). Deformation monitoring scheme using static GPS and continuous operating reference stations (CORS) in California, *12<sup>th</sup> Int. Technical Meeting of the Satellite Division of the Institute of Navigation*, Tennessee, 14-17 September, 63-70.
- Duffy, M. A., C. Hill, C. Whitaker, A. Chrzanowski, J. Lutes & G. Bastin (2001). An automated and integrated monitoring program for Diamond Valley Lake in California, *10th FIG Int. Symp. on Deformation Measurements*, Orange, California, 19-22 March, k1-k23.
- Dunnicliff, J. (1988). *Geotechnical Instrumentation for Monitoring Field Performance*, 1<sup>st</sup> Edition, John Wiley & Sons, New York, ISBN 0471096148, 577pp.
- Dunnicliff, J. (1993). *Geotechnical Instrumentation for Monitoring Field Performance*, 2<sup>nd</sup> Edition, John Wiley & Sons, New York, ISBN 047 1005460, 608pp.
- El-Mowafy, A. (1994). *Kinematic Attitude Determination From GPS*, UCGE Report Number 20074, The University of Calgary, 215pp.
- Embree, P. (1995). *C Algorithms for Real-Time DSP*, Prentice Hall, Englewood Cliffs, New Jersey, ISBN 0133373533, 248pp.
- Embree, P. & D. Danieli, (1999). *C++ Algorithms for Digital Signal Processing*, Second Edition, Prentice Hall, Englewood Cliffs, New Jersey, ISBN 0-13-179144-3, 579pp.
- Enge, P.K. & Van Dierendonck, A.J. (1996) Wide Area Augmentation System, In *Global Positioning System: Theory and Applications (Vol. 2)*, Edited by Parkinson & Spilker, American Institute of Aeronautics and Astronautics, Inc., Washington D.C., ISBN 1-56347-107-8, 117-142.
- Fraser, C. S. (1996). Design aspects utilizing digital photogrammetry for deformation measurements, *8th FIG Int. Symp. on Deformation Measurements*, Hong Kong, 25-28 June, 115-124.
- Garcia, D. & J. Orteu (2001). 3D deformation measurement using stereo-correlation applied to experimental mechanics, *10th FIG Int. Symp. on Deformation Measurements*, Orange, California, 19-22 March, 23-32.
- Ge, L., L. Dai, S. Han & C. Rizos (2000a). GPS seismometers: the implementing issues, *14th Int. Tech. Meeting of the Satellite Division of the U.S. Inst. of Navigation*, Salt Lake City, Utah, 19-22 September, 75-83.
- Ge, L., H. Y. Chen, S. Han & C. Rizos (2000b). Adaptive filtering of continuous GPS results, *Journal of Geodesy*, 74(7/8), 572-580.

- Ge, L., S. Han & C. Rizos (2000c). Multipath mitigation of continuous GPS measurements using an adaptive filter, *GPS Solutions*, 4(2), 19-30.
- Gentile, C., F. Martinez & Y. Cabrera (2001). Dynamic Assessment of a curved cable-stayed bridge at the Malpensa 2000 airport, *Structural Engineering International*, 11(1).
- Georgiadou, Y. & A. Kleusberg (1989) On carrier signal multipath effects in relative GPS positioning, *Manuscripta Geodaetica*, 14, 143-148.
- Gnanadesikan, R. (1997). *Methods for Statistical Data Analysis of Multivariate Observations*, John Wiley & Sons, New York, ISBN 0-471-16119-5, 384pp.
- Gnanadesikan, R. and Kettenring, J. R. (1972). Robust estimates, residuals and outlier detection with multiresponse data, *Biometrics* 28, 81-124.
- Goad, C.C. (1987) Precise positioning with the GPS, *In Applied Geodesy, Lecture Notes in Earth Sciences*, Edited by Turner, Springer-Verlag, Berlin, 12, 17-30.
- Gordon, S., D. Lichti & M. Stewart (2001). Application of a high-resolution, ground-based laser scanner for deformation measurements, *10th FIG Int. Symp. on Deformation Measurements*, Orange, California, 19-22 March, 23-32.
- Guo, J. & S. Ge (1997). Research of displacement and frequency of tall building under wind loading using GPS, *10th Int. Tech. Meeting of the Satellite Division of the U.S. Inst. of Navigation*, Kansas City, Missouri, 16-19 September, 1385-1388.
- Han, S. (1997) Quality control issues relating to instantaneous ambiguity resolution for real-time GPS kinematic positioning, *Journal of Geodesy*, 71, 351-361.
- Han, S. & C. Rizos. (1995). A suggested procedure for on-the-fly ambiguity resolution for long range kinematic positioning, *4th Int. Conf. On Differential Navigation Systems*, Norway, 24-28 April, Paper 67, 8pp.
- Han, S. & C. Rizos. (1996). Integrated method for instantaneous ambiguity resolution using new generation GPS receivers, *IEEE Position Location and Navigation Symp. PLAN'96*, Atlanta, Georgia, 22-26 April, 254-261.
- Han, S. & C. Rizos. (1997a). An instantaneous ambiguity resolution technique for medium-range GPS kinematic positioning, *10<sup>th</sup> Int. Tech. Meeting of the Satellite Division of the U.S. Inst. Of Navigation*, Kansas City, Missouri, 16-19 September, 1789-1800.
- Han, S. & C. Rizos (1997b). Multipath effects on GPS in mine environments, *X<sup>th</sup> Int. Congress on the International Society for Mine Surveying*, Fremantle, Australia, 2-6 November, 447-457.

- Hatch, R. (1986) Dynamic differential GPS at the centimetre level, *Fourth International Geodetic Symposium on Satellite Positioning*, Austin, Texas, 28 April-2 May, 1287-1298.
- Hatch, R. & H. J. Euler. (1994) Comparison of several AROF kinematic techniques, *7<sup>th</sup> International Technical Meeting of the Satellite Division of the Institute of Navigation*, Salt Lake City, Utah, 20-23 September, 363-370.
- Haykin, S. (1995). *Advances in Spectrum Analysis and Array Processing*, 1<sup>st</sup> ed. (Vol. 3), Prentice Hall, New Jersey, ISBN 0130615404, 560pp.
- Hearn, G. (1998). Condition data and bridge management systems, *Structural Engineering International*, 8(3), <http://www.iabse.ethz.ch/sei/backissues/sei9803toc.html>.
- Heinonen, P. & Y. Neuvo (1987). Fir-median hybrid filters, *IEEE Trans. Acoustics, Speech & Signal Processes*, 35, 832-838.
- Hill, B. (2000). Creating a CTabCtrl Application, <http://codeguru.earthweb.COM/controls/CMyTabCtrl.html>.
- Hinkley, D. (1970). Inference about the change point in a sequence of random variables, *Biometrika*, 57(1), 1-17.
- Hofmann-Wellenhof, B., H. Lichtenegger, & J. Collins (2001) *Global Positioning System: Theory and Practice*, 5<sup>th</sup> edition, Springer-Verlag, Berlin Heidelberg New York, ISBN 3211835342, 382pp.
- Hollmann, R. & W. M. Welsch. (1992). A high precision dam monitoring network observed with GPS or can GPS replace terrestrial measurements for high precision engineering networks? *6<sup>th</sup> International Geodetic Symposium on Satellite Positioning*, Columbus, Ohio, 17-20 March, 811-821.
- Hudnut, K. W. & J. A. Behr (1998). Continuous GPS monitoring of structural deformation at Pacoima Dam, *Seismological Research Letters*, 69(4), 299-308.
- Hudnut, K. W., Y. Bock, J. E. Galetzka, F. H. Webb & W. H. Young (2001). The Southern California Integrated GPS Network (SCIGN), *10th FIG Int. Symp. on Deformation Measurements*, Orange, California, 19-22 March, 129-148.
- IGS (2001). The International GPS Service, <http://igs.cb.jpl.nasa.gov/components/prods.html>.
- Jackson, J. E. (1985). Multivariate quality control, *Communications in Statistics*, 14(11), 2657-2688.
- Jian, Y., P. Zengfong & C. Baicong (1996). Laser alignment real-time system of deformation measurements, *8th FIG Int. Symp. on Deformation Measurements*, Hong Kong, 25-28 June, 171-174.

- Jonkman, N. F. & K. De Jong (2000a). Integrity monitoring of IGEX-98 data, part I: availability, *GPS Solutions*, 3(4), 10-23.
- Jonkman, N. F. & K. De Jong (2000b). Integrity monitoring of IGEX-98 data, part II: cycle slip and outlier detection, *GPS Solutions*, 3(4), 24-34.
- Jonkman, N. F. & K. De Jong (2000c). Integrity monitoring of IGEX-98 data, part III: broadcast navigation message validation, *GPS Solutions*, 4(2), 45-53.
- JPS (1998) A GPS Tutorial: Basics of High Precision Global Positioning Systems, Javad Positioning Systems, Inc., <http://www.topconps.com>
- Kälber, S., R. Jäger & R. Schwäble (2000). A GPS-based online control and alarm system, *GPS Solutions*, 3(3), 19-25.
- Kahmen, H. (1994). Optical 3-D measurement techniques with measurement robots: applications in inspection quality control and robotics, *XX FIG Congress on Engineering Surveys*, Melbourne, Australia, 5-12 March, 265-280.
- Kahmen, H., A. Kopacik, V. Stanek & P. Vybiral (1994). Determination of 2-D deformations with accelerometers, *XX FIG Congress on Engineering Surveys*, Melbourne, Australia, 5-12 March, 114-122.
- Kahmen, H. (1996). New developments in instrumentation for precise engineering and deformation surveys, *8th FIG Int. Symp. on Deformation Measurements*, Hong Kong, 25-28 June, 77-84.
- Kashima, S., Y. Yanaka, S. Suzuki & K. Mori (2001). Monitoring the Akashi Kaikyo Bridge: first experiences, *Structural Engineering International*, 11(2), 120-123.
- Katowski, O. (1995). Precision deformation measurement with automatic monitoring systems, *the 5th South East Asian and 36th Australian Surveyors Congress*, Singapore, 16-20 July, 499-508.
- Katowski, O. (1996). Machine guidance and deformation monitoring with automatic theodolite systems, *8th FIG Int. Symp. on Deformation Measurements*, Hong Kong, 25-28 June, 85-90.
- Katupitiya, J., & K. Bentley (2000). *C++ Programming with Electronic Interfacing University Teaching Aid*, 2<sup>nd</sup> edition, UNSW, Sydney, Australia. 379pp.
- Kavanagh, B. F. (2001). *Surveying: with Construction Applications*, 4<sup>th</sup> ed., Prentice Hall, New Jersey, ISBN 0130271438, 603pp.
- Kayser, J. & R. Schwarb (2001). Geotechnical and structural measurements for a deep excavation near an existing navigable lock, *10th FIG Int. Symp. on Deformation Measurements*, Orange, California, 19-22 March, 250-258.

- Keats, J. B., J. D. Miskulin & C. R. George (1995). Statistical process control design, *Quality Technology*, 27(3), 214-225.
- Klobuchar, J.A. (1991). Ionospheric effects on GPS, *GPS World*, 2(4), 48-51.
- Kondo, H. and M. E. Cannon (1995). Real-time landslide detection system using precise carrier phase GPS, *8<sup>th</sup> Int. Tech. Meeting of the Satellite Division of the U.S. Inst. Of Navigation*, Palm Springs, California, 12-15 September, 1877-1884.
- Kourti, T. & J. F. MacGregor (1996). Multivariate SPC methods for process and product monitoring, *Quality Technology*, 28(4), 409-427.
- Lachapelle, G. (1990). GPS observables and error sources for kinematic positioning, *IAG International Symposium No. 107 on Kinematic Systems in Geodesy, Surveying and Remote Sensing*, Springer Verlag, New York, 10-13 September, 17-26.
- Lachapelle, G., M. E. Cannon & G. Lu (1992). High precision GPS navigation with emphasis on carrier phase ambiguity resolution, *Marine Geodesy*, 15 (4), 253-269.
- Lam, S. Y. W. & C. H. W. Tang (2001). On monitoring the precise geometric models for tunnel construction in HongKong, *IAG Workshop on Monitoring of Constructions & Local Geodynamic Process*, Wuhan, China, 22-24 May, 84-87.
- Langley, R.B. (1993). The GPS observables, *GPS World*, 4(4), 52-59.
- Langley, R.B. (1998). RTK GPS, *GPS World*, 9(9), 70-76.
- Leica Geosystems (2002). Bridge Surveys: record breaking Tsing Ma Bridge, <http://www.leica-geosystems.com/civil/application/tsingma.htm>
- Leick, A. (1995). *GPS Satellite Surveying*, 2<sup>nd</sup> edition, John Wiley & Sons, Inc., New York, ISBN 047 1306266, 560pp.
- Lichti, D. D. & M. A. Chapman (1996). Evaluation of the finite element method of self-calibration for photogrammetric deformation measurements, *8th FIG Int. Symp. on Deformation Measurements*, Hong Kong, 25-28 June, 125-134.
- Lin, L.S. (1997) *Real-Time Estimation of Ionospheric Delay Using GPS Measurements*, Ph.D. thesis, School of Geomatic Engineering, The University of New South Wales, Sydney, Australia, 198pp.
- Lovse, J., W.F. Teskey, G. Lachapelle & M. E. Cannon (1995). Dynamic deformation monitoring of tall structures using GPS technology, *Journal of Surveying Engineering*, 121(1), 35-40.
- Lowry, A. & R. MacLeod (1997). Pmos – a real-time precise DGPS continuous deformation monitoring system, *10<sup>th</sup> Int. Tech. Meeting of the Satellite Division of the U.S. Inst. Of Navigation*, Kansas City, Missouri, 16-19 September, 923-927.

- Lu, C. (1999). Control charts for monitoring the mean and variance of autocorrelated processes, *Quality Technology*, 31(3), 259-274.
- McReynolds, P. (1994). *SPC Made Easy: Process Control Charting with Your Favourite Spreadsheet*, TitleWave Press, San Jose, California, ISBN 1-883327-46-6, 290pp.
- Mentes, G. & M. Fabian (2001a). Investigation of motions due to mechanical coupling between ground and the TV tower at Sopron, Hungary, *IAG Workshop on Monitoring of Constructions & Local Geodynamic Process*, Wuhan, China, 22-24 May, 56-62.
- Mentes, G. & M. Fabian (2001b). Investigation of ground and object motions at the TV tower in Sopron, Hungary, *Acta Geodaetica et Geophysica Hungarica*, 36(4), 391-398.
- Mertikas, S.P. (1998). Quality control and automatic deformation monitoring with GPS. 'Advances in GPS Deformation Monitoring', Perth, Australia, 24-25 September, Paper 12.
- Mertikas, S. (2001). Automatic and online detection of small but persistent shifts in GPS station coordinates and statistical process control, *GPS Solutions*, 5(1), 39-50.
- Mertikas, S. P. & C. Rizos (1996). Quality control of GPS measurements for real time applications, *8th FIG Int. Symp. on Deformation Measurements*, Hong Kong, 25-28 June, 27-36.
- Mertikas, S. P. & C. Rizos (1997). On-line detection of abrupt changes in the carrier phase measurements of GPS, *Journal of Geodesy*, 71, 469-482.
- Mertikas, S. P. & C. Rizos (1998). Real-time failure detection in the carrier phase measurements of GPS by robust and conventional Kalman filtering, *Marine Geodesy*, 21(1), 41-65.
- Mikhail, E. M., J. S. Bethel & J. C. McGlone (2001). *Introduction to modern photogrammetry*, Wiley & Sons, New York, ISBN 0471309249, 479pp.
- Moffitt, F. H. & J. D. Bossler (1998). *Surveying*, 10<sup>th</sup> ed., Addison Wesley, California. 738pp.
- Morley, T. G. (1997). Augmenting of GPS with Pseudolites in a marine environment, M.Sc. Thesis, The University of Calgary, Calgary, Alberta, 144pp.
- Murchison, D. E. (1977). *Surveying and Photogrammetry: Computation for Civil Engineers*, Newnes-Butterworths, Boston, ISBN 040800293X, 113pp.
- Nakamura, S. (2000). GPS measurement of wind-induced suspension bridge girder displacements, *Journal of Structural Engineering*, 126(12), 1413-1419.



- Niemeier, W. & D. Tengen (1988). PANDA - a menu driven software package on a PC for optimization, adjustment and deformation analysis of engineering networks, *5<sup>th</sup> Int. FIG Symposium "Deformationsmessungen"*, Fredericton, Canada, 374-376.
- NGS (2001). National Geodetic Survey web site: <http://www.ngs.noaa.gov/ANTCAL/>.
- Nolan, J. M. (1990). *Development of a Navigational System Utilizing the Global Positioning System in a Real-Time, Differential Mode*, Unisurv S-40, University of New South Wales, Sydney, Australia, 163pp.
- Ober, P. (2000). Position domain integrity assessment, *13th Int. Tech. Meeting of the Satellite Division of the U.S. Inst. of Navigation*, Salt Lake City, Utah, 19-22 September, 1948-1956.
- Obidowski, R. M. & W. F. Teskey (1996). Precise surveying techniques for machinery alignment, *8th FIG Int. Symp. on Deformation Measurements*, Hong Kong, 25-28 June, 135-142.
- Ochieng, W. Y., K. F. Sheridan, X. Han, P. A. Cross, S. Lannelongue, N. Ammour & K. Petit (2001). Integrity performance models for a combined Galileo/GPS navigation system, *Journal of Geospatial Engineering*, 3(1), 21-32.
- Ochieng, W. Y., K. F. Sheridan, K. Sauer, X. Han, P. A. Cross, S. Lannelongue, N. Ammour & K. Petit (2002). An assessment of the RAIM performance of a combined Galileo/GPS navigation system using the marginally detectable errors (MDE) algorithm. *GPS Solutions*, 5(3), 42-51.
- Ogaja, C. (2001). On-line GPS integrity monitoring and deformation analysis for structural monitoring applications, *14th Int. Tech. Meeting of the Satellite Division of the U.S. Inst. of Navigation*, Salt Lake City, Utah, 11-14 September, 989-999.
- Ogaja, C., C. Rizos & S. Han (2000). Is GPS good enough for monitoring the dynamics of high rise buildings? *2nd Trans Tasman Survey Congress*, Queenstown, New Zealand, 20-26 August, 150-164.
- Ogaja, C., C. Rizos, J. Wang & J. Brownjohn (2001a). Towards the implementation of on-line structural monitoring using RTK-GPS and analysis of results using the wavelet transform, *10th FIG Int. Symp. on Deformation Measurements*, Orange, California, 19-22 March, 284-293.
- Ogaja, C., C. Rizos, J. Wang, & J. Brownjohn (2001b). A dynamic GPS system for on-line structural monitoring, *Int. Symp. on Kinematic Systems in Geodesy, Geomatics & Navigation (KIS2001)*, Banff, Canada, 5-8 June, 290-297.
- Ogaja, C., C. Rizos, J. Wang, & J. Brownjohn (2001c). High precision dynamic GPS system for on-line structural monitoring, *5th Int. Symp. on Satellite Navigation Technology & Applications*, Canberra, Australia, 24-27 July, Paper 35, CD-ROM Proc.

- Olivier, R. & M. Vetterli (1991). Wavelets and signal processing, *IEEE Sig. Processing*, October, 8(4), 14-38.
- Page, E. (1954). Continuous inspection schemes, *Biometrika*, 41, 100-115.
- Page, E. (1957). Estimating the point of change in a continuous process, *Biometrika*, 44, 248-252.
- Pervan, B. S., C. E. Cohen & B. W. Parkinson (1994). Integrity monitoring for precision approach using kinematic GPS and a ground-based pseudolite, *Journal of the Institute of Navigation*, 41(2), 159-173.
- Parkinson, B.W. (1994). GPS eyewitness: the early years, *GPS World*, 5(9), 32-45.
- Parkinson, B.W. & P. K. Enge (1996). Differential GPS, In *Global Positioning System: Theory and Applications (Vol. 2)*, Edited by Parkinson & Spilker, American Institute of Aeronautics and Astronautics, Inc., Washington D.C., ISBN 1-56347-107-8, 3-50.
- Parkinson, B.W. & J. J. Spilker Jr. (eds.) (1996). *Global Positioning System: Theory and Applications (Vol. 1)*, American Institute of Aeronautics and Astronautics, Inc., Washington D.C., ISBN 1-56347-106-X, 793pp.
- Paxton, J. F. (2001). MILLIKEN Dam: Structural monitoring of a concrete arch dam, *10th FIG Int. Symp. on Deformation Measurements*, Orange, California, 19-22 March, 193-202.
- Perrott, S. W. (1970). *Surveying for Young Engineers*, 3<sup>rd</sup> ed., Chapman & Hall, London, ISBN 041209830X, 188pp.
- Petranovic, D., S. Stankovic & L. Stankovic (1997). Special purpose hardware for time frequency analysis, *Electron. Letters*, 33(6), 464-465.
- Pignatiello, J. J. & C. R. George (1990). Comparisons of multivariate CUSUM charts, *Quality Technology*, 22(3), 173-181.
- Pretorius, C. J., W. F. Schmidt, C. S. van Staden & K. Egger (2001). The extensive geodetic system used for the monitoring of 185 metre high arc dam in Southern Africa, *10th FIG Int. Symp. on Deformation Measurements*, Orange, California, 19-22 March, 203-213.
- Proszynski, W. & A. Stanczyk (2001). Erecting the inclined pylon legs in a cable-stayed bridge with the support of strain and stress analysis, *10th FIG Int. Symp. on Deformation Measurements*, Orange, California, 19-22 March, 276-283.
- Qian S. & D. Chen (1996). *Joint Time-Frequency Analysis: Methods and Applications*. Prentice Hall, New Jersey, ISBN 0132543842, 302pp.
- Qin, Z., P. Jianbin, W. Li & L. Wanlin (2001). The technical design and set-up of the GPS monitor network of the shore slope in the Hei River Reservoir, *IAG Workshop*

- on Monitoring of Constructions & Local Geodynamic Process*, Wuhan, China, 22-24 May, 278-287.
- Qiu, W. (1993). *An Analysis of Some Critical Error Sources in Static GPS Surveying*, UCGE Report Number 20054, The University of Calgary, 102pp.
- Radovanovic R. S. (2000). High accuracy deformation monitoring via multipath mitigation by day-to-day correlation analysis, *13th Int. Tech. Meeting of the Satellite Division of the U.S. Inst. of Navigation*, Salt Lake City, Utah, 19-22 September, 35-44.
- Radovanovic, R. S. & W. F. Teskey (2001). Dynamic monitoring of structures: GPS versus robotic tacheometry systems, *10th FIG Int. Symp. on Deformation Measurements*, Orange, California, 19-22 March, 61-70.
- Rao, P. & J. Taylor (1990). Estimation of instantaneous frequency using the Discrete Wigner Distribution, *Electron. Letters*, 26(4), 246-248.
- Ray, J. K. (1999). Use of multiple antennas to mitigate carrier phase multipath in reference stations, *12th Int. Tech. Meeting of the Satellite Division of the U.S. Inst. of Navigation*, Nashville, Tennessee, 14-17 September, 269-279.
- Ray, J. K., M. E. Cannon & P. Fenton (1998). Mitigation of static carrier phase multipath effects using multiple closely-spaced antennas, *11th Int. Tech. Meeting of the Satellite Division of the U.S. Inst. of Navigation*, Nashville, Tennessee, 15-18 September, 1025-1034.
- Remondi, B. W. (1985). Performing centimetre accuracy relative surveys in seconds using carrier phase, *First International Symposium on Precise Positioning with the Global Positioning System*, Rockville, Maryland, 15-19 April, 789-797.
- Remondi, B.W. & G. Brown (2000). Triple differencing with Kalman Filtering: making it work, *GPS Solutions*, 3(3), 58-64.
- Rizos, C. (1997). *Principles and Practice of GPS Surveying*, Monograph 17, School of Geomatic Engineering, The University of New South Wales, ISBN 0 85839 071, 555pp.
- Roberts, G.W., A.H. Dodson & V. Ashkenazi (1999). Twist and deflect: monitoring motion of the Humber Bridge, *GPS World*, 10(10), 24-34.
- Roberts, G.W., X. Meng & A.H. Dodson (2000). Structural dynamic and deflection monitoring using integrated GPS and triaxial accelerometers, *13th Int. Tech. Meeting of the Satellite Division of the U.S. Inst. of Navigation*, Salt Lake City, Utah, 19-22 September, 59-68.
- Roberts, G W, X. Meng & A. H. Dodson (2001). Data processing and multipath mitigation approaches for GPS/Accelerometer based hybrid structural deflection monitoring system, *14<sup>th</sup> Int. Tech. Meeting of the Satellite Division of the Satellite*

- Division of the U.S. Inst. of Navigation*, Salt Lake City, Utah, 11-14 September, 473-481.
- Roberts, G W, X. Meng & A. H. Dodson (2001). The use of kinematic GPS and triaxial accelerometers to monitor the deflections of large bridges, *10th FIG Int. Symp. on Deformation Measurements*, Orange, California, 19-22 March, 268-275.
- Rothacher, M., Beulter, G., Gurtner, W., Schneider, D., Wiget, A., Geiger, A. & Kahle, H.G. (1990). The role of atmosphere in small GPS networks, *Second International Symposium on Precise Positioning with the Global Positioning System*, Ottawa, Ontario, 3-7 September, 581-598.
- RTCM (1994). *Recommended Standards for Differential Navstar GPS Service* (version 2.1), RTCM SC-104, Washington, D.C.
- Rueger, J. M. (1996). *Electronic Distance Measurement – An Introduction*, 4<sup>th</sup> ed., Springer-Verlag, ISBN 0387611592, 276pp.
- Rutledge, D., J. Gnipp & J. Kramer (2001). Advances in real-time GPS deformation monitoring for landslides, volcanoes and structures, *10th FIG Int. Symp. on Deformation Measurements*, Orange, California, 19-22 March, 110-121.
- Samuel, T. R., J. P. Joseph Jnr. & J. A. Calvin (1998). Identifying the time of a step change with X-bar control charts, *Quality Engineering*, 10(3), 521-527.
- Sanchez, J. C., (2001). ScrollChart, [Http://codeguru.earthweb.com/controls/ScrollChart.html](http://codeguru.earthweb.com/controls/ScrollChart.html).
- Schaal, R. E. & A. P. C. Larocca (2002). A methodology for monitoring vertical dynamic sub-centimetre displacements with GPS, *GPS Solutions*, 5(3), 15-18.
- Schaal, R. E. & N. P. Netto (2000). Quantifying multipath using MNR ratios, *GPS Solutions*, 3(3), 44-48.
- Schwarz, K. P., Z. Li & A. El-Mowafy (1993). GPS multipath detection and reduction using spectral technique, *IAG General Meeting*, Beijing, China, 9-13 August.
- Seber, G. A. F. (1984). *Multivariate Observations*, John Wiley & Sons, New York, ISBN 047188104X, 712pp.
- Seeber, G. (1993) *Satellite Geodesy: Foundations, Methods & Applications*, Walter de Gruyter, Berlin New York, ISBN 3110127539, 531pp.
- Setan, H. & B. C. Nyet (2001). Development of a software system for least squares estimation, deformation detection and visualization analysis, *10th FIG Int. Symp. on Deformation Measurements*, Orange, California, 19-22 March, 122-128.

- Shengxiang, H. & L. Xianglin (2001). Data analysis of GPS dynamic monitoring for tall structure, *LAG Workshop on Monitoring of Constructions & Local Geodynamic Process*, Wuhan, China, 22-24 May, 243-249.
- Spilker, Jr., J.J. (1996). Tropospheric effects on GPS, In: Parkinson, B.W. et al. (eds.), *Global Positioning System: Theory and Applications*, Progress in Astronautics & Aeronautics, ISBN 1-56347-106-X, 163, 517-546.
- Stankovic, L. & V. Katkovnic (1998). Algorithm for instantaneous frequency estimation using time-frequency distributions with adaptive window width, *IEEE Sig. Processing Lett.*, 5(9), 224-227.
- Stewart, M. & M. Tsakiri (2001). The application of GPS to dam monitoring, *Journal of Geospatial Engineering*, 3(1), 45-57.
- Sullivan, J. H. & W. H. Woodall (1996). A comparison of multivariate control charts for individual observations, *Quality Technology*, 28(4), 398-408.
- Szostak-Chrzanowski, A., M. Massiera, A. Chrzanowski & C. J. Hill (2001). Use of geodetic monitoring surveys in verifying design parameters of large earthen dams at the stage of filling the reservoir, *10th FIG Int. Symp. on Deformation Measurements*, Orange, California, 19-22 March, 214-222.
- Talbot, N.C. (1993). Centimetre in the field, a user's perspective of real-time kinematic positioning in a production environment, *6<sup>th</sup> International Technical Meeting of the Satellite Division of the Institute of Navigation*, Salt Lake City, Utah, 22-24 September, 1049-1057.
- Tao N. F. & J. M. W. Brownjohn (1998). Estimation of ground motion acceleration and building response to a long distance earthquake, *Journal of Earthquake Engineering*, 2(3), 477-485.
- Townsend, B. & R. Fenton (1994). A practical approach to the reduction of pseudo-range multipath errors in an L1 GPS receiver, *6<sup>th</sup> Int. Tech. Meeting of the Satellite Division of the Satellite Division of the U.S. Inst. of Navigation*, Salt Lake City, Utah, 20-23 September, 143-148.
- Uren, J. & W. F. Price (1994). *Surveying for Engineers*, 3<sup>rd</sup> ed., Macmillan, London, ISBN 0333577051, 586pp.
- USACE, (1994). *Engineer Manual (EM 1110-1-1004): Deformation Monitoring and Control Surveying*, Department of the Army, U.S. Army Corps of Engineers (USACE), Washington, DC 20314-1000, 31 October, 191pp.
- USACE, (1996). *Engineer Manual (EM 1110-1-1003): NAVSTAR GPS Positioning Surveying*, Department of the Army, U.S. Army Corps of Engineers (USACE), Washington, DC 20314-1000, 1 August, 328pp.

- Wang, Y. (1995). Jump and sharp cusp detection by wavelets, *Biometrika*, 82(2), 385-397.
- Wang, J., T. Tsujii., C. Rizos, L. Dai, & M. Moore (2001). GPS and pseudolite satellites integration for precise positioning, *Geomatics Research Australasia*, 74, 103-118.
- Watson, C. & R. Coleman (1998). The Batman Bridge: structural monitoring using GPS, 'Advances in GPS Deformation Monitoring', Perth, Western Australia, 24-25 September, Paper 16.
- Wells, D.E., N. Beck, D. Delikaraohlou, A. Kleusberg, E. J. Krakiwsky, G. Lachapelle, R. B. Langley, M. Nakiboglu, K. P. Schwarz, J. M. Tranquilla & P. Venicek (1987). *Guide to GPS Positioning*, 2<sup>nd</sup> edition, Canadian GPS Associates, Fredericton, New Brunswick, Canada, ISBN 0920114733, 503pp.
- Wieser A. (2001). *Robust and Fuzzy Techniques for Parameter Estimation and Quality Assessment in GPS*, PhD dissertation, Technische Universität Graz, Shaker Verlag, ISBN 3-8265-9807-5, 253pp.
- Wong K., K. Man & W. Chan (2001). Monitoring Hong Kong's bridges: Real-Time Kinematic spans the gap, *GPS World*, 12(7), 10-18.
- Zumberge, J.F. (1999). Automated GPS data analysis service, *GPS Solutions*, 2(3), 76-78.
- Zumberge, J.F., M. B. Heflin, D. C. Jefferson, M. M. Watkins & F. H. Webb (1997). Precise point positioning for the efficient and robust analysis of GPS data from large networks, *Journal of Geophysical Research*, 102(B3), 5005-5017.

## APPENDIX I

### AUTHOR-DEVELOPED SOFTWARE

---

---

#### **I-1 Introduction**

This Appendix discusses some of the programming considerations for the software implementation of the mathematical algorithms discussed in this thesis (Chapters 6 & 7).

After some investigation, it was decided to develop the software to run under the Windows environment, and to develop all the source code in the object-oriented C++ programming language using a framework of Microsoft Visual C++ 6.0 classes. Section I-2 discusses some of the considerations behind these decisions, and Section I-3 describes a set of core C++ classes that were implemented in the development of the software.

When developing software it is prudent to write a test system that exercises its functions with some sets of input data. Such a test program requires a simple user interface through which parameters can be entered and the output can be verified. The user interfaces presented in Section I-4 are representative examples. When the software system is thoroughly tested (it is often difficult to know how much testing is adequate), it is then ready to be used for the intended purpose, including in real-time operations.

#### **I-2 Programming Language and Coding Style**

The choice of programming language was influenced by the fact that the application is intended for real-time performance, and that the test software requires a simple graphical user interface (GUI). C++ was considered the best choice due to its general popularity for commercial applications as well as its widespread use in research and development environments. The Windows libraries themselves are written in the C

language of which C++ is an extension that allows the use of constructs of the Object Oriented Programming System (OOPS).

Programs written using the OOPS constructs are much easier to maintain (Nolan, 1990). The coding encapsulates data types and their associated operations, centralising all access to the data type by using classes whose default behaviour is that no routine outside of a class can access any of its members. Hence when a “bug” shows up, for example, it can be associated with its data type and traced.

Considering the high cost of software development, it is also imperative that software is capable of adapting to a variety of future needs. Not only does C++ allow the programmer to fully encapsulate the data with the methods that operate on the data, its inherent modularity makes it easier to write well-structured code. Well-structured, modular, and clearly documented C++ source code makes it easier for other programmers to maintain, and enhance, the software in the future. Additional functionality can be added to existing C++ classes through Inheritance, a coding mechanism that allows code re-use, by *deriving* subclasses from them. Thus, there is the advantage of increased robustness by basing new functionality on previously tested modules, and the ability to combine at run time different objects with the same base class. The language also contains efficient methods of handling exceptions or errors, and portability is one of its key advantages. Subroutines or functions written during initial system development can be later re-used in other programs, and in other computing environments.

The process of software development involves a number of subtasks. It requires an *editor*, a *compiler* and a *linker*. In modern software development platforms, these subtasks are seamlessly integrated and the entire process is largely automatic. Such platforms are called *Integrated Development Environments* (IDEs). Most modern C++ packages (the software used to develop C++ programs) provide some sort of an IDE (Katupitiya & Bentley, 2000). Among these are the commercially available packages such as Borland C++, C++ Builder and Visual C++. Apart from the editor, compiler and linker, these packages provide extensive library support, for example in the form of run-time libraries (RTLs).



At the time this study was being undertaken, Microsoft Visual C++ 6.0 for the Windows 95/98/2000 Operating Systems was available. It was decided to develop the system using this package for a Wintel environment. Its IDE allows for the definition of a project with files containing the C++ source codes that can be edited, compiled and linked, on user command. Figure I-1 is an example of the Visual C++ 6.0 *workspace* showing the project files for the developed application.

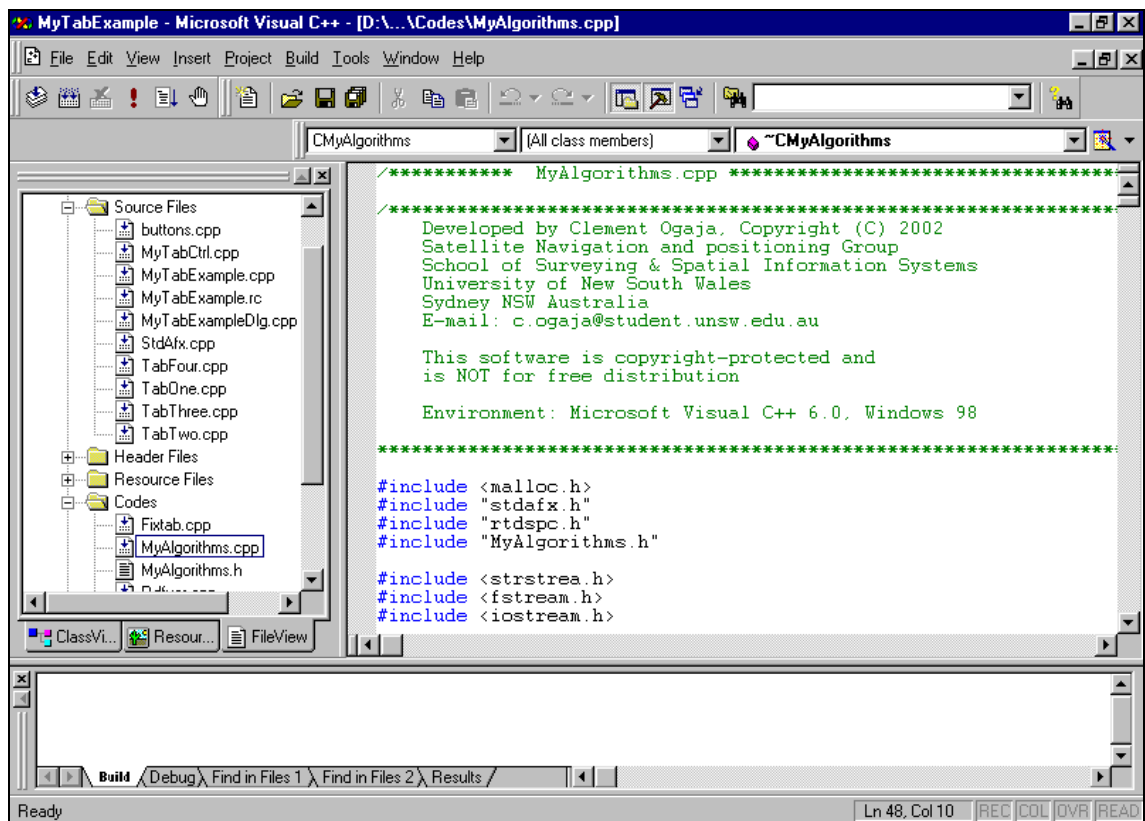


Figure I-1. Microsoft Visual C++ 6.0 project workspace

The project was defined so as to contain different folders for the individual files, of both the Microsoft Developer Studio generated, and the author-developed C++ classes or source codes. For example, the upper left window of Figure I-1 displays the project files under four different folders namely *Source Files*, *Header Files*, *Resource Files* and *Codes*. The developed C++ code was written to allow the software components to be as self-contained as possible. In other words, the software consists of discrete functional modules or parts, with each unit performing a specific function.

The following general rules were also adhered to, being part of the programming style requirements for *reliability*, *maintainability*, *extensibility* and *efficiency*:

- All constants or variables that may be altered were defined in a separate project file.
- Each part of the software system had a clear function and purpose.
- The *class member functions* were limited to roughly 200 lines or less in order to avoid having large *member functions*.
- Exception or errors were anticipated and appropriately handled.
- Header comments were used to convey important information concerning the various parts of the software.
- Consistent indentation highlighting statements executed in the same loop.
- Appropriate use of blank lines and paragraphing to enhance program readability.

With the project defined as in Figure I-1, the software developer can add or edit a *resource file* from the library of built-in routines. This allows for easy implementation of menus, dialogue boxes, dialogue tab controls and other components of a user-friendly interface. The Windows environment provides a user interface with which users of other Microsoft software products will be immediately familiar.

### I-3 Framework Core Classes

This section presents a set of core C++ classes that were used to develop the application. These classes encapsulate the various data types, C++ function prototypes and, in some instances, subclasses. Figure I-2 is the opened workspace of the project (shown earlier in Figure I-1), this time displaying the implemented C++ classes on the left-hand window. The project classes are:

- The class *CAboutDlg* creates a dialogue box named "About" (Hill, 2000). This dialogue is commonly used to display information such as the software version, ownership and copyright status.

- The classes *CButtonAuto*, *CButtonValue* and *CVirtualButton* implement the radio and edit buttons that are important for program settings and operation (Sanchez, 2001).
- The class *CMyAlgorithms* implements the algorithms of Chapters 5 & 6 of this study.
- The class *CMyTabCtrl* helps to create tabbed child dialogue boxes (Hill, 2000).
- The classes *CMyTabExampleApp* and *CMyTabExampleDlg* help to create the main dialogue on which the tabbed child dialogues are built (Hill, 2000).
- The class *CScrollChart* implements the real-time charting and plotting member functions (Sanchez, 2001).
- The class *CTabOne* creates a tabbed child dialogue named "RTK Data".
- The class *CTabTwo* creates a tabbed child dialogue named "MultiSensor Data".
- The class *CTabThree* creates a tabbed child dialogue named "Time Series Plots".
- The class *CTabFour* creates a tabbed child dialogue named "Program Author".
- The class *COMPLEX* defines complex variables and a prototype FFT function.

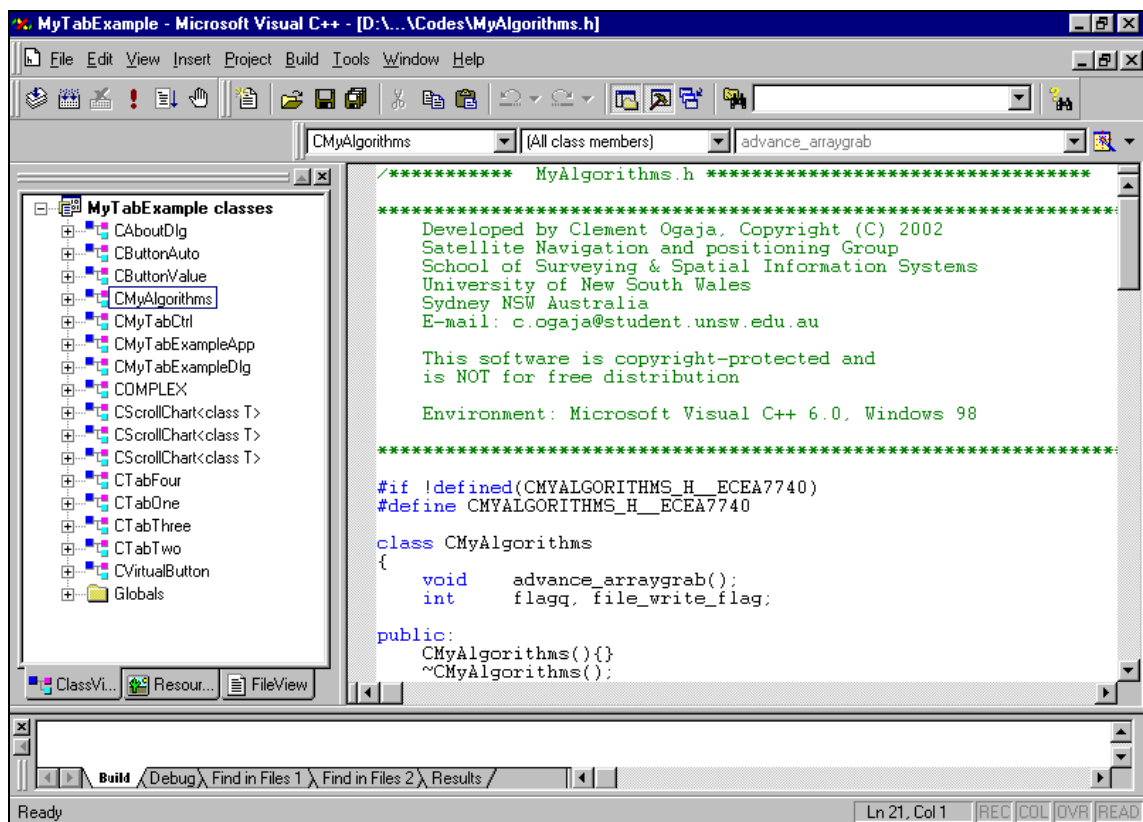


Figure I-2. An opened Microsoft Visual C++ 6.0 project workspace

All the classes named in italics were downloaded from the Internet and used by permission of their authors (references given). The classes in bold are discussed below.

Listing I-1 shows the class ***CMyAlgorithms***. This class is contained in the header file *CMYALGORITHMS.H*. It is implemented by including the header file in the C++ source file and linking with the *CMYALGORITHMS.CPP* object. All the member functions implementing the proposed algorithms (described in Chapter 5 & 6) are contained in the source file *CMYALGORITHMS.CPP*.

Listings I-2, I-3, I-4 and I-5 show the classes ***CTabOne***, ***CTabTwo***, ***CTabThree*** and ***CTabFour*** respectively, contained in *CTABONE.H*, *CTABTWO.H*, *CTABTHREE.H* and *CTABFOUR.H*. These classes are implemented by including the header files in the C++ source files and linking with the *CTABONE.CPP*, *CTABTWO.CPP*, *CTABTHREE.CPP* and *CTABFOUR.CPP* objects. The member functions in these classes perform similar functions. The following are some of the operations common to the member functions:

- A call to the member function ***OnCreate(LPCREATESTRUCT lpCreateStruct)*** creates the chart controls and attaches it to the object created by the constructors of the classes *CTabOne::CTabOne*, ..., *CTabFour::CTabFour*.
- A call to the member function ***OnInitDialog()*** will initialise the program parameter or variable settings as specified within the function.
- A call to the member function ***OnRealTimeUpdate()*** performs the real-time update of the timer-supported functions.

```

/*****
    Developed by Clement Ogaja, Copyright (2001)
    Environment: Microsoft Visual C++ 6.0, Windows 98
    *****/
class CMyAlgorithms
{
    void advance_arraygrab();
    int flagq, file_write_flag;
public:
    CMyAlgorithms(){}
    ~CMyAlgorithms();
    void ref_data_size(int &rows);
    void initialize();
    double runmean(int index, double value, double oldmean);
    double runupdate(int index, double oldvalue, double oldmean, double oldsum);
    double runvariance(int index, double value, double oldupdate, double oldmean);
    void grabarray(double &dY1, double &dX1, double &dZ1, double &dY2, double &dX2, double &dZ2,
        double &dY3, double &dX3, double &dZ3, double &dY4, double &dX4, double &dZ4);
    double mean(const double *array, int size);
    void init_mean_and_cov();
    double getmin(int l,double *v);
    double getmax(int l,double *v);
    void computeStatistics(int n,double new_value, double old_value,double old_mean, double &new_mean,
        double old_stdv, double &new_stdv,double old_update, double &new_update);
    void between_Receiver(int vector_comp,int epoch, double &d12, double &d23, double &d13, double dY1, double
        dX1,double dZ1,double dY2, double dX2,double dZ2,double dY3, double dX3,double dZ3);
    void cusums(int epoch, int old_flag,int &new_flag, int &reset_epoch,double c12_1, double old_c12_1,
        double c12_2, double old_c12_2,double c23_1, double old_c23_1,double c23_2, double old_c23_2,
        double c13_1, double old_c13_1,double c13_2, double old_c13_2,double &cusum12_1, double &cusum12_2,
        double &cusum13_1, double &cusum13_2,double &cusum23_1, double &cusum23_2,
        double old_reset12_1, double old_reset12_2,double old_reset13_1, double old_reset13_2,
        double old_reset23_1, double old_reset23_2,double &reset12_1, double &reset12_2,
        double &reset13_1, double &reset13_2,double &reset23_1, double &reset23_2,
        int old_r_flag, int &r_flag,double CUSUMCHK,double &inov12_1, double old_inov12_1,
        double &inov12_2, double old_inov12_2,double &inov23_1, double old_inov23_1,
        double &inov23_2, double old_inov23_2,double &inov13_1, double old_inov13_1,
        double &inov13_2, double old_inov13_2);
    void updatecusums(double &c12_1, double &c12_2, double &c23_1, double &c23_2,double &c13_1, double &c13_2,
        int epoch, double shift, double d12,double d23, double d13, double var1,double var2, double var3);
    void two_sided_cusumtest(int epoch, int cusum_delay, double threshold,double cusum12_1, double cusum12_2,
        double cusum23_1, double cusum23_2,double cusum13_1, double cusum13_2,
        double max12_1, double max12_2, double max23_1, double max23_2, double max13_1, double max13_2,
        double min12_1, double min12_2, double min23_1, double min23_2, double min13_1, double min13_2,
        double &testv1, double &testv2, double &testv3, int &sensorflag, double &cusm1, double &cusm2,
        double &cusm3,double transformer, double &CUSUMCHK);
    void cusum_stats(int n, int flag, double new_value, double old_value, double old_mean, double &new_mean,
        double &run_var, double old_update, double &new_update, double CUSUMCHK);
    double qstatistic(double *realtime_data);
    void Freq_and_Ampl(double *b,double &Freq,double &Amplitude,double cFs,int L_value, double lcut_off);
    void DominantFrequency(int numSamples, // total number of frequency samples in buffer
        int windowSize, // width of search window (experiment with this; try 4)
        double *real, // real coefficient buffer
        double *imag, // imaginary coefficient buffer
        double *ampl, // work buffer for holding r*r+i*i values
        double samplingRate, // sampling rate expressed in samples/second [Hz]
        double cut_off, // lower frequency cut off in Hz
        double &ampld, // amplitude
        double &freq); // peak frequency in Hz
    void passNormalisedMeans(double &muY1,double &muX1,double &muZ1,double &muY2,double &muX2,
        double &muZ2,double &muY3,double &muX3,double &muZ3,double &muY4,double &muX4,double &muZ4,
        double Y1mu,double X1mu,double Z1mu,double Y2mu,double X2mu,double Z2mu,double Y3mu
        double X3mu,double Z3mu,double Y4mu,double X4mu,double Z4mu);
    double NormalisedMean(const double *array, double mu, int size);
    void passMeans(double &Y1_mu,double &X1_mu,double &Z1_mu,double &Y2_mu,double &X2_mu,double &Z2_mu,
        double &Y3_mu,double &X3_mu,double &Z3_mu,double &Y4_mu,double &X4_mu,double &Z4_mu);
};

```

LISTING I-1. Class *CMyAlgorithms* (contained in *CMYALGORITHM.H*)

```

/*****
    Developed by Clement Ogaja, Copyright (2001)
    Environment: Microsoft Visual C++ 6.0, Windows 98
    *****/
class CTabOne : public CDialog
{
public:
    CMyAlgorithms Rn; int T;
protected:
    CScrollChart<float> m_wndChart13; CScrollChart<float> m_wndChart14;
    CScrollChart<float> m_wndChart15; CScrollChart<float> m_wndChart16;
    int m_nRedHorz; int m_nRedVert; CStatic m_TextHozMax;
    CStatic m_TextHozMin; CStatic m_TextVerMax; CStatic m_TextVerMin;
    CButtonValue m_button; CButtonAuto m_buttonAuto;
// Construction
public:
    CTabOne(CWnd* pParent = NULL); // standard constructor
// Dialog Data
   //{{AFX_DATA(CTabOne)
    enum { IDD = IDD_TAB_ONE };
    //}}AFX_DATA
// Overrides
    // ClassWizard generated virtual function overrides
    //{{AFX_VIRTUAL(CTabOne)
protected:
    virtual void DoDataExchange(CDataExchange* pDX); // DDX/DDV support
    //}}AFX_VIRTUAL
// Implementation
    void AddToListBox1(LPCTSTR szBuffer);
    void AddToListBox2(LPCTSTR szBuffer);

protected:
    // Generated message map functions
   //{{AFX_MSG(CTabOne)
    afx_msg void OnRealTimeUpdate();
    afx_msg void OnChangeEdit();
    afx_msg void OnBkColor();
    afx_msg void OnIdc();
    afx_msg void OnLineStyleChange();
    afx_msg void OnChangeWidth(UINT nID); // OnChangeWidth();
    virtual BOOL OnInitDialog();
    afx_msg int OnCreate(LPCREATESTRUCT lpCreateStruct);
    //}}AFX_MSG
    DECLARE_MESSAGE_MAP()
};
//{{AFX_INSERT_LOCATION}}
// Microsoft Visual C++ will insert additional declarations immediately before the previous line.
#endif // !defined(AFX_TABONE_H__4F1DD92C_C67D_48AE_A73F_02D7EDA0580E__INCLUDED_)

```

LISTING I-2. Class *CTabOne* (contained in *CTABONE.H*)

- A call to the member function *OnBkColor()* retrieves and sets the current background colour to the selected colour.
- A call to the member function *OnChangeEdit()* invokes the various edit button controls through which the user can edit input variables/parameters.
- A call to the member function *OnIdc()* changes the status of the chart's grid and points system.
- A call to the member function *OnLineStyleChange()* sets the plotting line style.

- A call to the member function *OnChangeWidth(UINT nID)* sets the width of the plotting line.
- A call to the member functions *AddToListBox1(LPCTSTR szBuffer)* and *AddToListBox2(LPCTSTR szBuffer)* will display numerical values on pre-defined windows screens.

The code for all the C++ member functions are available from the author.

```

*****
        Developed by Clement Ogaja, Copyright (2001)
        Environment: Microsoft Visual C++ 6.0, Windows 98
*****/
class CTabTwo : public CDialog
{
public:

        CMyAlgorithms Rn;
        int T;

protected:
        CScrollChart<float> m_wndChart1;CScrollChart<float> m_wndChart13;
        CScrollChart<float> m_wndChart14;CScrollChart<float> m_wndChart15;
        CScrollChart<float> m_wndChart16;CButtonValue m_button;
        CButtonAuto m_buttonAuto;

// Construction
public:
        CTabTwo(CWnd* pParent = NULL); // standard constructor

// Dialog Data
       //{{AFX_DATA(CTabTwo)
        enum { IDD = IDD_TAB_TWO };
                // NOTE: the ClassWizard will add data members here
        }}AFX_DATA

// Overrides
        // ClassWizard generated virtual function overrides
       //{{AFX_VIRTUAL(CTabTwo)
        protected:
        virtual void DoDataExchange(CDataExchange* pDX); // DDX/DDV support
        }}AFX_VIRTUAL

// Implementation
        void        AddToListBox2(LPCTSTR szBuffer);

protected:
        // Generated message map functions
       //{{AFX_MSG(CTabTwo)
        afx_msg void OnRealTimeUpdate();
        afx_msg void OnChangeEdit();
        afx_msg void OnIdc();
        afx_msg void OnLineStyleChange();
        afx_msg void OnBkColor();
        afx_msg int OnCreate(LPCREATESTRUCT lpCreateStruct);
        virtual BOOL OnInitDialog();
        afx_msg void OnChangeWidth(UINT nID);
        }}AFX_MSG
        DECLARE_MESSAGE_MAP()
};
//{{AFX_INSERT_LOCATION}}
// Microsoft Visual C++ will insert additional declarations immediately before the previous line.

#endif // !defined(AFX_TABTWO_H__7E062B52_3B6E_44C4_B58E_AAD73592C8E3__INCLUDED_)

```

LISTING I-3. Class *CTabTwo* (contained in *CTABTWO.H*)

```

*****
Developed by Clement Ogaja, Copyright (2001)
Environment: Microsoft Visual C++ 6.0, Windows 98
*****/
class CTabThree : public CDialog
{
public:
    CMyAlgorithms Rn; int T;
protected:
    CScrollChart<float> m_wndChart1; CScrollChart<float> m_wndChart4;
    CScrollChart<float> m_wndChart5; CScrollChart<float> m_wndChart7;
    CScrollChart<float> m_wndChart8; CScrollChart<float> m_wndChart9;
    CScrollChart<float> m_wndChart10; CScrollChart<float> m_wndChart13;
    CScrollChart<float> m_wndChart14; CScrollChart<float> m_wndChart15;
    CScrollChart<float> m_wndChart16; CScrollChart<float> m_wndChart17;
    CScrollChart<float> m_wndChart18; CScrollChart<float> m_wndChart19;
    CScrollChart<float> m_wndChart20; CScrollChart<float> m_wndChart21;
    CScrollChart<float> m_wndChart22;
// Construction
public:
    CTabThree(CWnd* pParent = NULL); // standard constructor
// Dialog Data
   //{{AFX_DATA(CTabThree)
    enum { IDD = IDD_TAB_THREE };
        // NOTE: the ClassWizard will add data members here
    //}}AFX_DATA
// Overrides
    // ClassWizard generated virtual function overrides
   //{{AFX_VIRTUAL(CTabThree)
    protected:
    virtual void DoDataExchange(CDataExchange* pDX); // DDX/DDV support
    //}}AFX_VIRTUAL
// Implementation
    void AddToListBox1(LPCTSTR szBuffer);
    void AddToListBox2(LPCTSTR szBuffer);
    void AddToListBox3(LPCTSTR szBuffer);
    void AddToListBox4(LPCTSTR szBuffer);
    void AddToListBox5(LPCTSTR szBuffer);
    void AddToListBox6(LPCTSTR szBuffer);
protected:
    // Generated message map functions
   //{{AFX_MSG(CTabThree)
    afx_msg void OnRealTimeUpdate();
    afx_msg void OnChangeEdit();
    afx_msg void OnLineStyleChange();
    afx_msg void OnIdc();
    afx_msg void OnBkColor();
    afx_msg void OnChangeWidth(UINT nID);
    afx_msg int OnCreate(LPCREATESTRUCT lpCreateStruct);
    virtual BOOL OnInitDialog();
    //}}AFX_MSG
    DECLARE_MESSAGE_MAP()
};
//{{AFX_INSERT_LOCATION}}
// Microsoft Visual C++ will insert additional declarations immediately before the previous line.

```

LISTING I-4. Class *CTabThree* (contained in *CTABTHREE.H*)



```

*****
        Developed by Clement Ogaja, Copyright (2001)
        Environment: Microsoft Visual C++ 6.0, Windows 98
*****/
class CTabFour : public CDialog
{
// Construction
public:
        CTabFour(CWnd* pParent = NULL); // standard constructor
// Dialog Data
        //{{AFX_DATA(CTabFour)
        enum { IDD = IDD_TAB_FOUR };
        // NOTE: the ClassWizard will add data members here
        //}}AFX_DATA
// Overrides
        // ClassWizard generated virtual function overrides
        //{{AFX_VIRTUAL(CTabFour)
        protected:
        virtual void DoDataExchange(CDataExchange* pDX); // DDX/DDV support
        //}}AFX_VIRTUAL
// Implementation
protected:
        // Generated message map functions
        //{{AFX_MSG(CTabFour)
        // NOTE: the ClassWizard will add member functions here
        //}}AFX_MSG
        DECLARE_MESSAGE_MAP()
};
//{{AFX_INSERT_LOCATION}}
// Microsoft Visual C++ will insert additional declarations immediately before the previous line.

#endif // !defined(AFX_TABFOUR_H_109F865C_727C_49A5_8091_5252D271861E__INCLUDED_)#endif //
!defined(AFX_TABTHREE_H_798A9124_C906_446C_822D_322B5AB6C4C4__INCLUDED_)

```

LISTING I-5. Class *CTabFour* (contained in *CTABFOUR.H*)

Listing I-6 shows the class called *COMPLEX*. This class is contained in the header file *RTDSPC.H*. It is implemented by including the header file in the *CMYALGORITHM-S.CPP* source file and linking with the *CMYALGORITHM.S.CPP* object. In this work, the class *COMPLEX* was used solely to define the variables *real* and *imag* as type *COMPLEX* and not to implement the prototype FFT function.

```

*****
        Developed by Clement Ogaja, Copyright (2001)
        Environment: Microsoft Visual C++ 6.0, Windows 98
*****/
typedef struct {
        float real, imag;
} COMPLEX;

/* function prototype for fft */
extern void fft(COMPLEX *,int);_

```

LISTING I-6. Class *COMPLEX* (contained in *RTDSPC.H*)

#### I-4 Software Modules and Sample Window Interfaces

The general flow of the software system developed in this study is as shown in Figure I-3. Its main objective is to analyse continuous data streams, and to compare outputs with specified criteria in order to extract deformation or biased signals, as well as to characterise the behaviour of the monitoring system or sub-system.

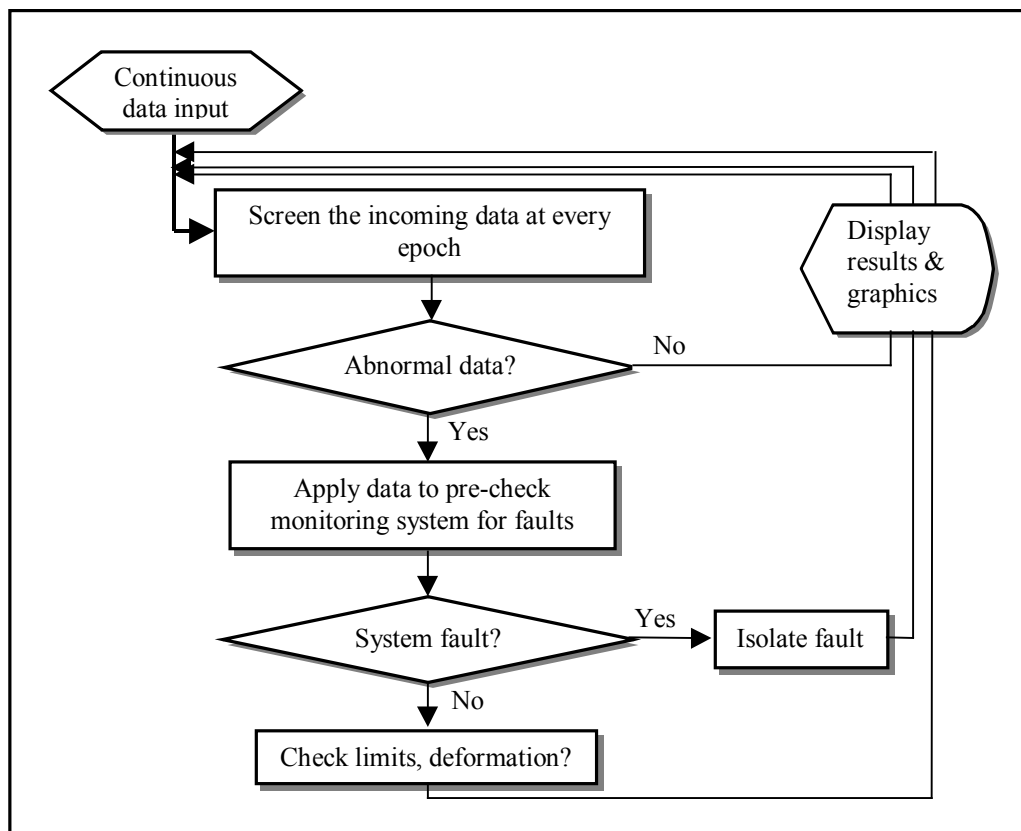


Figure I-3. Overall structure of the author-developed system

In Figure I-4, the key software components are shown with the general message (or data) flow. The function *OnRealTimeUpdate* reads the input data, program settings, user request and calls a range of other functions. The called functions in turn implement the appropriate algorithms with the new data input.

In Figures I-5 and I-6 are two key program modules that had been designed to implement the mathematical algorithms of GPS data integrity assessment and multi-

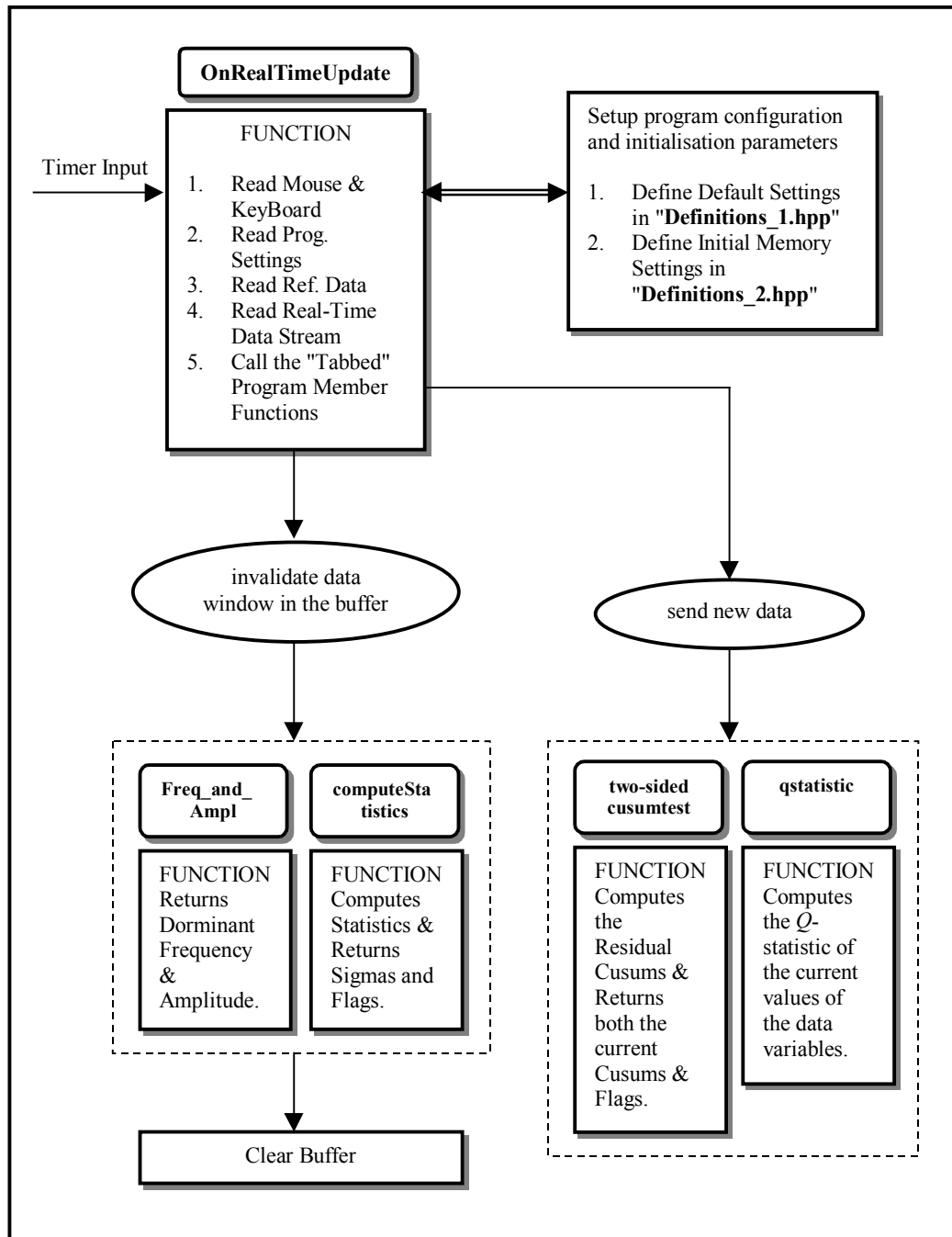


Figure I-4. Flowchart of some of the key functions of the author-developed system

sensor data monitoring. Though both modules use time domain data by default, additional functionality was created to monitor in the frequency domain as well. The modules include functions for online analysis that detect abnormal observations as quickly as possible, and either provide clues as to the possible cause (e.g. sensor faults), or simply issue an alert if a warning limit is exceeded. The tasks that cannot be carried out online can then be handled by offline analysis. The validity of the analysed results

and the efficiency of the monitoring system are both crucial to the overall system performance.

The main functions of the module illustrated in Figure I-5 are:

- To access the positioning residuals for multiple receivers from a GPS processing engine and to perform statistical calculations in real-time.
- To check the consistency between multiple 'rover' receivers in real-time, assuming that there is an independent check on the GPS base station(s).
- To display the data analysis results graphically in real-time.
- To perform alarm handling in case of abnormal observations or system sensor faults.

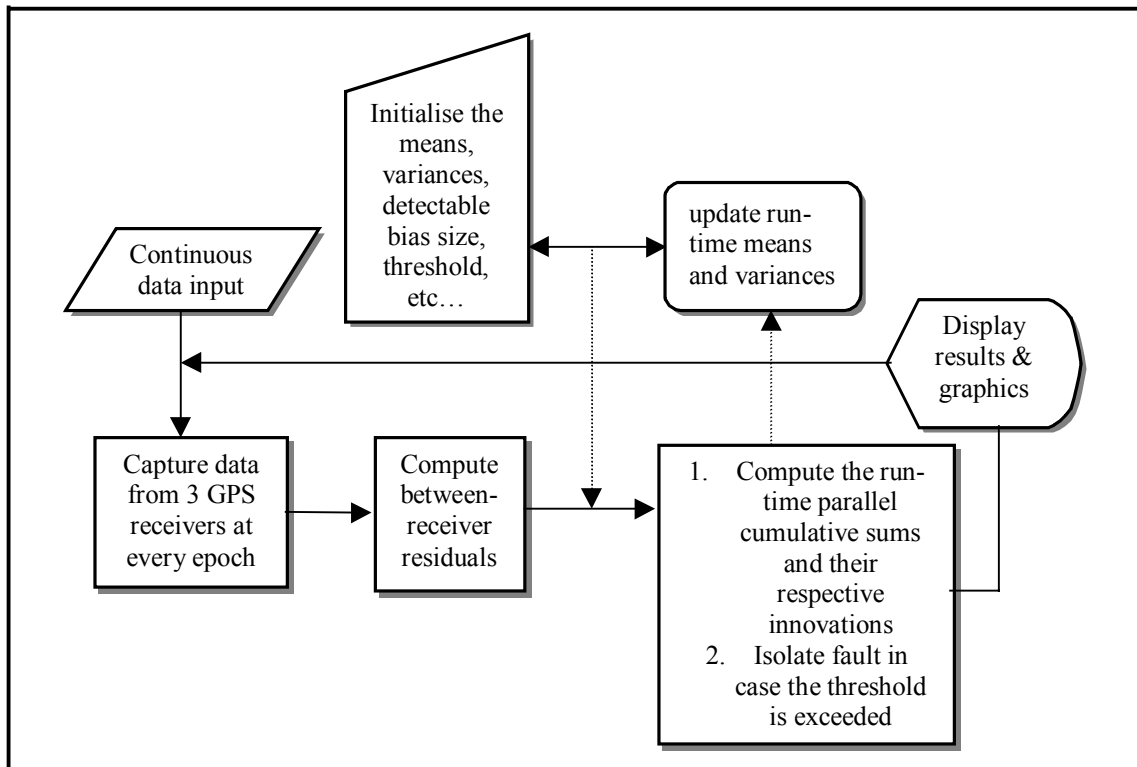


Figure I-5. Flow diagram of the module for RTK data integrity monitoring

The second module (Fig. I-6) combines both the integrity assessment algorithm (Chapter 5) and the multivariate SPC algorithm (Chapter 6). This module is more suited for the analysis of multi-sensor data. Its main functions are:

- Accessing both GPS data and auxiliary sensor data continuously, and performing statistical analysis in real-time.
- Performing online multisensor data monitoring.
- Checking the consistency between multiple 'rover' receivers in real-time, assuming that there is an independent check on the GPS base station(s).
- Displaying the data analysis results graphically in real-time.
- Performing alarm handling in case of abnormal observations or system sensor faults.

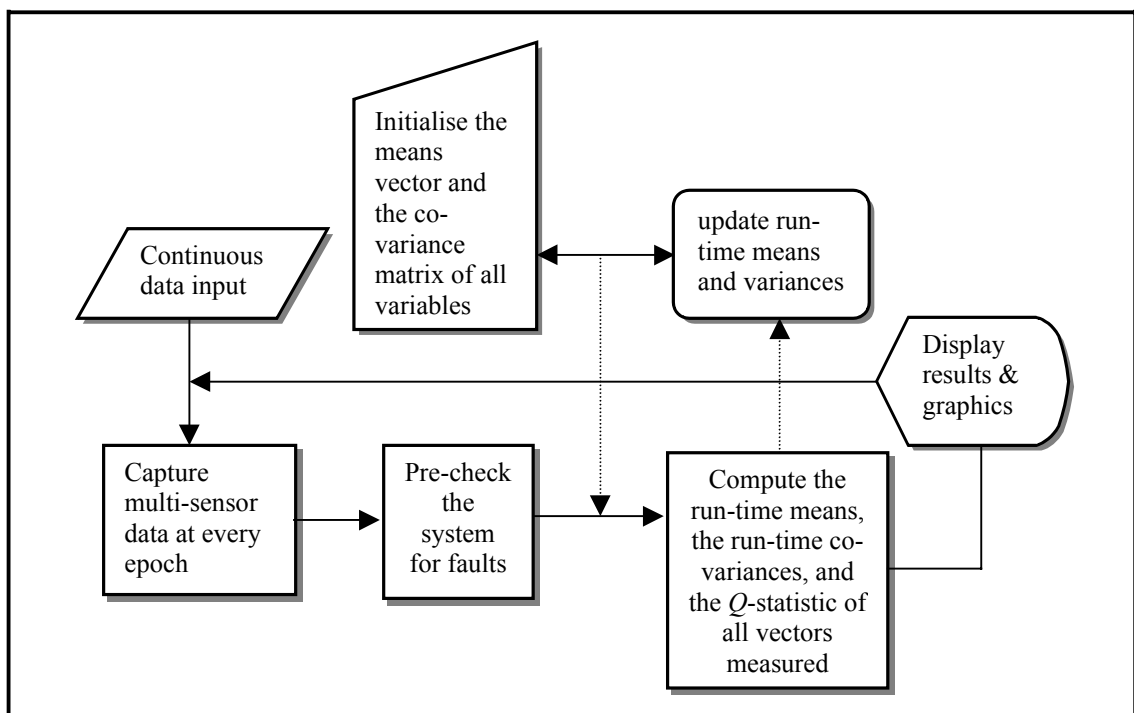


Figure I-6. *Flow diagram of the module for multisensor data analysis*

The main function of the two modules is to allow any PC to run the software system without user intervention, except when an alert condition is activated. The implementations are robust against both positive and negative observational or system biases.

The developed application software comprises a graphical user interface (GUI), named "Real-Time System Monitor" (RTSM). This GUI is designed to allow the user to input some information required by the application for processing the data streams. It also

offers the user the opportunity to select the mode in which to run the application through three main tabbed dialogues. Thus, the user can select whether to monitor by running the RTK-GPS data mode in both the time domain and frequency domain, the multisensor data mode, or just the time series plots.

Figure I-7 is a display of the first tabbed dialogue. Note how it presents a variety of user options for the display settings. For example, the CUSUMS control limit is activated, the data rate is 1Hz, the sensitivity to bias is 1.5 [cm or mm], the plotted line style is SOLID, the grids are active, the grid divisions are 20 and 10 for horizontal and vertical scales respectively, the plot range is 60 samples, and the background colour is white.

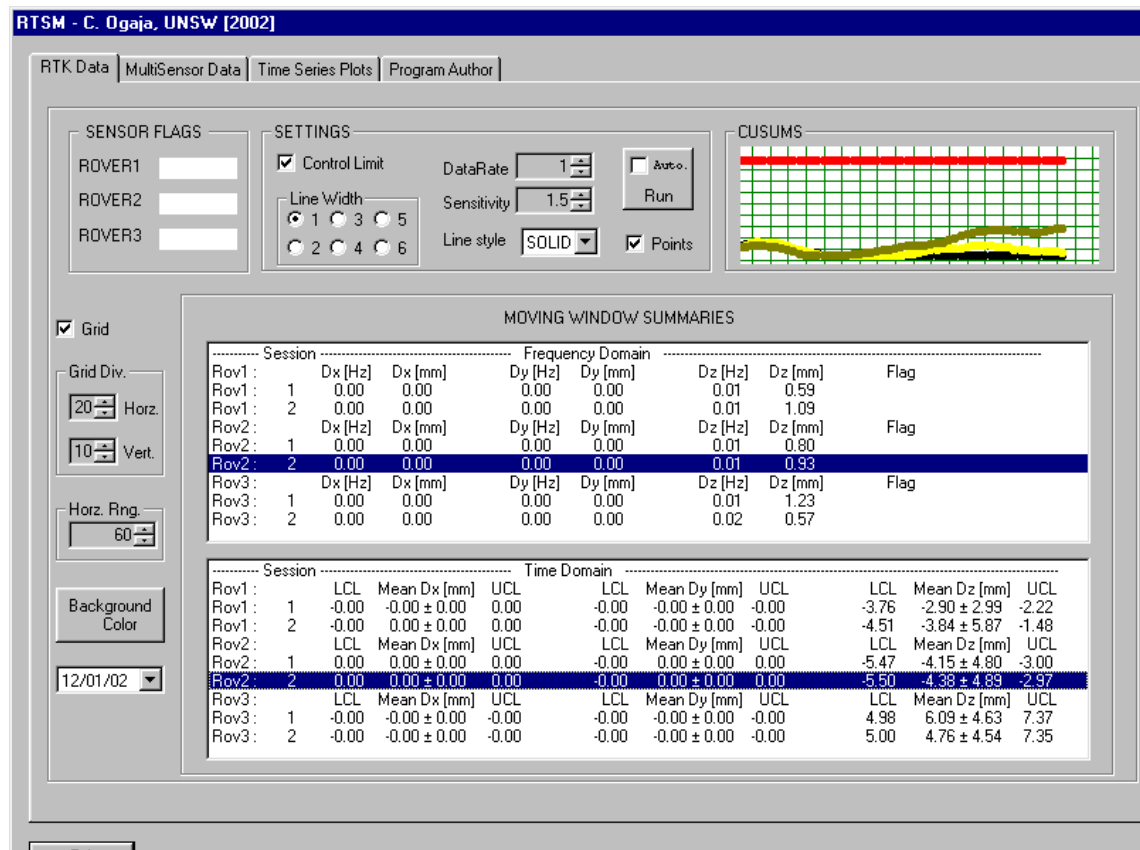


Figure I-7. "Dialogue One" of RTSM version 1.0 interface

The two screens at the bottom part of the dialogue display the results for a predefined moving window. The upper screen gives a session by session summary of the frequencies and amplitudes extracted from the fast RTK-GPS results (1Hz and higher). The lower screen displays the session by session summary of the time domain statistics

corresponding to the upper screen results. The cumulative sums (CUSUMS) display and the sensor flags are the key graphical displays for quality control monitoring. However, additional alarm handling and messaging is also provided through an alarm message box, such as shown in Figure I-8. This additional feature is available for monitoring of quality control in both the time domain (of the measurements) and the frequency domain (after transformation).

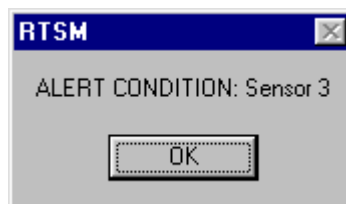


Figure I-8. Alarm message box of RTSM

Figure I-9 is the second tabbed display of the interface. It combines integrity assessment with the multisensor data handling. It allows the user to monitor sensor biases, the MSPC series and the 3D time domain moving window summaries for the RTK-GPS results.

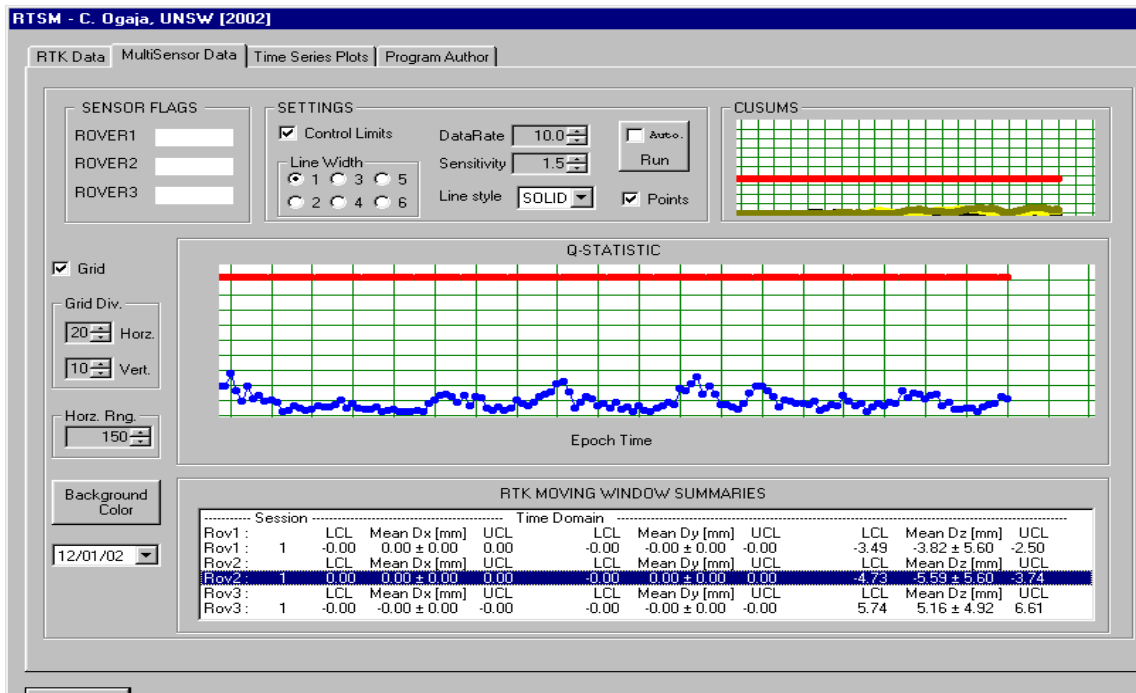


Figure I-9. "Dialogue Two" of RTSM version 1.0 interface

Figure I-10 is the third tabbed display of the interface. In this option the user can monitor a continuous series of graphs that have been grouped into horizontal components and height components. Respective legends tagged with small display screens for the current value display are also available to the user. At this point note that all the tabbed options of the software offer similar settings capability. For instance, whichever option is selected, a user will be able to perform an integrity check on the RTK-GPS data, set the sensitivity threshold and set the data rate.

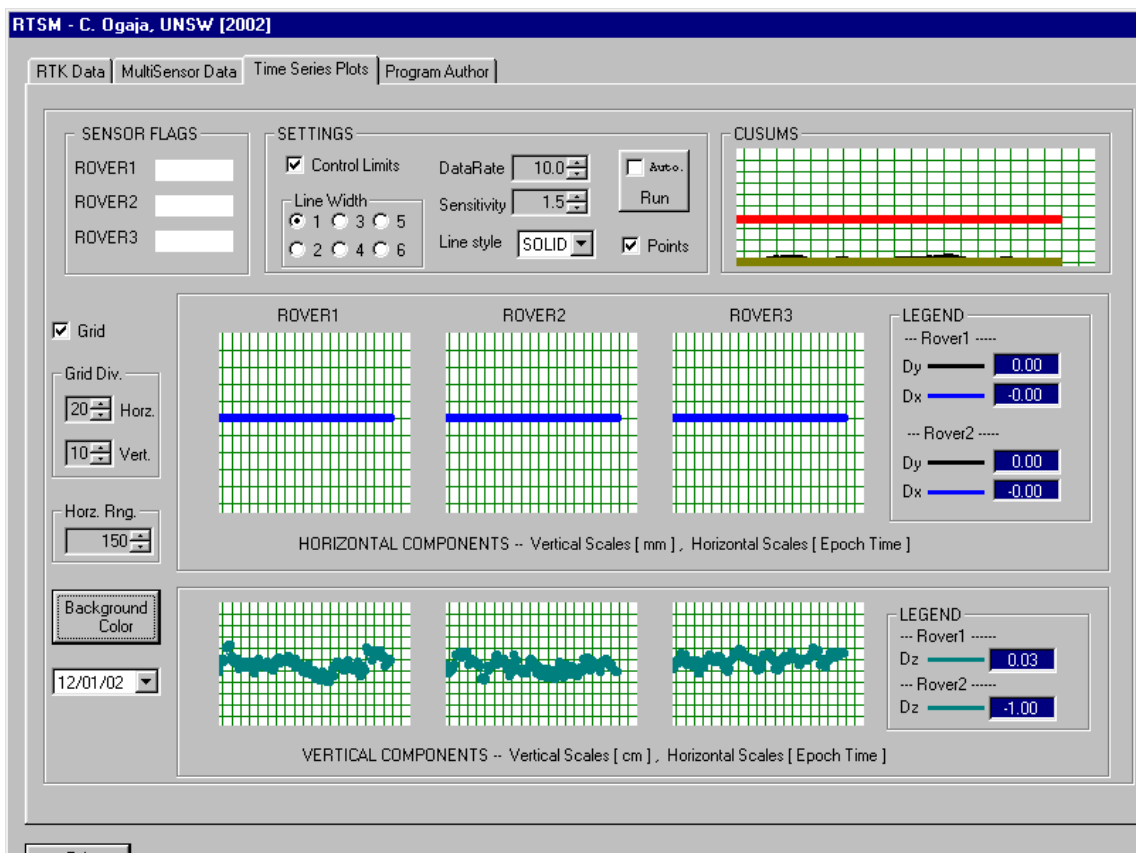


Figure I-10. "Dialogue Three" of RTSM version 1.0 interface

## I-5 Concluding Remarks

One of the principal aims of the author-developed software system is to provide the user with statistics concerning the quality of results and the monitoring system status. It has the basic functionality for the real-time display of three-dimensional standard deviations, sensor-related biases (or faults) and the trend of RTK-GPS residuals, among



other features. The system user can, in addition, monitor in real-time the ‘dynamic’ information in terms of the dominant frequencies and their corresponding amplitudes. At the time of writing of this report, the system design includes three main dialogue options, with the functionality for integrity check enabled for all three options. Though it is still undergoing further modification and development, the present system configuration is adequate for the initially intended tasks.

It is recognised that one of the strengths of the GUI is the ease with which it can be altered. The dialogue boxes can be added or restructured quite easily, altering the overall look of the program. Similarly, menus and sub-menus can be added. Every effort was made to allow develop the software system so that it is capable of adapting to future needs. The structure of the software code was designed to make it easy to maintain, and more features and improvements will be added, as well as the implementation of improved algorithms. It is also intended that this software will be able to address other application areas apart from structural monitoring. Such areas of expanded application might include INS-GPS positioning and attitude determination.

## APPENDIX II

### GLOSSARY OF TERMS

---

---

#### *Anti-Spoofing (AS)*

Is a policy of the U.S. Department of Defense by which the P-Code is encrypted (by the additional modulation of a so-called W-Code to generate a new "Y-Code"), to protect the militarily important P-Code signals from being "spoofed" through the transmission of false GPS signals by an adversary during times of war. Hence civilian GPS receivers are unable to make direct P-Code pseudo-range measurements and must use proprietary (indirect) signal tracking techniques to make measurements on the L2 carrier wave (for both pseudo-range and carrier phase). All dual-frequency instrumentation must therefore overcome AS using these special signal tracking and measurement techniques.

#### *Ambiguity*

Carrier phase measurements can only be made in relation to a cycle or wavelength of the L1 or L2 carrier waves because it is impossible to discriminate different carrier cycles (they are all "sine waves" if one ignores the modulated messages and PRN codes). Integrated carrier phase measurements may be made by those receivers intended for carrier phase-based positioning. In this case the change in receiver-satellite distance can be measured by counting the number of whole wavelengths since initial signal lock-on and adding the instantaneous fractional phase measurement. However, such a measurement is a biased range or distance measurement because the initial number of whole (integer) wavelengths in the receiver-satellite distance is unknown. This unknown value is referred to as the "ambiguity". It is different for the different satellites, and different for the L1 and L2 measurements. It is, however, a constant if signal tracking continues uninterrupted through an observation session. If there is signal blockage, then a "cycle slip" occurs, causing the new ambiguity after the cycle slip to be different from the value before. Cycle slip repair therefore restores the continuity of carrier cycle counts and ensures that there is only one ambiguity for each satellite-receiver pair.

***Ambiguity Resolution***

If the initial integer ambiguity value for each satellite-receiver pair could be determined, then the ambiguous integrated carrier phase measurement can be corrected to create an unambiguous, but very precise (millimetre observation accuracy), receiver-satellite distance measurement. A solution using the corrected carrier phase observations is known as an "ambiguity-fixed" or "bias-fixed" solution. The mathematical process or algorithm for determining the value for the ambiguities is Ambiguity Resolution. Tremendous progress has been made in AR techniques, making today's carrier phase-based GPS systems very efficient by cutting down the length of observation data needed (resulting in so-called "rapid static surveying" techniques) and even allowing this process to occur while the receiver is itself in motion (in so-called "on-the-fly" AR techniques). (In practice, the AR process and the ambiguity-fixed solutions are carried out on the double-differenced carrier phase observables, not on the one-way satellite-receiver measurements.)

***Bandwidth***

The range of frequencies in a signal.

***Baseline***

A Baseline consists of a pair of stations for which simultaneous GPS data have been collected. Mathematically expressed as a vector of coordinate differences between the two stations, or an expression of the coordinates of one station with respect to the other (whose coordinates are assumed known, and is typically referred to as a "Base" or "Reference" Station).

***Base Station***

Also called a Reference Station. In GPS navigation, this is a receiver that is set up on a known location specifically to collect data for differentially correcting data files of another receiver (which may be referred to as the "mobile" or "rover" receiver). In the case of pseudo-range-based Differential GPS (DGPS) the base station calculates the error for each satellite and, through differential correction, improves the accuracy of GPS positions collected at unknown locations by another (roving) GPS receiver. For GPS Surveying techniques, the receiver data from the base station is combined with the

data from the other receiver to form double-differenced observations, from which the baseline vector is determined.

### ***Bias***

All GPS measurements are affected by biases and errors. Their combined magnitudes will affect the accuracy of the positioning results (they will bias the position or baseline solution). Biases may be defined as being those systematic errors that cause the true measurements to be different from observed measurements by a "constant, predictable or systematic amount", such as, for example, all distances being measured too short, or too long. Biases must somehow be accounted for in the measurement model used for data processing if high accuracy is sought. There are several sources of biases with varying characteristics, such as magnitude, periodicity, satellite or receiver dependency, etc. Biases may have physical bases, such as the atmosphere effects on signal propagation or ambiguities in the carrier phase measurements, but may also enter at the data processing stage through imperfect knowledge of constants, for example any "fixed" parameters such as the satellite ephemeris information, station coordinates, velocity of light, antenna height errors, etc. Random errors will not bias a solution. However, outlier measurements, or measurements significantly affected by multipath disturbance (which may be considered a transient, unmodelled bias), will bias a solution if the proportion of affected measurements is relatively high compared to the number of unaffected measurements. For this reason, long period static GPS Surveying is more accurate (less likely to be biased) than "rapid static surveying" or kinematic (single-epoch) positioning.

### ***C/A-Code***

The standard (Clear/Acquisition) GPS PRN code, also known as the Civilian Code or S-Code. Only modulated on the L1 carrier. Used by the GPS receiver to acquire and decode the L1 satellite signal, and from which the L1 pseudo-range measurement is made.

### ***Carrier***

A radio wave having at least one characteristic (e.g., frequency, amplitude, phase) that can be varied from a known reference value by modulation. In the case of GPS there are

two transmitted carrier waves: (a) L1 at 1575.42MHz, (b) L2 at 1227.60MHz, modulated by the Navigation Message (both L1 and L2), the P-Code (both L1 and L2) and the C/A-Code (L1).

### ***Carrier Phase***

GPS measurements made on the L1 or L2 carrier signal. May refer to the fractional part of the L1 or L2 carrier wavelength (approximately 19cm for L1, 24cm for L2), expressed in units of metres, cycles, fraction of a wavelength or angle. (One cycle of L1 is equivalent to one wavelength, and similarly for L2.) In carrier phase-based positioning, such as employed in GPS Surveying techniques, carrier phase may also refer to the accumulated or integrated measurement which consists of the fractional part plus the whole number of wavelengths (or cycles) since signal lock-on.

### ***Code Phase***

GPS measurements based on the C/A-Code. The term is sometimes restricted to the C/A- or P-Code pseudo-range measurement when expressed in units of cycles.

### ***Cycle Slip***

A discontinuity of an integer number of cycles in the measured (integrated) carrier phase resulting from a temporary loss-of-lock in the carrier tracking loop of a GPS receiver. This corrupts the carrier phase measurement, causing the unknown Ambiguity value to be different after the cycle slip compared with its value before the slip. It must be "repaired" (the unknown number of "missing" cycles determined and the carrier observation subsequent to the cycle slip all corrected by this amount) before the phase data is processed in double-differenced observables for GPS Surveying techniques.

### ***Differential GPS (DGPS)***

A technique to improve GPS accuracy that uses pseudo-range errors measured at a known Base Station location to improve the measurements made by other GPS receivers within the same general geographic area. It may be implemented in real-time through the provision of a communication link between the GPS receivers, transmitting the correction information in the industry-standard RTCM format, or various proprietary formats. May be implemented in single Base Station mode, in the so-called Local Area

DGPS (LADGPS), or using a network of Base Stations, as in the Wide Area DGPS (WADGPS) implementation.

### ***Differential Positioning***

Also known as Relative Positioning. Precise measurement of the relative positions of two receivers tracking the same GPS signals. Maybe considered synonymous with DGPS, or the term may be reserved for the more precise carrier phase-based baseline determination technique associated with GPS Surveying.

### ***Double-Difference***

A data processing procedure by which the pseudo-range or carrier phase measurements made simultaneously by two GPS receivers are combined so that, for any measurement epoch, the observations from one receiver to two satellites are subtracted from each other (in a so-called "between-satellite single-difference") to remove that receiver's clock error (or bias). (Similarly for the other receiver's observations to the same two satellites.) Then the two single-differences are subtracted so as to eliminate the satellite clock errors as well as to reduce significantly the effect of unmodelled atmospheric biases and orbit errors. (The order may be reversed, i.e., take "between-receiver single-differences" to each satellite in turn, and then difference between the single-differences.) The resulting set of Double-Differenced observables (for all independent combinations of two-satellite-two-receiver combinations) can be processed to solve for the baseline (linking the two receivers) components and, in the case of ambiguous carrier phase measurements, the integer ambiguity parameters. All high precision positioning techniques use some form of Double-Difference processing: pseudo-range, unambiguous carrier phase within a "bias-fixed" solution (i.e., after the double-differenced ambiguity values have been estimated and applied to the original carrier measurements), or ambiguous carrier phase data within a "bias-free" solution.

### ***Dual-Frequency***

Refers to the instrumentation that can make measurements on both L-Band frequencies, or to the measurements themselves (e.g., L1 and L2 pseudo-range or carrier phase measurements). Dual-frequency measurements are useful for high precision (pseudo-range-based) navigation because the Ionospheric Delay bias can be determined, and the

data corrected for it. In the case of Double-Differenced carrier phase, dual-frequency observations can account for the residual ionospheric bias (for case of long baselines), or aid Ambiguity Resolution for "rapid static" or "kinematic" baseline determination. All "top-of-the-line" GPS receivers are of the dual-frequency variety, and are comparatively expensive because of the special signal processing techniques that must be implemented to make measurements on the L2 carrier under the policy of Anti-Spoofing.

### ***International GPS Service (IGS)***

An initiative of the International Association of Geodesy, as well as several other scientific organisations, that was established as a service at the beginning of 1994. The IGS comprises of many component civilian agencies working cooperatively to operate a permanent global GPS tracking network, to analyse the recorded data and to disseminate the results to users via the Internet. The range of "products" of the IGS include precise post-mission GPS satellite ephemerides, tracking station coordinates, earth orientation parameters, satellite clock corrections, tropospheric and ionospheric models. Although these were originally intended for the geodetic community as an aid to carrying out precise surveys for monitoring crustal motion, the range of users has since expanded dramatically, and the utility of the IGS is such that it is vital to the definition and maintenance of the International Terrestrial Reference System (and its various "frame realisations" ITRF92, ITRF94, ITRF96, etc.).

### ***Ionosphere, Ionospheric Delay***

The Ionosphere is that band of atmosphere extending from about 50 to 1000 kilometres above the earth's surface in which the sun's ultraviolet radiation ionises gas molecules which then lose an electron. These free electrons influence the propagation of microwave signals (speed, direction and polarisation) as they pass through the layer. The Ionospheric Delay on GPS signals is frequency-dependent and hence impacts on the L1 and L2 signals by a different amount (unlike that within the Troposphere). A linear combination of pseudo-range or carrier phase observations on the L1 and L2 carrier waves can be created to almost entirely eliminate the Ionospheric Delay. The resulting observable is known as the Ionosphere-Free carrier phase (or pseudo-range). For single-frequency receivers it is not possible to account for this signal bias in this

way. A broadcast model is contained within the transmitted Navigation Message, however, it is a relatively poor model (unlikely to account for more than 50% of the effect) as the Delay is very difficult to predict. The magnitude of the Ionospheric Delay is a function of the latitude of the receiver, the season, the time of day, and the level of solar activity. The Delay in the Zenith direction can be several tens of metres, increasing as the elevation angle of the satellite signal reduces (being 3-5 times greater than in the Zenith direction). The Delay is largely eliminated in Relative or Differential Positioning, however, the residual Ionospheric Delay increases as the baseline length increases and may be a significant source of error (especially in the height component) for very high precision GPS Geodesy. Even when using dual-frequency instrumentation, the Ionospheric Delay can still cause problems during the process of rapid Ambiguity Resolution when phase and range combinations other than the Ionosphere-Free one are used.

### ***Kalman Filter***

A numerical method used to track a time-varying signal in the presence of noise.

### ***L1 Frequency***

1575.42MHz GPS carrier frequency which contains the C/A-Code, the encrypted P-Code (or Y-Code) and the Navigation Message. Commercial GPS navigation receivers can track only the L1 carrier to make pseudo-range (and sometime carrier phase and Doppler frequency) measurements.

### ***L2 Frequency***

1227.60MHz GPS carrier frequency which contains only the encrypted P-Code (or Y-Code) and the Navigation Message. Military Y-Code capable receivers can, in addition to making L1 measurements, make pseudo-range measurements on the L2 carrier. The combination of the two measurements (on L1 and L2) permits the Ionospheric Delay to be corrected for. Dual-frequency GPS receivers intended for Surveying applications can make L2 measurements using proprietary signal processing techniques. Such measurements are essential if the Ionospheric Delay on carrier phase is to be corrected for (especially on baselines of length greater than about 20-30km) and/or where fast Ambiguity Resolution is needed.



***On-The-Fly (OTF)***

This is a form of Ambiguity Resolution (AR) which does not require that the receivers remain stationary for any length of time. Hence this AR technique is suitable for initialising carrier phase-based Kinematic Positioning. For many applications this introduces considerable flexibility. For example, aircraft do not have to be parked on the ground in order to resolve the carrier cycle ambiguities, and then require that signal lock-on be maintained throughout the kinematic survey. However, dual-frequency instrumentation capable of making both carrier phase and precise (P-Code level) pseudo-range measurements is required.

***P-Code***

The Precise or Protected code. A very long sequence of PRN binary biphasic modulations on the GPS L1 and L2 carrier at a chip rate of 10.23MHz, which repeats about every 267 days. Each one week segment of this code is unique to a GPS satellite and is reset each week. Under the policy of "Anti-Spoofing" the US Dept. of Defense has encrypted the P-Code (replacing it with a so-called Y-Code). Only US military and other authorised users are able to overcome AS using special receivers.

***Pseudolite***

A ground-based differential GPS receiver which transmits a signal like that of an actual GPS satellite, and can be used for ranging. Originally intended as an augmentation for Local Area Augmentation Systems to aid aircraft landings. However, pseudolites may also be used where signal obstructions are such that insufficient GPS satellites can be tracked. In fact, pseudolites are feasible in circumstances where no satellite signals are observable, e.g. for indoor applications.

***Pseudo-Range***

A distance measurement based on the correlation of a satellite's transmitted code (may be the C/A-Code or the encrypted P-Code) and the local receiver's reference code (for that PRN satellite number), that has not been corrected for errors in synchronisation between the transmitter's clock and the receiver's clock. Hence a pseudo-range measurement is a time-error biased distance measurement. The precision of the

measurement is a function of the resolution of the code, hence C/A-Code pseudo-range measurements may have a "noise" at the few metre level for standard GPS receivers (and at the sub-metre precision level in the case of so-called "narrow correlator" GPS receivers).

***Real Time Kinematic (RTK)***

The Relative Positioning procedure whereby carrier phase measurements (or corrections) are transmitted in real-time from a Reference or Base Station to the user's roving receiver. Centimetre accuracy is achieved without the need to record and post-process double-differenced carrier phase observables.

***Real-Time DGPS***

A Base Station computes, formats, and transmits pseudo-range corrections via some sort of data communication link (e.g., VHF or UHF radio, cellular telephone, FM radio sub-carrier or satellite com link). The roving receiver requires some sort of data link receiving equipment to receive the transmitted DGPS corrections so that they can be applied to its current observations. Most GPS receivers are so-called "RTCM-capable", which means that they can accept industry standard DGPS correction messages if the real-time data link is provided.

***Radio Technical Committee for Maritime Applications (RTCM)***

RTCM Special Committee 104 has developed standard message types for use by differential GPS transmitting stations. The message content has been defined and hence when the RTCM-104 standard (version 2.2 is the latest) is implemented within a user receiver, it is able to decode and apply the DGPS corrections to its raw data in order to generate a DGPS-corrected coordinate.

***RS-232***

A standard type of connection to a computer. It is a serial port that allows communication between a computer and a receiver.

***Selective Availability (SA)***

Intentional degradation of the Absolute Positioning performance capabilities of the NAVSTAR satellite system for civilian use (the Standard Positioning Service) by the U.S. military, accomplished by artificially "dithering" the clock error in the satellites. Has generally been mitigated through the use of Relative Positioning techniques. SA was activated on 25 March 1990, and was removed on the 1st May 2000 (midnight Washington D.C. time).

### ***Troposphere, Tropospheric Delay***

The Troposphere is the neutral atmosphere comprising the lower 8km of the atmosphere. The Tropospheric Delay on GPS signals is of the non-dispersive variety because it is not frequency-dependent and hence impacts on both the L1 and L2 signals by the same amount (unlike that within the Ionosphere). The wet and dry components of the Troposphere cause the Delay to the signals, with the wet component be responsible for approximately 10% of the total delay. Various Tropospheric Delay models have been developed to estimate the Delay as a function of the satellite elevation angle, receiver height, and meteorological parameters such as temperature, pressure and humidity. The Delay in the Zenith direction is approximately 2.5m, increasing as the elevation angle of the satellite signal reduces. (This behaviour is described by the so-called Mapping Function, so that the Delay near the horizon is 3-5 times higher than in the Zenith direction.) The Delay is largely eliminated in Relative or Differential Positioning, however the residual Tropospheric Delay increases as the baseline length increases and may be a significant source of error (especially in the height component) for very high precision GPS Geodesy.

### ***World Geodetic System***

A consistent set of parameters describing the size and shape of the Earth, the positions of a network of points with respect to the centre of mass of the Earth, transformations from major geodetic datums, and the potential of the Earth (usually in terms of harmonic coefficients).

### ***World Geodetic System 1984 (WGS-84)***

A global Geodetic Datum defined and maintained by the US Department of Defense. As the Control Segment coordinates and the Broadcast Ephemerides are expressed in this

Datum, the GPS positioning results are said to be in the WGS-84 Datum. In the case of Point Positioning this is largely true, although the level of accuracy achievable under the policy of Selective Availability is so poor that the link to the WGS-84 Datum is very approximate. In the case of Relative Positioning, the baseline vector may be determined to quite high accuracy (at the sub-centimetre level using precise GPS Surveying techniques), however the coordinate (and therefore the Datum) of the unknown point is almost completely defined by the Datum of the Base Station. This may not be coincident with the WGS-84 Datum at better than a few tens of metres! If GPS Geodesy techniques are used, with known station coordinates expressed in the ITRS and precise ephemerides obtained from the IGS, it is more correct to state that the subsequent set of coordinates are expressed in one of the ITRS frames (e.g. ITRF92, ITRF94, etc.). The WGS-84 and the ITRS are compatible at the one metre level. However, the ITRS is a more precise realisation of an earth-fixed, earth-centred terrestrial reference system.

## VITA

---

---

### **Biodata**

Full name: Clement Ogaja  
Gender: Male  
Date of birth: January 22, 1972  
Nationality: Kenyan  
Marital status: Married  
Religion: Christian  
Address: School of Surveying and Spatial Information Systems  
University of New South Wales  
Sydney NSW 2052, Australia

### **Universities attended and degrees obtained:**

1999-2002: Ph.D. (IPRS scholarship)  
School of Surveying and Spatial Information Systems  
*(formerly School of Geomatic Engineering)*  
The University of New South Wales  
Sydney, Australia

1992-1997: Bachelor of Science (Surveying)  
Department of Surveying  
University of Nairobi, Nairobi, Kenya

### **Awards and Prizes**

2002: Best Student Paper Award, IAG Special Commission IV, Berlin.

2001: Best Paper Award, the U.S. Institute of Navigation, USA.

2001: Student Competition Winner Award, the U.S. Institute of Navigation, USA.

2001: Navtech Seminars & GPS Supply Tutorial Scholarship Award, Navtech Seminars & GPS Supply, USA.

2001: U.S. Institute of Navigation's Scholarship Award to attend the 14<sup>th</sup> International Technical Meeting of the Satellite Division of the U.S. Institute of Navigation, USA.

1999-2002: International Postgraduate Research Scholarship (IPRS), Commonwealth of Australia.

1999-2002: Supplementary Engineering Postgraduate Award (SEPA), Faculty of Engineering, UNSW, Sydney, Australia.

1999-2002: Satellite Navigation and Positioning Scholarship Award, School of Surveying and Spatial Information Systems, UNSW, Sydney, Australia.

1999: Best Final Year Student Award by the Survey Consult Ltd. for being the best final year student at the Department of Surveying, University of Nairobi, Kenya.

1999: Best Final Year Student Award by the Institution of Surveyors of Kenya for being the best final year student at the Department of Surveying, University of Nairobi, Kenya.

### **Academic Contributions (2000-2002)**

#### ***Theses/Books***

OGAJA, C., 2002. PhD Thesis: A Framework in Support of Structural Monitoring by RTK-GPS and MultiSensor Data. School of Surveying and Spatial Information Systems, UNSW, Sydney, 207pp.

#### ***Refereed Journal Publications***

OGAJA, C., J. WANG, C. RIZOS & J. BROWNJOHN, 2002. Multivariate monitoring with GPS observations and auxiliary multi-sensor data. *GPS Solutions*, 5(4), 58-69.

OGAJA, C., J. WANG & C. RIZOS, 2002. Principal Component Analysis of wavelet transformed GPS data for deformation monitoring. In *Vistas for Geodesy in the New Millennium*, J. Adams & K.P. Schwarz (eds.), IAG Symp. Vol.125, Springer-Verlag, ISBN 3-540-43454-2, 341-346.

OGAJA, C., WANG, J., & RIZOS, C., 2001. Detection of Wind-Induced Response by Wavelet Transformed GPS Solutions. *Accepted for publication in the Journal of Surveying Engineering of the American Society of Civil Engineers (ASCE)*.

SATIRAPOD C., OGAJA C., WANG J. & RIZOS C. (2001) An Approach to GPS analysis incorporating Wavelet Decomposition. *Artificial Satellites, Vol. 36 No. 2, 27-35*.

OGAJA, C., RIZOS, C., WANG, J., & BROWNJOHN, J., 2001. GPS and building monitoring case study: Republic Plaza Building, Singapore. *Submitted to the Australian Surveyor*.

#### ***Refereed Conference Proceedings (Presentations)***

OGAJA, C., 2002. Software implementation of multi-sensor data reduction and integrity assessment of GPS data for structural monitoring applications. In Proc. *2nd Symp. on Geodesy for Geotechnical & Structural Engineering*, 21-24 May, Berlin, Germany, 27-37. *(won a best student paper award)*

OGAJA, C., 2001. On-line GPS integrity monitoring and deformation analysis for structural monitoring applications. In Proc. *14th Int. Tech. Meeting of the Satellite Division of the U.S. Inst. of Navigation*, 11-14 September, Salt Lake City, Utah, USA, 989-999. *(won best student paper and best presentation awards)*

OGAJA, C., WANG, J., & RIZOS, C., 2001. Principal Component Analysis of wavelet transformed GPS data for deformation monitoring. *IAG Scientific Meeting*, Budapest, Hungary, 3-8 September, CD-ROM proc.

SATIRAPOD C., C. OGAJA, J. WANG & C. RIZOS, 2001. GPS analysis with the aid of wavelets. *5th Int. Symp. on Satellite Navigation Technology & Applications*, Canberra, Australia, 24-27 July, paper 38, CD-ROM proc.

OGAJA, C., C. RIZOS, J. WANG & J. BROWNJOHN, 2001. High precision dynamic GPS system for on-line structural monitoring. *5th Int. Symp. on Satellite Navigation Technology & Applications*, Canberra, Australia, 24-27 July, paper 35, CD-ROM proc.

OGAJA, C., C. RIZOS., J. WANG, & J. BROWNJOHN, 2001. A dynamic GPS system for on-line structural monitoring. *Int. Symp. on Kinematic Systems in Geodesy, Geomatics & Navigation (KIS2001)*, 5-8 June, Banff, Canada, 290-297.

OGAJA, C., C. RIZOS, J. WANG & J. BROWNJOHN, 2001. Towards the implementation of on-line structural monitoring using RTK-GPS and analysis of results using the wavelet transform. *10th FIG Int. Symp. on Deformation Measurements*, 19-22 March, Orange, California, USA. 284-293.

OGAJA, C., C. RIZOS & S. HAN, 2000. Is GPS good enough for monitoring the dynamics of high rise buildings? *2nd Trans Tasman Survey Congress*, Queenstown, New Zealand, 20-26 August, 150-164.

#### *Non-refereed Contributions*

OGAJA, C., 2001. A Simplified Fault Detection Algorithm and its Application to Integrity Assessment of GPS Data for Real-Time Applications. *29th Annual Research Seminars*, School of Surveying and Spatial Information Systems, UNSW, Sydney, 6-7 November.

OGAJA, C., 2000. Wavelets Extract High and Low Frequencies: A Powerful Tool GPS Data Analysis. *28th Annual Research Seminars*, School of Surveying and Spatial Information Systems, The University of New South Wales, Sydney, Australia, 20-21 November.

The hard copy of this thesis is available as a UNISURV report of the School of Surveying and Spatial Information Systems. In order to purchase, contact the **UNISURV editor** at the following address:

A/Prof. Jean M. Rueger  
School of Surveying and Spatial Information Systems  
(formerly the School of Geomatic Engineering)  
University of New South Wales  
UNSW Sydney NSW 2052  
AUSTRALIA  
Email: [J.Rueger@unsw.edu.au](mailto:J.Rueger@unsw.edu.au)  
Phone: +61-2-9385-4173  
Fax: +61-2-9313-7493